UNIVERSIDADE FEDERAL DA PARAÍBA
CENTRO DE CIÊNCIAS DA SAÚDE
INSTITUTO DE PESQUISA EM FÁRMACOS E MEDICAMENTOS
PROGRAMA DE PÓS-GRADUAÇÃO EM PRODUTOS NATURAIS
E SINTÉTICOS BIOATIVOS

FERNANDO FERREIRA LEITE

# SÍNTESE DE DERIVADOS CHALCONAS E BICHALCONAS COM AVALIAÇÃO DA ATIVIDADE LEISHMANICIDA E ANTITUMORAL

JOÃO PESSOA - PB
2024

**FERNANDO FERREIRA LEITE**

# SÍNTESE DE DERIVADOS CHALCONAS E BICHALCONAS COM AVALIAÇÃO DA ATIVIDADE LEISHMANICIDA E ANTITUMORAL

*Tese apresentada ao Programa de Pós-graduação em Produtos Naturais e Sintéticos Bioativos, do Centro de Ciências da Saúde, da Universidade Federal da Paraíba, como requisito para obtenção do título de doutor em Produtos Naturais e Sintéticos Bioativos*.
Área de concentração: Farmacoquímica.

**Orientador: Prof. Dr. Francisco Jaime Bezerra Mendonça Junior**
**Coorientador: Prof. Dr. Luis Cezar Rodrigues**

**JOÃO PESSOA - PB**
**2024**

**Catalogação na publicação**
**Seção de Catalogação e Classificação**

L533s Leite, Fernando Ferreira.

Síntese de derivados Chalconas e Bichalconas com avaliação da atividade Leishmanicida e antitumoral / Fernando Ferreira Leite. - João Pessoa, 2024.
210 f. : il.

Orientação: Francisco Jaime Bezerra Mendonça Júnior. Coorientação: Luis Cezar Rodrigues.
Tese (Doutorado) - UFPB/CCS.

1. Produtos naturais. 2. Chalconas - Atividade anticancerígena. 3. Condensação de Claisem-Schimidt. 4. Leishmania infantum. 5. Leishmania brasiliensis. I. Mendonça Júnior, Francisco Jaime Bezerra. II. Rodrigues, Luis Cezar. III. Título.

UFPB/BC CDU 547.9(043)

Elaborado por ANNA REGINA DA SILVA RIBEIRO - CRB-15/24

**SÍNTESE DE DERIVADOS BICHALCONAS E BIFLAVONOIDES COM AVALIAÇÃO DA ATIVIDADE LEISHMANICIDA E ANTITUMORAL**

**BANCA EXAMINADORA**

Documento assinado digitalmente
gov.br FRANCISCO JAIME BEZERRA MENDONCA JUNIO
Data: 09/07/2024 21:20:15-0300
Verifique em https://validar.iti.gov.br

**Orientador: Prof. Dr. Francisco Jaime Bezerra Mendonça Junior – Universidade Estadual da Paraíba**

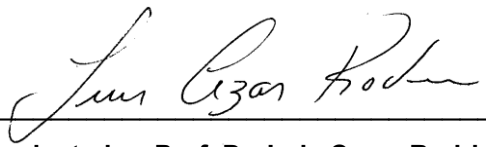

**Coorientador: Prof. Dr. Luis Cezar Rodrigues**
**Universidade Federal da Paraíba**

Documento assinado digitalmente
gov.br FLAVIO VALADARES PEREIRA BORGES
Data: 06/07/2024 00:00:24-0300
Verifique em https://validar.iti.gov.br

**Examinador I: Prof. Dr. Flavio Valadares Pereira Borges**
**Universidade Federal da Paraíba**

Documento assinado digitalmente
gov.br SOCRATES GOLZIO DOS SANTOS
Data: 09/07/2024 08:10:08-0300
Verifique em https://validar.iti.gov.br

**Examinador II: Prof. Dr. Socrates Golzio dos Santos**
**Universidade Federal da Paraíba**

Documento assinado digitalmente
gov.br RICARDO OLIMPIO DE MOURA
Data: 04/07/2024 15:18:56-0300
Verifique em https://validar.iti.gov.br

**Examinador III: Prof. Dr. Ricardo Olímpio de Moura**
**Universidade Estadual da Paraíba**

Documento assinado digitalmente
gov.br FRANCISCO HUMBERTO XAVIER JUNIOR
Data: 04/07/2024 14:37:55-0300
Verifique em https://validar.iti.gov.br

**Examinador IV: Prof. Dr. Francisco Humberto Xavier Júnior**
**Universidade Federal da Paraíba**

**JOÃO PESSOA – PB**

**2024**

*Dedico esse trabalho a minha mãe Dalila (In memorian), a pessoa mais guerreira com quem tive a oportunidade de conhecer ao longo dessa jornada, que chamamos de vida.*

AGRADECIMENTOS

Parafraseando Diego Sternhein “*Grandes realizações são sempre fruto de trabalho em equipe*”.

Com isso deixo aqui meus agradecimentos a todos que contribuíram de alguma forma para a realização deste trabalho e colaboraram para meu crescimento profissional e pessoal.

Inicialmente, expresso minha gratidão a Deus, pois até este momento, o Senhor tem sido meu auxílio constante, graças ao seu amor infinito e por ser a minha esperança constante nos momentos mais desafiadores ao longo desta jornada.

Em especial agradeço a minha mãe que mesmo não estando nesse plano, continua me dando forças para continuar em frente. Quero expressar meu eterno agradecimento por tudo o que fez por mim. Sua presença é eterna em minhas memórias, e seu legado vive em cada passo que dou.

Agradeço ao meu pai Luís de Sousa Leite e meus irmãos Fábio Ferreira Leite e Fernanda Ferreira Leite, além dos meus gatos Thomas, Nora e Frajola, pois sem eles eu não seria nada. Agradeço por todo apoio e suporte emocional em todos os momentos.

Agradeço aos meus tios Dione, Domício e Dejaci, por sempre estarem dispostos a me ajudarem em todas as situações difíceis e pelos conselhos dados.

Agradeço aos meus orientadores Dr Luis Cezar, Dr Francisco Jaime e a professora Bárbara Viviana pela paciência e por todos os ensinamentos. Por todo auxílio na bancada e por sempre estarem dispostos a me ensinar e colaborar com meu crescimento profissional. Sei que sem eles esse trabalho não seria possível.

Aos professores Marcus Túlius, Luciana Scott, Barbosa, Tatjane, Edeltrudes e Elisalva, além da minha prima Natália, pelas colaborações em trabalhos.

Aos técnicos Evandro, Marcelo e Nonato, pelos espectros, solventes e reagentes fornecidos e pelos bons papos nos corredores, sempre enriquecendo meu conhecimento.

Aos meus amigos de Pós-graduação Pedro, André, Ferreirinha, Vinicius e Bruno pelos momentos de descontração, deixando essa jornada mais leve.

A toda equipe do professor Luis, Gabi, Denise, além dos já citados acima.

A todos os meus amigos do “Clube do Bolinha”, John, Venâncio, Ricardo, Emmanuel, Kauê, Thyago, Bruno, Pedro, Felipe e Vinicius pelos laços de amizades que permaneceram após a graduação e por tornarem essa caminhada mais alegre.

A todos aqueles que colaboraram de forma direta ou indireta para a realização desse trabalho.

A Universidade Federal da Paraíba.

Ao Instituto de Pesquisa em Fármacos e Medicamentos (IPeFARM).

A todos os funcionários que pertencem ao Programa de Produtos Naturais e Sintéticos Bioativos.

Ao Conselho Nacional de Desenvolvimento Científico e Tecnológico

(CNPq) pelo apoio financeiro.

Deixo aqui minha gratidão!

***“Não espere por uma crise para descobrir o que é importante em sua vida.”***

***(Platão)***

***“Se eu pude enxergar mais longe, foi por estar apoiado sobre ombros de gigantes.”***

***(Isaac Newton)***

# RESUMO

As chalconas são uma classe de compostos gerados pelo metabolismo secundário dos vegetais. Estudos anteriores já relataram a gama de atividades farmacológicas apresentadas por esses compostos, dentre elas destacam-se as propriedades leishmanicidas, anticancerígeras, antimicrobianas e antioxidantes. Nesse trabalho buscamos sintetizar chalconas e dímeros de chalconas inéditos com rotas viáveis economicamente, elucidar estruturalmente os compostos por técnicas espectroscópicas de RMN $^{1}H$ e $^{13}C$, além de espectrometria de massas e avaliar as propriedades desses compostos frente as espécies de *Leishmania infantum* e *Leishmania brasiliensis*, e ainda relatar propriedades anticancerígenas de chalconas em estudos relatados nos últimos cinco anos, englobando o período de 2019 a 2023. Diferentes concentrações dos compostos foram avaliadas frente a formas promastigotas e amastigotas de *L. infantum e L. brasiliensis,* apresentando inibições promissoras com $IC_{50}$ de 10.96 e 13.64 μm. Estudos *in silico* foram feitos com enzimas importantes na sobrevivência e manutenção do parasita, dentre elas a tripanotiona redutase e a 14-αdemetilase (CYP-51). O Docking molecular revelou fortes interações dos compostos com esses alvos, com valores de MolDock score inferiores aos dos ligante cocristalizados variando entre -94.0758 (para CYP-51) e -50.5692 (para trypanotiona redutase) de energia negativa. Nossos achados reforçam o potencial dessa classe de metabólitos secundários e encorajam estudos posteriores para descobrir o real mecanismo de ação por análises *in vitro,* além de encontrar novos análogos ainda mais promissores para essa doença ainda negligenciada. Para uma melhor compreensão do leitor, o trabalho foi dividido em 4 capítulos, onde no capítulo 1 abordamos as etapas de síntese e caracterização dos compostos, seguido dos trabalhos publicados, englobando os capítulos 2, 3 e 4.

Palavras-Chave: Chalconas, Condensação de Claisem-Schimidt, Atividade anticancerígena, *Leishmania infantum, Leishmania brasiliensis*.

# ABSTRACT

Chalcones are a class of compounds generated by the secondary metabolism of plants. Previous studies have reported the range of pharmacological activities presented by these compounds, among which the leishmanicidal, anticancer, antimicrobial and antioxidant properties stand out. In this work, we aimed to synthesize novel chalcones and chalcone dimers with economically viable routes, structurally elucidate the compounds by $^{1}H$ and $^{13}C$ NMR spectroscopic techniques, in addition to mass spectrometry and evaluate the properties of these compounds against *Leishmania infantum* and *Leishmania brasiliensis* species, and also report anticancer properties of chalcones in studies reported in the last five years, covering the period from 2019 to 2023. Different concentrations of the compounds were evaluated against promastigote and amastigote forms of *L. infantum* and *L. brasiliensis*, showing promising inhibitions with $IC_{50}$ of 10.96 and 13.64 μm. In silico studies were performed with enzymes important in the survival and maintenance of the parasite, among them trypanothione reductase and 14-αdemethylase (CYP-51). Molecular docking revealed strong interactions of the compounds with these targets, with MolDock score values lower than those of the cocrystallized ligands, ranging from -94.0758 (for CYP-51) to -50.5692 (for trypanothione reductase) of negative energy. Our findings reinforce the potential of this class of secondary metabolites and encourage further studies to discover the real mechanism of action by in vitro analysis, in addition to finding new, even more promising analogues for this still neglected disease. For a better understanding of the reader, the work was divided into 4 chapters, where in chapter 1 we address the synthesis and characterization steps of the compounds, followed by the published works, encompassing chapters 2, 3 and 4.

Keywords: Chalcones, Claisem-Schimidt Condensation, Anticancer activity, *Leishmania infantum*, *Leishmania brasiliensis*.

# LISTA DE FIGURAS

# LISTA DE ESQUEMAS

# LISTA DE ABREVIAÇÕES, SIGLAS E FÓRMULAS

**AcOEt** Acetato de etila

**APT** Attached proton test

**$BF_3 \cdot Et_2O$** Trifluoreto de boro eterato

**CC** Cromatografia em coluna

**CCDA** Cromatografia em camada delgada analítica

**CCDP** Cromatografia em camada delgada preparativa

**$CH_2Cl_2$** Diclorometano

**$CHCl_3$** Clorofórmio

**d** Dubleto

**dd** Duplo dupleto

**DMF** Dimetilformamida

**Hz** Hertz

**$CI_{50}$** Concentração inibitória média

**J** Constante de acoplamento

**$K_2CO_3$** Carbonato de potássio

**L.** Leishmania

**m** Multipleto

**MeI** Iodeto de metila

**MHz** Megahertz

**OMS** Organização Mundial de Saúde

**P&D** Pesquisa e desenvolvimento

**ppm** Pulsos por minuto

**q** Quarteto

**RMN** Ressonância Magnética Nuclear

**RMN $^{13}C$** Ressonância magnética nuclear de carbono-13

**RMN $^{1}H$** Ressonância magnética nuclear de hidrogênio

**s** Sinpleto

**t** Tripleto

**WHO** World Health Organization

**δ** Deslocamento químico em ppm

**Sumário**

# Introdução

## INTRODUÇÃO

A busca por novos agentes terapêuticos e aperfeiçoamento dos mecanismos farmacológicos têm impulsionado a pesquisa na área de produtos bioativos, sejam eles de origem natural ou sintética (PIRES A L R, BIERHALZ A C K. & MORAE Â M, 2015). No contexto farmacêutico, a atenção voltada para substâncias capazes de modular processos fisiológicos, prevenir ou tratar doenças tem sido crescente.

Nesse cenário, os produtos naturais têm se destacado como fontes ricas em moléculas bioativas, oferecendo um vasto repertório de compostos com potencial farmacológico (SIMÕES, C.M.O. et al. 2016). O Brasil se torna protagonista nesse âmbito, possuindo em torno de 25 a 27% da maior biodiversidade mundial, segundo a CDB (Convenção da Diversidade Biológica) distribuída em 7 biomas, se tornando uma rica fonte de substâncias biologicamente ativas (ROMA, J.C. & CORADIN, L., 2016).

Os produtos naturais, provenientes de plantas, microorganismos e outros organismos, têm sido tradicionalmente utilizados na medicina popular e (NAGEEN, et al., 2018), ao longo do tempo, têm sido objeto de investigação científica intensa, fomentando cada vez mais a indústria farmacêutica no investimento a P&D (Pesquisa & Desenvolvimento). A diversidade estrutural química presente nesses compostos naturais oferece uma gama de oportunidades para a descoberta de novos fármacos e entendimento de seus mecanismos de ação (SOUZA G H B, MELLO J C P, 2011), dentre esses compostos naturais estão presentes alcalóides, flavonoides, cumarinas, lignanas, triterpenos, esteróides e as chalconas.

As chalconas são polifenóis de grande interesse químico-farmacológico que vem recebendo grande atenção pois além de possuírem estruturas relativamente simples, ainda possuem uma grande variedade de atividades farmacológicas (FERREIRA, et al., 2018), como: atividade antioxidante (VANANGAMUDI, et al., 2017), antinociceptiva (FERREIRA, et al., 2018), anti-convulsivante (NASSAR, et al., 2016), anti-inflamatória (ÖZDEMIR, et al., 2015), anti-viral contra o SARS-CoV (PARK, JI-YOUNG, et al., 2016) e vírus influenza H1N1 (MALBARI, K., et al., 2018).

Tanto na terapêutica convencional como na medicina tradicional encontramos diversos medicamentos à base de fitocomplexos ou fitoconstituintes, como a quercetina com propriedades antiinflamatórias (COSTA, ACF, 2020), antioxidante (BEHLING, E. V. et al. 2008), antiviral (AGRAWAL, Pawan K.; AGRAWAL, Chandan; BLUNDEN, Gerald, 2020) e gastroprotetora (MARTIN, MJ, et al, 2015).

Derivados das 1,3-diaril-2-propen-1-onas (Figura 1), apresentaram variadas atividades como ação anticonvulsivante (MORA-PEREZ PA & MEDEL MRH, 2016), antinociceptiva (BARROT M, 2012), antioxidante (PANDEY M M, et al., 2016) e antiinflamatória (MACHADO, et al., 2016), relatado por Ferreira e colaboradores em 2018. Leite e colaboradores (2023) relataram, em uma revisão sistemática, atividades anticancerígenas de chalconas naturais e sintéticas, demonstrando o amplo espectro de ações farmacológicas que esses metabólitos apresentam.

Figura 1: Esqueleto básico de chalconas.

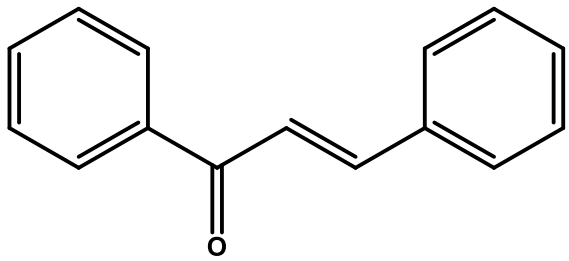


**1,3-diaril-2-propen-1-ona**

Fonte: MORA-PEREZ PA & MEDEL MRH, 2016.

No entanto, a crescente demanda por esses potenciais agentes terapêuticos, vem preocupando os pesquisadores uma vez que são encontrados baixos rendimentos quando obtidos por fontes naturais, sendo necessária uma grande demanda de matéria prima. Nesse cenário a química verde vem ganhando destaque, pois tem como objetivo final conduzir as ações científicas ecologicamente corretas, visando a preservação dos biomas (CGEE, 2010).

A síntese aliada aos produtos naturais proporciona uma obtenção de compostos bioativos sem agressões aos biomas, além de permitir realizar ajustes precisos em suas propriedades, visando a otimização de atividades farmacológicas e a minimização de efeitos colaterais indesejados (SANGI D P,

2016). Dessa forma, a interação sinérgica entre produtos naturais e sintéticos abre novas perspectivas para o avanço na descoberta de medicamentos.

A integração entre a síntese de compostos bioativos e o uso de produtos naturais não só facilita a descoberta de novos medicamentos, mas também oferece uma abordagem sustentável para o tratamento de doenças, especialmente aquelas que afetam de forma desproporcional países emergentes. Nesse contexto, a aplicação dessas técnicas na luta contra doenças negligenciadas, como a Leishmaniose, se torna ainda mais relevante. Com milhares de novos casos registrados anualmente, a exploração de estratégias inovadoras e eficazes para o combate a essa doença é essencial (Marques, L.G.A., et al. 2022).

A OMS (2018) estima que cerca de 0,7 a 1 milhão de novos casos surgem anualmente, além de 20 a 30 mil óbitos (Diotallevi et al, 2020). Dentre as espécies de maior interesse clínico estão a *Leishmania infantum*, *L. chagasi, L. donovani, L. brasiliensis* e *L. amazonensis* (Mauricio et al, 2018).

Os mesmos medicamentos desde o final da década de 1940 ainda são utilizados no combate ao parasita, como os antimoniais pentavalentes e, mais recentemente, a anfotericina B (Barbosa et al, 2015). Porém, além de caros, esses medicamentos não são mais tão eficazes ou seguros, e apresentam diversos efeitos colaterais. Além disso, provocaram seleção natural devido ao uso extensivo, o que levou ao surgimento de cepas resistentes de Leishmania sp. (Qin et al, 2020; Akbari et al, 2017).

Dada a importância que as chalconas e seus dímeros vem apresentando na terapêutica, e tendo em vista que a extração desses recursos por vias naturais necessita de uma alta demanda de nossa flora pelos baixos rendimentos sobretudo dos dímeros bichalconas, buscamos realizar a síntese desses compostos utilizando matérias primas de baixo custo e de fácil acesso, com técnicas já conhecidas na literatura, e analisar as atividades antileishmania apresentadas por essa classe de compostos.

## REFERÊNCIAS

AGRAWAL, Pawan K.; AGRAWAL, Chandan; BLUNDEN, Gerald. Quercetin: antiviral significance and possible COVID-19 integrative considerations. Natural Product Communications, v. 15, n. 12, p. 1934578X20976293, 2020.

BARBOSA, Juliana F et al. New approaches on leishmaniasis treatment and prevention: A review of recent patents. Recent patents on endocrine, metabolic & immune drug discovery, v. 9, n. 2, p. 90-102, 2015.

BARROT, Michel. Tests and models of nociception and pain in rodents. Neuroscience, v. 211, p. 39-50, 2012.

BEHLING, E. V. et al. Flavonóide quercetina: aspectos gerais e ações biológicas. Alimentos e Nutrição Araraquara, v. 15, n. 3, p. 285-292, 2008.

COSTA, Ana Carolina de Figueiredo. Efeito antinociceptivo e anti-inflamatório da quercetina na artrite reumatoide induzida por mBSA na ATM de ratos. Dissertação de Mestrado, 2020.

DIOTALLEVI, Aurora et al. Real-time PCR to differentiate among Leishmania (Viannia) subgenus, Leishmania (Leishmania) infantum and Leishmania (Leishmania) amazonensis: Application on Brazilian clinical samples. Acta tropica, v. 201, p. 105178, 2020.

FERREIRA, Maria Kueirislene A. et al. Potencial farmacológico de chalconas: Uma breve revisão. **Revista virtual de química**, v. 10, n. 5, 2018.

FERREIRA, Maria Kueirislene A. et al. Potencial farmacológico de chalconas: Uma breve revisão. Revista virtual de química, v. 10, n. 5, 2018.

MACHADO, Alessandra Cury et al. Atividade anti-inflamatória de produtos naturais em Odontologia: uma revisão sistemática. 2016.

MALBARI, K., et al. "In search of effective H1N1 neuraminidase inhibitor by molecular docking, antiviral evaluation and membrane interaction studies using NMR." Acta virologica 62.2 (2018): 179-190.

MARQUES, Lana Grasiela Alves et al. O impacto da bioprospecção para o descobrimento de novas moléculas terapêuticas. **Revista Fitos**, v. 16, n. Supl. 2, p. 293-314, 2022.

MARTIN, M. J. et al. Anti-oxidant mechanisms involved in gastroprotective effects of quercetin. Zeitschrift für Naturforschung C, v. 53, n. 1-2, p. 82-88, 2015.

MARDHATILLAH, Athina; MUTAKIN, Mutakin; LEVITA, Jutti. FeCl3-catalyzed Synthesis of Dehydrodiisoeugenol. International Journal of Chemistry, v. 8, n. 1, 2016.

MAURÍCIO, I. L.; BRUSCHI, F.; GRADONI, L. The Leishmaniases: Old Neglected Tropical Diseases. The leishmaniases: old neglected tropical diseases. Cham: Springer International Publishing, p. 15-30, 2018.

MORA-PÉREZ, A.; HERNÁNDEZ-MEDEL, M. del R. Actividad anticonvulsivante del extracto metanólico de tallo y raíz de Kalanchoe pinnata Lam. en ratones: comparación con diazepam. Neurología, v. 31, n. 3, p. 161-168, 2016.

NAGEEN, Bushra, et al. "Eupatilin: a natural pharmacologically active flavone compound with its wide range applications." Journal of Asian natural products research 22.1 (2018): 1-16.

Nassar, E. M.; Abdelrazek, F. M.; Ayyad, R. R.; El-Farargy, A. F. Synthesis and Some Reactions of 1-aryl-4-acetyl-5-methyl-1,2,3- triazole Derivatives with Anticonvulsant Activity. Mini reviews in medicinal chemistry 2016, 16, 926.

Organização Mundial da Saúde. Leishmaniasis. 2018. Disponível online em: http://www.who.int/mediacentre/factsheets/fs375/en/

ÖZDEMIR, Ahmet, et al. "Synthesis and evaluation of new indole-based chalcones as potential antiinflammatory agents." European journal of medicinal chemistry 89 (2015): 304-309.

PANDEY, Madan Mohan et al. Determination of flavonoids, polyphenols and antioxidant activity of Tephrosia purpurea: a seasonal study. Journal of integrative medicine, v. 14, n. 6, p. 447-455, 2016.

PARK, Ji-Young, et al. "Chalcones isolated from Angelica keiskei inhibit cysteine proteases of SARS-CoV." Journal of enzyme inhibition and medicinal chemistry 31.1 (2016): 23-30.

PIRES, Ana Luiza R.; BIERHALZ, Andréa CK; MORAES, Ângela M. Biomateriais: tipos, aplicações e mercado. Química nova, v. 38, p. 957-971, 2015.

QIN, Hua-Li et al. Chalcone hybrids as privileged scaffolds in antimalarial drug discovery: A key review. European journal of medicinal chemistry, v. 193, p. 112215, 2020.

ROMA, Júlio Cesar; CORADIN, Lidio. A Governança da Convenção sobre Diversidade Biológica e sua implementação no Brasil. 2016.

SANGI, Diego Pereira. Estratégias de síntese na descoberta de fármacos: o emprego da síntese orientada pela diversidade estrutural. Química nova, v. 39, p. 995-1006, 2016.

SIMÕES, Cláudia Maria Oliveira et al. **Farmacognosia: do produto natural ao medicamento**. Artmed Editora, 2016.

SOUZA, Gustavo Henrique Bianco de; MELLO, João Carlos Palazzo de; LOPES, Norberto Peporine. Farmacognosia: coletânea científica. Editora UFOP, 2011.

VANANGAMUDI, Ganesan, Muthuvel Subramanian, and Ganesamoorthy Thirunarayanan. "Synthesis, spectral linearity, antimicrobial, antioxidant and insect antifeedant activities of some 2, 5-dimethyl-3-thienyl chalcones." Arabian Journal of Chemistry 10 (2017): S1254-S1266.

Waldvogel, Siegfried R. "Comprehensive Organic Name Reactions and Re." (2010): 892-892.

# CAPÍTULO 1

## SÍNTESE E CARACTERIZAÇÃO DOS COMPOSTOS

## PROPOSTA DE SÍNTESE E CARACTERIZAÇÃO DOS COMPOSTOS

Um total de 18 compostos foram sintetizados, dentre eles chalconas e dímeros de chalconas, das quais 9 são compostos inéditos, sendo eles, FER26, FER23(A), FER23(B), FER89, FER08, FER13, FER12, FER36 e FER37.

Os compostos foram obtidos via condensações de Claisem Schimidt (Esquema 1), utilizando em quase todos os casos um reagente em comum, sendo a 3,4-metilenodioxi acetofenona, com benzaldeídos previamente sintetizados e/ou modificados sinteticamente.

Esquema 1: Esquema geral de síntese das chalconas.

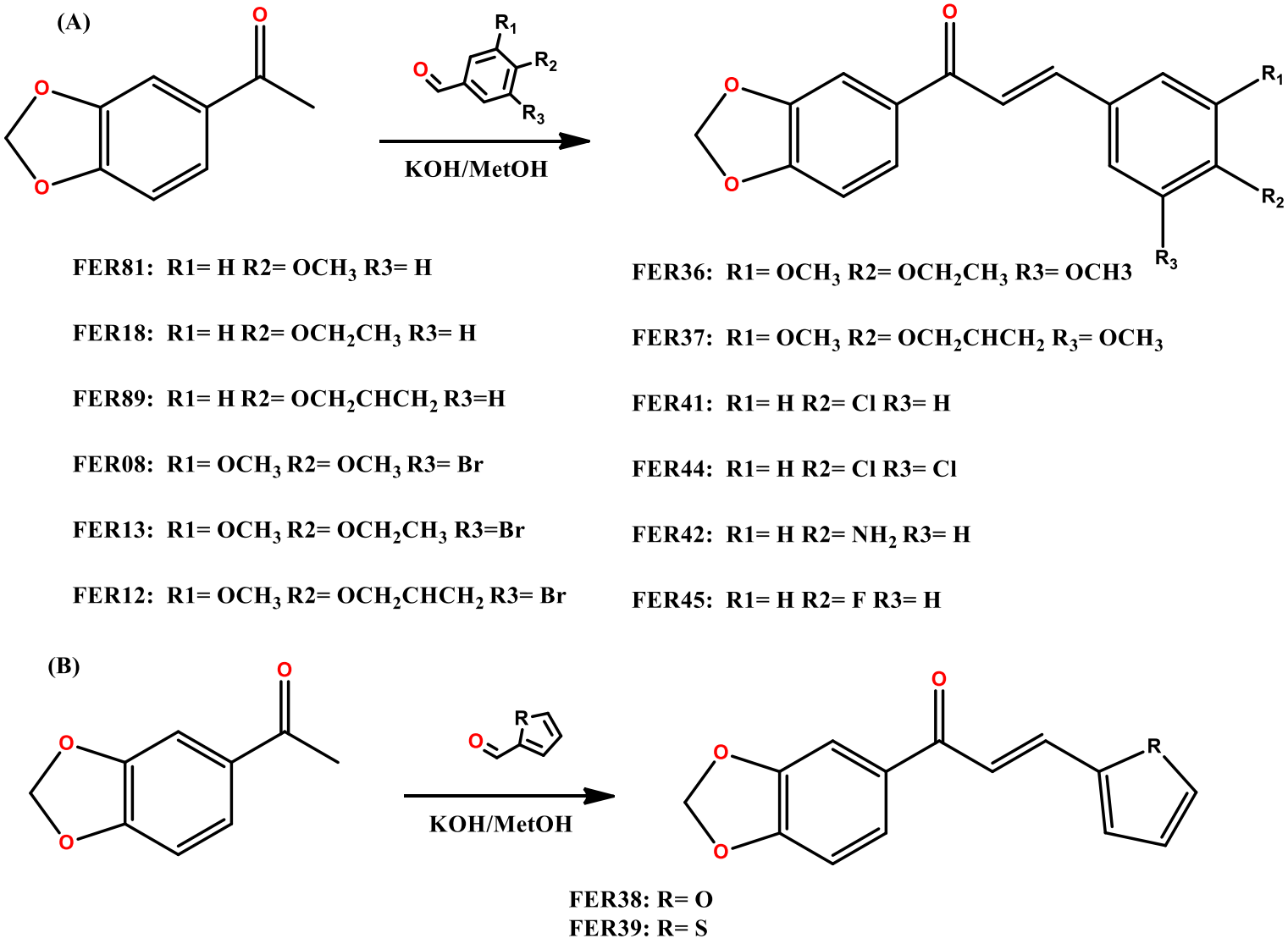


Fonte: autor, 2024.

O mecanismo de condensação via Claisen-Schimidt foi relatado pela primeira vez em 1881 pelos pesquisadores Ludwig Claisen e J. G. Schmidt

(CLAISEN L, 1881), e consiste em uma reação de condensação entre aldeídos e cetonas na presença de um catalisador ácido ou básico, formando compostos carbonílicos α,β-insaturado. Essas reações se tornaram populares por apresentar altos rendimentos, além de possuir um baixo custo para sua execução. No mecanismo das reações via Claisen via catalise básica, a base capta um próton da acetofenona que possui caráter ácido, um carbânion então é formado entrando em conjugação com a carbonila da cetona, formando um enol (Esquema 2).

Os elétrons em ressonância do grupo enol atacam o carbono do benzaldeído formando uma ponte de ligação entre a acetofenona e o benzaldeído. Em meio aquoso a base atua retirando o próton do carbono alfa-carbonila, ocasionando uma desidratação e formando um sistema conjulgado, concluindo assim a formação de compostos do tipo chalcona (WALDVOGEL, 2010).

Esquema 2: Mecanismo da condensação de Claisen Schmidt.

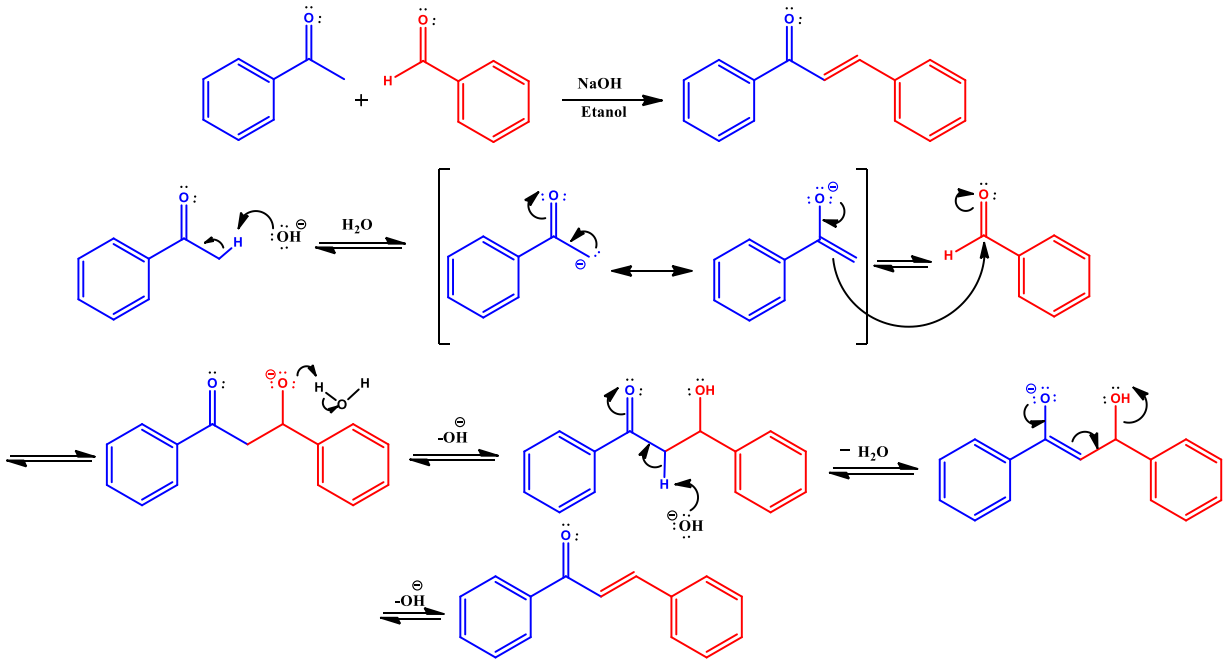


Fonte: Adaptado de Waldvogel, 2010.

Na síntese dos dímeros, foi feito um acoplamento oxidativo entre duas moléculas de vanilina, utilizando o cloreto férrico como catalisador. O mecanismo proposto para essa reação se inicia pela clivagem homolítica do hidrogênio da

hidroxila (Figura 2 [1]) formando um complexo com o cloreto férrico. O sistema ressonante desloca o elétron até a posição orto (Figura 2 [2]), onde posteriormente é formado uma ponte bifenil entre duas moléculas de vanilina (Figura 2 [3]). Após a formação da ponte bifenil o sistema ressonante é restabelecido promovendo a formação do dímero (Mardhatillah A., et al. 2016). Posteriormente a obtenção da divanilina, foi realizada uma etapa de alquilação, metilando as hidroxilas livres presente no dímero, finalizando o preparo do primeiro reagente na síntese da bichalcona.

Figura 2: Mecanismo proposto na síntese da divanilina.

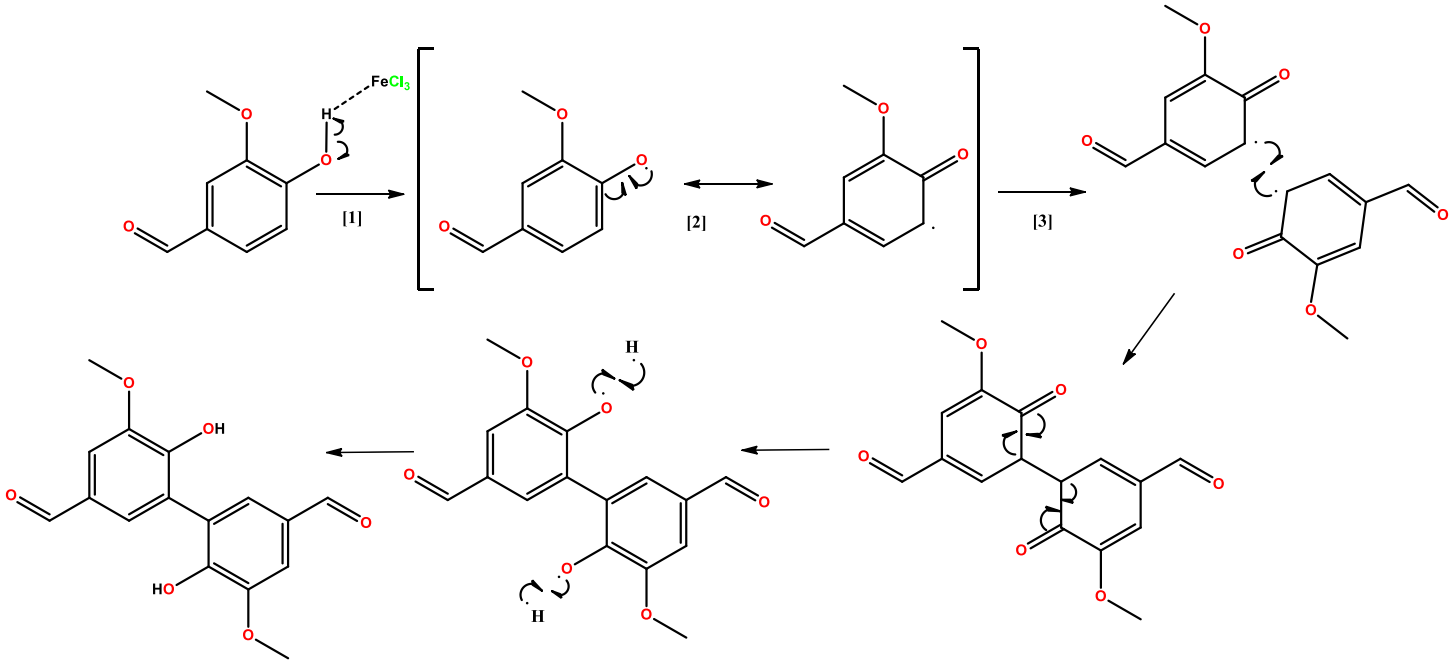


Fonte: Adaptado de Mardhatillah A., et al. 2016

No preparo do segundo reagente, foi feita uma acilação via Friedel-Crafts com trifluoreto de boto eterato. A acilação ocorre preferencialmente na posição orto-hidroxila, uma vez que esse grupo é um ativante do anel aromático, sendo orto/para dirigente. Pela posição de ambas hidroxilas, a posição orto se torna duplamente favorecida. Por fim, foi feita uma condensação de Claisem-Schimidt entre a divanilina e a acetofenona da resorcina para gerar a bichalcona (FER26).

## 1.1. DETERMINAÇÃO ESTRUTURAL DA (2E,2'E)-3,3'-(5,5',6,6'-TETRAMETOXI-[1,1'-BIFENIL]-3,3'-DIIL)BIS(1-(2,4-DIMETOXIFENIL)PROP-2-EN-1-ONA) (FER26)

Por se tratar de um dímero com um plano de simetria (Figura 3), é esperado que se observe sinais compatíveis com uma estrutura de chalcona, porém com sinais equivalentes ao dobro da massa molecular, sendo mais intensos e com um acoplamento bifenílico, correspondente da divanilina (Figura 4).

Evidenciamos a formação da chalcona, através dos dupletos em $\delta_H$ 7.60 e $\delta_H$ 7.39 ppm (Figura 6) acoplando entre si com uma constante de 15.7 Hz no espectro de $^1H$ (400MHz, $CDCl_3$), indicando a presença do sistema olefínico obtido após a condensação de Claisen-Schimidt. As alquilações podem ser confirmadas pelas metoxilas presentes em $\delta_H$ 3.713 (s, 6H), $\delta_H$ 3.86 (s, 6H), $\delta_H$ 3.87 (s, 6H) e $\delta_H$ 3,95 ppm (s, 6H) (Figura 5) no espectro de $^1H$ em conjunto com os dados do espectro de $^{13}C$ com deslocamentos em $\delta_C$ 60.83, $\delta_C$ 55.89, $\delta_C$ 55.78 e $\delta_C$ 55.52 ppm (Figura 7). No espectro de $^{13}C$ (100MHz, $CDCl_3$) verificamos a presença de 7 sinais para carbonos metínicos aromáticos e 8 sinais para carbonos não hidrogenados (Figura 8), sugerindo a formação da ponte bifenil da divanilina resultante do acoplamento oxidativo.

O espectro de massas (Figura 9) revelou uma massa molar de 665.2537 no modo positivo, e uma fórmula química compatível com o dímero de chalcona $C_{38}H_{39}O_{10}$ [M+]. A partir desses dados de RMN $^1H$ e $^{13}C$, aliado aos dados obtidos do espectro de massas, podemos identificar o composto FER26 sendo a bichalcona (2E,2'E)-3,3'-(5,5',6,6'-tetrametoxi-[1,1'-bifenil]-3,3'-diil)bis(1-(2,4-dimetoxifenil)prop-2-en-1-ona).

Figura 3: (2E,2'E)-3,3'-(5,5',6,6'-tetrametoxi-[1,1'-bifenil]-3,3'-diil)bis(1-(2,4-dimetoxifenil)prop-2-en-1-ona) (FER26).

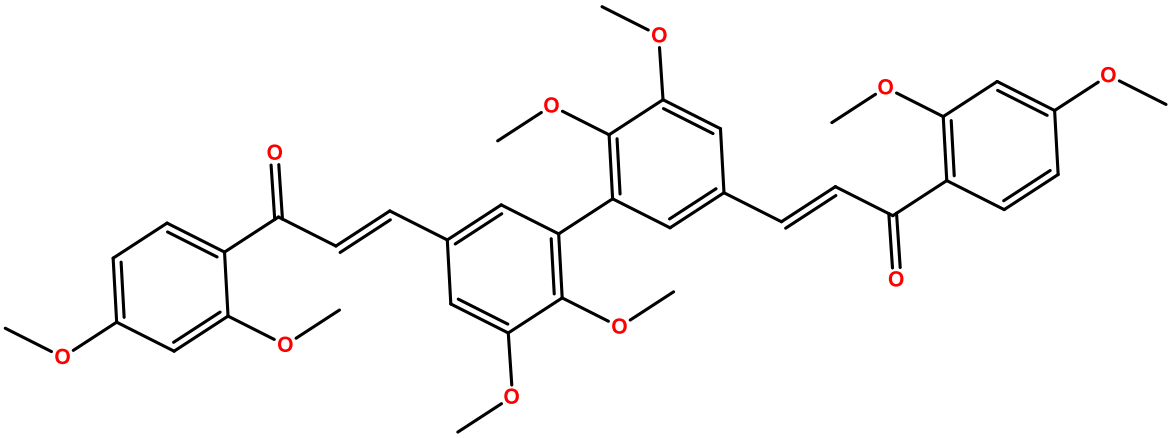

**Chemical Formula:** $C_{38}H_{38}O_{10}$
**Exact Mass: 654,25**

Figura 4: Espectro de RMN $^{1}H$ (400 MHz, $CDCl_3$) de FER26.

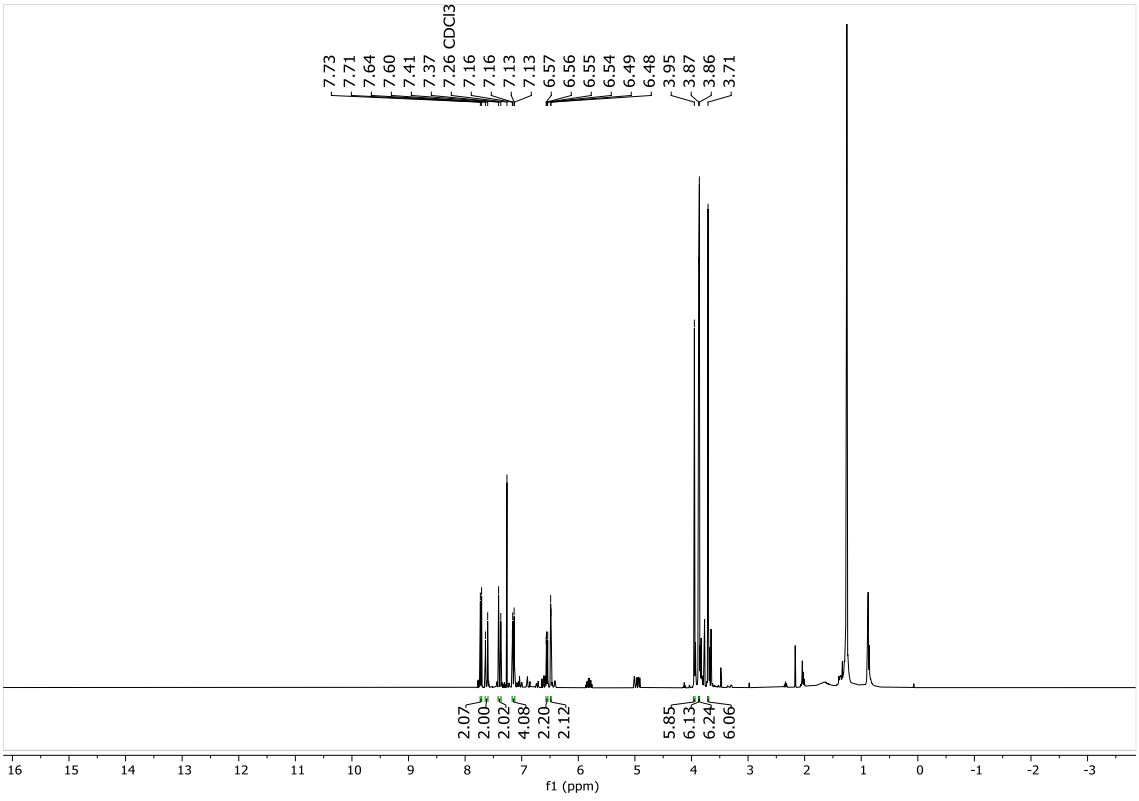

Figura 5: Expansão do espectro de RMN $^{1}H$ (400 MHz, $CDCl_3$) de FER26 na região 3.66 a 3.99 ppm.

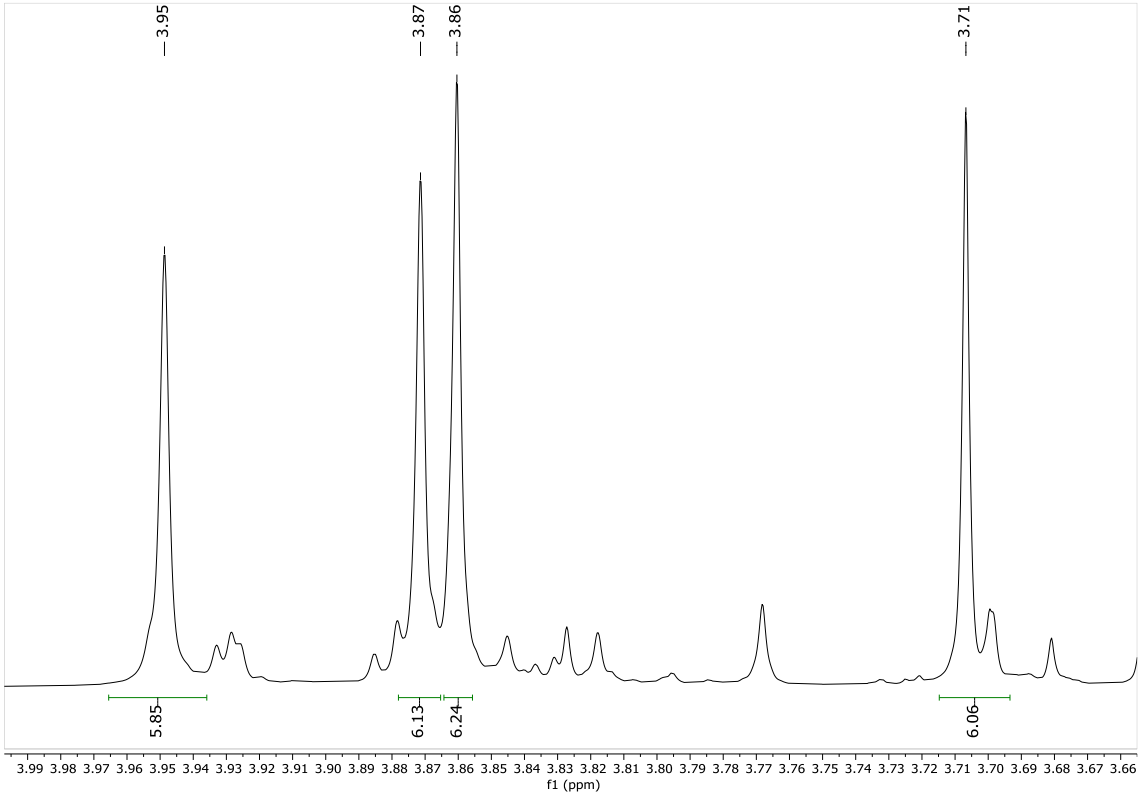


Figura 6: Expansão do espectro de RMN $^{1}H$ (400 MHz, $CDCl_3$) de FER26 na região 6.45 a 7.80 ppm.

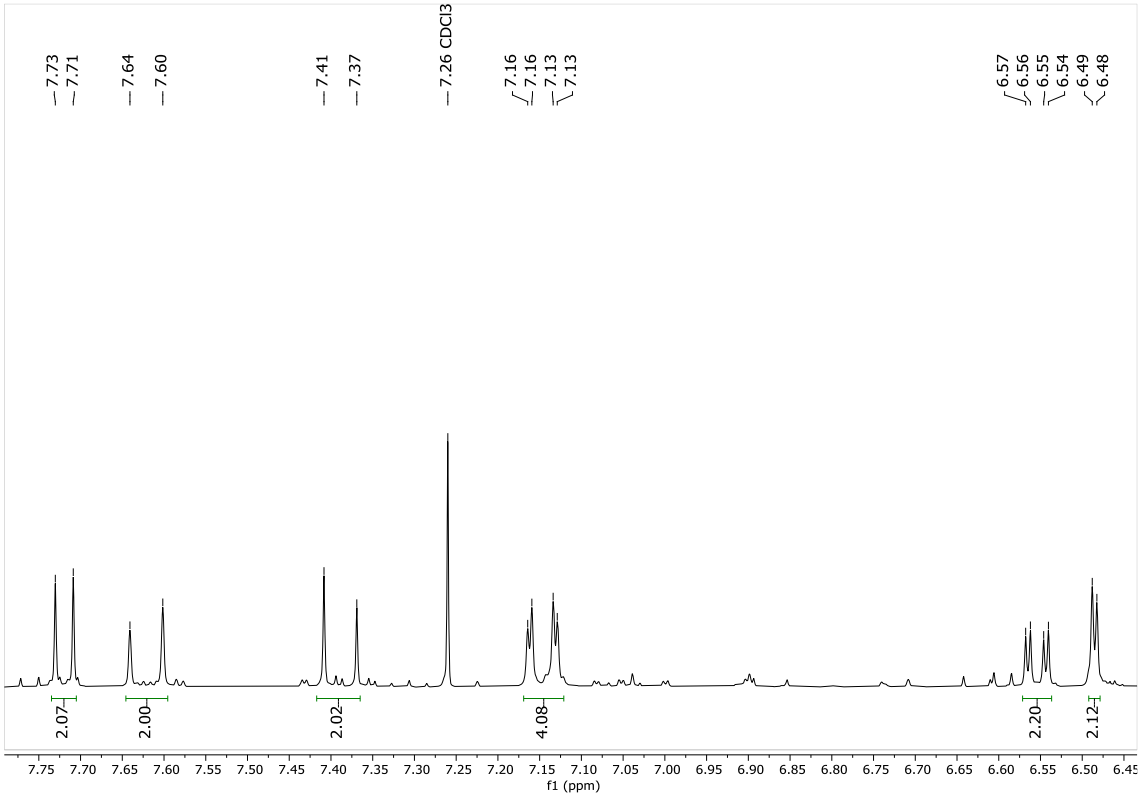

Figura 7: Espectro de RMN $^{13}C$ (100 MHz, $CDCl_3$) de FER26.

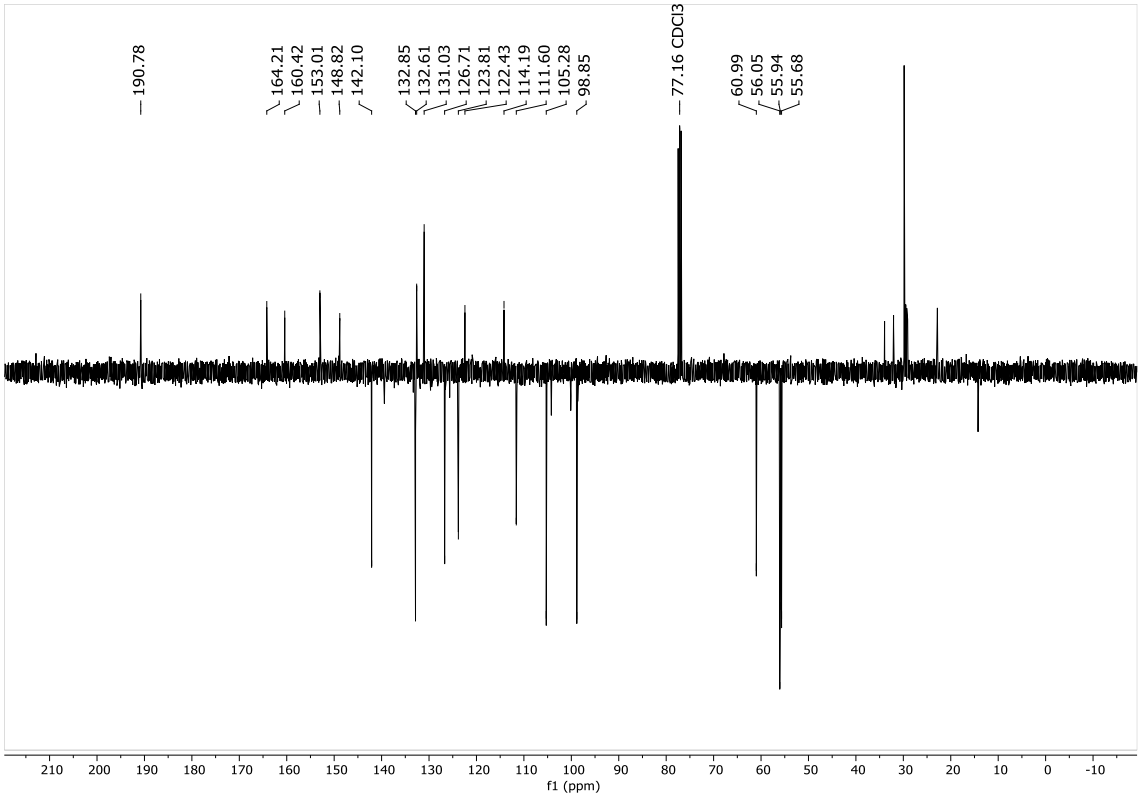


Figura 8: Expansão do espectro de RMN $^{13}C$ (100 MHz, $CDCl_3$) de FER26 na região 97 a 165 ppm.

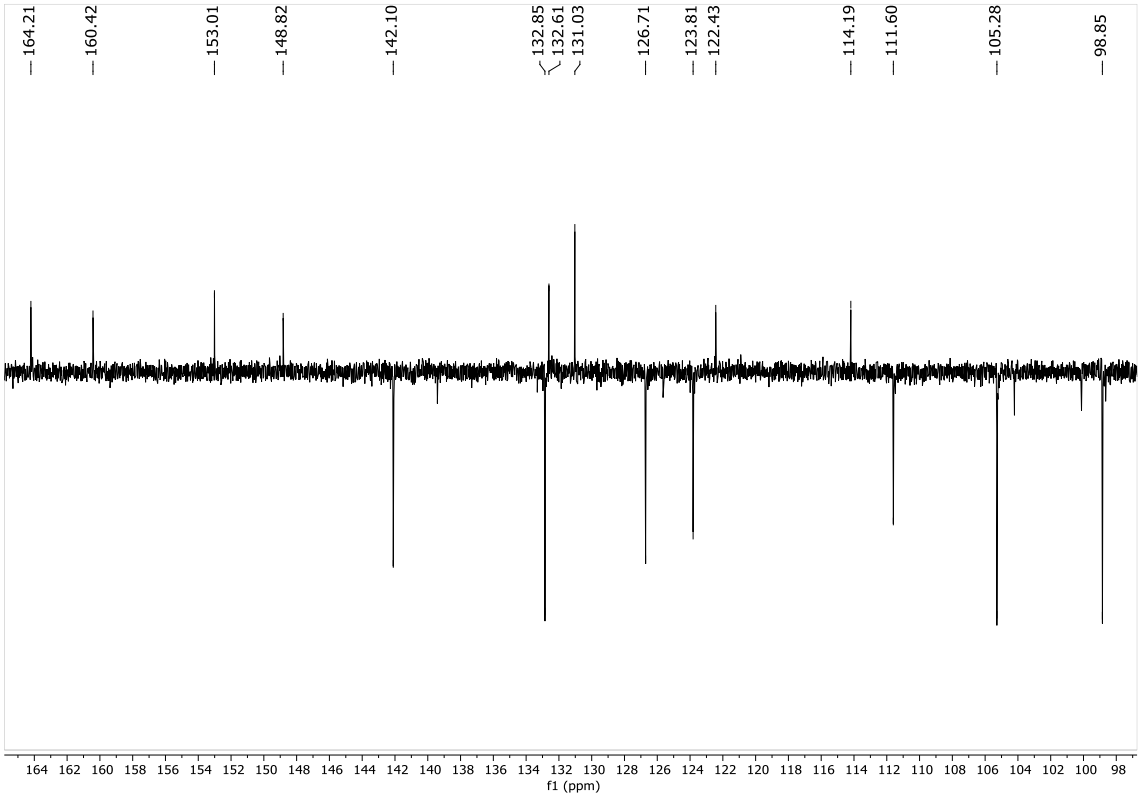

Figura 9: Espectro de massas [M+] do composto FER26.

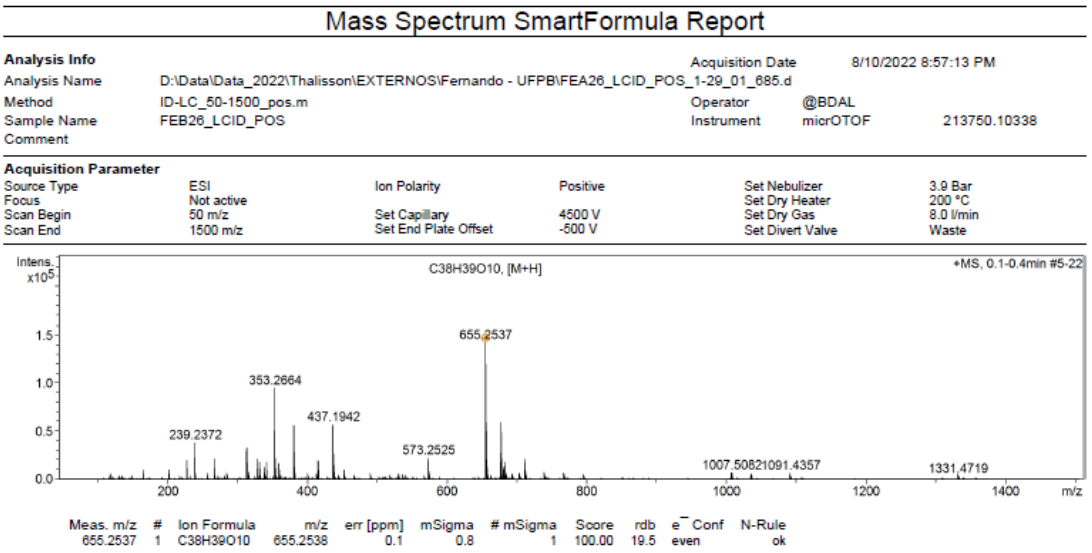


## 1.2. DETERMINAÇÃO ESTRUTURAL DA (2E,2'E)-3,3'-(5,5',6,6'-tetrametoxi-[1,1'-bifenil]-3,3'-diil)bis(1-(benzo[d][1,3]dioxol-5-il)prop-2-en-1-ona) (FER23(A))

Para obtenção do composto FER23(A) (Figura 10) foi feita uma condensação de Claisem entre a divanilina metilada e a 3,4-metilenodioxi acetofenona, gerando o segundo dímero. Após 48 horas a reação foi parada e purificada em CCDP com hexano e acetato de etila como eluentes, na proporção de 8:2. Na placa foi observado a formação de 2 produtos, sendo isolados e codificados de FER23(A) e FER23(B). Posteriormente foi feito o espectro de RMN $^{1}H$ e $^{13}C$ de ambos.

No espectro de FER23(A) observamos sinais compatíveis aos da chalcona, porém essa molécula, assim como no dímero anterior, apresenta um plano de simetria, absorvendo na mesma região. As integrais foram então duplicadas no espectro de $^{1}H$ (Figura 11). Os sinais presentes em $\delta_H$ 7.76 (d, *J* = 15.6 Hz, 2H) e $\delta_H$ 7.41 (d, *J* = 15.6 Hz, 2H) (Figura 12) confirmam a formação da chalcona pela condensação de Claisem. As metoxilas são confirmadas em $\delta_H$ 3.98 (s, 6H) e $\delta_H$ 3.73 (s, 3H) (Figura 11) no espectro de $^{1}H$ aliado aos sinais em $\delta_C$ 61.04 e $\delta_C$ 56.15 ppm no espectro de $^{13}C$. Os sinais em $\delta_C$ 6.05 (s, 2H) e $\delta_C$ 102.00 (Figura 13) confirmam a presença do metilenodioxi. A presença de 30 prótons reforça a formação do dímero, aliado a isso temos a comparação entre os espectros da chalcona FER23 e do dímero FER23(A), onde no dímero temos

a ausência de um dupleto em $\delta_H$ 7.15 (d, *J* = 2.1 Hz, 1H), isso se deve a presença do acoplamento bifenílico da divanilina. A presença de 7 sinais para carbonos não hidrogenados (Figura 13) confirma o acoplamento bifenílico, que é evidenciado quando comparamos com o espectro de $^{13}C$ de FER23 (Figura 23), onde notamos a presença de apenas 6 sinais para carbonos não hidrogenados, indicando a presença de 1 próton a mais.

Com base nos dados obtidos no espectro de $^{1}H$, $^{13}C$ em comparação aos espectros de $^{1}H$ e $^{13}C$ de FER23, concluímos que o composto FER13(A) trata-se do dímero de chalcona (2E,2'E)-3,3'-(5,5',6,6'-tetrametoxi-[1,1'-bifenil]-3,3'-diil)bis(1-(benzo[d][1,3]dioxol-5-il)prop-2-en-1-ona).

Figura 10: (2E,2'E)-3,3'-(5,5',6,6'-tetrametoxi-[1,1'-bifenil]-3,3'-diil)bis(1-(benzo[d][1,3]dioxol-5-il)prop-2-en-1-ona) (FER(A)).

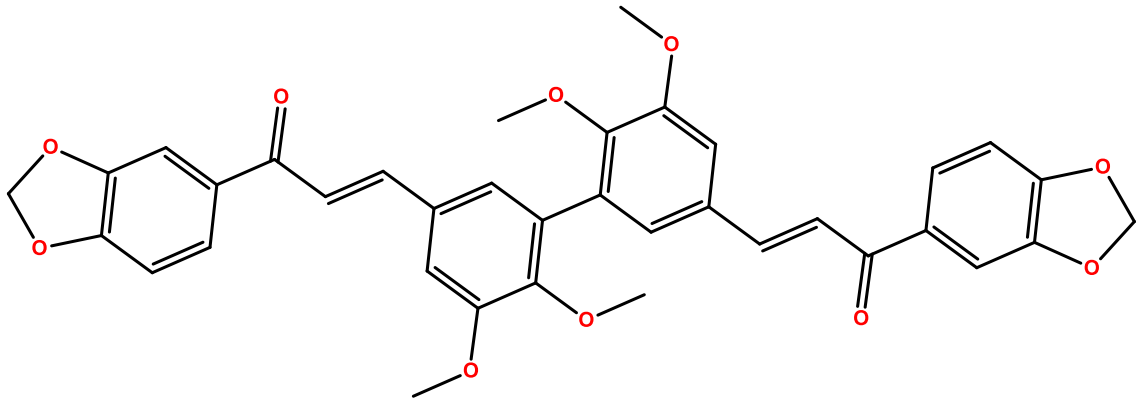

**Chemical Formula:** $C_{36}H_{30}O_{10}$
**Exact Mass: 622,18**

Figura 11: Espectro de RMN $^{1}H$ (400 MHz, $CDCl_3$) de FER23(A).

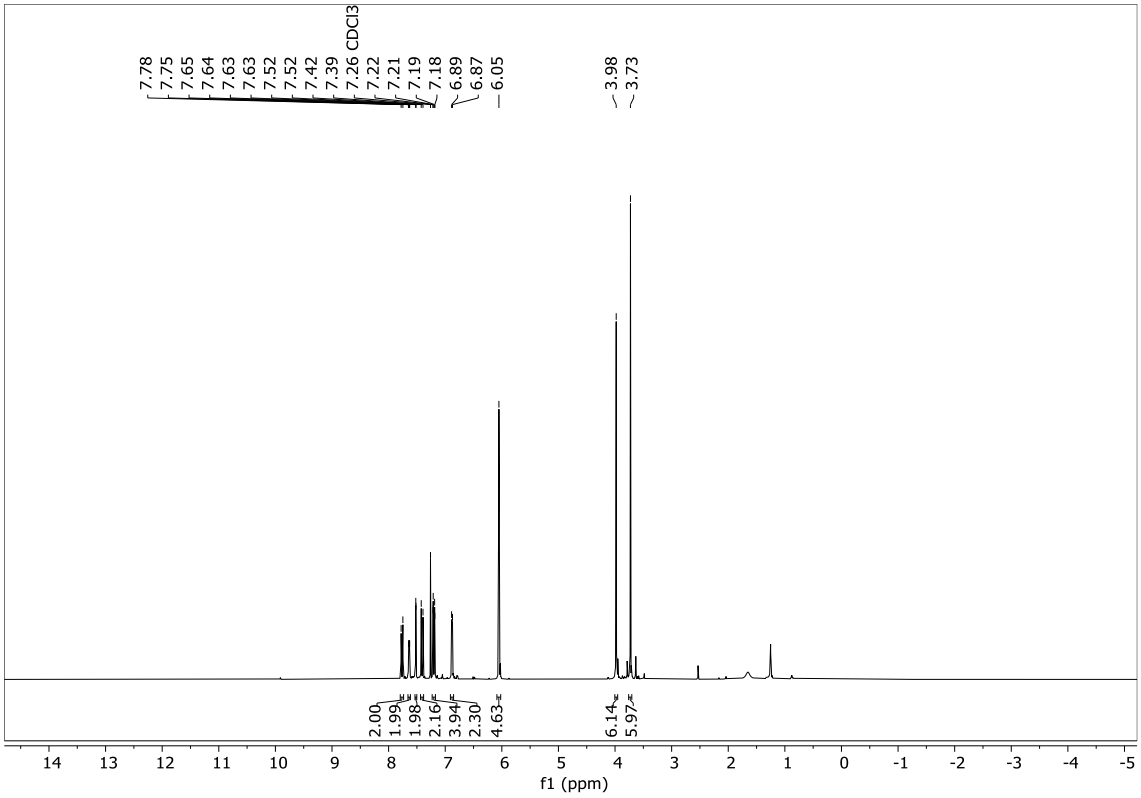


Figura 12: Expansão do espectro de RMN $^{1}H$ (400 MHz, $CDCl_3$) de FER23(A) na região 6.70 a 7.95 ppm.

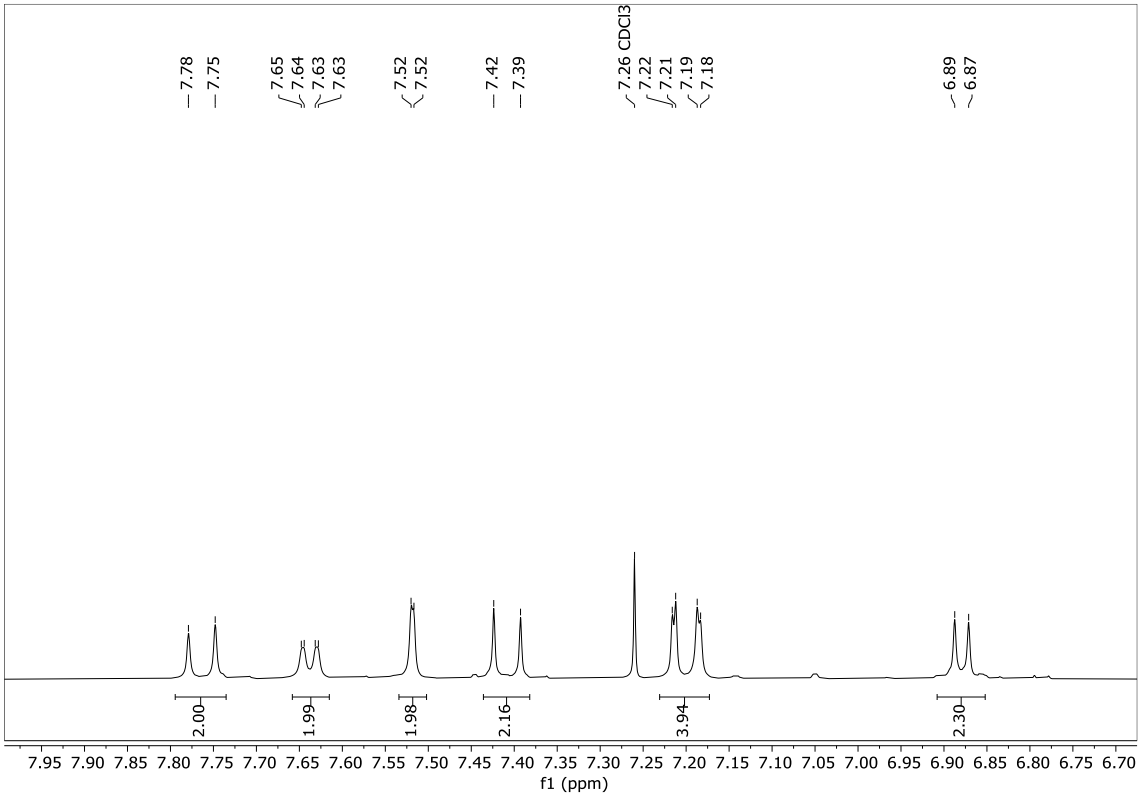

Figura 13: Espectro de RMN $^{13}C$ (100 MHz, $CDCl_3$) de FER23(A).

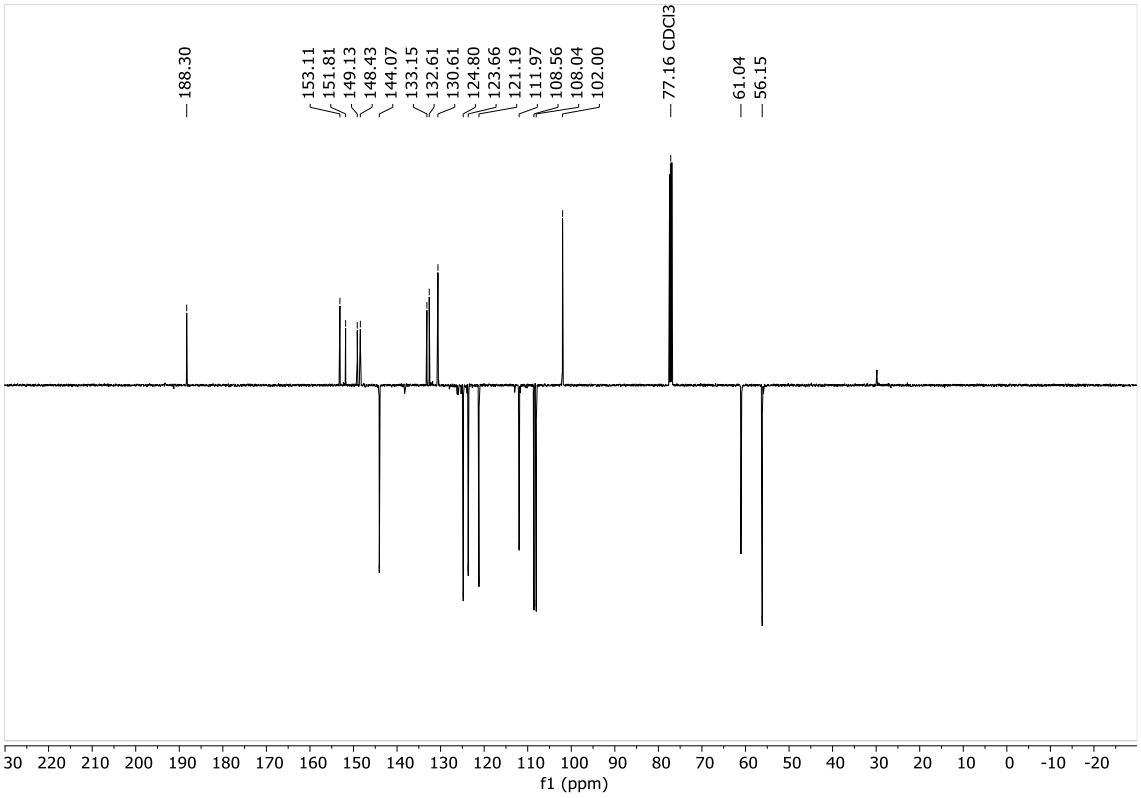


Figura 14: Expansão do espectro de RMN $^{13}C$ (100 MHz, $CDCl_3$) de FER26 na região 100 a 155 ppm.

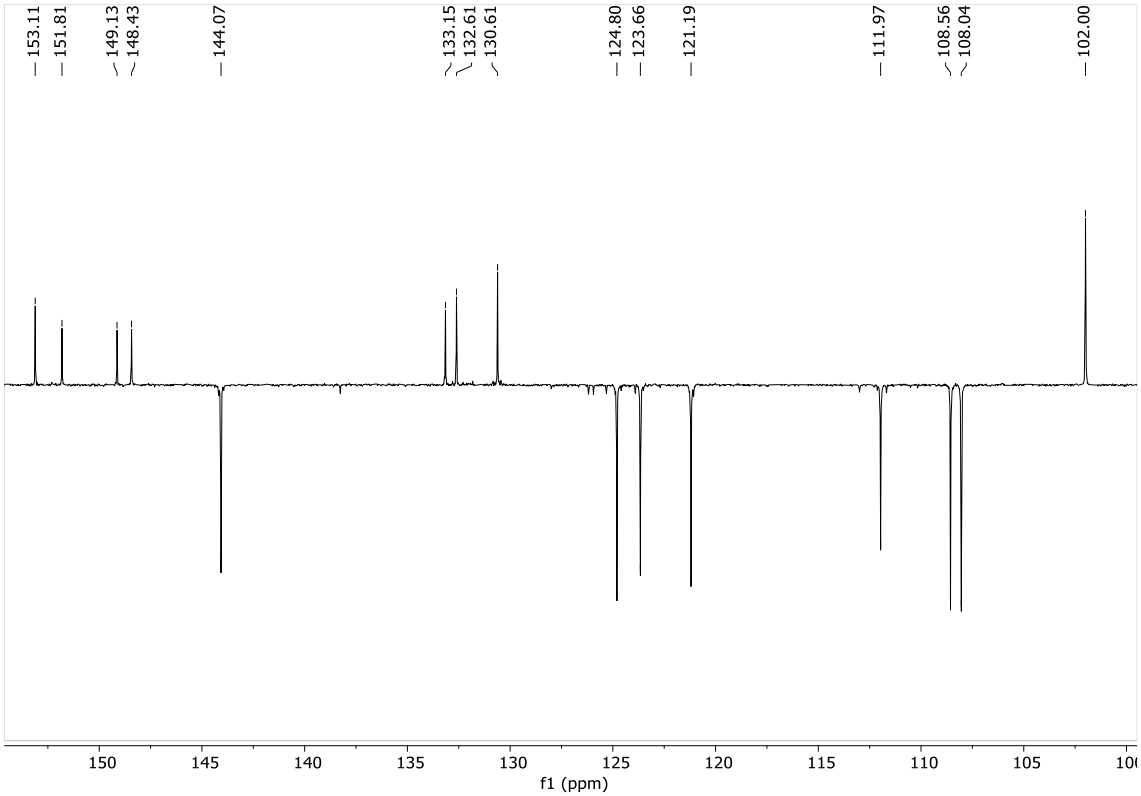

## 1.3. DETERMINAÇÃO ESTRUTURAL DA (E)-5'-(3-(BENZO[D][1,3]DIOXOL-5-IL)-3-OXOPROP-1-EN-1-IL)-2',3',5,6-TETRAMETOXI-[1,1'-BIFENIL]-3-CARBALDEIDO (FER23(B))

O composto FER23(B) (Figura 21) foi obtido como produto secundário da condensação de Claisem-Schimidt entre a divanilina metilada e a 3,4-metilenodioxi acetofenona. O composto FER23(B) foi obtido na forma incompleta do dímero, em que houve a condensação de Claisem em apenas uma porção do aldeído.

Figura 15: Espectro de RMN $^{1}H$ (400 MHz, $CDCl_3$) de FER23(B).

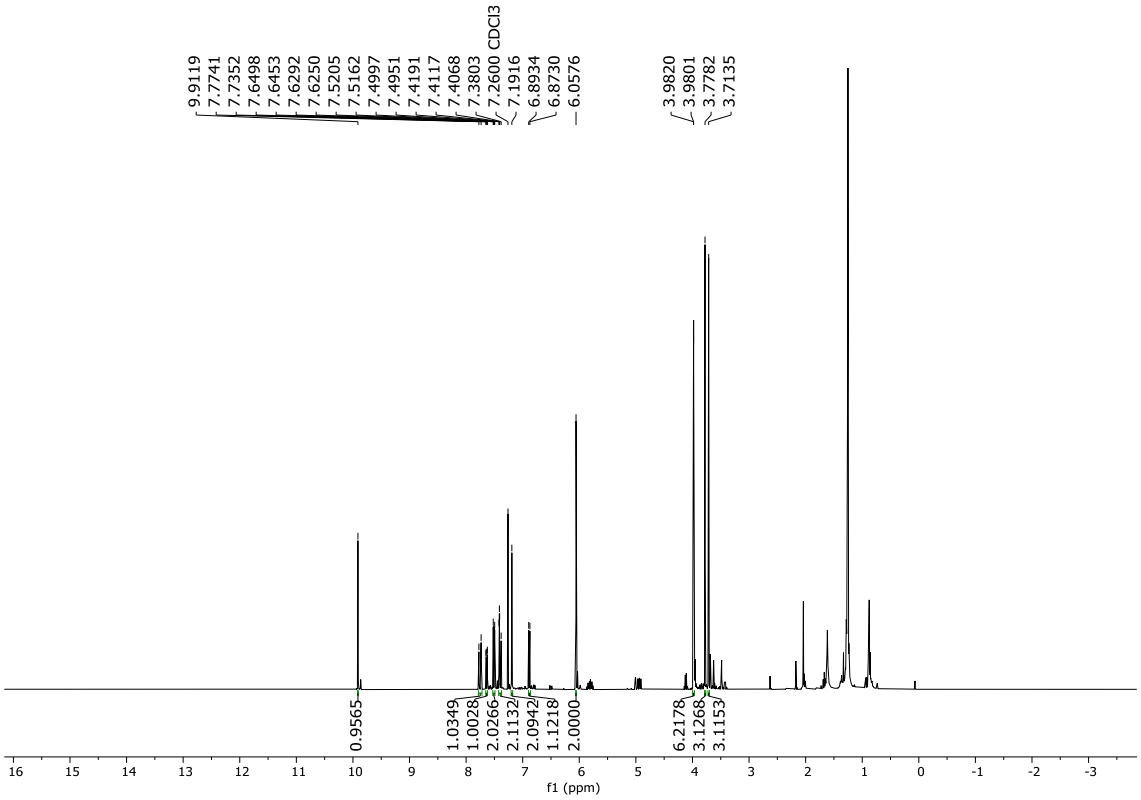

Figura 16: Expansão do espectro de RMN $^{1}H$ (400 MHz, $CDCl_3$) de FER23(B) na região 3.70 a 4.00 ppm.

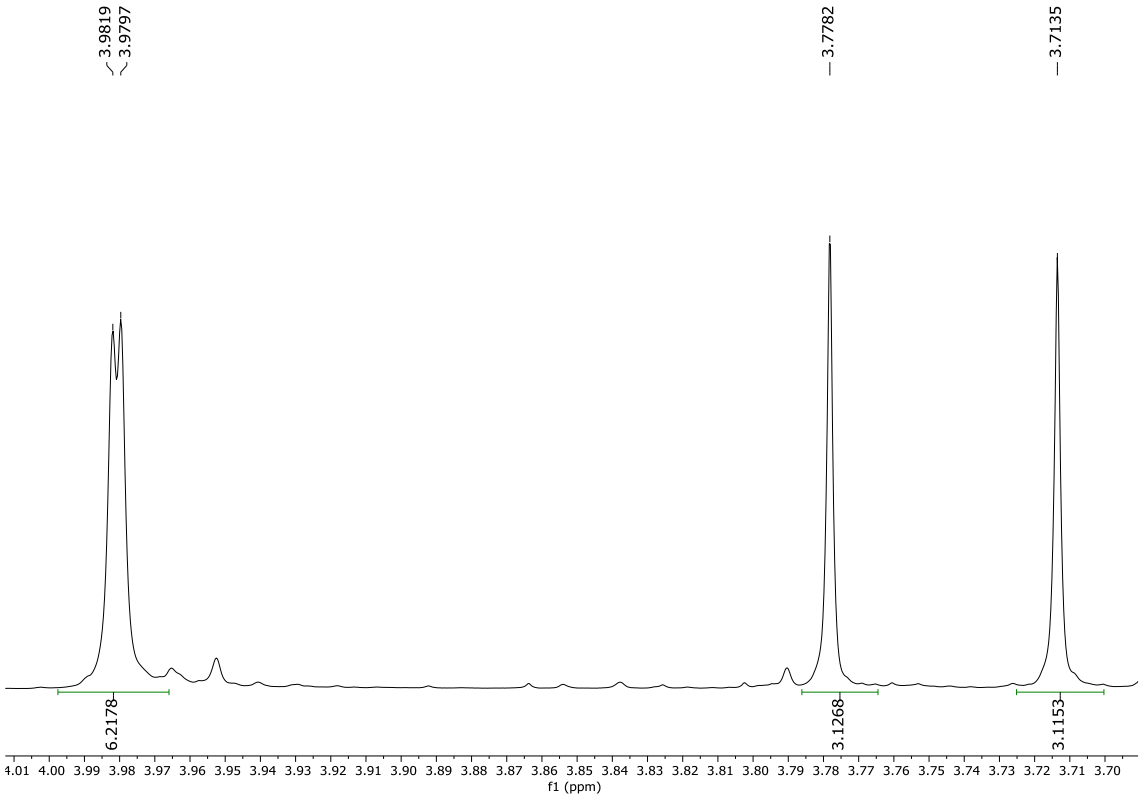


Figura 17: Expansão do espectro de RMN $^{1}H$ (400 MHz, $CDCl_3$) de FER23(B) na região 6.85 a 7.75 ppm.

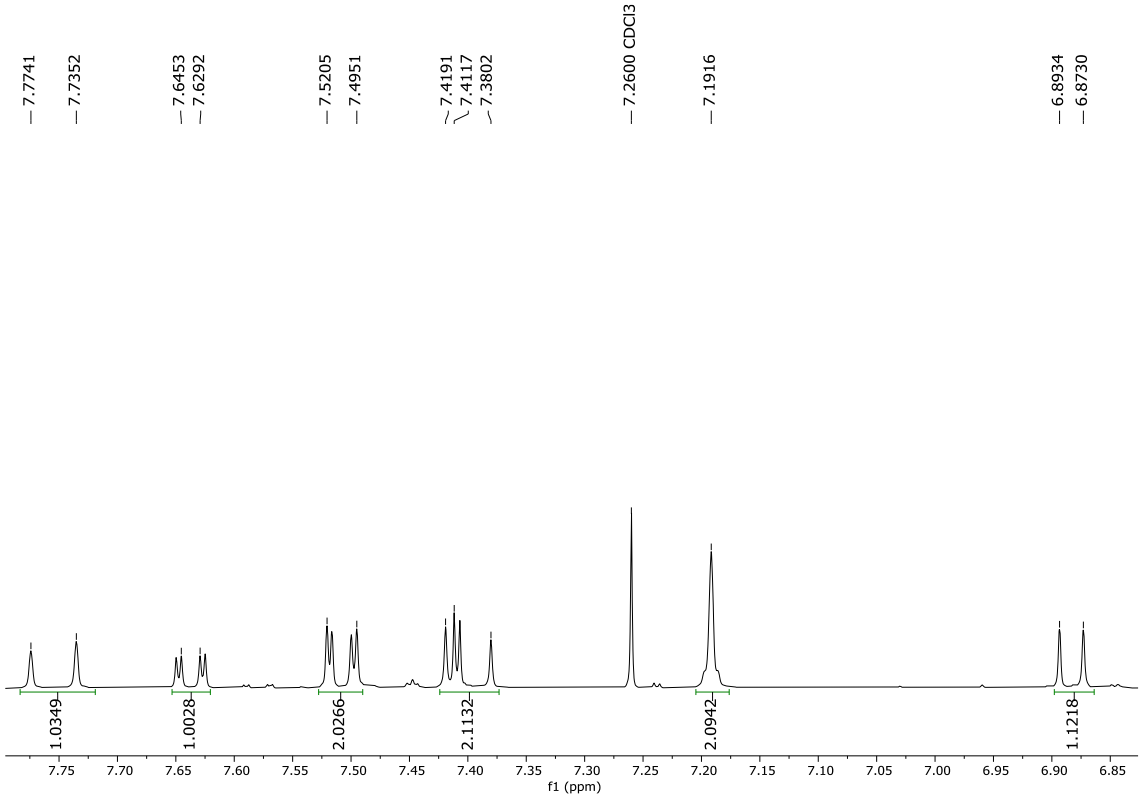

Figura 18: Espectro de RMN $^{13}C$ (100 MHz, $CDCl_3$) de FER23(B).

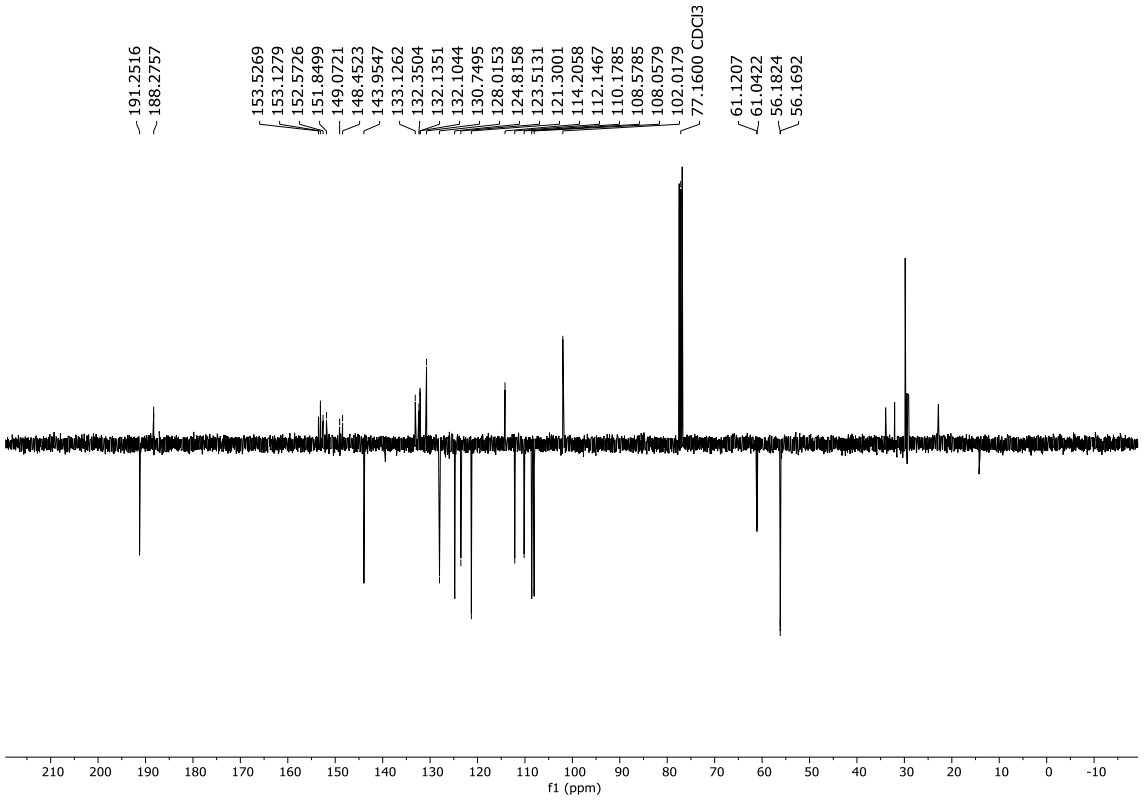


Figura 19: Expansão do espectro de RMN $^{13}C$ (100 MHz, $CDCl_3$) de FER23(B) na região 100 a 155 ppm.

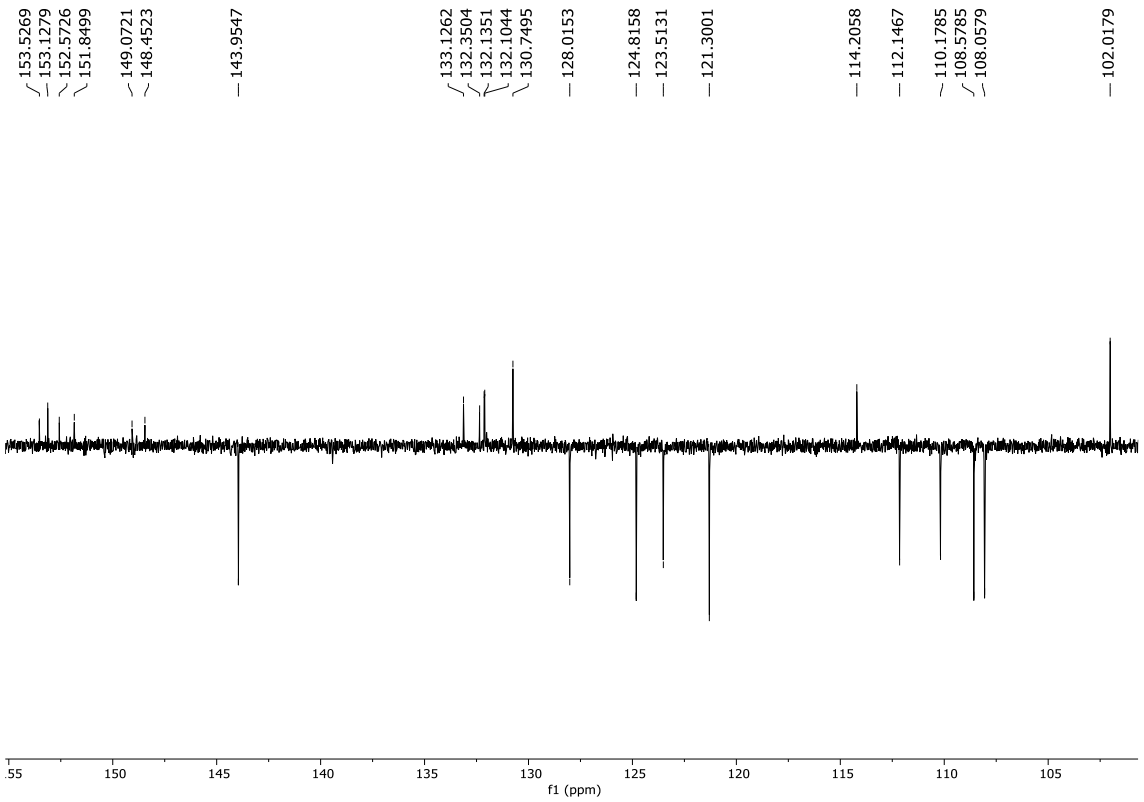

Figura 20: Espectro de massas [M+] de FER23(B).

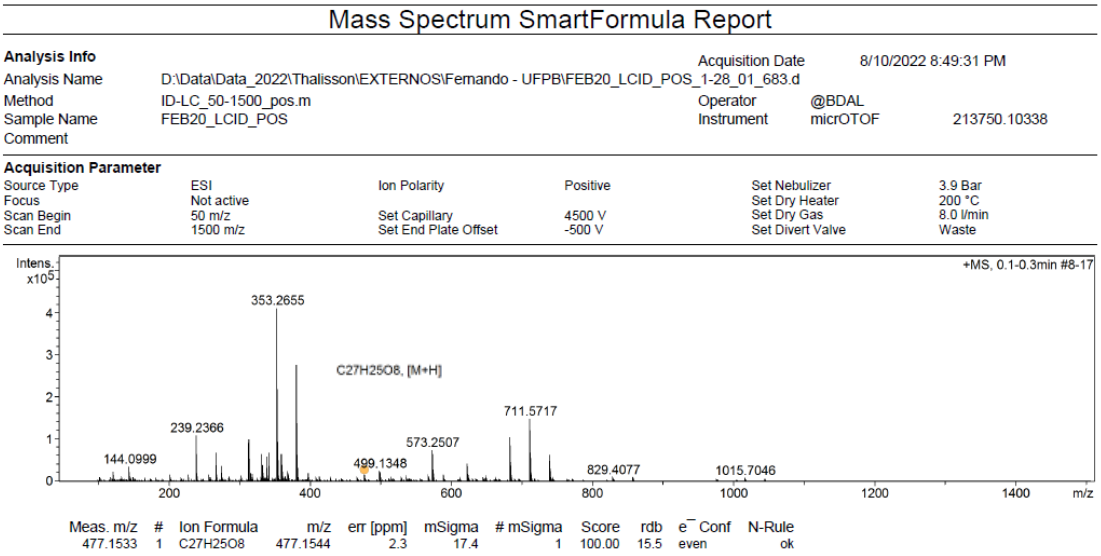


No espectro de $^{1}H$ (400 MHz, $CDCl_3$) (Figura 15) observamos a presença do sistema olefínico em $\delta_H$ 7.75 (d, *J* = 15.6 Hz, 1H) e $\delta_H$ 7.40 (d, *J* = 15.6 Hz, 1H) (Figura 16) acoplando entre si, aliado a isso ainda observamos uma carbonila de cetona deslocada em $\delta_C$ 188.28 ppm no espectro de $^{13}C$ (100 MHz, $CDCl_3$) (Figura 17), indicando a formação da chalcona pela condensação de Claisem. As metoxilas presentes no espectro de $^{1}H$ nas regiões de $\delta_H$ 3.98 (s, 3H), $\delta_H$ 3.98 (s, 3H), $\delta_H$ 3.78 (s, 3H) e $\delta_H$ 3.71 (s, 3H) (Figura 16) em conjunto com as absorções no espectro de $^{13}C$ em $\delta_C$ 61.12, $\delta_C$ 61.04, $\delta_C$ 56.18 e $\delta_C$ 56.17 ppm (Figura 18), corroboram com as alquilações realizadas na divanilina. A presença das carbonilas de cetona em $\delta_C$ 188.27 e de aldeído em $\delta_C$ 191.25 ppm (Figura 18) corroboram com o acoplamento em apenas um lado da divanilina.

Por fim, a presença de 9 sinais compatíveis com carbonos metínicos e 11 sinais para carbonos não hidrogenados, aliado aos dados obtidos no espectro de massas (Figura 20) com a uma massa total de 477.1532 e fórmula molecular de $C_{27}H_{25}O_8$, confirmam que o composto FER23(B) se trata do (E)-5'-(3-(benzo[d][1,3]dioxol-5-il)-3-oxoprop-1-en-1-il)-2',3',5,6-tetrametoxi-[1,1'-bifenil]-3-carbaldeido, havendo a formação da chalcona em apenas uma porção aldeído da divanilina.

Figura 21: (E)-5'-(3-(benzo[d][1,3]dioxol-5-yl)-3-oxoprop-1-en-1-il)-2',3',5,6-tetrametoxi-[1,1'-bifenil]-3-carbaldeido (FER23(B)).

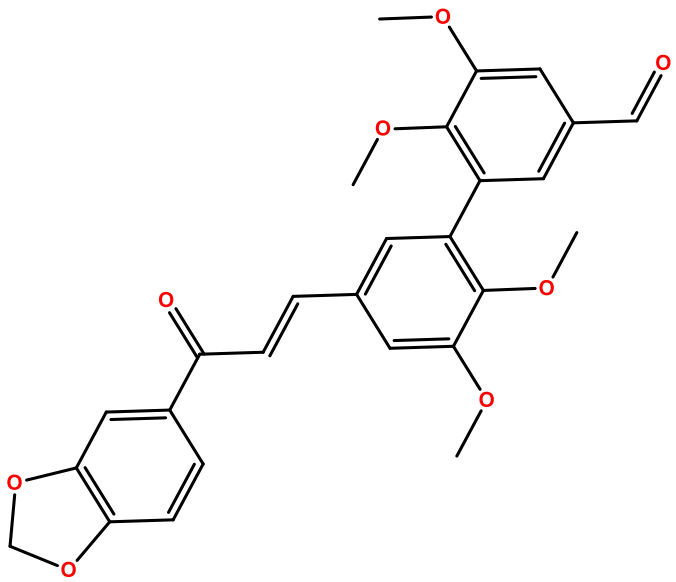

**Chemical Formula:** $C_{27}H_{24}O_8$
**Exact Mass: 476,15**

## 1.4. ELUCIDAÇÃO ESTRUTURAL DAS CHALCONAS

Um total de 15 chalconas foram obtidas via condensação de Claisem (Figura 2). As chalconas são uma classe de metabólitos conhecidas no reino vegetal e com um grande volume de estudos anteriores, com isso guiamos a elucidação estrutural com base em seus sinais norteadores, sendo sua principal característica a presença de um sistema olefínico com carbonila α,β-insaturada, gerando dois dupletos na região aproximada de $\delta_H$ 7,6 e $\delta_H$ 7,3 ppm (Figura 24) acoplando entre si com uma constante de aproximadamente 15 Hz e ambos integrando para 1 H cada, além da absorção de carbonila de cetona deslocada em torno 188 ppm (Figura 25) no espectro de $^{13}C$. Uma riqueza de sinais aromáticos na região entre $\delta_H$ 6.7~7.9 ppm (Figura 23) também é observada nessa classe de compostos. Aliado aos sinais norteadores da classe, foi verificado ainda a preservação de grupos funcionais presentes nos reagentes, e grupos protetores adicionados em etapas anteriores a condensação. Em conjunto com os dados de RMN foram obtidos dados de espectroscopia de massas (**ver seção "Material Suplementar" Pág. 158**), confirmando as estruturas pela presença da massa total e da fórmula molecular.

Figura 22: (E)-1-(benzo[d][1,3]dioxol-5-yl)-3-(3,4-dimetoxifenil)prop-2-en-1-ona (FER23).

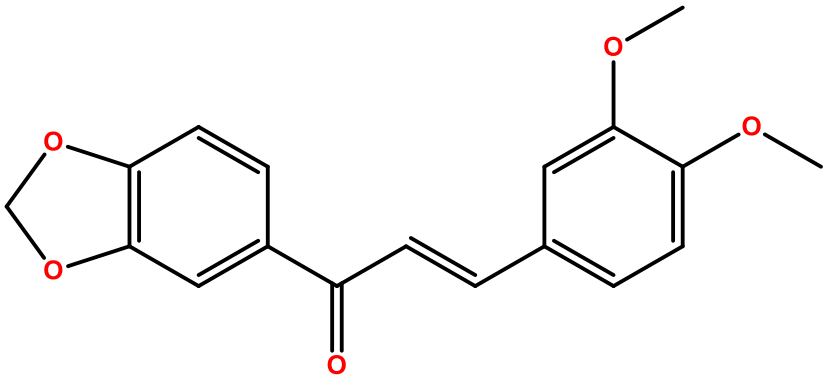


Figura 23: Espectro de RMN $^{1}H$ (400 MHz, $CDCl_3$) de FER23.

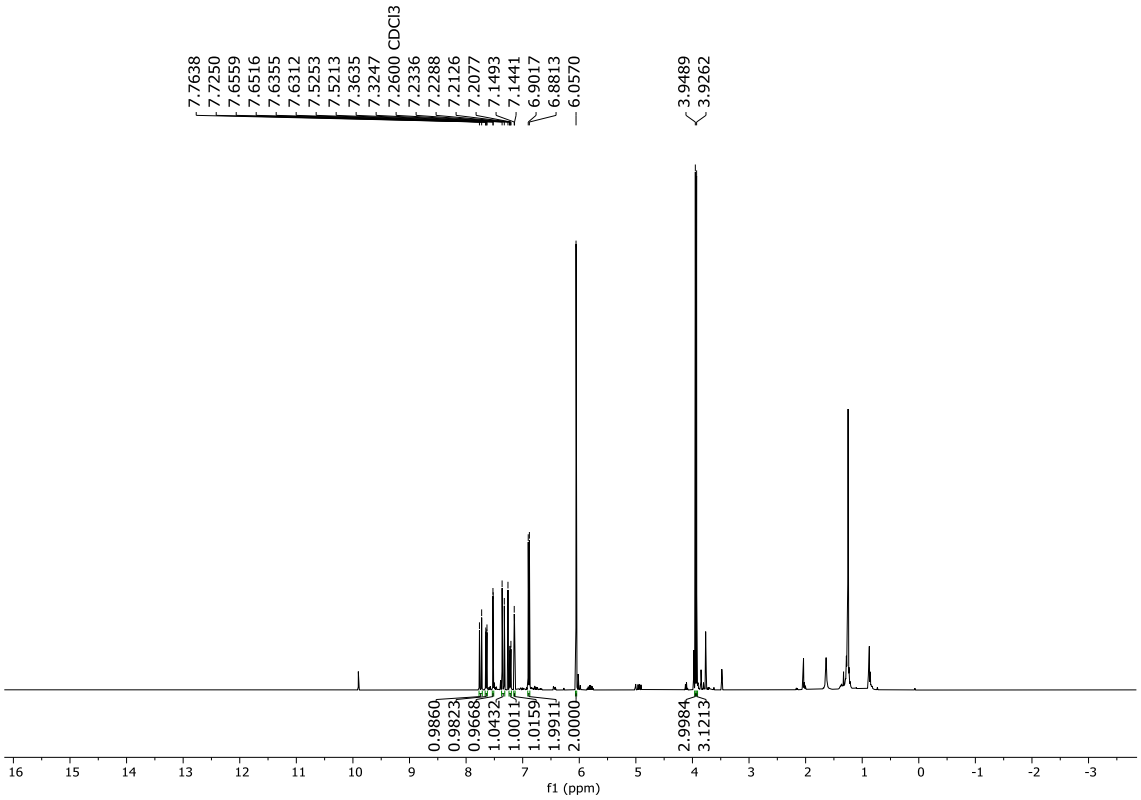

Figura 24: Expansão do espectro de RMN $^{1}H$ (400 MHz, $CDCl_3$) de FER23 na região 6.80 a 7.95 ppm.

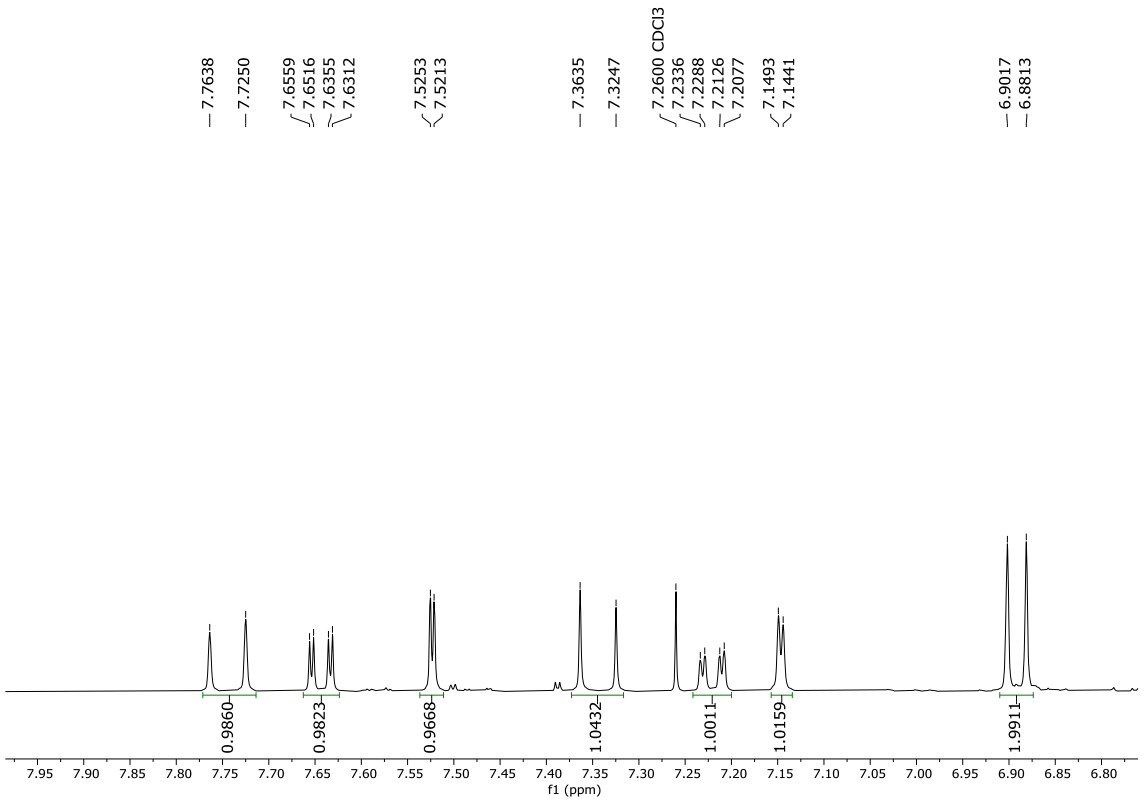


Figura 25: Espectro de RMN $^{13}C$ (100 MHz, $CDCl_3$) de FER23.

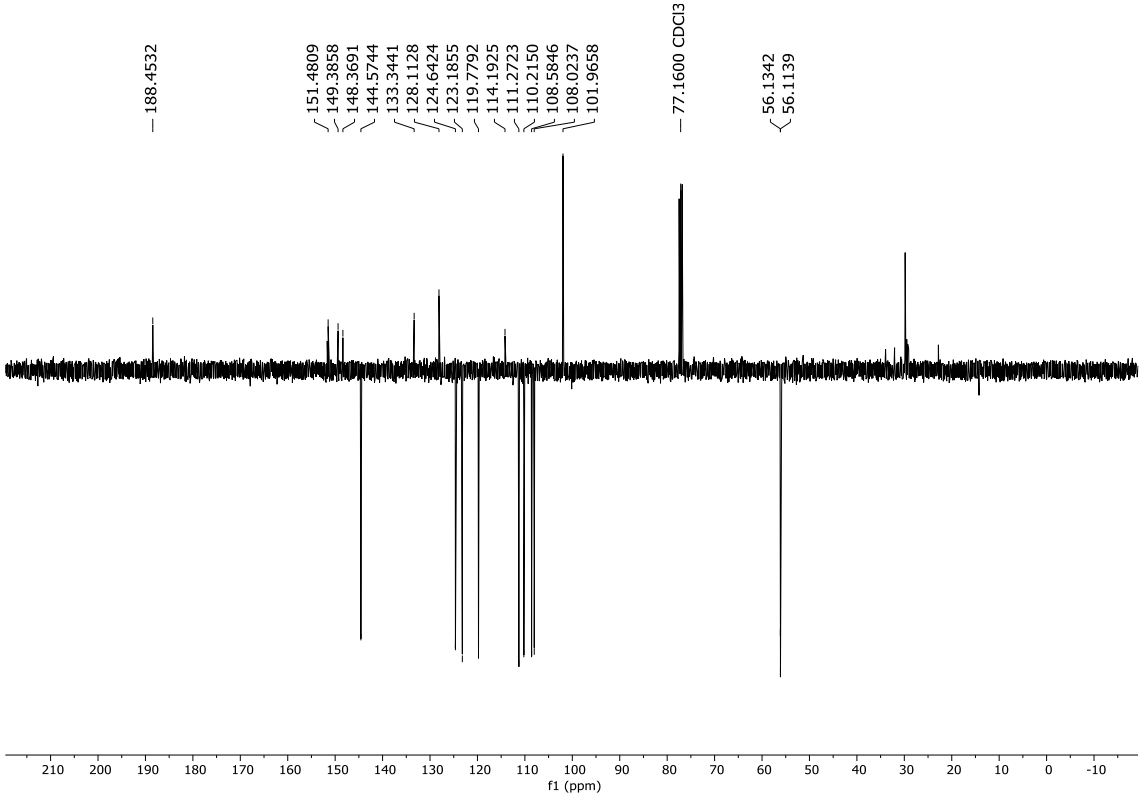

# CAPÍTULO 2

## Anticancer Activity of Chalcones and Its Derivatives: Review and *In Silico* Studies

As chalconas são uma classe de metabólitos amplamente conhecida na literatura, são precursoras direto dos flavonoides onde a etapa de ciclação do anel C não é concretizada. Esses compostos possuem um sistema olefínico constituído de uma cetona conjugada na posição α,β, sendo essa sua principal característica. As chalconas apresentam diversas atividades farmacológicas, já relatadas, dentre elas propriedades anticancerígenas.

Nessa perspectiva buscamos explorar o papel das chalconas naturais e sintéticas e sua atividade anticâncer *in vitro* relatadas nos últimos quatro anos compreendendo de 2019 a 2023. Além disso, realizamos uma análise de mínimos quadrados parciais (PLS) dos dados biológicos relatados para linhagem de adenocarcinoma de cólon HCT-116.

As informações foram obtidas na base de dados Web of Science. Nossa análise *in silico* identificou que a presença de radicais polares como hidroxila e metoxila contribuíram para a atividade anticancerígena dos derivados de chalconas. Esperamos que os dados apresentados neste trabalho ajudem os pesquisadores a desenvolver medicamentos eficazes para inibir o adenocarcinoma de cólon em trabalhos futuros.

Esse trabalho foi publicado na revista “molecules” no ano de 2023, disponível em: **https://doi.org/10.3390/molecules28104009**.

Qualis Capes: A2

Fatos de Impacto: 4.2

Cite Score: 7.4

Ano vigente 2023

# Anticancer Activity of Chalcones and Its Derivatives: Review and *In Silico* Studies

**Fernando Ferreira Leite [1,†], Natália Ferreira de Sousa [1,†], Bruno Hanrry Melo de Oliveira [1], Gabrielly Diniz Duarte [2], Maria Denise Leite Ferreira [1], Marcus Tullius Scotti [1], José Maria Barbosa Filho [1], Luís Cezar Rodrigues [2], Ricardo Olímpio de Moura [3], Francisco Jaime Bezerra Mendonça-Junior [4,*] and Luciana Scotti [1]**

[1] Post-Graduate Program in Natural and Synthetic Bioactive Products, Federal University of Paraíba, João Pessoa 58051-900, Brazil; fernandoferreira_15@hotmail.com (F.F.L.); nataliafsousa@ltf.ufpb.br (N.F.d.S.); hanrygb@hotmail.com (B.H.M.d.O.); denisecaiana@yahoo.com.br (M.D.L.F.); mtscotti@ccae.ufpb.br (M.T.S.); barbosa.ufpb@gmail.com (J.M.B.F.); luciana.scotti@gmail.com (L.S.)

[2] Post-Graduate Program in Development and Innovation of Drugs and Medicines, Federal University of Paraíba, João Pessoa 58051-900, Brazil; gabriellydduarte@hotmail.com (G.D.D.); luiscezarodrigues@acedmico.ufpb.br (L.C.R.)

[3] Post-Graduate Program in Pharmaceuticals Sciences Paraiba State University, Campina Grande 58429-500, Brazil; ricardo.olimpiodemoura@servidor.uepb.edu.br

[4] Laboratory of Synthesis and Drug Delivery, Department of Biological Science, Paraiba State University, João Pessoa 58071-160, Brazil

* Correspondence: franciscojaime@servidor.uepb.edu.br

† These authors contributed equally to this work.

**Abstract:** Chalcones are direct precursors in the biosynthesis of flavonoids. They have an α,β- unsaturated carbonyl system which gives them broad biological properties. Among the biological properties exerted by chalcones, their ability to suppress tumors stands out, in addition to their low toxicity. In this perspective, the present work explores the role of natural and synthetic chalcones and their anticancer activity *in vitro* reported in the last four years from 2019 to 2023. Moreover, we carried out a partial least square (PLS) analysis of the biologic data reported for colon adenocarcinoma lineage HCT-116. Information was obtained from the Web of Science database. Our *in silico* analysis identified that the presence of polar radicals such as hydroxyl and methoxyl contributed to the anticancer activity of chalcones derivatives. We hope that the data presented in this work will help researchers to develop effective drugs to inhibit colon adenocarcinoma in future works.

**Keywords:** chalcones; anticancer activity; *in vitro*; drug discovery; natural products; synthesis

## 1. Introduction

Chalcones are direct precursors in the biosynthesis of flavonoids. They have an α,β- unsaturated carbonyl system (Figure 1), which gives them broad biological properties [1].

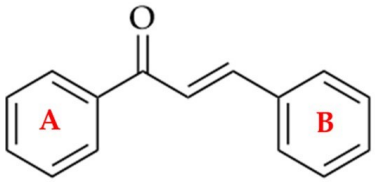


**Figure 1.** Chemical structure of a chalcone.

Their privileged structure also opens up possibilities for substitutions in aromatic rings [2], directly impacting its biological activity and development of

formulations capable of improving its pharmacokinetic characteristics [3]. Due to their high biological value, the literature also reports on the anti-inflammatory [4], antiviral [5], antimicrobial [6], anticancer [7], antioxidant [8], and antifungal [9] properties of these compounds.

Cancer is generally characterized by the uncontrolled growth of cells, resulting from a regulatory dysfunction, which can be caused by several factors, both hereditary and environmental [10]. In addition to presenting a difficult prognosis, it still has a very aggressive treatment and a high mortality rate, caused both by the disease and by the impacts of its treatment [11]. Natural products such as chalcones of the type (1,3-diaryl-2- propen-1-ones) have been the focus of research for the treatment of this disease, as they have a conjugated carbonyl system that acts by inhibiting the polymerization of tubulin in tumor cells, interrupting its disordered reproduction cycle [12].

Colorectal cancer can be cited as an example, since the fatality rate is reduced by the removal of intestinal polyps through surgical procedures; however, in more advanced stages the surgery becomes ineffective, requiring the use of alternative therapies such as chemotherapy. Thus, a molecular target therapy becomes efficient because it has selectivity in abnormal cells [13].

According to the WHO (World Health Organization), in 2018 alone, cancer was respon- sible for more than 9.6 million deaths globally. Leukemia accounts for one in three cases of cancer, and is the most common type in children and adolescents (WHO, 2018) [14,15]. In women, breast cancer is the most common type found, corresponding to 25% of re- ported cases. The chemotherapy choice for this type of tumor aims to reach specific targets, usually using monoclonal antibodies such as trastuzumab [16]. New candidates derived

from chalcones such as benzocoumarin-chalcones (Figure 2) have shown promise against breast tumors, as they are capable of inhibiting ERα and ERβ receptors, preventing the proliferation of abnormal cells [17].

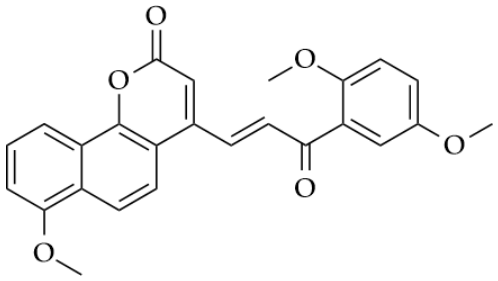


**Figure 2.** Chemical structure of benzocoumarin-chalcones.

Among these activities, studies of anticancer activity involving chalcones have been widely explored in recent years due to the difficulty in treating multidrug-resistant tumors with traditional medicines [18] in addition to the high toxic loads due to the association of drugs to combat the disease.

Chalcones with anticancer activity already known in the literature, such as MIPP and MOMIPP (Figure 3), act in the induction of methuosis *in vitro*, a type of non-apoptotic programmed cell death, while other chalcones act in different ways in the dysfunction of cell metabolism, causing death cell by

apoptosis [12].

Given the importance of researching alternative treatments for different types of cancer, the present work focused on the report of natural and synthetic products based on the chalcone scaffold as potential candidates for the treatment of the most diverse types of cancer. The review was combined with a partial least square (PLS) analysis of the biologic data obtained from previous authors and the chemical structures with reported inhibitory activity of the HCT-116 lineage of colon adenocarcinoma, in order to identify descriptors that favor the anticancer activity of the compounds.

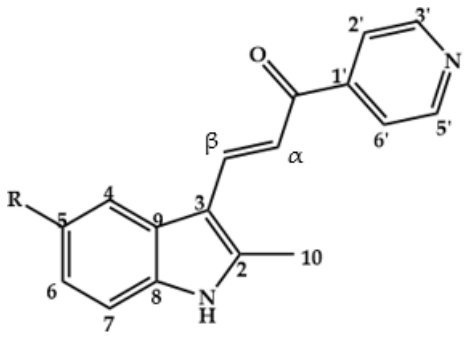


**Figure 3.** Chemical structure of chalcones, MIPP and MOMIPP.

## 2. Review Approaches

The present review was written with the aim of presenting the anticancer activities of chalcones' synthetic derivatives, aiming to demonstrate the physicochemical characteristics of these compounds that can contribute to their activity; however, it must be noted that this theme presents literature review papers that were previously published and which present different approaches and objectives that should be mentioned. The following types of approach were observed:

(1) The first type refers to the description of the complete action mechanism of chal- cones with emphasis on the biological targets and signaling pathways involved. Ouyang et al. (2021) [19] carried out a summary of recent advances in compounds belonging to the class of chalcones as potential anticancer agents and reported on the action mechanisms of these compounds. Furthermore, the authors presented future applications and scope of the chalcone family for cancer treatment and prevention. It is important to mention that in this work the authors emphasized the need for a complete description of the toxicity of chalcones. Also, it was possible to observe that the authors mentioned chalcones of natural origin, but emphasized the importance of the anticancer activity of chalcone hybrid compounds, mentioning the biological activity of artemisinin-chalcone hybrids, chalcone-azole hybrids, chalcone-coumarin hybrids, and chalcone-indole hybrids. In addition, the biological activity was ad- dressed by describing the mechanism of action emphasizing the pathways responsible for anti-inflammatory activity,

inhibition of MDR (multidrug resistance) channels, and anti-angiogenic, apoptotic, and tubulin polymerization. The authors emphasized the excellent activity of synthetic derivatives such as sofalcone (antiulcer agent) and methoxychalcone (choleretic drug), which both represent a promising strategy for developing chalcones as new anticancer agents. Another point mentioned referred to the lack of studies on chalcones in natural marine products. Thus, the authors concluded that chalcones are easy to synthesize, as well as easy to chemically modify, being able to generate compounds with a wide variety and structural diversity.

The second approach observed mainly emphasized synthetic compounds with the analysis of the chemical group related to activity, characterizing an approach of structure and activity approach. Among these articles, the main objective of the work developed by Shukla et al. (2021) [20] was to analyze the antitumor activity of chalcones 1,3-diaryl-2-propen-1-one through different mechanisms. The chemical groups related to activity and mentioned as being of greater importance referred to chalcone analogues with electron donating groups, indolyl, quinolone, pyrazolol, hydroxyaminobenzamide, hydroxamic acid, and pyridyl-indole groups. Among the activities evaluated were mechanisms related to apoptosis (emphasizing the importance of mitochondrial pathways), microtubule binding and cell cycle regulation, and inhibition of drug-metabolizing enzymes and new signaling pathways such as Notch (cell-surface Notch receiver). Thus, the authors concluded that the presence of electron donating groups such as $OCH_3$, OH, halogens in the ring A or B of chalcones, induce apoptosis through the intrinsic or extrinsic pathway as they stabilize the enzyme-inhibitor complex through electrostatic interactions. Several chalcones with indolyl, quinolone, and pyrazole act as potential anti-thymicrotubule agents and interrupt the cell cycle, mainly in the G2/M phase. Apoptosis by enzyme inhibition is achieved by hydroxyaminobenzamide, hydroxamic acid groups, and pyridylindole.

(2) The third approach found refers to synthetic chalcones and the reactions involved in their production. An article developed by Mastachi-Loza et al. (2021) [21] also emphasizes synthetic chalcones, but the authors mention cycloaddition mechanisms [4+2], which correspond to cycloadditions between a diene and a dienophile. The authors concluded that chalcones have not only been used as precursors of natural and synthetic molecules, but also in the development of new protocols and catalysts for asymmetric Diels–Alder nullification, reflecting their versatility. Furthermore, it is also possible that chalcones behave like dienes in Diels–Alder cycloadditions with inverse electron demand kinetics, as well as formal [4+2] cycloadditions, which are Diels–Alder cancellations. Therefore, due to their dual role in Diels–Alder cycloaddi- tions, chalcones have wide possibilities in organic synthesis. Rani et al. (2019) [22] also addressed synthetic and conjugated chalcones, but presented the addition of a relationship and activity study as a differential, with an emphasis on their mechanism of action and anchorage studies along with their future therapeutic applications.

(3) The fourth approach deals with the elucidation of the mechanism and performance of in vivo studies. This form of work was observed in the review

conducted by Souza et al. (2021) [23], in which the authors aimed to describe the anticancer poten- tial of chalcones related to some of the characteristics of cancer with emphasis on sustaining proliferative signaling, tumor-promoting inflammation, activation of invasion and metastasis, induction of angiogenesis and resistance to cell death; however, in this work no emphasis was shown on the chemical structure–the discussion was made in relation to the mechanism under study, and the chalcones which stood out were natural chalcones such as flavokawain B. Thus, the authors concluded that the chalcones and their derivatives had an anticancer effect by acting on the tumor microenvironment.

The following sections demonstrate articles that address the anticancer activity of chalcones.

## 3. Chalcones with Anticancer Activity

Chalcones of natural origin present a pattern of phenolic hydroxyls that originate from the biosynthetic reactions of flavonoids. As chalcones are metabolites derived from the mixed pathway, all natural chalcones have phenolic hydroxyls at positions 5 and 7 [24]. According to Leonte (2021) [25], this class of chalcones is very important, as they are crucial precursors in the biosynthesis of several metabolites with potential antitumor activity, such as flavones, flavanones, aurones, pyrazolines, pyrazoles, and epoxides.

Among the most used synthetic routes for the production of chalcones, the main route is through the Claisen–Schmidt condensation, which involves a condensation between a benzaldehyde and an acetophenone. They also have a conjugated ketone system, which can be functionalized through chemical reactions such as, for example, the addition of thiazole groups, producing a range of chalcone derivatives [25–27].

### *3.1 TNF-α*

The TNF-α factor was discovered in the 1970s, and the function of a serum mediation of innate immunity that is responsible for the induction of hemorrhagic necrosis in tumors is attributed to this signaling pathway [28]. After a few years of studies, it was noticeable that this factor has a dual action in cancer, especially in breast cancer, in which TNF-α can be a target that causes the disease as well as a therapeutic agent [29].

Articles that address TNF-α and natural chalcones correspond to research carried out by Roh and collaborators (2020) [30], which addressed the structural optimization of natural chalcones: isoliquiritigenin, which corresponds to a trihydroxy chalcone (1), as well as butein (2), which represents a tetrahydroxychalcone. Compounds that have already been reported as good inhibitors of histone deacetylases (HDAC) [31] are also considered to be inhibitors of this inflammatory mediator, but their physical-chemical characteristic of solu- bility is inconvenient for their study and use, because despite having polar groups, these compounds have low solubility (79 mM, 21.0 mg/mL) and a partition coefficient (Log P) of only 0.42, in addition to demonstrating low potency (IC50, 43.3 mM) and insufficient efficacy, with only 21% inhibition at 20 mM *in vitro*. Due to these limitations, the authors carried out pro-drug optimization strategies by conducting structural modifications in the two mentioned chalcones, with the main objective of improving their pharmacokinetic properties. Based on this information, derivatives of butein were synthesized, correspond- ing to compounds **3**, **4**, and **5** (Figure 4), which showed the power to suppress up to

50% of TNF-α production in peritoneal macrophages of mice after stimulation with lipopolysac- charides. Compound **5** was shown to be the most potent inhibitor, with an *in vitro* IC50 of 14.6 mM and limb volume suppressed by 70% in a murine lymphedema model. Thus, the authors concluded that the pro-drug strategy allowed a six-fold increase in the kinetic solubility of compound **1** and five-fold higher levels of the active metabolite in the blood for compound **5** with oral administration in the pharmacokinetic study. When undergoing modifications in their structure in order to facilitate solubility and permeability, an increase in potency was equivalent to three times (17.3 mM) for anti-inflammatory effects *in vitro* than the unmodified compound (43.3 mM). Compound **4**, despite its insufficient solubility (28 mg/mL), showed greater permeability and was able to suppress limb swelling by 53% orally (100 mg/kg/day). Compound **5** was the most potent (14.6 mM) and had five times greater solubility (136 mg/mL). As a pro-drug, compound **5** was rapidly converted to compound **2** by liver microsomes of three species, including mice, rats, and humans. Thus, the authors suggested that compound **5** could be developed as a potential therapeutic agent targeting anti-inflammatory activity to alleviate the progression of lymphedema.

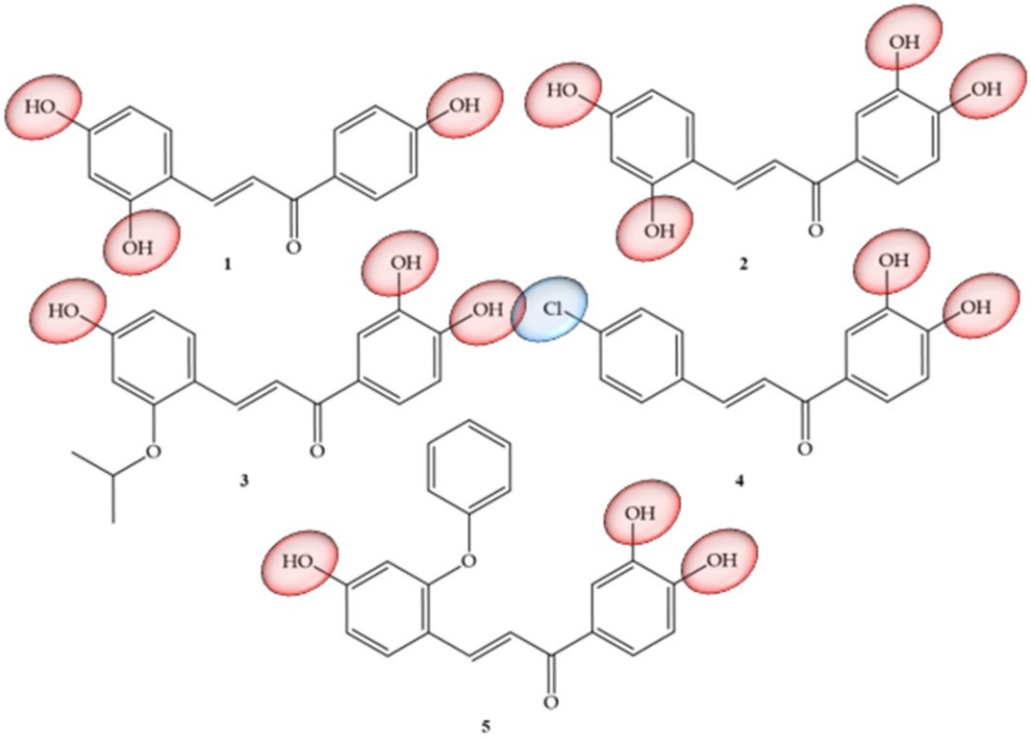


**Figure 4.** Chemical structure of TNF-α inhibitor compounds.

In a study carried out in 2019, Hashid and collaborators [32] observed that chalcones that have hydroxy, methoxy, and chlorine groups in the ortho and para positions, have strong inhibitory actions against mechanisms of inflammatory action, such as inhibition of cyclooxygenase. It was also revealed in this study that treatment with these compounds was able to inhibit up to 90% of inflammatory edemas.

### *3.2. Colon Cancer*

As potential therapeutic agents for colon cancer, articles that reported synthetic chalcones were observed with chalcones-ciprofloxacins linked to 1,2,3-triazole (6) (Figure 5), which showed an IC50 ranging from 2.53–8.67 mM, 8.67–62.47

mM, and 4.19–24.37 mM for HCT116, HT29, and Caco-2 cell lines, respectively; while doxorubicin showed IC50 values of 1.22, 0.88, and 4.15 mM. In addition, the compounds in studies still showed Topoisomerase I and II inhibitory activity [33]. Based on the properties of anthocyanidins and aglycones, Păus, escu and collaborators (2022) [34] carried out a synthesis of derivatives of the flavilium cation (7) (Figure 5), these being evaluated for anticancer activities in HCT116 and HepG2 strains. The anticancer effect was influenced by the position (6-, 7-, or 8-) of the methoxy group on the β-ring for the methoxy-4′-hydroxy-3′ methoxyflavilyl cation. Thus, the authors concluded that the evaluation of the anticancer activities of derivatives containing methoxy groups in the flavilium cation in hepatocellular carcinoma cells (HepG2) and colon cells of the HCT116 lineage, showed greater efficiency even at low concentrations (26 μM). Formation of the inclusion complex of Compound **5** with the cyclodextrin derivative SBECD led to a 1.5-fold increase in water solubility, preserving 70% of the cytotoxic effect in HepG2 cells.

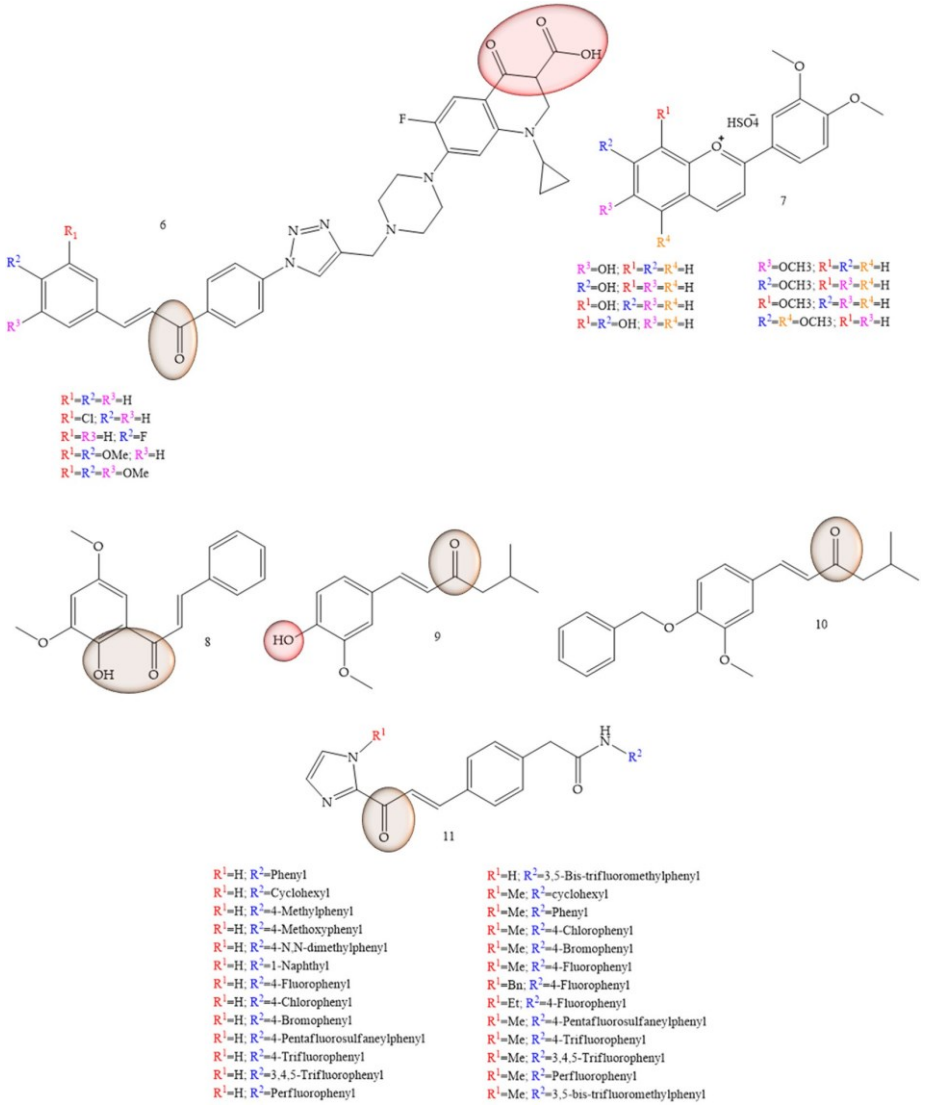


**Figure 5.** Chemical structure of colon cancer inhibitor compounds.

In a study conducted by Palko-Labuz and collaborators (2020) [35], the natural chal- cone found in the Kawa plant, flavokawain B (3) was evaluated for its inhibitory capacity of LoVo/Dx cells. The results showed that the natural

chalcone under study showed strong cytotoxic activity, as well as strongly inhibited cell proliferation of the strain under study. Furthermore, at low concentrations the chalcone flavokawain B (8) contributed to apoptosis, as it led to an increase in the expression of caspase-3 activity.

Vanillin-based chalcone analogues were discussed by Lukovic and collaborators (2020) [36]. The IC50 values observed in the HCT-116 cell models were equivalent to 6.85 ± 0.71 µg/mL for Compound **9** (Figure 5) and 7.9 ± 1.37 µg/mL for Compound **10** (Figure 5). Furthermore, vanillin-based chalcone analogues caused overexpression and activation of mitochondrial Bax protein and caspase-3 in HCT-116 cells, indicating that their antitumor mechanism of action was mediated by activation of the internal apoptotic pathway.

Inhibition of HCT-116 cells for evaluation of new tubulin inhibitors was performed by Hamashi and collaborators (2021) [37], through the aldol reaction of N-tosyl imidazolketone with the respective aldehyde group (Compound **11**) (Figure 5), thus obtaining 26 compounds that obtained GI50 values corresponding to 5.14 ± 6.81 µM. Regarding the IC50 values of the enzyme histone deacetylase (HDAC), these were equivalent to 1.8 ± 9.0 µM.

The presence of groups that favor hydrogen bonds, as well as the presence of halo genated elements may be related to the activity, since among the compounds considered the most active, they have these characteristics in common. In contrast, these groups demonstrate large cytotoxic loads, as demonstrated by Palko-Lobuz and collaborators [35].

### *3.3. Lung Cancer*

To obtain new therapeutic agents for lung cancer, Mphahlele and collaborators (2021) [38], carried out a sulfonylation reaction on compounds of the type 5-styryl-2-aminochalcones with p-toluenesulfonyl chloride in pyridine providing new hybrids of 5-styryl-2-sulfonamidochalco- nes. The *in vitro* results of the compounds (**12**) and (**13**) (Figure 6) against A549 and vero cell lines with LPS, showed a suppression capacity of up to 55% of ROS in vero cells and 35% in A549 cells. These compounds also reduced the cytotoxicity against the A549 cell line and did not affect the viability of vero cells. Another mechanism used for the discovery of drugs against lung cancer was addressed by Sherikar and collaborators (2021) [39]; in this work, the authors evaluated synthetic chalcone derivatives for blocking calcium channels, the study being carried out through pharmacophore modeling combined with experimental evaluation. Pharmacophore modeling revealed that hydrogen bonding receptors and hy- drophobic groups are important features for calcium channel-blocking activity. The docking study showed the existence of hydrophobic interactions, hydrogen bonds, and Van der Waals interactions between the amino acid residues and the ligands. *In vitro* screening showed that compounds **14**, **15**, and **16** were potent, yielding an IC50 of 4756, 3608, and 5211 µM, respectively, while the standard drug, Nifedipine, showed an IC50 of 1.30 µM. Furthermore, it is important to mention that synthetic chalcone derivatives with NO (nitric oxide) donating capacity is promising for designing new calcium channel blockers.

Another class under study was approached by El-wakil and collaborators (2020) [40], which refers to a series of 1,3,5-triazines linked to chalcones. The results showed that compounds (**17**) and (**18**) (Figure 6) significantly inhibited the viability of cancer cells of the A549 lineage, and their IC50 values were 24.5 and 17 µM, respectively, in reference to cisplatin (IC50 = 21.5 µM). Furthermore, mechanistic studies employing MALDI-TOF MS (matrix-assisted laser desorption ionization—time of flight mass spectrometry) and fluorescence spectroscopy using the EvaGreen probe inferred that (17) and

(18) induced DNA double-stranded breaks, in contrast to cisplatin, which induces crosslinks between DNA strands' DNA.

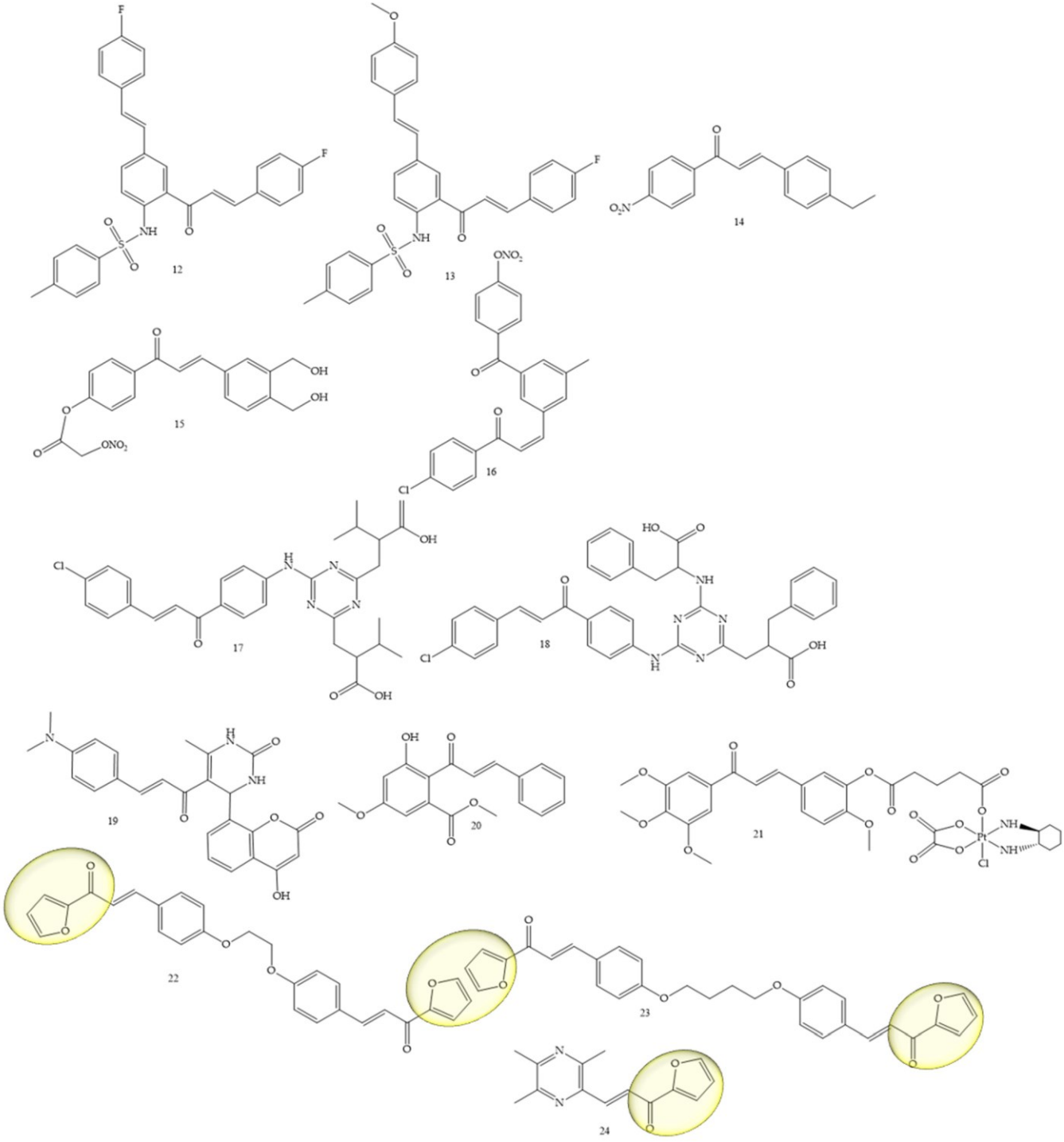

**Figure 6.** Chemical structure of lung cancer inhibitor compounds.

The functionalization of coumarins to chalcones as potent agents for lung cancer, among other activities, was mentioned by Kumar and collaborators (2021) [41]. In this article, the authors synthesized coumaryl–chalcone derivatives and it was observed that the compound lead (**19**) (Figure 6) is very potent against the A-549 (lung) strain, and also showed satisfactory results for the Jurkat (leukemia) and MCF-7 (breast). The IC50 values were, respectively, equivalent to 70.90, 79.34, and 79.13 µg/mL.

The natural chalcone flavokawain B (Compound **20**) (Figure 6) was studied by Hseu and collaborators (2019) [42] as an inhibitor of A459 cells and NSCLC cells (H1299). IC50 values of 11 µg/mL were observed for A549 cells and 5.1 µg/mL for H1299 cells. Further- more, at concentrations of 5–15 µg/mL, the chalcone under study induced apoptosis and autophagy in A-549 cells.

The platinum complex functionalization in the chalcone structure was a strategy adopted by Wang and collaborators (2021) [43]. Compound **21** (Figure 6) was the best performing complex, showing high apopytotic capacity, as well as IC50 values of 0.31 ± 0.09 and 0.71 ± 0.18 µM for the resistant strains A549/CDDP and SGC-7901/CDDP, while IC50 values for cisplatin corresponded to 35.05 ± 1.39 and 26.81 ± 1.73 µM, respectively.

Bischalcone derivatives linked to aliphatic ligands, with furan units in the A or B rings were synthesized by Fathi and collaborators (2021) [44]. Substances 22 and 23 (Figure 6) were considered the most promising, with IC50 (24.9 and 13.7 µg/mL, respectively) against A549, compared with the reference drug doxorubicin (IC50, 28.3 µg/mL), in addition to presenting IC50 (26.1 and 14.4 µg/mL, respectively) against A431 compared with the reference drug doxorubicin (IC50, 24.9 µg/mL). A ligustrazine chalcone was synthesized by Bukhari (2022) [45]. Compound **24** (Figure 6) showed an IC50 of 5.11 µM, as well as an inhibitory potential of other strains such as MCF-7.

A study led by Gaur and collaborators [46] pointed out that compounds of the chalcone class which have indole and furan groups in their structure, present high cytotoxicity against cell lines of this specific type of cancer, capable of combating these cells with an IC50 of 1 µg/mL, as well as cyclized chalcones with groups of diazoles, as reported by Bracke et al., 2008 [47].

### *3.4. Breast Cancer*

Breast cancer was one of the most mentioned pathologies, Wang and collaborators (2020) [48] reported the synthesis of new chalcones containing a diaryl ether moiety (25) (Figure 7). The results showed that among the synthesized compounds, the compound (**25**) with the 4-methoxy substitution on the right aromatic ring was considered the most active in cancer for MCF-7, HepG2, and HCT116 cell lines, showing IC50 values of 3.44 ± 0.19, 4.64 ± 0.23, and 6.31 ± 0.27 µM, respectively. *In vitro* tests showed that the compound (**25**) can effectively inhibit tubulin polymerization. Further studies of the mechanism of action revealed that the compound (**25**) was able to induce G2/M phase arrest and cell apoptosis. Furthermore, molecular docking studies revealed that compound (**25**) interacts and binds at the colchicine binding site of tubulin.

In another work Guruswamy and Jayarama (2020) [49] carried out synthesis of chalcone derivatives by the Claisen–Schmidt method. The resulting compound (**26**) (Figure 7) demonstrated incredible anticancer potential in MCF7 cells, with IC50 estimates of 6.55–10.14 µM. In addition, this induced apoptosis, since the increase in the expression level of Caspase 9 and Caspase 3 was noticeable. These results demonstrated expressive apoptotic activity.

The authors Homerin and collaborators (2020) [50], carried out synthesis of chalcones with thienyl groups as potential inhibitors of the farnesyltransferase enzyme as well as of the MCF-7 cell line. The bis(thienyl) chalcone (compound **27**) (Figure 7) was the most active compound in the series (IC50 = 7.4 µM), thus showing antiproliferative potential against the MCF7 cancer cell lines.

Another reported class refers to ethoxychalcones; these were studied by

Harshitha and collaborators (2020) [51] and were obtained by classic aldol condensation. The best compound was derivative (28) (Figure 7), which showed IC50 value = 53.47 μM for breast cancer cell line MDA-MB-231 and metastatic melanoma cells (A-375).

Al-kaabi and collaborators (2021) [52] synthesized chalcones from 1,2-bis(2-methoxy-4- vinylphenoxy)ethane. Compounds (**29**), (**30**) and (**31**) (Figure 7) showed the highest inhibition rate against the human breast cancer cell line Cal51, 64.1% 60.2%, and 50.4%, respectively.

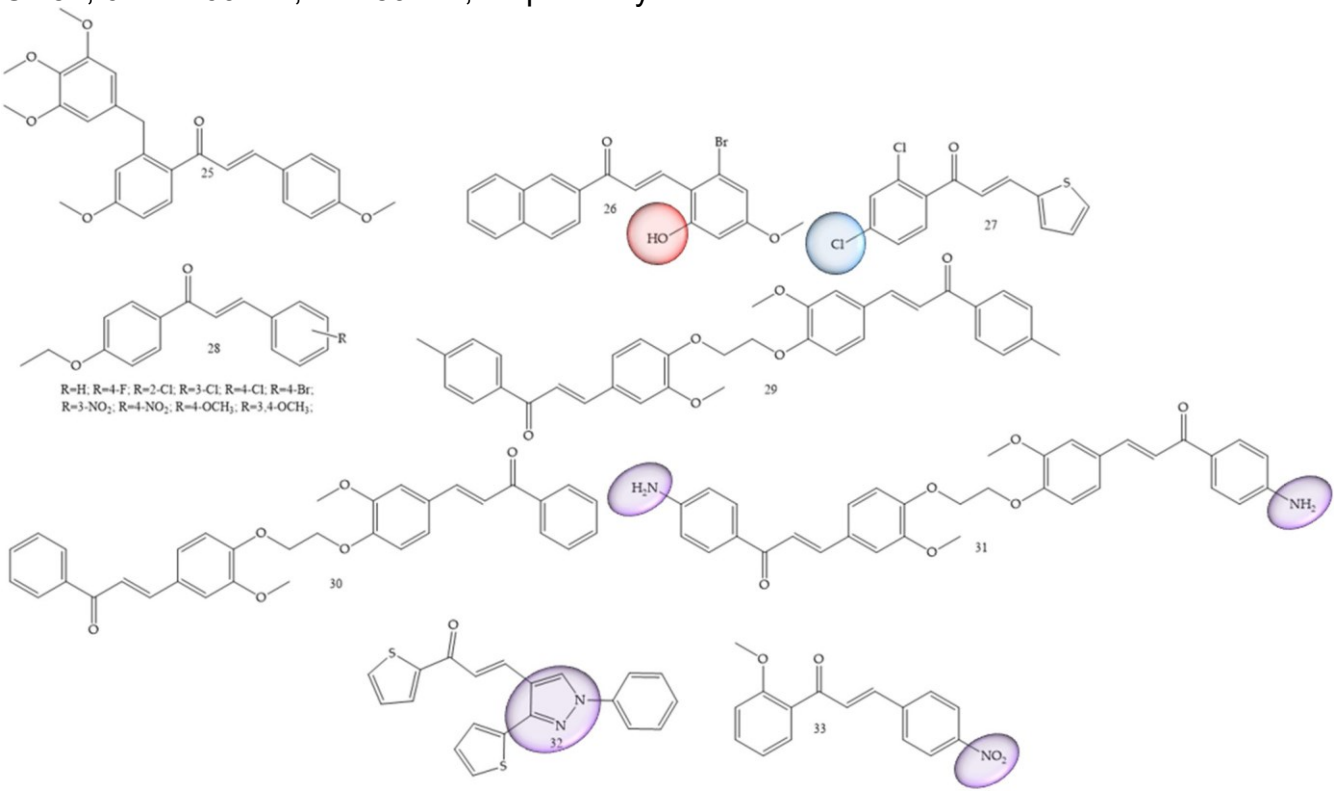


**Figure 7.** Chemical structure of breast cancer inhibitor compounds.

Chalcones with thiophene groups were synthesized by Mangoud and collaborators (2020) [53]. The results showed that chalcone 32 (Figure 7) had an inhibition percentage of 56.90% against T-47 D.

Polymethoxylated chalcones substituted with nitro groups ($NO_2$) were synthesized by Ahn and collaborators (2022) [54]. IC50 values for the MCF-7 cell line were around 1.33 and 172.20 μM, with compound **33** (Figure 7) being considered the best performer.

### *3.5. Oral Cancer*

In cases where the search for new therapeutic agents for oral cancer was mentioned, this was related to the suppression of inflammatory mediators such as interleukins. Ra- jeswari and collaborators (2022) [55], performed the functionalization of chalcones with other natural products belonging to the coumarin class, which are considered pharma- cophoric groups and which have already reported activity against oral cancer. In addition, pyrazolone aldehydes were produced using the Vilsmeier–Haack reaction, via the reaction between aldehydes and ketones in an alcoholic medium with sodium hydroxide. The *in vitro* assays were combined with *in silico* simulations that demonstrated high affinity of the compounds under study with mediators such as interleukins, as it

was also possible to observe that the *in vitro* cell viability studies of the series show that chalcones (34), (35), and (36) (Figure 8) presented IC50 values of 2.96, 2.97, and 2.82 µM against CAl27 oral cancer cell lines.

The inhibitory activity of the AW13516 cell line was studied by Kode and collab- orators (2020) [56]. In this work, the authors synthesized the compound **37** (*E*)-1-(3,4- dimethoxyphenyl)-3-(1-methyl-5-(3,4,5-trimethoxybenzoyl)-1H-indol-3-yl)prop -2-in-1-one
(37) (Figure 8). This derivative has 1-methyl, 2 and 3-methoxy substituents on the aromatic ring and was effective in inhibiting the AW13516 strain, showing GI50 values of 0.96 µM.

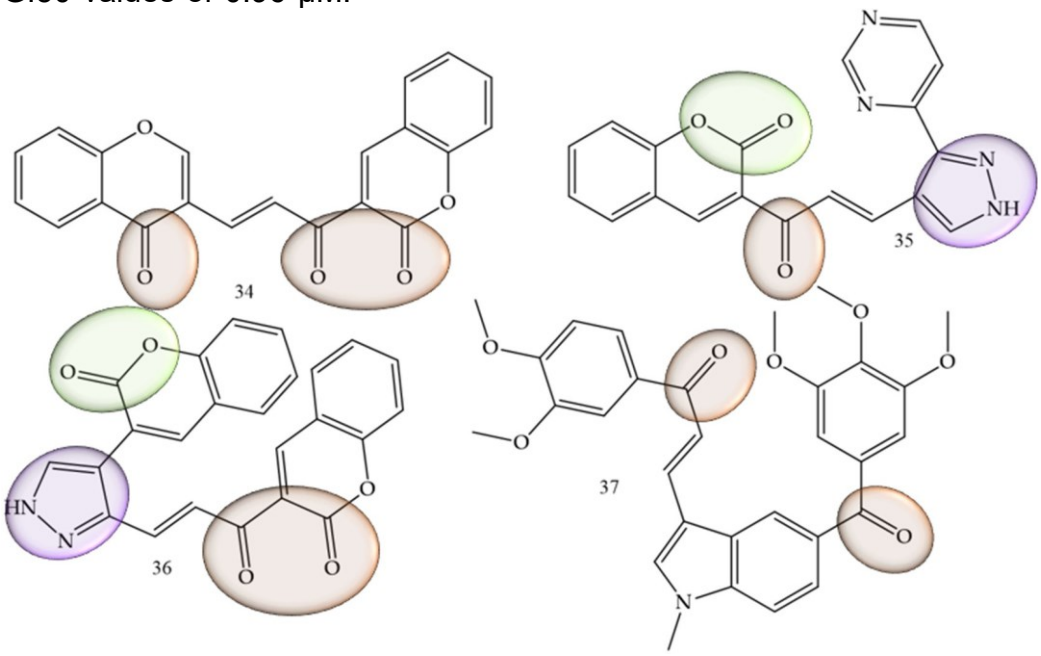


**Figure 8.** Chemical structure of oral cancer inhibitor compounds.

A study guided by Gul and collaborators [57] demonstrated that chalcone-like com- pounds have a greater selectivity for cells of the oral cancer lineage when they are trimethoxy- lated. In addition to the selectivity, based on *in vitro* experiments the authors concluded that these groups increase the potency of the compounds, showing promise in the fight against this type of cancer.

### *3.6. Leukemia*

Leukemia was also one of the most prevalent pathologies; synthetic derivatives of chalcones were reported in research by Mphahlele and collaborators (2022) [58], a series of 2- hydroxy-3-nitrochalcones substituted by 5-methyl, 5-bromo, and 5-chloro were synthesized. The results showed that chalcones 38 to 45 (Figure 9) exhibited inhibitory effect against α- glucosidase and α-amylase enzymes, in addition, it exhibited minimal cytotoxicity against Raw-264.7 macrophage cells (murine) in comparison with the anticancer drug, curcumin. For acute lymphoblastic leukemia, Kudlic˘ková and collaborators (2020) [59] performed the synthesis of 20 chalcone derivatives substituted with nitro groups ($NO_2$) and (CF3). Of the synthesized compounds, four derivatives (compounds **46**, **47**, **48**, and **49**), presented IC50 values between 6.1 and 8.9 µM for the inhibition of T lymphocytes, thus demonstrating a high antiproliferative role.
Del Rosário and collaborators (2022) [60], carried out the synthesis of 50 chalcones through a standard aldol condensation reaction of three acetophenones with three ben- zaldehydes. These compounds were

evaluated by means of the inhibition capacity of the strains HL-60 and U-937. Chalcone 2,2′-furoyloxy-4-methoxychalcone (Compound **50**) (Figure 9) was the most active compound, with IC50 values corresponding to 4.9 ± 1.3 μM.
In a differentiated methodology, Li and collaborators (2021) [61] aimed to search for new inhibitors of the specific histone lysine demethylase 1 (LSD1) enzyme, for which the synthesis was carried out through the aldol condensation of acetophenone and benzalde- hyde. Compound (**51**) (Figure 9), characterized as a piperidine oxazole chalcone, presented IC50 values corresponding to 0.14 μM, thus being about 100 times more potent than its precursor, in addition to representing a highly promising compound for the treatment of leukemia.

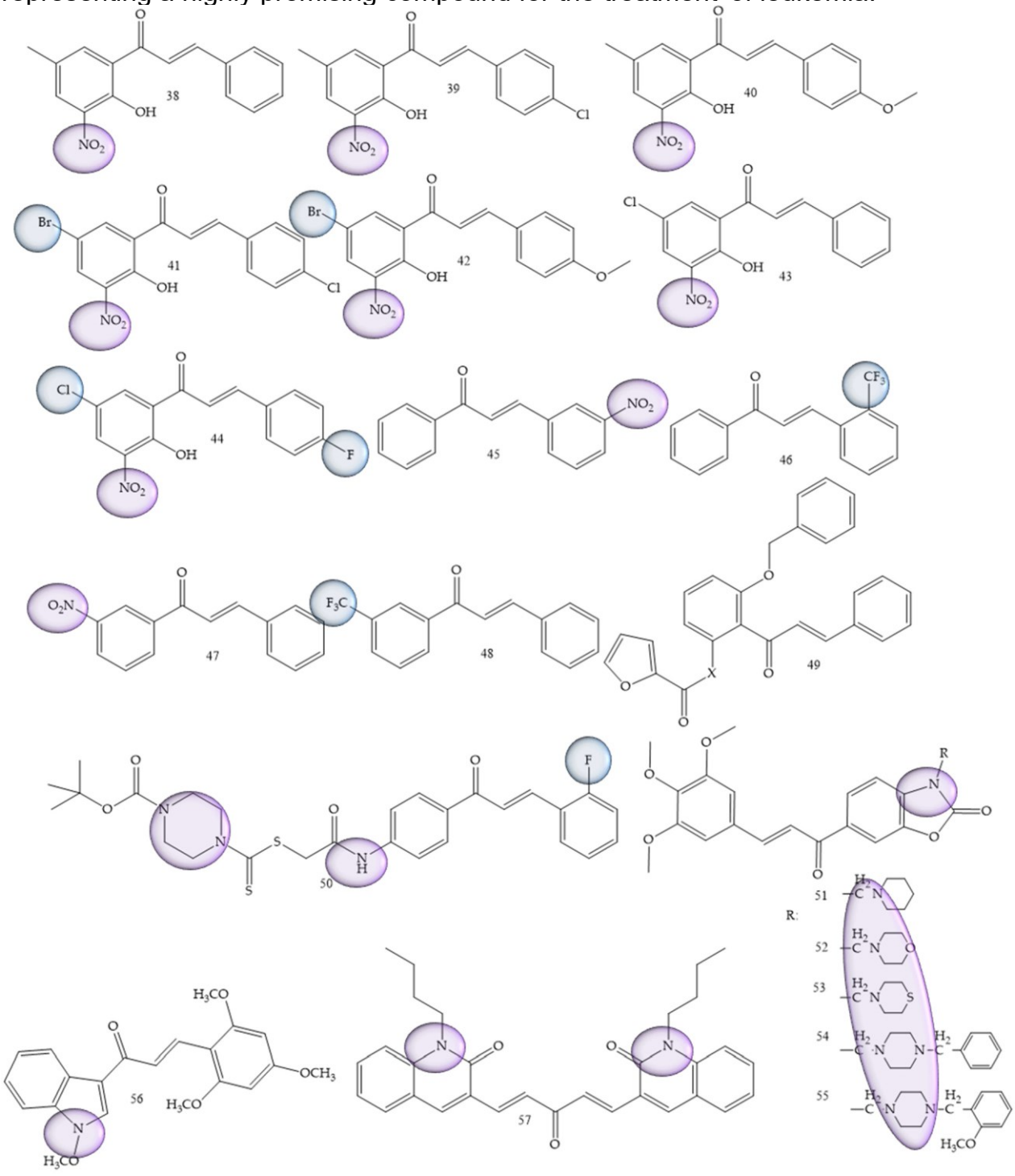


**Figure 9.** Chemical structure of leukemia inhibitor compounds.

Petrov and collaborators (2020) [62], carried out the synthesis of benzoxazolone deriva- tives to evaluate the inhibition of human leukemia strains. Compound (**52**) (Figure 9) demonstrated dose-dependent effect of cytotoxicity, being more sensitive for BV-173, SKW-3 and HL-60 strains (IC50 = 3.6–10.7 μM). The introduction of the aminomethyl group at position 3 of benzoxazolone was considered a structural prerequisite for the cytotoxic activity of the synthesized molecules.

For acute lymphoblastic leukemia, Kudlicˇková and collaborators (2021) [59] performed the synthesis of 20 chalcone derivatives substituted with nitro groups ($NO_2$) and (CF3). Of the synthesized compounds, four derivatives (compounds **46**, **47**, **48**, and **49**), presented IC50 values between 6.1 and 8.9 μM for the inhibition of T lymphocytes, thus demonstrating a high antiproliferative role. The greatest efficacy was demonstrated by chalcones against Jurkat leukemic cells, which are rapidly proliferative and more sensitive cells. IC50 values (excluding three compounds) ranged from 3.9 to 15 μM. The best results were obtained by compound **53** (Figure 9).

Bis-quinolinyl-chalcone compounds were synthesized by Insuasty and collaborators (2020) [63]. Compound **54** (Figure 9) showed significant activity against leukemia cells K-562 (GI50 = 0.88 μM), RPMI-8226 (GI50 = 0.32 μM) and SR (GI50 = 0.32 μM).

Studies led by Vrontaki (2017) [64] and Mercader (2012) [65] showed that nitrogenated and halogenated chalcones have high cytotoxicity against leukemic cells, being able to limit their growth, in addition to inducing the process of cell apoptosis.

### *3.7. Hepatocarcinoma*

A study conducted by Wang and collaborators (2022) [66] showed two series of chalcone derivatives containing aminoguanidine or bis-chalcone that were designed, synthesized, and screened for their cytotoxicity, proliferation inhibition, and apoptosis- promoting activity *in vitro*. The results showed that 2-((*E*)-4-((*E*)-3-oxo-3-(p-tolyl)prop-1- en-1-yl)benzylidene)hydrazine-1-carboximidamide (58) (Figure 10) was the most potent compound, with IC50 values of 7.17 μM and 3.05 μM of *in vitro* anti-proliferative activity against HepG2 human hepatocarcinoma cells and SMMC-7721 cells, respectively. This result showed that the compound had a certain degree of selectivity for human hepatocel- lular carcinoma cells, especially for SMMC-7721, affirming this compound as a potential drug candidate.

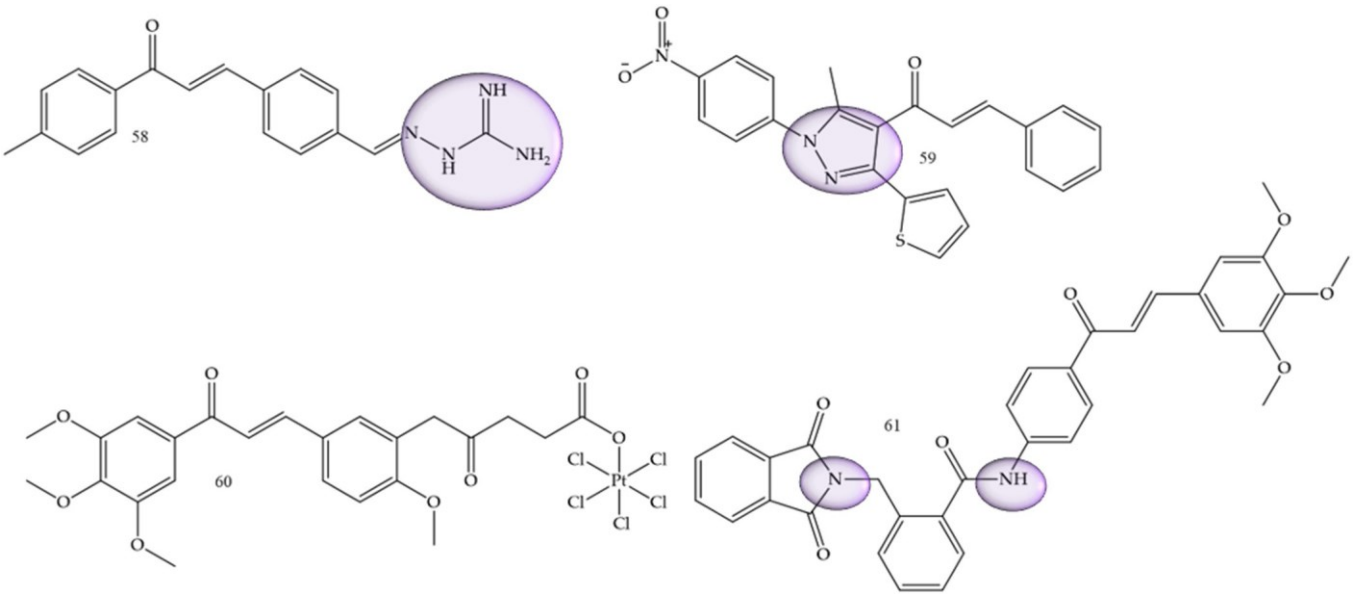


**Figure 10.** Chemical structure of hepatocarcinoma inhibitor compounds.

Helmy and collaborators (2022) [2], synthesized 4-acetyl-5-furan/thiophene-pyrazole derivatives. Compound (**59**) (Figure 10) showed to be the most promising compound, with IC50 = 26.6 µg/mL against HepG2 cells compared with the reference drug doxorubicin (IC50 = 21.6 µg/mL), and with IC50 = 27.7 µg/mL against A549 cells compared with the reference drug doxorubicin (IC50 = 28.3 µg/mL).

Huang and collaborators (2020) [67], reported functionalized platinum complexes to chalcones. Chalcone 60 (Figure 10) showed the best IC50 value for the HepG-2 strain IC50 of 0.33 µM, as well as other good values 0.41 µM, 0.30 µM, 0.45 µM, and 11.85 µM for HeLa, MGC-803, NCI-H460, and HL-7702, respectively.

α-phthalimido-chalcones were synthesized by Mourad and collaborators (2020) [68]. Trimethoxy derivative 61 (Figure 10) demonstrated the most potent anticancer activity, with an IC50 of 1.62 µM for Hep G2 and 1.88 µM for MCF-7. Thiophenic, nitrogenous, and diazolic chalcones have a strong antioxidant power, in addition to acting significantly against breast cancer and hepatocellular carcinoma cells, as reported in studies led by Zahrani in 2020 [69].

### *3.8. Cervical Cancer*

Methoxylation and hydroxylation reactions in chalcones were the strategies used by Sangpheak and collaborators (2019) [70] for the elaboration of new topoisomerase enzyme inhibitors. The synthesized compound corresponded to a derivative that had 2,4-dimethoxy and 6-hydroxy groups in ring A and 3′,4′,5′-trimethoxy in ring B (Compound **62**) (Figure 11), and showed the highest cytotoxicity in *in vitro* against HeLa, HT-1376, and MCF-7 strains, whose IC50 values corresponded to 3.2, 10.8, and 21.1 µM. In addition, it was demonstrated that the test compound had a high affinity for the topoisomerase enzyme, which was confirmed by molecular docking and molecular dynamics simulations.

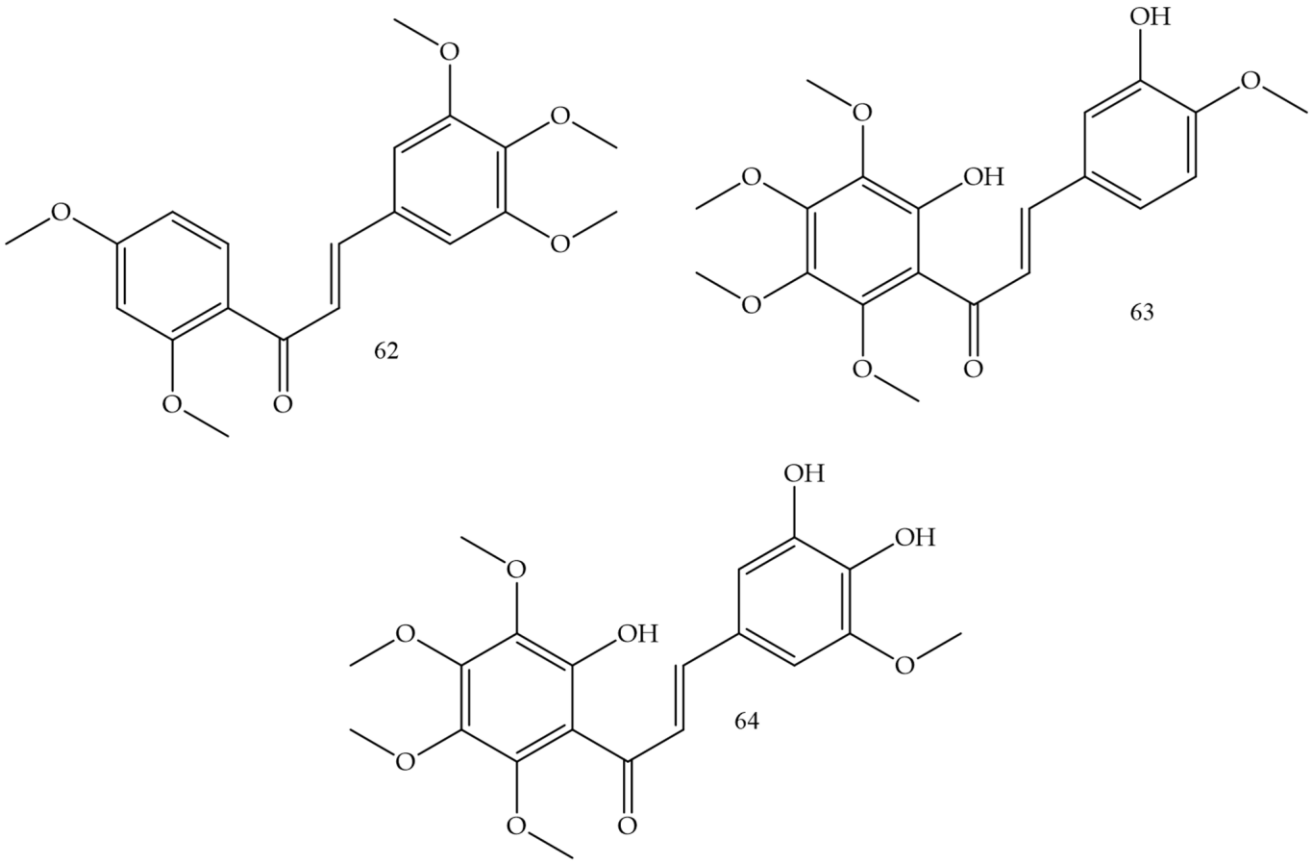


**Figure 11.** Chemical structure of cervical cancer inhibitor compounds.

HeLa cell inhibition was evaluated by Vongdeth and collaborators (2019) [71]. In this work, polyhydroxychalcones were synthesized by the classic Claisen–Schmidt con- densation pathway of 2-hydroxy-4,6-dimethoxyacetophenone with several aldehydes. Compound (**63**) (Figure 11) was the most potent, with greater selectivity for HeLa cells (IC50 1.44 μM) and SK-OV-3 cells (IC50 1.60 μM).

### *3.9. Glioblastoma*

Medanha and collaborators (2021) [72] reported the synthesis of new chalcones as promising inhibitors of human glioblastoma lines U98 and GL261. Chalcone 65 (Figure 12) was the compound with the best performance and reduced cell proliferation by 40% for U87 cells and 25% for GL261, not dependent on exposure time. The number of viable cells was significantly lower in treated cells and the invasive capacity of U87 cells was reduced by 50% after treatment with chalcone 65. These results demonstrate chalcone 65 as a promising agent.

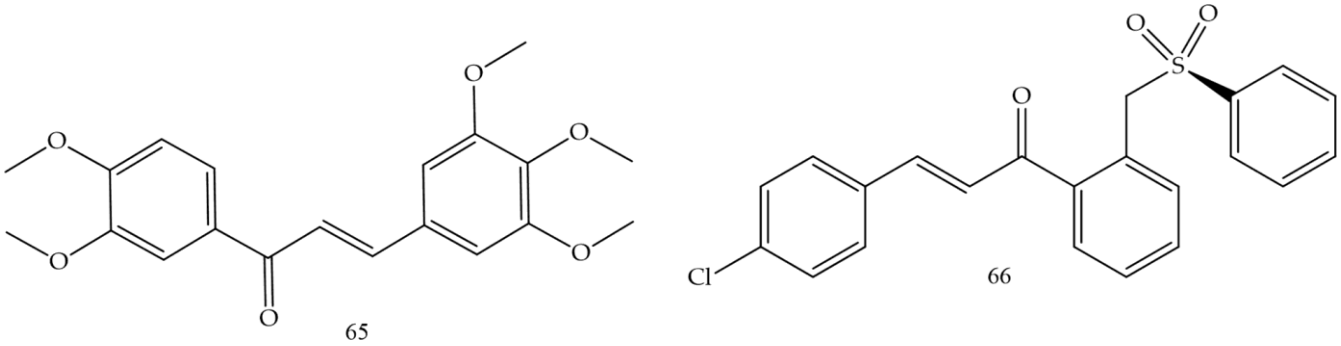

**Figure 12.** Chemical structure of glioblastoma inhibitor compounds.

Sulfonamide groups in chalcones were reported by Custodio and collaborators (2020) [73]. Compound (**66**) (Figure 12) had the lowest values of IC50 (2.1 e 2.4 $\mu g.mL^{-1}$ against SF-295 e PC-3, respectively).

*3.10. Melanoma*

Castano and collaborators (2022) [74], synthesized chalcone-sulfonamide hybrids. Since the compound (**67**) (Figure 13) presented the best inhibition profile for LOX IMVI (melanoma) with IC50 = 0.34 µM, it also showed good results for MCF7 and MDA-MB-468 (breast cancer) with IC50 values of 0.97 and 1.20 µM, respectively; K-562 (leukemia) with IC50 = 1.50 µM, and HCT-116 (colon cancer) with IC50 = 1.49 µM.

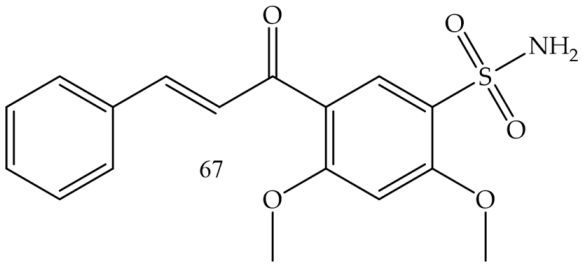

**Figure 13.** Chemical structure of melanoma inhibitor compounds.

## 4. Other Studies

This section includes compounds that are derived from chalcones, but have a different structure, as well as other mediators of anticancer activity. The results are described in Table 1.

**Table 1.** Other articles related to chalcones with anticancer activity.

| Compounds | Number of Compounds under Study | Obtaining Method | In Vitro Activity | Cell Lineage | References |
|---|---|---|---|---|---|
| Pyrimidine derivatives linked to chloropyrazine | 18 | Synthesis | 5 ± 1 µg/mL (IC50) | DU-145 (prostate cancer) | [75] |
| chalcone-thienopyrimidine | 06 | Synthesis | 5.3 ± 2.1 µg/mL (IC50) | Hep-G2 (Hepatocarcinoma) | [76] |
| Natural chalcones | Various compounds | Literature review | - | Antimitotic activity (cell cycle inhibition in the G2/M phase) | [77] |
| 1,3-diaryl-2-propen-1-one synthetic chalcones | Various compounds | Literature review | - | Inhibition of erythroid nuclear factor-related factor 2 (Nrf2) | [78] |
| Natural, synthetic, and semi-synthetic chalcones | Various compounds | Literature review | - | Biological activity of chalcones in negative undulating breast cancers (TNBCs) | [79] |
| Isoquinoline chalcone | 01 | Synthesis | Qualitative evaluation of marker expression | Evaluation of antioxidant and antiproliferative activity, as well as the action on p-53 and BAX markers | [80] |
| Spirooxindole hybrids | 37 | Synthesis | 7 ± 0.27 µM (IC50) 5.5 ± 0.2 µM (IC50) | HCT-116 and HepG2 (colon cancer) | [81] |
| Pyrimidodiazepine derivatives containing the 2-chloro-4-anilinoquinazoline fragment | 14 | Synthesis | 0.622 µM (GI50) | K-562 (Leukemia) | [82] |

| | | | | | |
|---|---|---|---|---|---|
| Benzothiazepine derivatives | 20 | Synthesis | 16 ± 18 µg/mL (IC50)<br>12 ± 13 µg/mL (IC50)<br>15 ± 18 µg/mL (IC50) | HT-29 (colon cancer)<br>MCF-7 (breast cancer)<br>DU-145 (prostate cancer) | [83] |
| Homocyclic and heterocyclic chalcones | Various compounds | Literature review | - | Biological activity of chalcones in breast cancer. | [84] |
| Natural and synthetic chalcone derivatives | Various compounds | Literature review | 50 ± 6 nM (GI50)<br>1–53.4 nM (GI50) | MDR A549/T (lung cancer)<br>HCT-116/L (colon cancer)<br>HL60/DOX (leukemia) | [85] |
| Natural and synthetic chalcone derivatives | Various compounds | Literature review | 6.20 ± 2.82 µg/mL (IC50) | A-549 (lung cancer)<br>HepG2 (colon cancer)<br>MCF-7 (breast cancer)<br>MDA-MB-231 (breast cancer)<br>ALL-SIL (leukemia)<br>SW1990 (pancreatic cancer)<br>Vascular endothelial growth factor (VEGF) (anti-angiogenesis) | [86] |
| Derivatives of indole chalcones | Various compounds | Literature review | 4 µM (IC50) | PaCa2 (pancreatic carcinoma)<br>RT112 (bladder carcinoma) | [87] |
| Substituted natural chalcones | Various compounds | Literature review | - | Evaluation of the induction of apoptosis by the caspase-3 pathway | [88] |
| Natural chalcones present in the Sophora kingdom | Various compounds | Literature review | - | It does not mention a specific cell or mechanism; it only informs that the compounds have anticancer activity | [89] |
| Glycosidic derivatives of chalcones | Various compounds | Literature review | 2.97 µM (IC50) | HL-60 (leukemia) | [90] |
| Natural and synthetic chalcone derivatives | Various compounds | Literature review | 0.17–0.19 µM (IC50) | ABCG2 transport protein inhibition | [91] |
| Natural and synthetic chalcone derivatives | Various compounds | Literature review | - | It does not mention a specific cell or mechanism; it only informs that the compounds have anticancer activity. | [92] |
| Triazole-chalcone-conjugates | 7 | Synthesis | 0.94–1.92 µM (IC50) | MCF-7 (breast cancer)<br>Leukemia SR | [93] |
| Amino-naftil-chalcona | 1 | Synthesis | 8 µg/mL (IC50) | U2OS (humanosteosarcoma cell line) | [94] |
| Polycyclic chalcone based acrylamides | 4 | Synthesis | 38.46–48.25 µg/mL (IC50)<br>38.02–36.35 µg/mL (IC50) | MCF-7 (breast cancer)<br>HeLa (cervical cancer) | [95] |
| Arylpropenone aminochalcone conjugates | 17 | Synthesis | 6.7–9.8 µM (IC50) | MCF-7 (breast cancer) | [96] |
| Synthetic chalcones | Various compounds | Review article | - | NRF2, apoptosis, and BCL2 | [97] |
| Natural and synthetic chalcone derivatives | Various compounds | Review article | - | Evaluation of the activity of chalcones in multiple mechanisms | [20] |
| Natural and synthetic chalcone derivatives | Various compounds | Review article | Survey of several studies and explanation of the mechanisms | Mechanisms related to gastric cancer | [98] |
| Synthetic chalcones | Various compounds | Review article about synthesis | Survey of several studies and explanation of the mechanisms | Various mechanisms | [19] |
| Natural and synthetic chalcone derivatives | Various compounds | Review articles on mechanisms of action of chalcones | Survey of several studies and explanation of the mechanisms | Various mechanisms | [22] |
| Natural and synthetic chalcone derivatives | Various compounds | Review articles on mechanisms the enzyme p53 | Survey of several studies and explanation of the mechanisms | Action on p-53 protein | [99] |
| Chalcone hybrids | Various compounds | Review article on obtaining hybrid chalcone compounds combined with structure-activity studies | Survey of several studies and explanation of the mechanisms | The article emphasizes various synthetic compounds and various mechanisms to achieve cancer | [100] |
| Ferrocenyl chalcones | Various synthetic compounds | Review about application | Survey of several studies and explanation of the mechanisms | The article emphasizes various synthetic compounds and various mechanisms to achieve cancer | [101] |
| Natural chalcones | Various compounds | Review on compounds reported in specific mechanism | Compost survey with action on histones | Histone deacetylase | [31] |
| Natural flavans and (iso)flavanones | Various compounds | Review and application of synthetic compounds anticancer | Survey of several studies and explanation of the mechanisms | Various mechanisms | [102] |
| Chalcone based metal cordination | Various compounds | Review and application of synthetic compounds anticancer | Survey of several studies and explanation of the mechanisms | Various mechanisms for obtaining synthetic chalcones | [103] |
| Chalcone heterocycles synthesis | Various compounds | Review and application of synthetic chalcones in cancer | Various mechanisms for obtaining synthetic chalcones | Various mechanisms for obtaining synthetic chalcones | [25] |
| Quinoline chalcone hybrids | Various compounds | Review and application of synthetic chalcones in cancer | Various mechanisms for obtaining synthetic chalcones | Various mechanisms for obtaining synthetic chalcones | [104] |
| Flavonoids overview addressing natural chalcones | Various compounds | Review about application of phytochemical constituents | - | Blade cancer | [105] |
| Chalcones and other compounds | Various compounds | Review on bioisosterism and obtaining drugs | - | Various mechanisms | [106] |

**Table 1.** *Cont.*

| Compounds | Number of Compounds under Study | Obtaining Method | In Vitro Activity | Cell Lineage | References |
|---|---|---|---|---|---|
| Coumarin-chalcone hybrids | Various compounds | Review and application of synthetic chalcones in cancer | Various mechanisms for obtaining synthetic chalcones | Various mechanisms | [107] |
| Phytochemical constituents of the Didymorcarpus wall (Gesneriaceae) | Various compounds | Review about application of phytochemical constituents | Survey of several studies and explanation of the mechanisms | Various mechanisms | [108] |
| Phytochemical constituents of the Kawa (piper methistycum) | Various compounds | Review about application of phytochemical constituents | Survey of several studies and explanation of the mechanisms | Various mechanisms | [109] |
| Flavonoids overview addressing natural chalcones | Various compounds | Review about application of phytochemical constituents | Survey of several studies and explanation of the mechanisms | Various mechanisms | [110] |
| Flavonoids overview addressing natural chalcones | Various compounds | Review article that addresses the antiviral activity for Herpes virus and a correlation with cancer pictures | Survey of several studies and explanation of the mechanisms | Antiviral activity and antitumor activity | [111] |
| Phenolic compounds of the *Mous alba*–natural chalcones | Various compounds | Review about application of phytochemical constituents | Survey of several studies and explanation of the mechanisms | Various mechanisms | [112] |
| Licochalcones | Various compounds | Review about application of phytochemical constituents | Survey of several studies and explanation of the mechanisms | Various mechanisms | [113] |
| Chalcone heterocycles synthesis | Various compounds | Review articles on mechanisms of action of chalcones | Survey of several studies and explanation of the mechanisms | Various mechanisms | [114] |
| Natural chalcones present in licorice–Chinese materia medica | Various compounds | Review articles on mechanisms of action of chalcones and other compounds | Survey of several studies and explanation of the mechanisms | Various mechanisms | [115] |

## 5. Chemometric Analyses

The PLS analysis was performed with the training set of 128 descriptors, assigning classification criteria to the compounds according to the activity value of the compounds obtained in the literature review. The activity values included were equivalent to the IC50, GI50, or percentage of inhibition (%) obtained for the cell lines under study. The selection of compounds related to the HCT-116 lineage of colon adenocarcinoma was carried out. This series corresponded to 28 compounds that presented the activity value in IC50 (µg/mL). The total series under study was divided into active and inactive compounds, with a value of +1 for active compounds and -1 for inactive compounds. Compounds **01**, **02**, **03**, **04**, **05**, **06**, **07**, **08**, **09**, **11**, **12**, **14**, **22**, **27**, and **28** were classified as active, as they presented IC50 values < 10 µg/mL (Figure 14A). The other compounds in the model, referring to compounds with IC50 values > 10 µg/mL, were classified as inactive (Figure 14B). To improve the statistical validation of the model, compounds **14** and **22** were excluded. The model validation was performed with the leave-one-out (LOO) cross-validation correlation coefficient method, resulting in a good observed statistical index in the calculation of the latent variable LV5, having a good predictive coefficient ($Q^2$ = 0.847) and an excellent determination coefficient ($R^2$ = 0.960), reinforcing the quality of the physical-chemical descriptors of VolSurf and the biological activity data used in this study.

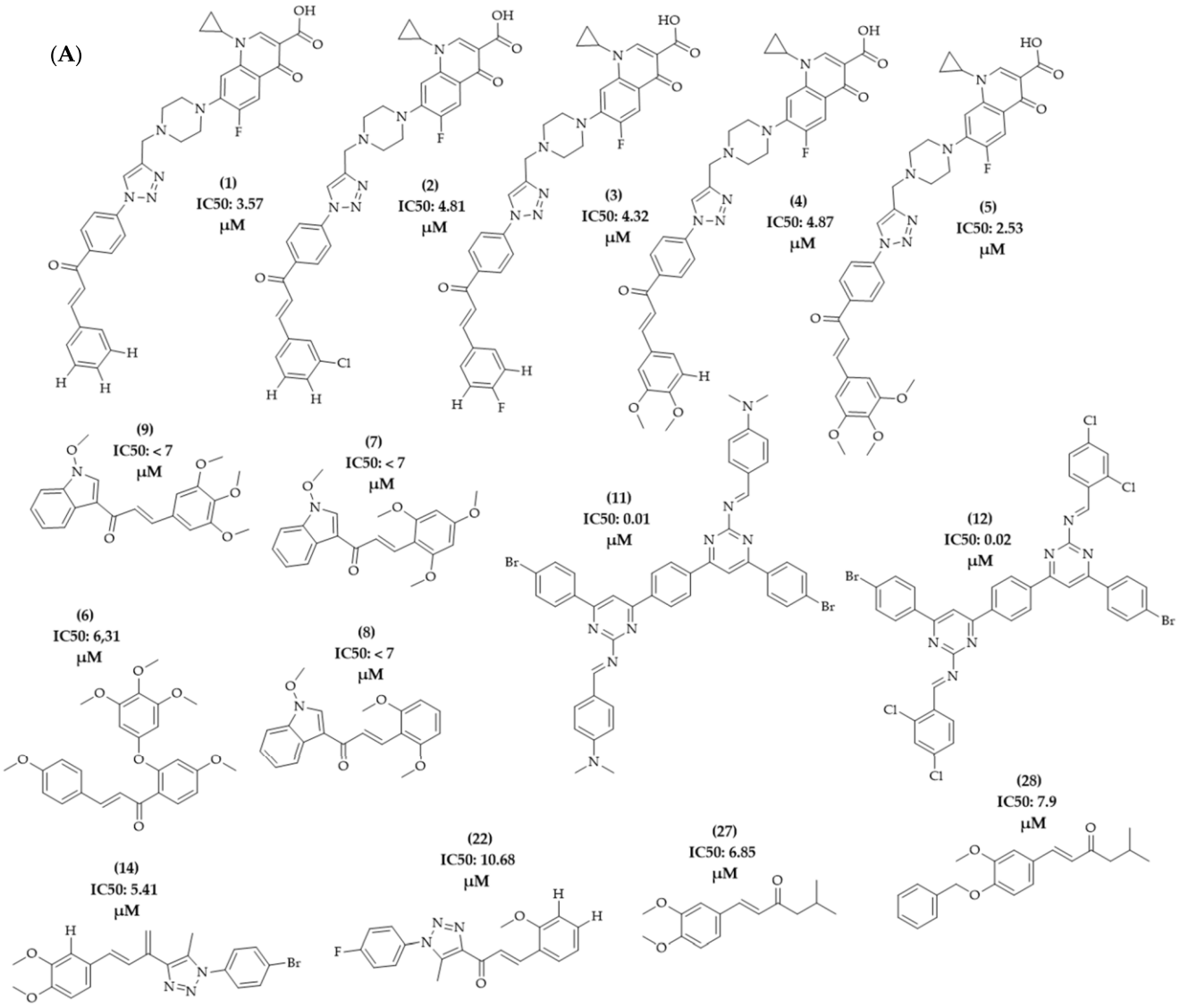


**Figure 14.** *Cont*.

**(B)**

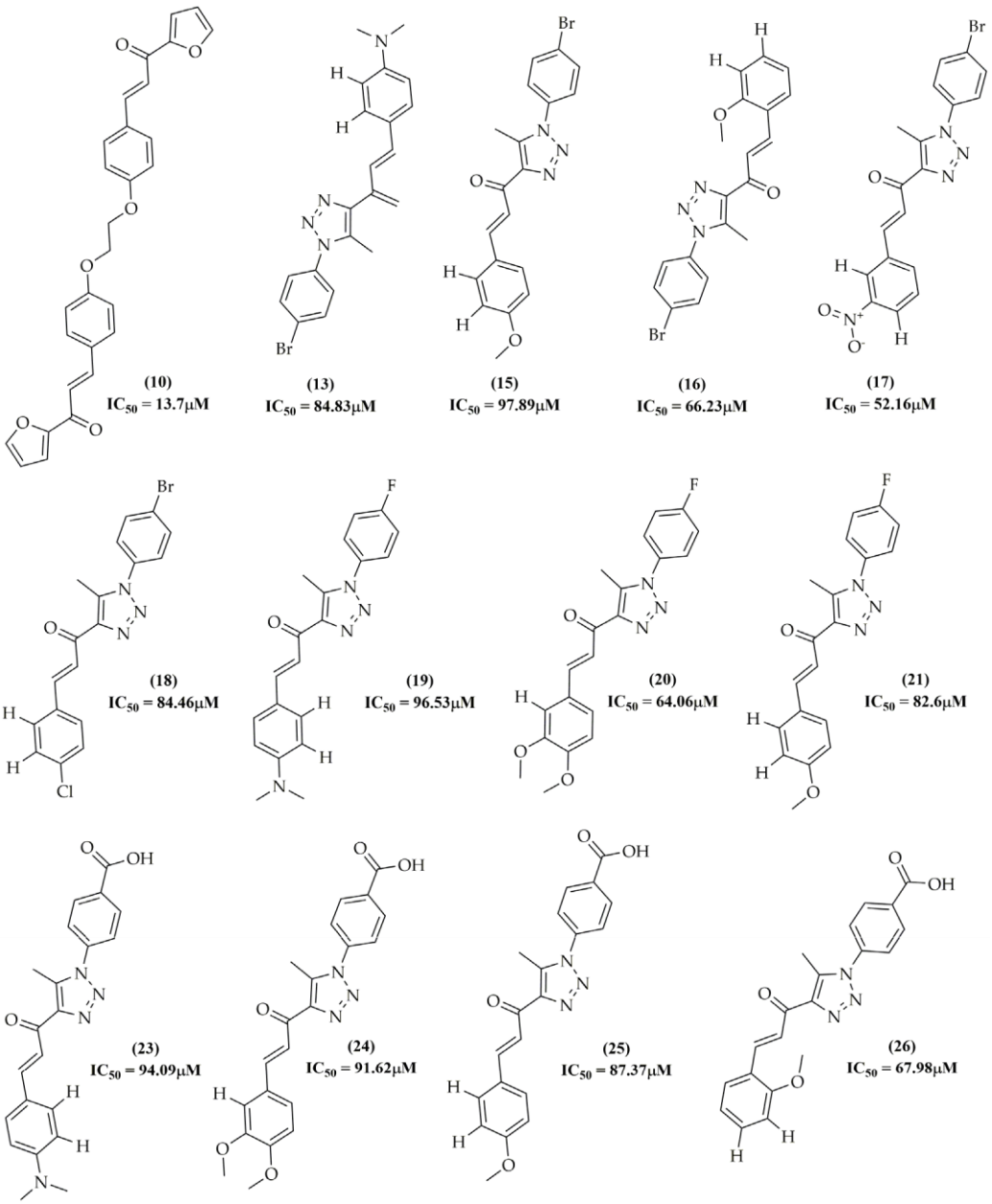


**Figure 14.** Chemical structure of the series of compounds submitted to PLS analysis. (**A**) Active compounds; (**B**) inactive compounds.

The t1-t2 PLS Score plot is shown in Figure 15. Regarding the plot, the selected model provides good discrimination between active and inactive class of compounds according to the statistically significant quality of the derived PLS model.

Based on the developed model, the contribution coefficients of the most significant descriptors for the activity were analyzed, that is, we sought to highlight the descriptors that favor the biological activity of the active compounds and the descriptors that disfavor the biological activity of the compounds. Among these descriptors, it is possible to observe the positive influence of the

descriptors Flex, G, W1, and Pol while the negative influence can be highlighted by the MetSab descriptor, as shown in Figure 16.

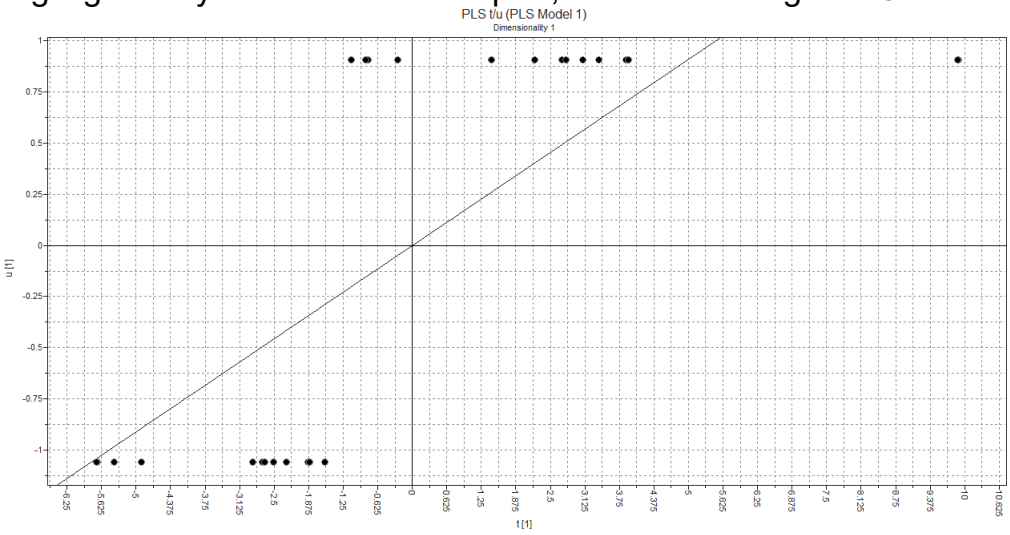


**Figure 15.** Arrangement of objects in relation to the activity of compounds.

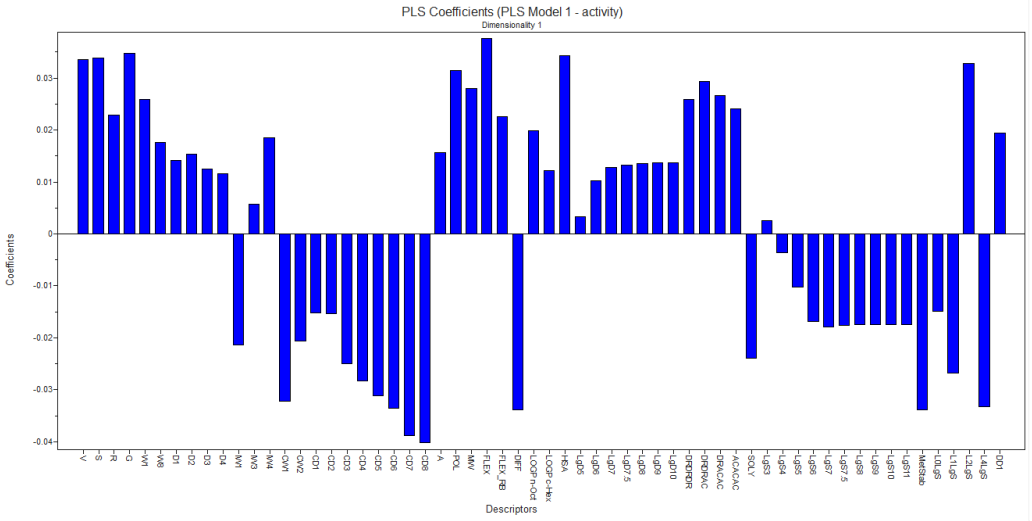


**Figure 16.** Coefficient graph generated from the PLS model.

The mentioned descriptors take into account the structural characteristics of the com- pounds without declaring the interference of biological activity. As positive contributions, the following stand out:

- The W1 descriptor belongs to the hydrophilic volume descriptor block, which describes the accessible molecular envelope that interacts attractively with water molecules.
- The FLEX descriptor is related to flexibility parameters and represents the maximum flexibility of a molecule.
- Another descriptor is the POL, which represents an estimate of the average molecular polarizability and is based on the structure of the compounds.
- Molecular globularity (G) is related to molecular flexibility and is defined as S/Sequiv with Sequiv = surface area of a sphere of volume V, where S and V are the molecular surface and volume described above, respectively.

As negative contributions, the following stand out:

The MetSab descriptor is an ADMET (absorption, distribution, metabolism, excretion, toxicity) descriptor, which represents the metabolic stability after incubation with the human CYP3A4 enzyme.

So in this way, it is understood that the series under study has hydrophilic characteris- tics and may present metabolization inconveniently.

## 6. Discussion

According to Michalkova and collaborators (2021) [116], chalcones are molecules chemically derived from aromatic ketones, and their chemical structure is considered simple, which may explain the ease of modifications in their structure. This information can be confirmed in the analyzed data, since most of the articles found referred to obtaining synthetic or semi-synthetic chalcones. The only natural chalcones mentioned referred to the butein and isoliquiritigenin derivatives and the chalcone present in the Kawa plant, known as flavokawain B.

Regarding the semi-synthetic chalcones that were observed, the most used synthesis reaction corresponded to the Claisen condensation, which is configured as a standard in obtaining chalcones, however, it was noticeable that the structural modifications carried out referred to hydroxylation reactions and methoxylation. The addition of halogens such as chlorine, bromine, and fluorine was also observed. In addition, the high occurrence of thiophene rings and azole substituents was noticeable. Another strategy used refers to the elaboration of complexes with platinum.

It was observed that the addition of the metal complex to the chalcone structure significantly increased the potency of the chalcone under study, being noticeable by the decrease in the IC50 values. According to Hacker (2009) [117] platinum complexes such as cisplatin and carboplatin demonstrate their antitumor action through the formation of DNA adducts that consequently contribute to the inhibition of DNA replication and transcription.

The high use of the strategy of adding polar radicals such as the hydroxyl and methoxyl was identified in the analyses related to the PLS regression, since the descriptors that are most related to the activity of the compounds under study are descriptors related to polar features, such as the W1 descriptor and the G descriptor.

Among the types of strains under study, the strains related to lung cancer were the most prevalent, reported in nine studies with the A-549 strain being the most mentioned strain. In addition, it was also observed that the compounds in question have multi-target potential since, in several cases, it was observed that natural chalcones and chalcone derivatives under study showed inhibitory capacity in more than one cell lineage, such as the natural chalcone flavokawain B.

Based on the observed results, the class of chalcones can be confirmed as potent anticancer agents, as well as their low level of toxicity and ease of procurement.

## 7. Material and Methods

### *7.2. Literature Review*

A literature review was carried out with articles that addressed the anticancer activity of natural chalcones, synthetic chalcones, and chalcone derivatives. The search was carried out on the Web of Sciences database (https://www.webofscience.com/wos/woscc/basic- search (accessed on 10 January 2023)); the period comprised the last four years, from 2019 to 2023, and the words used as descriptors were chalcones, anticancer activity, and *in vitro*. The inclusion criteria were full articles published in English that were reporting anticancer activity of natural or synthetic chalcones and chalcone derivatives. The exclusion criteria were in vivo and *in silico* studies, chalcone analogs, and other biological activities. In the search were found 159 articles from the Web of Science database, but only 101 met the review eligibility criteria mentioned above. The SMILES referring to all the compounds reported in the bibliographic survey are described in Table S1 of the Supplementary Material.

### *7.3. Data Set*

The chemical structures of the compounds under study were drawn in the software Marvin Sketch 22.13., 2022, ChemAxon (https://chemaxon.com/ (accessed on 10 January 2023)) [118]. After drawing, the structures were converted into SMILES, which consist of the canonical representation of the structure.

### *7.4. Chemometric Studies*

The structures in three dimensions (3D) saved in SDF format were imported in the program VolSurf+ v.1.0.7 [119] and subjected to molecular interaction fields (MIF) to generate descriptors using the following probes: N1 (nitrogen-amide binding donor probe—N1); O (carbonyl oxygen-hydrogen bond receptor probe); OH2 (water probe) and a DRY (hydrophobic probe). Non-MIF-derived descriptors were generated to create 128 descriptors [120].

### *7.5. Partial Least Squares (PLS)*

The QSAR analysis with PLS involves working with matrices X and Y, respectively, corresponding to chemical variables and biological descriptors. The PLS method approxi- mates the X and Y matrices to model the relationship between them. The PLS methodology was applied to build models. A discriminant PLS analysis was performed, with active com- pounds assigned the value of 1 (totaling 14 compounds) and inactive compounds assigned the value of −1 (totaling 14 compounds) separated according to the values of the IC50 (μg/mL), where the compounds that showed IC50 values < 10 μg/mL were considered active and the molecules that showed IC50 values > 10 μg/mL were considered inactive. The number of latent variables (LV) as well as the original value of the variables was selected using a graph of coefficients together with a graph that responds for each PLS com- ponent; the variation explained in the inflow ($R^2$) and the variation explained in forecast ($Q^2$) cv; cross-validation performed by LOO. The model with the highest cross-validation correlation based on the coefficient value ($Q^2$ cv) was selected.

## 8. Conclusions

Based on the literature review, it is possible to state that the class of chalcones that presents inhibitory activity against several cancer strains can be attributed to natural and synthetic chalcones. In addition, it was observed that the chalcone flavokawain B showed a high potential for cell inhibition in two cell lines, presenting multi-target potential. Another important point is the low toxicity reported in this class of compounds.

**Supplementary Materials:** The following supporting information can be downloaded at: https:// www.mdpi.com/article/10.3390/molecules28104009/s1. Table S1: Anticancer activity of chalcone-like compounds for various types of cancer with their respective cell lineage.

**Author Contributions:** Conceptualization: F.F.L., L.S. and N.F.d.S.; Methodology: F.F.L., M.T.S., L.C.R., M.D.L.F., J.M.B.F., F.J.B.M.-J., L.S. and N.F.d.S.; validation, R.O.d.M. and M.T.S.; writing—original draft preparation: F.F.L., N.F.d.S., B.H.M.d.O. and G.D.D.; writing—review and editing; M.T.S., L.S., R.O.d.M., L.C.R., J.M.B.F. and F.J.B.M.-J.; supervision: M.T.S., L.S., J.M.B.F., F.J.B.M.-J. and L.C.R., funding: M.T.S., L.S., J.M.B.F. and F.J.B.M.-J. All authors have read and agreed to the published version of the manuscript.

**Funding:** Coordination of Improvement of Higher Education Personnel—Brazil (CAPES)—Finance Code 001. This work was partially supported by the Conselho Nacional de Desenvolvimento Científico e Tecnológico (CNPq), grant numbers #431254/2018-4, #309648/2019-0, #308590/2017-1, and #306798/2020-4. The APC was funded by FAPESQ, funding No. 04/2022—Apoio ao Desenvolvi- mento Científico e Tecnológico do Estado da Paraíba—grant number #3783/2022-0, Paraíba State Research Foundation (FAPESQ).

**Institutional Review Board Statement:** Not applicable.

**Informed Consent Statement:** Not applicable.

**Data Availability Statement:** Not applicable.

**Acknowledgments:** Coordination of Improvement of Higher Education Personnel—Brazil (CAPES)— Financing Code 001 and Conselho Nacional de Desenvolvimento Científico e Tecnológico (CNPq), grant numbers grant numbers #431254/2018-4, #309648/2019-0, #308590/2017-1, and #306798/2020-4.

**Conflicts of Interest:** The authors declare no conflict of interest.

**Sample Availability:** Not applicable.

## References

1. Neto, R.A.d.M.; Santos, C.B.R.; Henriques, S.V.C.; Machado, L.d.O.; Cruz, J.N.; da Silva, C.H.T.d.P.; Federico, L.B.; de Oliveira, E.H.C.; de Souza, M.P.C.; da Silva, P.N.B. Novel Chalcones Derivatives with Potential Antineoplastic Activ- ity Investigated by Docking and Molecular Dynamics Simulations. *J. Biomol. Struct. Dyn.* **2022**, *40*, 2204–2216.

[CrossRef] [PubMed]
2. Helmy, M.T.; Sroor, F.M.; Mahrous, K.F.; Mahmoud, K.; Hassaneen, H.M.; Saleh, F.M.; Abdelhamid, I.A.; Mohamed Teleb, M.A. Anticancer Activity of Novel 3-(Furan-2-yl) Pyrazolyl and 3-(Thiophen-2-yl) Pyrazolyl Hybrid Chalcones: Synthesis and *In Vitro* Studies. *Arch. Pharm.* **2022**, *355*, 2100381. [CrossRef] [PubMed]
3. Rioux, B.; Pouget, C.; Ndong-Ntoutoume, G.M.A.; Granet, R.; Gamond, A.; Laurent, A.; Pinon, A.; Champavier, Y.; Liagre, B.; Fagnère, C. Enhancement of Hydrosolubility and *In Vitro* Antiproliferative Properties of Chalcones Following Encapsulation into β-Cyclodextrin/Cellulose-Nanocrystal Complexes. *Bioorganic Med. Chem. Lett.* **2019**, *29*, 1895–1898. [CrossRef]
4. Escribano-Ferrer, E.; Queralt Regue, J.; Garcia-Sala, X.; Boix Montanes, A.; Lamuela-Raventos, R.M. In Vivo Anti-Inflammatory and Antiallergic Activity of Pure Naringenin, Naringenin Chalcone, and Quercetin in Mice. *J. Nat. Prod.* **2019**, *82*, 177–182. [CrossRef]
5. Alaaeldin, R.; Mustafa, M.; Abuo-Rahma, G.E.A.; Fathy, M. *In Vitro* Inhibition and Molecular Docking of a New Ciprofloxacin- chalcone against SARS-CoV-2 Main Protease. *Fundam. Clin. Pharmacol.* **2022**, *36*, 160–170. [CrossRef]
6. Durairaju, P.; Umarani, C.; Periyasami, G.; Vivekanand, P.A.; Rahaman, M. Synthesis and *In Vitro* Antimicrobial Evaluation of Photoactive Multi—Block Chalcone Conjugate Phthalimide and 1, 8-Naphthalimide Novolacs. *Polymers* **2021**, *13*, 1859. [CrossRef] [PubMed]
7. Noser, A.A.; Shehadi, I.A.; Abdelmonsef, A.H.; Salem, M.M. Newly Synthesized Pyrazolinone Chalcones as Anticancer Agents via Inhibiting the PI3K/Akt/ERK1/2 Signaling Pathway. *ACS Omega* **2022**, *7*, 25265–25277. [CrossRef] [PubMed]
8. Aktar, W.; Sengupta, D.; Chowdhury, A. Impact of Pesticides Use in Agriculture: Their Benefits and Hazards. *Interdiscip. Toxicol.* **2009**, *2*, 1–12. [CrossRef]
9. Silva, P.T.; Lopes, P.T.; Xavier, L.M.A.; Carvalho, M.C.S.; Moraes, M.O.; Pessoa, C.; Barros, F.W.A.; Bandeira, P.N.; Cavalvante, C.S.P.; Teixeira, A.M.R. Atividade Citotóxica e Antifúngica de Chalconas Sintetizadas a Partir de Uma Acetofenona Natural Isolada de Croton Anisodontus. *Rev. Virtual Quim.* **2020**, *12*, 712–723.
10. Alman, A.A.; Daniel, K.; Killedar, S.G. Chalcone-Promising Entity for Anticancer Activity: An Overview. *Int. J. Pharm. Sci. Res* **2020**, *11*, 2027–2041.
11. Constantinescu, T.; Lungu, C.N. Anticancer Activity of Natural and Synthetic Chalcones. *Int. J. Mol. Sci.* **2021**, *22*, 11306. [CrossRef]
12. Dandawate, P.; Ahmed, K.; Padhye, S.; Ahmad, A.; Biersack, B. Anticancer Active Heterocyclic Chalcones: Recent Developments. *Anti-Cancer Agents Med. Chem.* **2021**, *21*, 558–566. [CrossRef] [PubMed]
13. Phang, C.-W.; Abd Malek, S.N.; Karsani, S.A. Flavokawain C Exhibits Anti-Tumor Effects on In Vivo HCT 116 Xenograft and Identification of Its Apoptosis-Linked Serum Biomarkers via Proteomic Analysis. *Biomed. Pharmacother.* **2021**, *137*, 110846. [CrossRef]
14. World Health Organization (WHO). CANCER. Available online: https://www.who.int/health-topics/cancer#tab=tab_1 (ac- cessed on 23 February 2023).
15. World Health Organization. Cancer Burden Rise to 18.1 Million New

Cases and 9.6 Million Cancer Deaths in 2018. *Int. Agency Res. Cancer* **2018**, *2018*, 3.
16. Dos Santos, M.B.; Bertholin Anselmo, D.; de Oliveira, J.G.; Jardim-Perassi, B.V.; Alves Monteiro, D.; Silva, G.; Gomes, E.; Lucia Fachin, A.; Marins, M.; de Campos Zuccari, D.A.P. Antiproliferative Activity and P53 Upregulation Effects of Chalcones on Human Breast Cancer Cells. *J. Enzym. Inhib. Med. Chem.* **2019**, *34*, 1093–1099. [CrossRef] [PubMed]
17. Saquib, M.; Baig, M.H.; Khan, M.F.; Azmi, S.; Khatoon, S.; Rawat, A.K.; Dong, J.J.; Asad, M.; Arshad, M.; Hussain, M.K. Design and Synthesis of Bioinspired Benzocoumarin-Chalcones Chimeras as Potential Anti-Breast Cancer Agents. *ChemistrySelect* **2021**, *6*, 8754–8765. [CrossRef]
18. Dallavalle, S.; Dobricˇic´, V.; Lazzarato, L.; Gazzano, E.; Machuqueiro, M.; Pajeva, I.; Tsakovska, I.; Zidar, N.; Fruttero, R. Improvement of Conventional Anti-Cancer Drugs as New Tools against Multidrug Resistant Tumors. *Drug Resist. Updat.* **2020**, *50*, 100682. [CrossRef] [PubMed]
19. Ouyang, Y.; Li, J.; Chen, X.; Fu, X.; Sun, S.; Wu, Q. Chalcone Derivatives: Role in Anticancer Therapy. *Biomolecules* **2021**, *11*, 894. [CrossRef]
20. Shukla, S.; Sood, A.K.; Goyal, K.; Singh, A.; Sharma, V.; Guliya, N.; Gulati, S.; Kumar, S. Chalcone Scaffolds as Anticancer Drugs: A Review on Molecular Insight in Action of Mechanisms and Anticancer Properties. *Anti-Cancer Agents Med. Chem.* **2021**, *21*, 1650–1670. [CrossRef]
21. Mastachi-Loza, S.; Ramírez-Candelero, T.I.; Benítez-Puebla, L.J.; Fuentes-Benítes, A.; González-Romero, C.; Vázquez, M.A. Chalcones, a Privileged Scaffold: Highly Versatile Molecules in [4+2] Cycloadditions. *Chem. Asian J.* **2022**, *17*, e202200706. [CrossRef]
22. Rani, A.; Anand, A.; Kumar, K.; Kumar, V. Recent Developments in Biological Aspects of Chalcones: The Odyssey Continues. *Expert Opin. Drug Discov.* **2019**, *14*, 249–288. [CrossRef]
23. de Souza, P.S.; Bibá, G.C.C.; Melo, E.D.d.N.; Muzitano, M.F. Chalcones against the Hallmarks of Cancer: A Mini-Review. *Nat. Prod. Res.* **2021**, *36*, 4803–4820. [CrossRef] [PubMed]
24. Elkanzi, N.A.A.; Hrichi, H.; Alolayan, R.A.; Derafa, W.; Zahou, F.M.; Bakr, R.B. Synthesis of Chalcones Derivatives and Their Biological Activities: A Review. *ACS Omega* **2022**, *7*, 27769–27786. [CrossRef] [PubMed]
25. Leonte, D.; Coman, F.-M.; Fotso, G.W.; Ngadjui, B.T.; Zaharia, V.; Ngameni, B. Heterocycles 49. Synthesis, Chemical Behaviour and Biological Properties of Heterocyclic Chalcones. Review from Our Research. *Farmacia* **2021**, *69*, 821–836. [CrossRef]
26. Yadav, G.D.; Wagh, D.P. Claisen-Schmidt Condensation Using Green Catalytic Processes: A Critical Review. *ChemistrySelect* **2020**, *5*, 9059–9085. [CrossRef]
27. Liu, B.; Zhao, D.; Xu, D.; Xu, Z. Facile Aldol Reaction between Unmodified Aldehydes and Ketones in Bronsted Acid Ionic Liquids. *Chem. Res. Chinese Univ.* **2007**, *23*, 549–553. [CrossRef]
28. Josephs, S.F.; Ichim, T.E.; Prince, S.M.; Kesari, S.; Marincola, F.M.; Escobedo, A.R.; Jafri, A. Unleashing Endogenous TNF-Alpha as a Cancer Immunotherapeutic. *J. Transl. Med.* **2018**, *16*, 242. [CrossRef]
29. Cruceriu, D.; Baldasici, O.; Balacescu, O.; Berindan-Neagoe, I. The Dual Role of Tumor Necrosis Factor-Alpha (TNF-α) in Breast Cancer: Molecular Insights and Therapeutic Approaches. *Cell. Oncol.* **2020**, *43*, 1–18.

[CrossRef]
30. Koh, J.-J.; Lin, S.; Aung, T.T.; Lim, F.; Zou, H.; Bai, Y.; Li, J.; Lin, H.; Pang, L.M.; Koh, W.L.; et al. Amino Acid Modified Xanthone Derivatives: Novel, Highly Promising Membrane-Active Antimicrobials for Multidrug-Resistant Gram-Positive Bacterial Infections. *J. Med. Chem.* **2015**, *58*, 739–752. [CrossRef]
31. Verza, F.A.; Das, U.; Fachin, A.L.; Dimmock, J.R.; Marins, M. Roles of Histone Deacetylases and Inhibitors in Anticancer Therapy. *Cancers* **2020**, *12*, 1664. [CrossRef]
32. Rashid, H.U.; Xu, Y.; Ahmad, N.; Muhammad, Y.; Wang, L. Promising Anti-Inflammatory Effects of Chalcones via Inhibition of Cyclooxygenase, Prostaglandin E2, Inducible NO Synthase and Nuclear Factor Kb Activities. *Bioorganic Chem.* **2019**, *87*, 335–365. [CrossRef] [PubMed]
33. Mohammed, H.H.H.; Abd El-Hafeez, A.A.; Ebeid, K.; Mekkawy, A.I.; Abourehab, M.A.S.; Wafa, E.I.; Alhaj-Suliman, S.O.; Salem, A.K.; Ghosh, P.; Abuo-Rahma, G.E.-D.A. New 1, 2, 3-Triazole Linked Ciprofloxacin-Chalcones Induce DNA Damage by Inhibiting Human Topoisomerase I& II and Tubulin Polymerization. *J. Enzym. Inhib. Med. Chem.* **2022**, *37*, 1346–1363.
34. Păuș escu, I.; Kántor, I.; Babos, G.; May, Z.; Fodor-Kardos, A.; Miskolczy, Z.; Biczók, L.; Péter, F.; Medeleanu, M.; Feczkó, T. Halochromic Behavior and Anticancer Effect of New Synthetic Anthocyanidins Complexed with β-Cyclodextrin Derivatives. *Int. J. Mol. Sci.* **2022**, *23*, 8103. [CrossRef] [PubMed]
35. Palko-Łabuz, A.; Kostrzewa-Susłow, E.; Janeczko, T.; S´roda-Pomianek, K.; Poła, A.; Uryga, A.; Michalak, K. Cyclization of Flavokawain B Reduces Its Activity against Human Colon Cancer Cells. *Hum. Exp. Toxicol.* **2020**, *39*, 262–275. [CrossRef] [PubMed]
36. Lukovic´, J.; Mitrovic´, M.; Popovic´, S.; Milosavljevic´, Z.; Stanojevic´-Pirkovic´, M.; And¯elkovic´, M.; Zelen, I.; Šorak, M.; Muškinja, J.; Ratkovic´, Z. Antitumor Effects of Vanillin Based Chalcone Analogues *In Vitro*. *Acta Pol. Pharm. Res.* **2020**, *77*, 57–67. [CrossRef]
37. Al-Hamashi, A.A.; Koranne, R.; Dlamini, S.; Alqahtani, A.; Karaj, E.; Rashid, M.S.; Knoff, J.R.; Dunworth, M.; Pflum, M.K.H.; Casero Jr, R.A. A New Class of Cytotoxic Agents Targets Tubulin and Disrupts Microtubule Dynamics. *Bioorganic Chem.* **2021**, *116*, 105297. [CrossRef]
38. Mphahlele, M.J.; Gildenhuys, S.; Agbo, E.N. *In Vitro* Evaluation and Docking Studies of 5-Oxo-5H-Furo [3, 2-g] Chromene-6- Carbaldehyde Derivatives as Potential Anti-Alzheimer's Agents. *Int. J. Mol. Sci.* **2019**, *20*, 5451. [CrossRef]
39. Sherikar, A.S.; Bhatia, M.S.; Dhavale, R.P. Identification and Investigation of Chalcone Derivatives as Calcium Channel Blockers: Pharmacophore Modeling, Docking Studies, *In Vitro* Screening, and 3D-QSAR Analysis. *Curr. Comput. Aided. Drug Des.* **2021**, *17*, 676–686. [CrossRef]
40. El-Wakil, M.H.; Khattab, S.N.; El-Yazbi, A.F.; El-Nikhely, N.; Soffar, A.; Khalil, H.H. New Chalcone-Tethered 1, 3, 5-Triazines Potentiate the Anticancer Effect of Cisplatin against Human Lung Adenocarcinoma A549 Cells by Enhancing DNA Damage and Cell Apoptosis. *Bioorganic Chem.* **2020**, *105*, 104393. [CrossRef]
41. Kumar, K.S.; Kotra, V.; Kola, P.K.; Devi, C.H.B.P.; Anusha, N.; Babu, B.H.;

Adil, S.F.; Shaik, M.R.; Khan, M.; Al-Warthan, A. $ZnCl_2$ Catalyzed New Coumarinyl-Chalcones as Cytotoxic Agents. *Saudi J. Biol. Sci.* **2021**, *28*, 386–394. [CrossRef]

42. Hseu, Y.; Huang, Y.; Thiyagarajan, V.; Mathew, D.C.; Lin, K.; Chen, S.; Liu, J.; Hsu, L.; Li, M.; Yang, H. Anticancer Activities of Chalcone Flavokawain B from Alpinia Pricei Hayata in Human Lung Adenocarcinoma (A549) Cells via Induction of Reactive Oxygen Species-mediated Apoptotic and Autophagic Cell Death. *J. Cell. Physiol.* **2019**, *234*, 17514–17526. [CrossRef] [PubMed]
43. Wang, M.; Liu, Z.; Huang, X.; Chen, Y.; Wang, Y.; Kong, J.; Yang, Y.; Yu, C.; Li, J.; Wang, X. Dual-Target Platinum (IV) Complexes Exhibit Antiproliferative Activity through DNA Damage and Induce ER-Stress-Mediated Apoptosis in A549 Cells. *Bioorganic Chem.* **2021**, *110*, 104741. [CrossRef] [PubMed]
44. Fathi, E.M.; Sroor, F.M.; Mahrous, K.F.; Mohamed, M.F.; Mahmoud, K.; Emara, M.; Elwahy, A.H.M.; Abdelhamid, I.A. Design, Synthesis, *In Silico* and *In Vitro* Anticancer Activity of Novel Bis-Furanyl-Chalcone Derivatives Linked through Alkyl Spacers. *ChemistrySelect* **2021**, *6*, 6202–6211. [CrossRef]
45. Bukhari, S.N.A. Synthesis and Evaluation of New Chalcones and Oximes as Anticancer Agents. *RSC Adv.* **2022**, *12*, 10307–10320. [CrossRef]
46. Gaur, R.; Yadav, D.K.; Kumar, S.; Darokar, M.P.; Khan, F.; Singh Bhakuni, R. Molecular Modeling Based Synthesis and Evaluation of *in Vitro* Anticancer Activity of Indolyl Chalcones. *Curr. Top. Med. Chem.* **2015**, *15*, 1003–1012. [CrossRef]
47. Parmar, V.S.; Bracke, M.E.; Vanhoecke, B.W.A.; Derycke, L.; Bolca, S.; Possemiers, S.; Heyerick, A.; Stevens, C.V.; Keukeleire, D.D.; Depypere, H.T. Plant Polyphenolics as Anti-Invasive Cancer Agents. *Anti-Cancer Agents Med. Chem.* **2008**, *8*, 171–185. [CrossRef] [PubMed]
48. Wang, G.; Liu, W.; Gong, Z.; Huang, Y.; Li, Y.; Peng, Z. Design, Synthesis, Biological Evaluation and Molecular Docking Studies of New Chalcone Derivatives Containing Diaryl Ether Moiety as Potential Anticancer Agents and Tubulin Polymerization Inhibitors. *Bioorganic Chem.* **2020**, *95*, 103565. [CrossRef]
49. Guruswamy, D.K.M.; Jayarama, S. Proapoptotic and Anti-Angiogenic Activity of (2E)-3-(2-Bromo-6-Hydroxy-4-Methoxyphenyl)- 1-(Naphthalene-2-Yl) Prop-2-En-1-One in MCF7 Cell Line. *Chem. Pap.* **2020**, *74*, 2229–2237. [CrossRef]
50. Homerin, G.; Nica, A.S.; Farce, A.; Dubois, J.; Ghinet, A. Ultrasounds-Mediated 10-Seconds Synthesis of Chalcones as Potential Farnesyltransferase Inhibitors. *Bioorganic Med. Chem. Lett.* **2020**, *30*, 127149. [CrossRef]
51. Harshitha, K.R.; Sarojini, B.K.; Narayana, B.; Lobo, A.G.; Kalal, B.S. Molecular Docking of 4-Ethoxychalcones on Oxidoreduc- tase/Pirin Inhibitors and Cytotoxic Evaluation on Breast/Skin Cancer Cell Lines. *Lett. Drug Des. Discov.* **2020**, *17*, 1245–1260. [CrossRef]
52. Al-Kaabi, M.M.; Rady Al-Hazam, H.A.; Arwa, H.M. Microwave Assisted Synthesis, Characterization and Biochemical Study of New Chalcones. *Egypt. J. Chem.* **2021**, *64*, 4027–4035. [CrossRef]
53. Mangoud, M.M.; Hussein, M.Z.; El-Bordany, E.A. Design and Synthesis

of Novel Pyrazoles, Pyrazolines, and Pyridines from Chalcone Derivatives with Evaluation of Their *In Vitro* Anticancer Activity Against T-47D and UACC-257 Cell Lines. *Egypt. J. Chem.* **2020**, *63*, 5203–5218.

54. Ahn, S.; Truong, V.N.-P.; Kim, B.; Yoo, M.; Lim, Y.; Cho, S.K.; Koh, D. Design, Synthesis, and Biological Evaluation of Chalcones for Anticancer Properties Targeting Glycogen Synthase Kinase 3 Beta. *Appl. Biol. Chem.* **2022**, *65*, 17. [CrossRef]
55. Rajeswari, K.; Manturthi, S.; Sirisha, K.; Velidandi, A.N. Anchoring and Hydrophobic Nature of Coumarin in Newer Coumarin Based Chalcones: Synthesis, *In Silico*, and *In Vitro* Cell Viability Studies. *Russ. J. Bioorganic Chem.* **2022**, *48*, 636–642. [CrossRef]
56. Kode, J.; Kovvuri, J.; Nagaraju, B.; Jadhav, S.; Barkume, M.; Sen, S.; Kasinathan, N.K.; Chaudhari, P.; Mohanty, B.S.; Gour, J. Synthesis, Biological Evaluation, and Molecular Docking Analysis of Phenstatin Based Indole Linked Chalcones as Anticancer Agents and Tubulin Polymerization Inhibitors. *Bioorganic Chem.* **2020**, *105*, 104447. [CrossRef]
57. Gul, H.I.; Yamali, C.; Gunesacar, G.; Sakagami, H.; Okudaira, N.; Uesawa, Y.; Kagaya, H. Cytotoxicity, Apoptosis, and QSAR Studies of Phenothiazine Derived Methoxylated Chalcones as Anticancer Drug Candidates. *Med. Chem. Res.* **2018**, *27*, 2366–2378. [CrossRef]
58. Mphahlele, M.J.; Maluleka, M.M.; Choong, Y.S.; Monchusi, B.A.; Mbazima, V.G. An *In Vitro* Study of the 5-Methyl-and 5-Bromo/Chloro Substituted 2-Hydroxy-3-Nitrochalcones as α-Glucosidase and/or α-Amylase Inhibitors with Potential Anti- Inflammatory Activity. *Med. Chem. Res.* **2022**, *31*, 2243–2259. [CrossRef]
59. Kudlic̆ková, Z.; Takác̆, P.; Sabolová, D.; Vilková, M.; Baláž, M.; Béres, T.; Mojžiš, J. Novel 1-Methoxyindole-and 2-Alkoxyindole- Based Chalcones: Design, Synthesis, Characterization, Antiproliferative Activity and DNA, BSA Binding Interactions. *Med. Chem. Res.* **2021**, *30*, 897–912. [CrossRef]
60. Del Rosario, H.; Saavedra, E.; Brouard, I.; González-Santana, D.; García, C.; Spínola-Lasso, E.; Tabraue, C.; Quintana, J.; Estévez, F. Structure-Activity Relationships Reveal a 2-Furoyloxychalcone as a Potent Cytotoxic and Apoptosis Inducer for Human U-937 and HL-60 Leukaemia Cells. *Bioorganic Chem.* **2022**, *127*, 105926. [CrossRef]
61. Li, Y.; Sun, Y.; Zhou, Y.; Li, X.; Zhang, H.; Zhang, G. Discovery of Orally Active Chalcones as Histone Lysine Specific Demethylase 1 Inhibitors for the Treatment of Leukaemia. *J. Enzym. Inhib. Med. Chem.* **2021**, *36*, 207–217. [CrossRef]
62. Petrov, O.I.; Ivanova, Y.B.; Gerova, M.S.; Momekov, G.T. Synthesis and Cytotoxicity of New Mannich Bases of 6-[3-(3,4,5- Trimetoxyphenyl)-2-Propenoyl]-2 (3H)-Benzoxazolone. *Lett. Drug Des. Discov.* **2020**, *17*, 512–517. [CrossRef]
63. Insuasty, D.; García, S.; Abonia, R.; Insuasty, B.; Quiroga, J.; Nogueras, M.; Cobo, J.; Borosky, G.L.; Laali, K.K. Design, Synthesis, and Molecular Docking Study of Novel Quinoline-based Bis-chalcones as Potential Antitumor Agents. *Arch. Pharm.* **2021**, *354*, 2100094. [CrossRef] [PubMed]
64. Vrontaki, E.; Melagraki, G.; Voskou, S.; Phylactides, M.S.; Mavromoustakos, T.; Kleanthous, M.; Afantitis, A. Development of a Predictive Pharmacophore Model and a 3D-QSAR Study for an *In Silico* Screening of New Potent Bcr-Abl Kinase Inhibitors. *Mini Rev. Med. Chem.* **2017**, *17*, 188–204. [CrossRef] [PubMed]

65. Mercader, A.G.; Pomilio, A.B. (Iso)Flav(an)Ones, Chalcones, Catechins, and Theaflavins as Anticarcinogens: Mechanisms, Anti-Multidrug Resistance and QSAR Studies. *Curr. Med. Chem.* **2012**, *19*, 4324–4347. [CrossRef]
66. Wang, Y.; Li, L.; Ma, T.; Cheng, X.; Liu, D. Design, Synthesis, and Apoptosis-Promoting Effect Evaluation of Chalcone Derivatives Containing Aminoguanidine Units. *Anti-Cancer Agents Med. Chem.* **2022**, *22*, 2116–2124.
67. Huang, X.; Liu, Z.; Wang, M.; Yin, X.; Wang, Y.; Dai, L.; Wang, H. Platinum (IV) Complexes Conjugated with Chalcone Analogs as Dual Targeting Anticancer Agents: *In Vitro* and In Vivo Studies. *Bioorganic Chem.* **2020**, *105*, 104430. [CrossRef]
68. Mourad, A.A.E.; Mourad, M.A.E.; Jones, P.G. Novel HDAC/Tubulin Dual Inhibitor: Design, Synthesis and Docking Studies of α-Phthalimido-Chalcone Hybrids as Potential Anticancer Agents with Apoptosis-Inducing Activity. *Drug Des. Devel. Ther.* **2020**, *14*, 3111–3130. [CrossRef]
69. Al Zahrani, N.A.; El-Shishtawy, R.M.; Elaasser, M.M.; Asiri, A.M. Synthesis of Novel Chalcone-Based Phenothiazine Derivatives as Antioxidant and Anticancer Agents. *Molecules* **2020**, *25*, 4566. [CrossRef]
70. Sangpheak, K.; Mueller, M.; Darai, N.; Wolschann, P.; Suwattanasophon, C.; Ruga, R.; Chavasiri, W.; Seetaha, S.; Choowongkomon, K.; Kungwan, N. Computational Screening of Chalcones Acting against Topoisomerase IIα and Their Cytotoxicity towards Cancer Cell Lines. *J. Enzym. Inhib. Med. Chem.* **2019**, *34*, 134–143. [CrossRef]
71. Vongdeth, K.; Han, P.; Li, W.; Wang, Q.-A. Synthesis and Antiproliferative Activity of Natural and Non-Natural Polymethoxychal- cones and Polymethoxyflavones. *Chem. Nat. Compd.* **2019**, *55*, 11–17. [CrossRef]
72. Mendanha, D.; Vieira de Castro, J.; Moreira, J.; Costa, B.M.; Cidade, H.; Pinto, M.; Ferreira, H.; Neves, N.M. A New Chalcone Derivative with Promising Antiproliferative and Anti-Invasion Activities in Glioblastoma Cells. *Molecules* **2021**, *26*, 3383. [CrossRef] [PubMed]
73. Custodio, J.M.F.; Moura, A.F.; de Moraes, M.O.; Perez, C.N.; Napolitano, H.B. On the *In Silico* and *In Vitro* Anticancer Activity of Sulfonamide Chalcones: Potential JNKK3 Inhibitors. *New J. Chem.* **2020**, *44*, 3294–3309. [CrossRef]
74. Castaño, L.F.; Quiroga, J.; Abonia, R.; Insuasty, D.; Vidal, O.M.; Seña, R.; Rubio, V.; Puerto, G.; Nogueras, M.; Cobo, J. Synthesis, Anticancer and Antitubercular Properties of New Chalcones and Their Nitrogen-Containing Five-Membered Heterocyclic Hybrids Bearing Sulfonamide Moiety. *Int. J. Mol. Sci.* **2022**, *23*, 12589. [CrossRef] [PubMed]
75. Bhandare, R.R.; Shaik, A.B. Assessment of the Antimicrobial and Antiproliferative Activities of Chloropyrazine-Tethered Pyrimidine Derivatives: *In Vitro*, Molecular Docking, and In-Silico Drug-Likeness Studies. *Appl. Sci.* **2021**, *11*, 10734. [CrossRef]
76. Safwat, G.M.; Hassanin, K.; Mohammed, E.T.; Ahmed, E.K.; Abdel Rheim, M.R.; Ameen, M.A.; Abdel-Aziz, M.; Gouda, A.M.; Peluso, I.; Almeer, R. Synthesis, Anticancer Assessment, and Molecular Docking of Novel Chalcone-Thienopyrimidine Derivatives in HepG2 and MCF-7 Cell Lines. *Oxid. Med. Cell. Longev.* **2021**, *2021*, 4759821. [CrossRef] [PubMed]
77. Liu, W.; He, M.; Li, Y.; Peng, Z.; Wang, G. A Review on Synthetic Chalcone Derivatives as Tubulin Polymerisation Inhibitors.

*J. Enzym. Inhib. Med. Chem.* **2022**, *37*, 9–38. [CrossRef] [PubMed]
78. Egbujor, M.C.; Saha, S.; Buttari, B.; Profumo, E.; Saso, L. Activation of Nrf2 Signaling Pathway by Natural and Synthetic Chalcones: A Therapeutic Road Map for Oxidative Stress. *Expert Rev. Clin. Pharmacol.* **2021**, *14*, 465–480. [CrossRef]
79. Elkhalifa, D.; Alali, F.; Al Moustafa, A.-E.; Khalil, A. Targeting Triple Negative Breast Cancer Heterogeneity with Chalcones: A Molecular Insight. *J. Drug Target.* **2019**, *27*, 830–838. [CrossRef]
80. WalyEldeen, A.A.; El-Shorbagy, H.M.; Hassaneen, H.M.; Abdelhamid, I.A.; Sabet, S.; Ibrahim, S.A. [1,2,4] Triazolo [3,4-a] Isoquinoline Chalcone Derivative Exhibits Anticancer Activity via Induction of Oxidative Stress, DNA Damage, and Apoptosis in Ehrlich Solid Carcinoma-Bearing Mice. *Naunyn-Schmiedebergs Arch. Pharmacol.* **2022**, *395*, 1225–1238. [CrossRef]
81. Islam, M.S.; Al-Majid, A.M.; Azam, M.; Verma, V.P.; Barakat, A.; Haukka, M.; Elgazar, A.A.; Mira, A.; Badria, F.A. Construction of Spirooxindole Analogues Engrafted with Indole and Pyrazole Scaffolds as Acetylcholinesterase Inhibitors. *ACS Omega* **2021**, *6*, 31539–31556. [CrossRef]
82. Cuartas, V.; Aragón-Muriel, A.; Liscano, Y.; Polo-Cerón, D.; del Pilar Crespo-Ortiz, M.; Quiroga, J.; Abonia, R.; Insuasty, B. Anticancer Activity of Pyrimidodiazepines Based on 2-Chloro-4-Anilinoquinazoline: Synthesis, DNA Binding and Molecular Docking. *RSC Adv.* **2021**, *11*, 23310–23329. [CrossRef]
83. Shaik, A.B.; Prasad, Y.R.; Nissankararao, S.; Shahanaaz, S. Synthesis, Biological and Computational Evaluation of Novel 2, 3-Dihydro-2-Aryl-4-(4-Isobutylphenyl)-1, 5-Benzothiazepine Derivatives as Anticancer and Anti-EGFR Tyrosine Kinase Agents. *Anti-Cancer Agents Med. Chem.* **2020**, *20*, 1115–1128. [CrossRef] [PubMed]
84. Rajendran, G.; Bhanu, D.; Aruchamy, B.; Ramani, P.; Pandurangan, N.; Bobba, K.N.; Oh, E.J.; Chung, H.Y.; Gangadaran, P.; Ahn, B.-C. Chalcone: A Promising Bioactive Scaffold in Medicinal Chemistry. *Pharmaceuticals* **2022**, *15*, 1250. [CrossRef] [PubMed]
85. Xiao, J.; Gao, M.; Diao, Q.; Gao, F. Chalcone Derivatives and Their Activities against Drug-Resistant Cancers: An Overview. *Curr. Top. Med. Chem.* **2021**, *21*, 348–362. [CrossRef] [PubMed]
86. Chen, J.; Liu, C.-F.; Rao, G.-W. Progress in the Synthesis, Angiogenesis Activity and Mechanism of Chalcone Derivatives. *Mini. Rev. Org. Chem.* **2020**, *17*, 814–827. [CrossRef]
87. Han, Y.; Dong, W.; Guo, Q.; Li, X.; Huang, L. The Importance of Indole and Azaindole Scaffold in the Development of Antitumor Agents. *Eur. J. Med. Chem.* **2020**, *203*, 112506. [CrossRef]
88. Dhaliwal, J.S.; Moshawih, S.; Goh, K.W.; Loy, M.J.; Hossain, M.S.; Hermansyah, A.; Kotra, V.; Kifli, N.; Goh, H.P.; Dhaliwal, S.K.S. Pharmacotherapeutics Applications and Chemistry of Chalcone Derivatives. *Molecules* **2022**, *27*, 7062. [CrossRef]
89. Abd-Alla, H.I.; Souguir, D.; Radwan, M.O. Genus Sophora: A Comprehensive Review on Secondary Chemical Metabolites and Their Biological Aspects from Past Achievements to Future Perspectives. *Arch. Pharm. Res.* **2021**, *44*, 903–998. [CrossRef]
90. Rout, S.; Mahapatra, R.K. *In Silico* Screening of Novel Inhibitors of M17

Leucine Amino Peptidase (LAP) of Plasmodium Vivax as Therapeutic Candidate. *Biomed. Pharmacother.* **2016**, *82*, 192–201. [CrossRef]
91. Constantinescu, T.; Mihis, A.G. Two Important Anticancer Mechanisms of Natural and Synthetic Chalcones. *Int. J. Mol. Sci.* **2022**, *23*, 11595. [CrossRef]
92. WalyEldeen, A.A.; Sabet, S.; El-Shorbagy, H.M.; Abdelhamid, I.A.; Ibrahim, S.A. Chalcones: Promising Therapeutic Agents Targeting Key Players and Signaling Pathways Regulating the Hallmarks of Cancer. *Chem. Biol. Interact.* **2022**, *369*, 110297. [CrossRef] [PubMed]
93. Othman, E.M.; Fayed, E.A.; Husseiny, E.M.; Abulkhair, H.S. Apoptosis Induction, PARP-1 Inhibition, and Cell Cycle Analysis of Leukemia Cancer Cells Treated with Novel Synthetic 1,2,3-Triazole-Chalcone Conjugates. *Bioorganic Chem.* **2022**, *123*, 105762. [CrossRef]
94. Seba, V.; de Lima, G.G.; Pereira, B.L.; Silva, G.; Reinhardt, L.S.; Arantes, P.R.; Chee, B.S.; Dos Santos, M.B.; França, S.C.; Regasini, L.O.; et al. Development, Characterization and Cell Viability Inhibition of Pva Spheres Loaded with Doxorubicin and 4′-Amino-1-Naphthyl-Chalcone (D14) for Osteosarcoma. *Polymers* **2021**, *13*, 2611. [CrossRef] [PubMed]
95. Gunasekaran, V.; Yuvakkumar, R.; Ganesan, R.; Palapetta, S.C.; Gurusamy, H. Biological Evaluation of Polycyclic Chalcone Based Acrylamides in Human MCF-7 and HeLa Cancer Cell Lines. *Environ. Res.* **2023**, *222*, 115395. [CrossRef]
96. Khan, I.; Ganapathi, T.; Shareef, M.A.; Shaik, A.B.; Akbar, S.; Rajanna, A.; Kamal, A.; Kumar, C.G. One-Pot Synthesis and Biological Evaluation of Arylpropenone Aminochalcone Conjugates as Potential Apoptotic Inducers. *ChemistrySelect* **2019**, *4*, 4672–4678. [CrossRef]
97. Jasim, H.A.; Nahar, L.; Jasim, M.A.; Moore, S.A.; Ritchie, K.J.; Sarker, S.D. Chalcones: Synthetic Chemistry Follows Where Nature Leads. *Biomolecules* **2021**, *11*, 1203. [CrossRef] [PubMed]
98. Michalkova, R.; Kello, M.; Cizmarikova, M.; Bardelcikova, A.; Mirossay, L.; Mojzis, J. Chalcones and Gastrointestinal Cancers: Experimental Evidence. *Int. J. Mol. Sci.* **2023**, *24*, 5964. [CrossRef] [PubMed]
99. Moreira, J.; Almeida, J.; Saraiva, L.; Cidade, H.; Pinto, M. Chalcones as Promising Antitumor Agents by Targeting the P53 Pathway: An Overview and New Insights in Drug-Likeness. *Molecules* **2021**, *26*, 3737. [CrossRef] [PubMed]
100. Gao, F.; Huang, G.; Xiao, J. Chalcone Hybrids as Potential Anticancer Agents: Current Development, Mechanism of Action, and Structure-activity Relationship. *Med. Res. Rev.* **2020**, *40*, 2049–2084. [CrossRef]
101. Montes-González, I.; Alsina-Sánchez, A.M.; Aponte-Santini, J.C.; Delgado-Rivera, S.M.; Durán-Camacho, G.L. Perspectives of Ferrocenyl Chalcones: Synthetic Scaffolds toward Biomedical and Materials Science Applications. *Pure Appl. Chem.* **2019**, *91*, 653–669. [CrossRef]
102. Gangopadhyay, A. Natural Flavans and (Iso) Flavanones with Anticancer Activity: A Review. *Curr. Org. Chem.* **2021**, *25*, 1028–1046. [CrossRef]
103. Mahapatra, D.K.; Bharti, S.K.; Asati, V.; Singh, S.K. Perspectives of Medicinally Privileged Chalcone Based Metal Coordination Compounds for Biomedical Applications. *Eur. J. Med. Chem.* **2019**, *174*, 142–158. [CrossRef] [PubMed]
104. Raj, V.; Aboumanei, M.H.; Rai, A.; Verma, S.P.; Singh, A.K.; Keshari,

A.K.; Saha, S. Pharmacophore and 3d-Qsar Modeling of New 1, 3, 4-Thiadiazole Derivatives: Specificity to Colorectal Cancer. *Pharm. Chem. J.* **2020**, *54*, 12–25. [CrossRef]
105. Lv, Y.; Liu, Z.; Jia, H.; Xiu, Y.; Liu, Z.; Deng, L. Properties of Flavonoids in the Treatment of Bladder Cancer. *Exp. Ther. Med.* **2022**, *24*, 1–19. [CrossRef]
106. Jayashree, B.S.; Nikhil, P.S.; Paul, S. Bioisosterism in Drug Discovery and Development-An Overview. *Med. Chem.* **2022**, *18*, 915–925. [CrossRef] [PubMed]
107. Pasricha, S.; Gahlot, P. Synthetic Strategies and Biological Potential of Coumarin-Chalcone Hybrids: A New Dimension to Drug Design. *Curr. Org. Chem.* **2020**, *24*, 402–438. [CrossRef]
108. Nanjala, C.; Odago, W.O.; Rono, P.C.; Waswa, E.N.; Mutinda, E.S.; Oulo, M.A.; Muema, F.W.; Wanga, V.O.; Mkala, E.M.; Kuja, J. A Review on Ethnobotany, Phytochemistry, and Pharmacology of the Genus *Didymocarpus* Wall. (Gesneriaceae). *J. Ethnopharmacol.* **2022**, *295*, 115404. [CrossRef]
109. Celentano, A.; Tran, A.; Testa, C.; Thayanantha, K.; Tan-Orders, W.; Tan, S.; Syamal, M.; McCullough, M.J.; Yap, T. The Protective Effects of Kava (Piper Methysticum) Constituents in Cancers: A Systematic Review. *J. Oral Pathol. Med.* **2019**, *48*, 510–529. [CrossRef]
110. Hosseinzadeh, E.; Hassanzadeh, A.; Marofi, F.; Alivand, M.R.; Solali, S. Flavonoid-Based Cancer Therapy: An Updated Review. *Anti-Cancer Agents Med. Chem.* **2020**, *20*, 1398–1414. [CrossRef]
111. Hassan, S.T.S.; Šudomová, M. Molecular Mechanisms of Flavonoids against Tumor Gamma-Herpesviruses and Their Correlated Cancers—A Focus on EBV and KSHV Life Cycles and Carcinogenesis. *Int. J. Mol. Sci.* **2022**, *24*, 247. [CrossRef]
112. Chan, E.W.C.; Wong, S.K.; Tangah, J.; Inoue, T.; Chan, H.T. Phenolic Constituents and Anticancer Properties of Morus Alba (White Mulberry) Leaves. *J. Integr. Med.* **2020**, *18*, 189–195. [CrossRef]
113. Maria Pia, G.D.; Sara, F.; Mario, F.; Lorenza, S. Biological Effects of Licochalcones. *Mini Rev. Med. Chem.* **2019**, *19*, 647–656. [CrossRef] [PubMed]
114. Kumar, V.; Dhawan, S.; Girase, P.S.; Awolade, P.; Shinde, S.R.; Karpoormath, R.; Singh, P. Recent Advances in Chalcone-Based Anticancer Heterocycles: A Structural and Molecular Target Perspective. *Curr. Med. Chem.* **2021**, *28*, 6805–6845. [CrossRef] [PubMed]
115. Wang, D.; Liang, J.; Zhang, J.; Wang, Y.; Chai, X. Natural Chalcones in Chinese Materia Medica: Licorice. *Evid.-Based Complement. Altern. Med.* **2020**, *2020*, 3821248. [CrossRef] [PubMed]
116. Michalkova, R.; Mirossay, L.; Gazdova, M.; Kello, M.; Mojzis, J. Molecular Mechanisms of Antiproliferative Effects of Natural Chalcones. *Cancers* **2021**, *13*, 2730. [CrossRef] [PubMed]
117. Hacker, M. Adverse Drug Reactions. In *Pharmacology*; Elsevier: Amsterdam, The Netherlands, 2009; pp. 327–352.
118. hemAxon Ltd. ChemAxon Marvin Sketch 22.13. 2022. Available online: https://chemaxon.com/ (accessed on 10 January 2023).
119. *USFC Modeller 9.20—Program for Comparative Protein Structure Modelling by Satisfaction of Spatial Restraints*; University of California San Francisco: San Francisco, CA, USA, 2020.
120. Cruciani, G.; Crivori, P.; Carrupt, P.A.; Testa, B. Molecular Fields in Quantitative Structure-Permeation Relationships: The VolSurf Approach. *J.*

*Mol. Struct. Theochem* **2000**, *503*, 17–30. [CrossRef]

# CAPÍTULO 3

## *In vitro* and *in silico* evaluation of the anti-leishmania activity of synthetic chalcones

Apesar dos graves problemas de saúde que causa, a Leishmaniose ainda é uma das doenças negligenciadas. Segundo a OMS (2018) cerca de 700 mil a 1milhão de novos, além de 20 a 30 mil mortes são registradas todos os anos. É prevalente em países emergentes como o Brasil. Dentre suas espécies as de maior interesse clínico são a *L.  Leishmania infantum, L. chagasi, L. donovani, L. brasiliensis and L. Amazonenses.*

Na literatura já possuem relatos do uso de chalconas no combate a esses parasitas, apresentando um potencial alternativa aos tratamentos convencionais na terapêutica atual.

Nesse estudo um total de 10 compostos da classe chalcona foram sintetizados e avaliados frente a formas promastigotas e amastigotas de *Leishmania infantum.* Estudos *in sílico* demonstraram fortes interações entre os compostos e os alvos propostos (Trypanotiona redutase e a 14,α-redutase) sugerindo uma via de ação dos compostos. Dos compostos avaliados 6 apresentaram atividade, desses 3 ganharam destaque sendo o composto CP03 considerado o mais promissor.

Esses compostos podem servir de modelo para novos protótipos, afim de potencializar essas interações. Um estudo de mecanismo de ação também pode ser considerado para determinar os alvos *in vitro*.

Qualis Capes: A3

Fatos de Impacto: 2.2

Cite Score: 4.5

Ano vigente 2024

Esse trabalho foi aceito para publicação na revista “Natural Products Research”, onde se encontra na etapa de revisões, como demonstra o email abaixo.

Taylor & Francis
Taylor & Francis Group

Dear FRANCISCO MENDONÇA,

Thank you for submitting your revised manuscript.

| | |
|---|---|
| **Submission ID** | **249160885** |
| **Manuscript Title** | **In vitro and in silico evaluation of the anti-leishmania activity of synthetic chalcones** |
| **Journal** | **Natural Product Research** |

If you made the submission, you can check its progress and make any requested revisions on the Author Portal.

Thank you for submitting your work to our journal.
If you have any queries, please get in touch with GNPL-peerreview@journals.tandf.co.uk.

Kind Regards,
*Natural Product Research* Editorial Office

**_In vitro_ and _in silico_ evaluation of the anti-leishmania activity of synthetic chalcones**

Fernando Ferreira Leite [a], Luis Cezar Rodrigues[b], Bruno Hanrry Melo de Oliveira[a], Gabrielly Diniz Duarte[b], Maria Denise Leite Ferreira[a], Natália Ferreira de Sousa [a], Shayenne Eduarda Ramos Vanderley [a,c], Leonardo Lima Cardoso [a,c], Tatjana Souza Lima Keesen[a,c], Rodrigo Santos Aquino de Araújo [a,d], Luciana Scotti[a], Marcus Tullius Scotti[a], and Francisco Jaime Bezerra Mendonça-Junior [a,d],*

*[a]Postgraduate Program in Natural and Synthetic Bioactive Products, Federal University of Paraíba, João Pessoa 58051-900, Brazil; [b]Postgraduate Program in Development and Innovation of Drugs and Medicines, Federal University of Paraíba, João Pessoa 58051-900, Brazil; [c]Laboratory of Infectious Disease Immunology of the Department of Cellular and Molecular Biology; Federal University of Paraíba, João Pessoa 58051-900, PB, Brazil; [d] Synthesis and Drug Delivery Laboratory, Department of Biological Sciences, State University of Paraíba, João Pessoa 58071-160, Brazil*

* *Correspondence author: franciscojaime@servidor.uepb.edu.br*

# *In vitro* and *in silico* evaluation of the anti-leishmania activity of synthetic chalcones

**Abstract:** Leishmaniasis is a group of neglected, vector-borne infectious diseases that affect millions of people around the world. The medications available for its treatment, especially in cases of visceral leishmaniasis, are old, outdated and have serious side effects. In this work, 10 chalcones were synthesized and evaluated *in vitro* against promastigotes and axenic amastigotes of *Leishmania infantum*. Compounds CP04 and CP06 were the most promising, presenting respectively $IC_{50}$ values = 13.64 ± 0.25 and 11.19 ± 0.22 µM against promastigotes, and $IC_{50}$ = 18.92 ± 0.05 and 22.42 ± 0.05 µM against axenic amastigotes. Only compound CP04 did not show cytotoxicity against Peripheral Blood Mononuclear Cells (PBMCs). Molecular docking studies carried out with the enzyme's sterol 14-alpha demethylase (CYP-51) (PDB: 3L4D) and trypanothione reductase (PDB: 5EBK) from *L. infantum* evidenced the great affinity of the CP04 for these targets, presenting values Moldock score of -94.0758 and -50.5692 $KJ/mol^{-1}$.

**Keywords:** chalcones, anti-leishmania activity, cytotoxicity, molecular docking, molecular dynamic.

## 1. Introduction

Despite the serious public health problems it causes, leishmaniasis is still one of the neglected diseases. According to the World Health Organization (WHO) (2018), the highest concentration of cases occurs in emerging countries, with highest incidences in Brazil, China, Ethiopia, Eritrea, Kenya and Somalia, where there are records of approximately 0.7 to 1 million new cases. cases, in addition to 20 to 30 thousand deaths annually (Diotallevi et al, 2020). Among the Leishmania species, *Leishmania infantum*, *L. chagasi*, *L. donovani*, *L. brasiliensis* and *L. amazonensis* are those with greatest clinical interest (Mauricio et al, 2018).

Upon entering a human host in its reproductive cycle, the promastigote forms infest defense cells such as neutrophils and macrophages, transforming into amastigotes and becoming immune to the body's defense mechanisms. Cell lysis is caused by massive intracellular reproduction, releasing more amastigotes into the body. The cycle repeats itself causing a generalized infection (Rougeron et al, 2017). As a result, treatment in humans becomes difficult and fighting sandfly transmission is often preferable. The same medications since the late 1940s are still used to combat the parasite, such as pentavalent antimonials and, more recently, amphotericin B. However, in addition to being expensive, these medications are no longer as effective or safe, and have several side effects. collaterals associated with its use are widely known; Furthermore, they provoked natural selection due to extensive use, which led to the emergence of resistant strains of *Leishmania sp.* (Qin et al, 2020; Akbari et al, 2017; Barbosa et al, 2015).

These facts by themselves already demonstrate the need to develop new drug candidates which represent new therapeutic alternatives and demonstrate efficacy and safety in combating these infections (Ortalli et al, 2018; Moreno et al, 2014). One of the strategies that has been widely used to help and direct this

search is through the use of alternative therapeutic targets, preferably exclusive to the parasite, or that present greater selectivity for the parasite, thus reducing its potential toxicity and increasing its selectivity, and in turn its effectiveness (Moreno et al. 2014; Hermoso et al., 2003).

Among the various classes of natural products that have been used as prototypes for the design of new anti-leishmania agents (Rodrigues, 2015), our group is interested in chalcones are chemical compounds which are natural synthesis precursors of some secondary metabolite classes, being structurally constituted by two phenyl rings united through an α,β-unsaturated ketone (Souza et al, 2020; Rosa et al, 2019; Ali et al, 2021), being the 1,3-diaryl-2-propen-1-one (Figure 1) its simplest substructure (Moreno et al., 2014; Passalacqua et al, 2015). They are known as privileged structures due to their extensive pharmacological applications, associated with their affinity to bind to several known molecular targets (Xiang et al, 2023), as well as due to the relative synthetic simplicity, which allows numerous molecular changes to be made to its main skeleton, allowing different classes of derivatives to be obtained (Romagnoli et al, 2009; Zhang et al, 2023).

The anti-leishmania activity of chalcones is widely described in the literature, for example: Lophirone E (Figure 1) presented an $IC_{50}$ of 15.3 μM against promastigotes of *L. infantum* (Pozzetti et al, 2022); Licochalcone A (Figure 1) presented, *in vitro*, $IC_{50}$ values of 3.88 and 12.47 μM against promastigotes of *L. amazonensis* and *L. infantum*, and $IC_{50}$ values of 36.84 and 29.58 μM against amastigotes of the same species. *In vivo*, administered at 50 mg/kg, Licochalcone A was able to reduce the parasite load by 43.67% and 39.81% in the liver and spleen, respectively (Souza et al, 2020); Ortalli et al, 2018 analyzed the anti-leishmania potential of 31 chalcones, of which two stood out (compounds 6 and 16 - Figure 01) as being active against four Leishmania species (*L. donovani*, *L. tropica*, *L. major* and *L. infantum*). Compound 6 presented $IC_{50}$ values lower than 5.2 μM, and compound 16 lower than 13 μM against the promastigotes forms of the four analyzed species. These two compounds also showed anti-amastigote

activity against *L. donovani* with $IC_{50}$ values of 14 μM (compound 6) and 4.5 μM (compound 16).

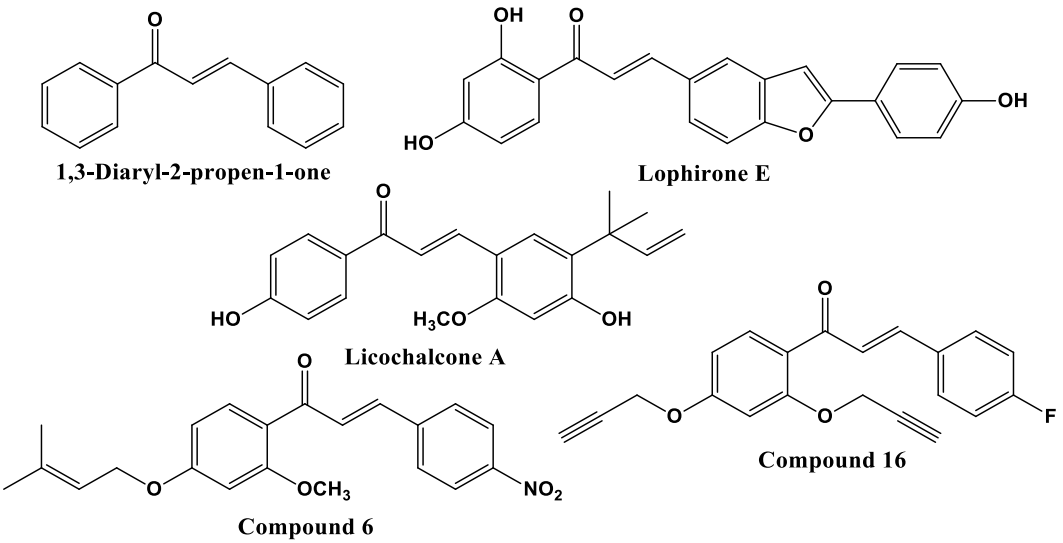


**Figure 1:** Chemical structures of 1,3-diaryl-2-propen-1-one and other chalcone derivatives with anti-leishmania activity.

Although the action mechanism associated with the anti-leishmania activity of chalcones is not fully known, some more recent studies have described the metabolic importance of many essential macromolecules for the protozoan growth and life cycle, which may represent molecular targets to be explored in molecular docking studies (Garcia et al, 2021; Escrivani et al, 2021). Trypanothione reductase (TR) stands out among these important molecular targets, as it is involved in maintaining the redox balance of the parasite cell. It also represents an enzyme specific to trypanosomatids (not present in humans), and is essential in the biochemical pathway for the survival of the parasite (Battista et al, 2020). Inhibition of this enzyme can lead to the accumulation of reactive oxygen species (ROS), causing cellular damage and parasite death, making it a promising target for the development of new treatments (Juan et al, 2021).

Another potential target to be explored is Sterol 14α-demethylase (CYP51). Its inhibition destabilizes the parasite membrane, leading to its death (Lepesheva et al., 2011). This enzyme acts directly on the biosynthesis of ergosterol, an essential component of the parasite's cell membrane, making it a specific therapeutic target. This allows for the development of drugs that affect the parasite but not the human host (Lepesheva et al., 2018). Furthermore, understanding CYP51 (PDB: 3L4D) is crucial for combating drug resistance. CYP51 inhibitors, such as azoles, have demonstrated potential in the treatment of Leishmania infections (Capela et al., 2019).

Considering the importance of this class of natural products such as chalcones, combined with the search for alternative treatments for Leishmaniasis, our group sought to apply the potential of these compounds against forms of the parasite to investigate their anti-leishmanial power.

## 2. Results and discussion

### *2.1. Chemistry*

Claisen-Schmidt condensation was performed between 3,4-methylenedioxyacetophenone and substituted benzaldehydes to synthesize the 10 chalcones of the present work. They were previously prepared according to procedures widely described in the literature (Scheme 1). The compounds had their chemical structures confirmed by Nuclear Magnetic Resonance (NMR) and mass spectrometry (MS).

The $^{1}H$ NMR showed the presence of the carbonyl system conjugated with two doublets (coupling diagnostic signal) with chemical shifts between 7.30 and 7.60 ppm and α,β type constant couplings (*J*) appearing in the range between δH 15.3~15.7 Hz being typical of the *E*-alkene system. A singlet at 6.00 ppm referring to methylenedioxy hydrogens is also observed. Signs of aromatic hydrogens with couplings in *ortho*, *meta* and *para* are also observed according to the pattern of substituents of each aromatic ring.

The $^{13}C$ NMR also confirm the success of the reactions. It was observed at 101 ppm the methylenedioxy carbon. The methoxyl (around 55 ppm), ethyloxyl (around 70 and 15 ppm) and allyloxyl (around 70, 118 and 133 ppm) carbons in their specific regions. The presence of a carbon shifted around 188 ppm, referring to ketone carbonyl, helps confirm the *E* stereochemistry of the alkene (Goyal et al, 2021).

The compounds were obtained in the form of a pale yellow amorphous solid for all compounds, with the exception of CP08 which presented an orange color and CP09 which presented a brownish tone. Yields varied between 87~97%. The purity of all compounds was determined by HPLC and presented values above 95% (spectra in supplementary material).

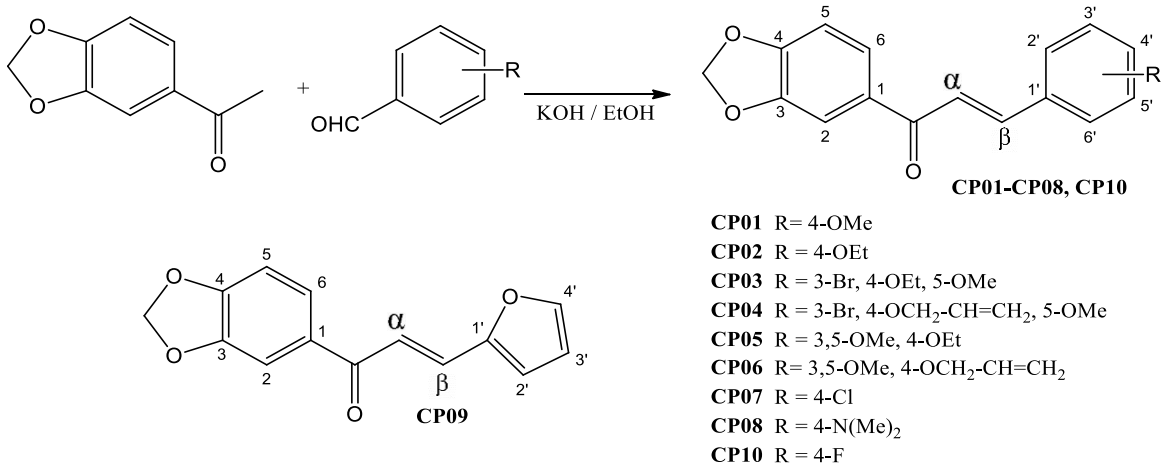


**CP01** R= 4-OMe
**CP02** R = 4-OEt
**CP03** R = 3-Br, 4-OEt, 5-OMe
**CP04** R = 3-Br, 4-$OCH_2$-CH=$CH_2$, 5-OMe
**CP05** R = 3,5-OMe, 4-OEt
**CP06** R= 3,5-OMe, 4-$OCH_2$-CH=$CH_2$
**CP07** R = 4-Cl
**CP08** R = 4-$N(Me)_2$
**CP10** R = 4-F

**Scheme 1:** General synthesis of chalcones via Claisen-Schmidt condensation between 3,4-methylenedioxyacetophenone and benzaldehydes.

### *2.2. Anti-Leishmania activity*

In order to evaluate the anti-leishmania potential of the synthesized compounds, *in vitro* assays against promastigote and axenic amastigote forms *of L. infantum* were carried aou with the aim to determining the inhibitory concentration of 50% ($IC_{50}$) against promastigotes and the effective concentration of 50% ($EC_{50}$) against axenic amastigotes, using amphotericin B as reference drug. $IC_{50}$ corresponds to the potency of the drug to inhibit promastigote forms in

their log phase of growth, thus evaluating the inhibition of parasite growth, while $EC_{50}$ evaluates the cytotoxic power of amastigote forms in their stationary phase, defining the potential of the drug at effective concentrations. A screening was initially performed to evaluate the anti-promastigote activity, in which it was observed that four compounds (CP01, CP02, CP07 and CP08) were inactive, three showed moderate activity (CP05, CP09 and CP10, with $IC_{50}$ values ranging between 39 and 60 µM), and three compounds (CP03, CP04 and CP06) showed good activity ($IC_{50}$ less than 14 µM) (Table 1).

**Table 1.** Inhibitory concentration of 50% ($IC_{50}$) in log phase of growth of *L. infantum* promastigotes and effective concentration of 50% ($EC_{50}$) of axenic amastigotes of *L. infantum* in stationary phase, treated with chalcones.

| Compound | $IC_{50}$ (uM) | $EC_{50}$ (uM) |
|---|---|---|
| CP01 | >1012 | |
| CP02 | >1012 | |
| CP03 | 10.96 ± 0.27 | 62.52 ± 0.05 |
| CP04 | 13.64 ± 0.25 | 18.92 ± 0.05 |
| CP05 | 39.04 ± 0.19 | |
| CP06 | 11.19 ± 0.22 | 22.42 ± 0.05 |
| CP07 | >1012 | |
| CP08 | >1012 | |
| CP09 | 60.48 ± 0.27 | |
| CP10 | 42.21 ± 0.25 | |
| AmpB | 0.31 ± 0.02 | 0.15 ± 0.02 |

Data represent the mean ± SEM of three independent triplicate experiments evaluating growth inhibition of promastigote forms of *L. infantum* ($IC_{50}$) and anti-leishmania potency in stationary forms of axenic amastigotes of *L. infantum* ($EC_{50}$) treated with chalcones and amphotericin B as positive control.

The three most promising compounds (CP03, CP04 and CP06) were evaluated *in vitro* for anti-amastigote activity (Table 1; Graph 1). The CP04 and CP06 chalcones showed cytotoxicity above 75% at concentrations from 126 to 63.30 µM, while CP03 showed the same effect from 126 to 31.60 µM. However, CP04 and CP06 showed a 50% drop in anti-amastigote activity at concentrations between 31.60 and 15.80 µM, respectively, constituting results in agreement with their $EC_{50}$ values, which were 18.92 ± 0.05 µM for CP04 and 22.42 ± 0.05 µM for CP06, thereby showing its potential against the evolutionary form of the parasite which promotes disease in humans.

As expected, Amphotericin B showed great potential for inhibiting amastigotes, showing cytotoxicity against parasites in concentrations from 10 to 0.31 µM (Graph 1), with biological activity against *L. infantum* amastigotes reduced by half in concentrations of 0.15 µM, as indicated by the drug's $EC_{50}$ value of 0.15 ± 0.02 µM.

**Graph 1.** Cell viability percentage of axenic amastigotes treated with CP04, CP03, CP06 and Amphotericin B.

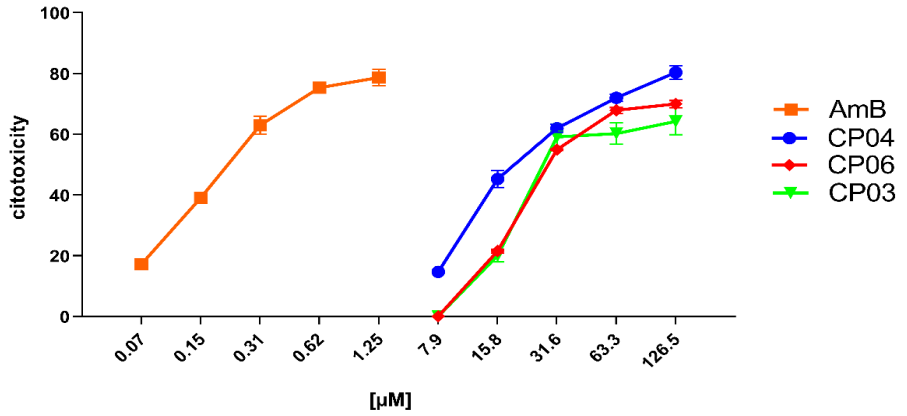


### *2.3. Cytotoxicity on Peripheral Blood Mononuclear Cells (PBMCs) and Red Blood cells*

In order to assess the safety of the most active compounds CP03, CP04 and CP06 compared to amphotericin B (AmpB), *in vitro* cytotoxicity tests were carried out against Peripheral Blood Mononuclear Cells (PBMCs) and Red Blood cells. The results are presented in table 2.

The hemolysis test demonstrated that both the chalcones and AmpB have low cytotoxicity against Red Blood cells. The selectivity indices (SI) observed were greater than 74 for chalcones and greater than 245 for AmpB.

However, the same profile was not observed in PBMCs, where it was observed that the compounds exhibited significant cytotoxicity, especially for CP03 and CP06 even at low concentrations, resulting in SI of 1. Compound CP04 was the only chalcone that presented a safety margin against PBMCs, presenting $CC_{50}$ value of 185.60 µM, and SI of 9.8.

**Table 2.** Compound selectivity index against red blood and Peripheral Blood Mononuclear Cells (PBMCs)

| Compound | *L. infantum* | | Red Blood cells | | PBMC cells | |
|---|---|---|---|---|---|---|
| | $IC_{50}$ (µM) | $EC_{50}$ (µM) | $HC_{50}$ (µM) | SI | $CC_{50}$ (µM) | SI |
| CP03 | 10.96 ± 0.27 | 62.52 ± 0.05 | >1,012 | >92.33 | 62.72 ± 0.05 | 1.00 |
| CP04 | 13.64 ± 0.25 | 18.92 ± 0.05 | >1,012 | >74.19 | 185.6 ± 0.03 | 9.80 |
| CP06 | 11.19 ± 0.22 | 22.42 ± 0.05 | >1,012 | >90.43 | 23.29 ± 0.05 | 1.03 |
| AmpB | 0.13 ± 0.02 | 0.15 ± 0.02 | 58.9 ± 0.14 | 245.41 | 53.88 ± 0.01 | 359.20 |

Data represent mean ± SEM of three independent experiments in triplicate of *L. infantum* promastigotes ($IC_{50}$) and amastigotes ($EC_{50}$) treated with chalcone compounds and amphotericin B as positive control, respectively during 72 and 24 hours of treatment. Red Blood cell citotoxicity ($HC_{50}$) and selectivity indices (SI, $HC_{50}/IC_{50}$). PBMCs cytotoxicity ($CC_{50}$) and selectivity indices (SI, $CC_{50}/EC_{50}$).

### *2.4. Computational chemistry*

*2.4.1. Docking molecular*

Molecular docking simulations were performed with compounds derived from chalcones that showed the best inhibition results of the parasite under study in the *in vitro* test for evaluating their affinity to enzymes related to important survival mechanisms of *L. infantum*, such as Sterol enzyme 14-alpha demethylase (CYP-51) (PDB: 3L4D) and the trypanothione reductase enzyme from *L. infantum* (PDB: 5EBK). Molecular docking results were generated based on the energy value of the MolDock Score algorithm. More negative values indicate better predictions for all scoring functions.

Redocking was performed prior to molecular docking simulations in order to validate the compounds under study. For the proteins under study, the RMSD (Root Mean Square Deviation) values corresponded to: 0.2122 for the PDB ligand Fluconazole complexed to the target CYP-51 (PDB: 3L4D) and 1.5733 for the ligand 6-sec-Butoxy-2-[(3-chlorophenyl)sulfanyl]-4-pyrimidinamine (RDS) complexed to the target Trypanothione Reductase (PDB: 5EBK), and it was observed that all compounds obtained values below the recommended limit (below 2.0 Å), validating the docking simulations performed. The molecular docking simulation results can be viewed in Table 3.

**Table 3.** Affinity values of chalcone derivatives for the enzymes under study according to the MolDock Score algorithm.

| Compound | CYP-51 (PDB: 3L4D) | Trypanothione Reductase (PDB: 5EBK) |
|---|---|---|
| CP01 | -82.2604 | -28.1816 |
| CP02 | -92.3169 | -20.2976 |
| CP03 | -85.9169 | -45.2721 |
| CP04 | **-94.0758** | **-50.5692** |
| CP05 | -89.5499 | -17.9649 |
| CP06 | -91.2791 | -28.3599 |
| CP07 | -75.0916 | -29.6601 |
| CP08 | -84.5501 | -27.6151 |
| CP09 | -71.7698 | -36.0213 |
| CP10 | -75.2075 | -29.9171 |
| PDB ligand (fluconazole) | -72.482 | -16.29 |

Legend: The most negative energy compound is in bold.

According to the results of the analyzed, the compounds under study obtained negative energies, thus demonstrating that they have the potential to interact with the two 3D structures under study generating stable complexes. Only the CP09 compound did not show a more negative affinity score for the CYP-51 enzyme (PDB: 5RG1) than the PDB ligand, while all the other compounds in the series were considered more potent and demonstrating greater affinity; the CP04 compound presented the highest affinity among the studied compounds corresponding to -94.0758 KJ/mol$^{-1}$, while the PDB ligand fluconazole presented a score of -72.482 KJ/mol$^{-1}$. All 10 compounds derived from chalcones showed a higher affinity for the trypanothione reductase enzyme (PDB: 5EBK) when compared to the PDB ligand, with the CP04 compound presenting the lowest energy -50.5692 KJ/mol$^{-1}$, while the PDB ligand presented a score of -16.19 KJ/mol$^{-1}$. (Figure S30) shows the molecular interaction between the CP04

compound, the PDB ligand fluconazole and the CYP-51 enzyme (PDB: 3L4D), and (Figure S31) shows the molecular interaction between the CP04 compound, the pyridine-derived PDB ligand and the trypanothione reductase enzyme for *L. infantum* (PDB: 5EBK).

Molecular interactions in the CP04 compound present in the methylenedioxy groups were visualized through hydrogen bond interactions via the Tyr 115 residue (1 interaction) and three alkyl and pi-alkyl interactions, which represent hydrophobic interactions resulting from van der Waals bonds (pink dashed line) through the Phe 109 (1 interaction), Leu 126 (1 interaction) and Tyr 115 (1 interaction) residues. The alkyl and pi-alkyl interactions were also visualized in the aromatic rings of the compound through the Ala 286 (1 interaction), Ala 290 (1 interaction), Leu 355 (2 interactions) residues, and additionally 1 hydrogen bond interaction with the Ala 290 residue and a halogen interaction with the Bromine (Br) atom. The allyl group presented three alkyl and pi-alkyl interactions through Val 212 (interaction), Pro 209 (1 interaction) and Met 359 (1 interaction) residues. The last group that interacted with the studied macromolecule corresponded to the methoxy group through the Met 359 (1 interaction), Phe 104 (1 interaction) and Tyr 102 (1 interaction) residues. It is worth mentioning that the CP09 compound presented similar interactions to the PDB ligand fluconazole through alkyl and pi-alkyl interactions of the Ala 290 and Ala 286 residues, as well as through hydrogen bond interactions through the Ala 290 amino acid.

The molecular interaction established between the CP04 compound and the trypanothione reductase enzyme from *L. infantum* (PDB: 5EBK) involved the allyl group, with an alkyl-type interaction being observed with the Trp 21 residue. The second group observed corresponded to the methoxy group through alkyl and pi-alkyl interactions (pink dashed line) through the Leu 17 (1 interaction), Val 53 (1 interaction), Tyr 110 (1 interaction) residues, and additionally, a hydrogen bond interaction was observed through the Gly 49 residue. The third group involved in the interactions corresponded to the Bromine (Br) atom, in which an alkyl-type interaction with the Ile residue 339 and a halogen-type interaction with the Glu 18 residue were observed. It is important to mention that similar interactions were observed between the CP04 test compound and PDB ligand which corresponded to alkyl-type interactions of the Val 53 residue.

### *2.4.2. Molecular Dynamics Simulation*

After analyzing the activity potential of the CP04 test compound against important mechanisms for evaluating anti-leishmania activity, molecular dynamics simulations were conducted with the CP04 compound to evaluate the flexibility of the enzyme and the stability of interactions in the presence of factors such as solvent, ions, pressure and temperature. This information is important because it complements the docking results and allows evaluating whether the compounds remain strongly bound to the studied enzymes in the presence of factors which are found in the host organism. Therefore, the following enzymes were chosen for analysis: CYP-51 (PDB: 3L4D) and trypanothione reductase from *L. infantum* (PDB: 5EBK), since the CP04 test compound showed a higher affinity for these proteins. Then, the RMSD was calculated separately for the Cα atoms of the complexed enzyme and the structures of each ligand.

For the enzyme CYP-51 (PDB: 3L4D) (Figure S32) the RMSD metric of the protein demonstrated that the test compound CP04 (red dashed line) was the most stable compound, when compared to the protein complex (line black) and

the PDB ligand fluconazole (green line), as it presented lower RMSD values, corresponding to 0.3 nm. It is worth noting that the stability of the CYP-51 protein (PDB: 3L4D) is essential to keep compounds bound to the active site. Regarding the binder's RMSD metric (Figure S33), which refers to the compound's ability to resist variations in temperature and pressure conditions, it was observed that the fluconazole control (black line) presented lower RMSD values when compared to compound CP04 (red line). This result can be justified by the fact that the fluconazole compound has a more rigid structure which is composed of three rings that configure the compound as a molecular system with a lower degree of freedom in terms of Cartesian atomic coordinates, which makes it difficult to move the complex, but also reduces structure overlap. Regarding the RMSF metric (Figure S34) in which the fluctuation of amino acids and their contribution to the flexibility of the structure was observed, as this is contributed by values above 0.3, it was noticed that that residues among the amino acids present in the protein at positions 29, 30, 36, 41, 253, 310, 409 and 476 contribute to the conformational change of the protein complexed to the CP04 compound (red dashed line).

For the TR enzyme (PDB: 5EBK) (Figure S35), it was observed that the compound CP4 (red dashed line) presented stability between the period of 20 to 40 ns with RMSD values corresponding to 0.35 nm, with subsequent fluctuation until reaching 0.5 nm. The most stable complex corresponded to the TR protein (black line), as it presented lower RMSD values corresponding to 0.35 nm and the PDB ligand (green line) was the most unstable with RMSD values corresponding to 0.5 nm. For the RMSD of the ligand (Figure S36), a greater stability of the PDB ligand (red line) was observed. showing that it remains in the active site of the enzyme after changes in pressure and temperature conditions. In the RMSF metric (Figure S37) it was observed that among the amino acids present in the protein, those in positions 1, 76 -82, 85, 86, 302, 305, 353, 399-405, 407, 419, 457-462 and 486 contribute to the conformational change of the protein complexed to the CP04 compound (red line).

## 3. Conclusions

This study involved the design, synthesis, and evaluation of a series of chalcone-based compounds as potential anti-leishmania agents, both *in vitro* and *in silico*. Six of the synthesized compounds exhibited activity against *L. infantum* promastigotes, with three compounds (CP03, CP04, and CP06) identified as the most promising. Against *L. infantum* amastigotes CP04 and CP06 showed the highest activity, with $IC_{50}$ values of 18.92 ± 0.05 μM and 22.42 ± 0.05 μM, respectively. The compounds did not demonstrated cytotoxicity against red blood cells, meanwhile only CP04 did not present cytotoxicity against PBMCs with $CC_{50}$ value of 185.60 μM, and SI of 9.8.

Molecular docking studies against two key molecular targets of the parasite, sterol 14-alpha demethylase (CYP-51) (PDB: 3L4D) and trypanothione reductase (PDB: 5EBK), revealed strong affinity of the CP04 molecule for these targets. Significant interactions with several amino acid residues were observed, resulting in Moldock score values of -94.0758 and -50.5692 KJ/mol, which are lower than those of the co-crystallized ligands. Additionally, molecular dynamics simulations demonstrated the high stability of CP04 with these targets, indicating a robust interaction potential.

Our findings underscore the potential of chalcones as candidates for anti-leishmania drugs and highlight CP04 as a particularly promising compound for the design and development of more active chalcone-based analogs for leishmaniasis therapy.

**Supplementary Materials:** The supporting information can be downloaded at: xxxxxxxxxxxxx

**Funding:** This research was funded by Conselho Nacional de Desenvolvimento Científico e Tecnológico (CNPq) from Brazil, grants number #306798/2020-4 and #141683/2019-8. Additionally, this study received financial support from the Coordenação de Aperfeiçoamento de Pessoal de Nível Superior (CAPES) from Brazil, finance code 001; This work was also funded by Paraíba State Research Foundation (FAPESQ) through: Program to Support the Settlement of Young Doctors in Paraíba grant number #150859/2023-6; Funding n° 04/2022, grant 116/2022 —Apoio ao Desenvolvimento Científico e Tecnológico do Estado da Paraíba—grant number #3783/2022-0; and PRONEX/FAPESQ grant number 030/2023.

**Disclosure statement:** No potential conflict of interest was reported by the authors.

## References

Abraham MJ, Murtola T, Schulz R, Páll S, Smith JC, Hess B, 2015. GROMACS: High performance molecular simulations through multi-level parallelism from laptops to supercomputers. SoftwareX. 1:19–25.

Akbari M, Oryan A, Hatam G, 2017. Application of nanotechnology in treatment of leshmaniasis: A Review. Acta Trop. 172:86-90.

Ali M, Khan M, Zaman K, Wadood A, Iqbal M, Alam A, Khan KM. 2021. Chalcones: as potent α-amylase enzyme inhibitors; synthesis, *in vitro*, and *in silico* studies. Med Chem. 17: 903-912.

Almeida FS, Moreira VP, Silva ES, Cardoso LL, 2003. Leishmanicidal Activity of Guanidine Derivatives against *Leishmania infantum*. Trop Med Infect Dis. 8:141.

Barbosa JF, Figueiredo SM, Monteiro FM, 2015. New approaches on Leishmaniasis treatment and prevention: A review of recent patents. Recent Pat Endocr Metab Immune Drug Discov. 9:90-102.

Berendsen HJC, van der Spoel D, van Drunen R, 1995. GROMACS: a message-passing parallel molecular dynamics implementation. Comp Phys Comm. 91(1–3), 43–56.

Battista T, Colotti G, Ilari A, Fiorillo A. 2020. Targeting trypanothione reductase, a key enzyme in the redox trypanosomatid metabolism, to develop new drugs against leishmaniasis and trypanosomiases. Molecules, 25: 1924.

Capela R, Moreira R, Lopes F. 2019. An overview of drug resistance in protozoal diseases. Int J Mol Sci. 20: 5748.

Ciccotti G, Ryckaert J-P. 1986. Molecular dynamics simulation of rigid molecules. Comp Phys Rep. 4(6):346–392.

De Santiago-Silva KM, Bortoleti BTS, Oliveira LN, Maia FLdA, Castro JC, Costa IC, Lazarin DB, Wardell JL, Wardell SMSV, Albuquerque MG. 2022.

Antileishmanial Activity of 4,8-Dimethoxynaphthalenyl Chalcones on Leishmania amazonensis. Antibiotics 11(2022):1402.

Debrabant A, Joshi MB, Pimenta PFP. 2004. Generation of Leishmania Donovani Axenic Amastigotes: Their Growth and Biological Characteristics. Int J Parasit. 34(2):205–217.

Diotallevi A, Buffi G, Ceccarelli M, Neitzke-Abreu HC. 2020. Real-time PCR to differentiate among Leishmania (Viannia) subgenus, Leishmania (Leishmania) infantum and Leishmania (Leishmania) amazonensis: Application on Brazilian clinical samples. Acta Trop. 201:105178.

Escrivani DO, Charlton RL, Caruso MB. 2021. Chalcones identify cTXNPx as a potential antileishmanial drug target. PLoS Neglect Trop Dis. 15(11):9951.

Garcia AR, Oliveira DMP, Jesus JB, Souza AMT. 2021. Identification of chalcone derivatives as inhibitors of *Leishmania infantum* arginase and promising antileishmanial agents. Front Chem. (8):624678.

Guilbert C, James TL. 2008. Docking to RNA via root-mean-square-deviation-driven energy minimization with flexible ligands and flexible targets. J Chem. Inf Model. 48(6):1257-1268.

Gupta O, Pradhan,T Bhatia R, Monga V. 2021. Recent advancements in anti-leishmanial research: Synthetic strategies and structural activity relationships. Eur J Med Chem. 223:113606.

Goyal K, Kaur R, Goyal A, Awasthi R. 2021. Chalcones: A review on synthesis and pharmacological activities. J Appl Pharm Sci. 11(1):001-014.

Hermoso A, Jiménez IA, Mamani ZA, Bazzocchi IL. 2003. Antileishmanial activities of dihydrochalcones from Piper elongatum and synthetic related compounds. Structural requirements for activity. Bioorg Med Chem. 11(18):3975-3980.

Jain K, Verma AK, Mishra PR. 2015. Surface-Engineered Dendrimeric Nanoconjugates for Macrophage-Targeted Delivery of Amphotericin B: Formulation Development and *in Vitro* and in Vivo Evaluation. Antimicrob Agents Chemother. 59:2479–2487.

Juan CA, Pérez de la Lastra JM, Plou FJ, Pérez-Lebeña, E. 2021. The chemistry of reactive oxygen species (ROS) revisited: outlining their role in biological macromolecules (DNA, lipids and proteins) and induced pathologies. Int. J. Mol. Sci. 22: 4642.

Lepesheva GI, Waterman MR. 2011. Sterol 14alpha-Demethylase (CYP51) as a Therapeutic Target for Human Trypanosomiasis and Leishmaniasis. Curr Top Med Chem. 11(16):2060–2071.

Lepesheva GI, Friggeri L, Waterman M R. 2018. CYP51 as drug targets for fungi and protozoan parasites: past, present and future. Parasitol. 145: 1820-1836.

Maiorov VN, Crippen GM. 1994. Significance of root-mean-square deviation in comparing three-dimensional structures of globular proteins. J Mol Biol. 235:625-634.

Maurício IL, Bruschi F, Gradoni Maurício L, Bruschi F, Gradoni L. 2018. Leishmania Taxonomy. In: The Leishmaniases: Old Neglected Tropical Diseases. Springer International Publishing. New York City. USA. pp. 15–30.

Moreno MA, Alonso A, Alcolea PJ, Abramov A. 2014. Tyrosine aminotransferase from *Leishmania infantum*: A new drug target candidate. Int J Parasitol Drugs Resist. 4(3):347-354.

Ortalli M, Ilari A, Colotti G, De Ionna I, Battista T, Bisi A. 2018. Identification of chalcone-based antileishmanial agents targeting trypanothione reductase. Eur J Med Chem. 152:527-541.

Passalacqua TG, Torres FAE, Nogueira CT. 2015. The 2',4'-dihydroxychalcone could be explored to develop new inhibitors against the glycerol-3-phosphate dehydrogenase from Leishmania species. Bioorg Med Chem Lett. 25:3564-3568.

Pozzetti L, Ibba R, Rossi S. 2022. O Taglialatela-Scafati, Total synthesis of the natural chalcone lophirone E, synthetic studies toward benzofuran and indole-based analogues, and investigation of anti-leishmanial activity. Molecules. 27:463.

Qin HL, Zhang ZW, Lekkala R, Alsulami H, Rakesh KP. 2020. Chalcone hybrids as privileged scaffolds in antimalarial drug discovery: A key review. Eur J Med Chem. 193: 112215.

Rodrigues IA, Mazotto AM, Cardoso V, Alves RL. 2015. Natural products: Insights into Leishmaniasis inflammatory response. Mediators Inflamm. 2015:835910.

Romagnoli R, Baraldi PG, Carrion MD, Cruz-Lopez O. 2009. Hybrid α-bromoacryloylamido chalcones. Design, synthesis and biological evaluation. Bioorg Med Chem Lett. 19:2022-2028.

Rosa GP, Seca AML, Barreto MC, Silva AMS. 2019. Chalcones and flavanones bearing hydroxyl and/or methoxyl groups: Synthesis and biological assessments. Appl Sci. 9:2846.

Rougeron V, De Meeûs T, Bañuls AL. 2017. Reproduction in Leishmania: a focus on genetic exchange. Infect Genet Evol. 50:128-132.

Souza JM, Carvalho ÉAA, Candido ACBB. 2020. Licochalcone a exhibits leishmanicidal activity *in vitro* and in experimental model of Leishmania (Leishmania) infantum. Front Vet Sci. 7:527.

Vijayakumar S, and Das P. 2019. Structural, molecular motions, and free-energy landscape of Leishmania sterol-14α-demethylase wild type and drug resistant mutant: A comparative molecular dynamics study. J Biomol Struct Dyn. 37: 1477-1493.

Xiang J, Mlambo R, Shaw I, Seid Y, Shah H, He Y. 2023. Cryopreservation of bioflavonoid-rich plant sources and bioflavonoid-microcapsules: emerging technologies for preserving bioactivity and enhancing nutraceutical applications. Front Nutr. 10:1232129.

World Health Organization. Leishmaniasis. 2018. Available online: http://www.who.int/mediacentre/factsheets/fs375/en/

Zhang Z, Zhang W, Hou ZW, Li P, Wang L. 2023. Electrophilic halospirocyclization of N-benzylacrylamides to access 4-halomethyl-2-azaspiro[4.5]decanes. J Org Chem. 19: 13610-13621.

**Supplementary Material**

# *In vitro* and *in silico* evaluation of the anti-leishmania activity of synthetic chalcones

Fernando Ferreira Leite [1], Luis Cezar Rodrigues[2], Bruno Hanrry Melo de Oliveira[1], Gabrielly Diniz Duarte[2], Maria Denise Leite Ferreira[1], Natália Ferreira de Sousa [1], Shayenne Eduarda Ramos Vanderley[1,3], Leonardo Lima Cardoso[1,3], Tatjana Souza Lima Keesen[1,3], Rodrigo Santos Aquino de Araújo[1,4], Luciana Scotti[1], Marcus Tullius Scotti[1], and Francisco Jaime Bezerra Mendonça-Junior [1,4,*]

*[1] Postgraduate Program in Natural and Synthetic Bioactive Products, Federal University of Paraíba, João Pessoa 58051-900, Brazil;*

*[2] Postgraduate Program in Development and Innovation of Drugs and Medicines, Federal University of Paraíba, João Pessoa 58051-900, Brazil;*

*[3] Laboratory of Infectious Disease Immunology of the Department of Cellular and Molecular Biology; Federal University of Paraíba, João Pessoa 58051-900, PB, Brazil*

*[4] Synthesis and Drug Delivery Laboratory, Department of Biological Sciences, State University of Paraíba, João Pessoa 58071-160, Brazil*

** Correspondence: franciscojaime@servidor.uepb.edu.br*

## Experimental

### 1. Chemical

All chemicals, solvents, and reagents (reagent grade) used were purchased from Sigma-Aldrich (St. Louis, MO, USA) and used without further purification. The reaction was monitored by TLC, run on silica gel-coated aluminum sheets (silica gel 60 GF254, E. Merck, Germany) and revealed by UV light (254 or 365 nm). 1H, 13C Nuclear Magnetic Resonance (NMR) spectra were registered in a Bruker Avance 400 MHz NMR spectrometer in deuterated chloroform. The chemical shifts (δ) are reported in parts per million (ppm) downfield to tetramethylsilane (δ = 0). The coupling constant (J) is expressed in Hertz (Hz). High Resolution Mass Spectra (HRMS) was performed using direct infusion on a micrOTOF II mass spectrometer (Bruker Daltonics, Billerica, MA, USA) containing an electrospray ion (ESI) source to obtain high resolution mass spectra. The parameters applied were as follows: capillary 4.5 kV, ESI in negative mode, final plate offset 500 V, 40 psi nebulizer, dry gas (N2) with a flow rate of 8 mL/min and a temperature of 200 ℃. The mass spectra (m/z 50–1000) were recorded every 2 s.

#### 1.1. Synthesis of 3-bromo-4-hydroxy-5-methoxybenzaldehyde

A solution with glacial acetic acid (100 mL) and bromine (25 mL) was prepared, adding 2 g of vanillin (31-333-CAS-6108306) and left under magnetic stirring for 24 hat room temperature (28-30 °C). A white precipitate was formed by filtering and washing with water and methanol three times, respectively. The solid was then dried at room temperature, with an approximate yield of 98%.

##### 1.1.1. General procedure for etherifications in bromine vanillin, 4-hydroxybenzaldehyde and syringealdehyde

In a 500 mL flask, the respective aldehyde, bromo-vanillin (8.7 mmol, 1 equiv), 4-hydroxybenzaldehyde (31-614-CAS-32142740) (16.4 mmol, 1equiv), and syringealdehyde (31-331-CAS-7026331) (10.1 mmol, 1 equiv) was added and

solubilized in dimethylformamide (DMF), followed by potassium carbonate (4 eq) and finally the methylating (iodomethane, 1 eq), ethylating (bromoethane, 1 equiv) and allylating (allyl bromide, 1 eq) agents, respectively. The reaction medium was left under magnetic stirring for 24 hours at room temperature (28-30 °C), being monitored by Thin Layer Chromatography (TLC). At the end of the reaction, a partition was made with ethyl acetate for 3 times, the organic phase was dried with anhydrous sodium sulfate and rotary evaporated, resulting in the etherified product, with yields ranging from 95 to 98%.

### 1.1.2. General procedure for chalcone synthesis

First, 3,4-methylenedioxyacetophenone (31-614-CAS-31805209) (6.1 mmol, 1 eq) was added in a 500 mL flask and solubilized in ethanol. Then the respective aldehyde (6.1 mmol, 1 eq) was added and finally potassium hydroxide (24.4 mmol, 4 eq). The reaction medium was left under magnetic stirring for 24 hours at room temperature (28-30 °C), being monitored by TLC. A yellow solid was formed. The solid was filtered, washed with ethanol and dried in a desiccator. This process was repeated for all chalcones, with yields ranging from 87 to 97%.

### 1.1.3. Spectral data and physicochemical characteristics of the synthesized compounds

(E)-1-(benzo[d][1,3]dioxol-5-yl)-3-(4-methoxyphenyl)prop-2-en-1-one (CP01) [47]: Yellowish amorphous solid, yield of 95%, Weight 1.63 g (5,78 mmol), melting point 147.1 – 148.0 °C, C17H14O4, mm: 282.09 g/mol, HPLC-UV: 4.36 min/ 96%. 1H NMR (400 MHz, CDCl3) δ 7.75 (d, J = 15.5 Hz, 1H), 7.62 (dd, J = 8.1, 1.7 Hz, 1H), 7.57 (d, J = 8.7 Hz, 2H), 7.51 (d, J = 1.7 Hz, 1H), 7.35 (d, J = 15.5 Hz, 1H), 6.91 (d, J = 8.8 Hz, 2H), 6.87 (d, J = 8.1 Hz, 1H), 6.03 (s, 2H), 3.83 (s, 3H). 13C NMR (101 MHz, CDCl3) δ 188.33, 161.66, 151.59, 148.31, 144.14, 133.32, 130.20, 127.81, 124.54, 119.47, 114.48, 108.49, 107.95, 101.90, 55.47.

(E)-1-(benzo[d][1,3]dioxol-5-yl)-3-(4-ethoxyphenyl)prop-2-en-1-one (CP02): Yellowish amorphous solid, yield of 95%, Weight 1.72 g (5,79 mmol), melting point 125.0 - 126.0 °C; HRMS (ESI-TOF+) C18H17O4, mm: 296.10 g/mol, HPLC-UV: 5.23 min/ 99%, [M+H]+: calcd m/z = 297.1049; found 297.1132; 1H NMR

(400 MHz, CDCl3) δ 7.73 (d, J = 15.5 Hz, 1H), 7.60 (dd, J = 8.2, 1.7 Hz, 1H), 7.54 (d, J = 8.7 Hz, 2H), 7.49 (d, J = 1.7 Hz, 1H), 7.33 (d, J = 15.5 Hz, 1H), 6.88 (d, J = 8.8 Hz, 2H), 6.85 (d, J = 8.1 Hz, 1H), 6.01 (s, 2H), 4.04 (q, J = 7.0 Hz, 2H), 1.40 (t, J = 7.0 Hz, 3H). 13C NMR (101 MHz, CDCl3) δ 188.19, 160.94, 151.42, 148.15, 144.08, 133.20, 130.07, 127.47, 124.38, 119.17, 114.80, 108.34, 107.79, 101.74, 63.57, 14.65.

(E)-1-(benzo[d][1,3]dioxol-5-yl)-3-(3-bromo-4-ethoxy-5-methoxyphenyl)prop-2-en-1-one (CP03) – pale yellow crystals, yield of 87%, Weight 2.14 g (5,30 mmol), melting point 112.6 - 115.2 °C, C19H17BrO5, mm: 404.03 g/mol, HPLC-UV: 6.99 min/ 98%. 1H NMR (400 MHz, CDCl3) δ 7.37 (d, J = 15.5 Hz, 1H), 7.64 (dd, J = 8.2, 1.7 Hz, 1H), 7.52 (d, J = 1.4 Hz, 1H), 7.46 (d, J = 1.9 Hz, 1H), 7.37 (d, J = 15.5 Hz, 1H), 7.05 (d, J = 1.9 Hz, 1H), 6.90 (d, J = 8.1 Hz, 1H), 6.07 (s, 2H), 4.13 (q, J = 7.1 Hz, 2H), 3.91 (s, 3H), 1.43 (t, J = 7.1 Hz, 3H). 13C NMR (101 MHz, CDCl3) δ 187.89, 153.91, 151.81, 148.34, 147.53, 142.61, 132.80, 131.83, 124.80, 124.73, 121.88, 118.63, 111.50, 108.40, 107.93, 101.90, 69.43, 56.19, 15.58.

(E)-3-(4-(allyloxy)-3-bromo-5-methoxyphenyl)-1-(benzo[d][1,3]dioxol-5-yl)prop-2-en-1-one (CP04) - pale yellow crystals, yield of 95%, Weight 2.41 g (5,79 mmol), melting point 123.7 - 125.8 °C; HRMS (ESI-TOF+) C20H17BrO5, mm: 416.03 g/mol, HPLC-UV: 7.04 min/ 92%, [M+H]+: calcd m/z = 417.0259; found 417.0335; 1H NMR (400 MHz, CDCl3) δ 7.62 (d, J = 15.6 Hz, 1H), 7.62 (dd, J = 8.2, 1.7 Hz, 2H), .49 (d, J = 1.6 Hz, 1H), 7.43 (d, J = 1.8 Hz, 1H), 7.34 (d, J = 15.6 Hz, 1H), 7.03 (d, J = 1.9 Hz, 1H), 6.87 (d, J = 8.2 Hz, 1H), 6.11 (ddt, J = 17.2, 10.3, 6.0 Hz, 1H), 6.04 (s, 2H), 5.37 (dq, J = 17.2, 1.5 Hz, 1H), 5.23 (dq, J = 10.4, 1.1 Hz, 1H), 4.57 (dt, J = 6.0, 1.3 Hz, 2H), 3.89 (s, 3H). 13C NMR (101 MHz, CDCl3) δ 187.86, 153.85, 151.84, 148.37, 147.08, 142.54, 133.56, 132.82, 132.04, 124.82, 124.76, 122.00, 118.59, 118.47, 111.54, 108.43, 107.95, 101.93, 74.25, 56.22.

(E)-1-(benzo[d][1,3]dioxol-5-yl)-3-(4-ethoxy-3,5-dimethoxyphenyl)prop-2-en-1-one (CP05) - pale yellow crystals, yield of 87%, Weight 1.89 g (5,30 mmol), melting point 131.0 – 133.0 °C; HRMS (ESI-TOF+) C20H21O6, mm: 356.13 g/mol, HPLC-UV: 4.50 min/ 98%, [M+H]+: calcd m/z = 357.1260; found 357.1346; 1H NMR (400 MHz, CDCl3) δ 7.69 (d, J = 15.6 Hz, 1H), 7.63 (dd, J = 8.2, 1.8 Hz,

1H), 7.51 (d, J = 1.8 Hz, 1H), 7.35 (d, J = 15.6 Hz, 1H), 6.88 (d, J = 8.1 Hz, 1H), 6.84 (s, 2H), 6.05 (s, 2H), 4.10 (q, J = 7.1 Hz, 2H), 3.89 (s, 6H), 1.36 (t, J = 7.0 Hz, 3H). 13C NMR (101 MHz, CDCl3) δ 188.36, 153.89, 151.76, 148.38, 144.64, 139.48, 133.13, 130.43, 124.74, 121.02, 108.55, 108.02, 105.76, 101.98, 69.24, 56.34, 15.64.

(E)-3-(4-(allyloxy)-3,5-dimethoxyphenyl)-1-(benzo[d][1,3]dioxol-5-yl)prop-2-en-1-one (CP06) - greenish yellow crystals, yield of 92%, Weight 2.06 g (5,61 mmol), melting point 136.0 – 137.0 °C; HRMS (ESI-TOF+) C21H20O6, mm: 368.13 g/mol, HPLC-UV: 4.66 min/ 91%, [M+H]+: calcd m/z = 369.1260; found 369.1339; 1H NMR (400 MHz, CDCl3) δ 7.60 (d, J = 15.5 Hz, 1H), 7.68 – 7.55 (m, 2H), 7.49 – 7.42 (m, 1H), 7.32 (d, J = 15.5 Hz, 1H), 6.85 – 6.75 (m, 3H), 5.99 (s, 2H), 6.11 – 6.01 (m, 1H), 5.28 (dt, J = 17.2, 1.7 Hz, 1H), 5.15 (dt, J = 10.4, 1.5 Hz, 1H), 5.15 (dt, J = 10.4, 1.5 Hz, 1H), 3.85 (d, J = 2.4 Hz, 8H). 13C NMR (101 MHz, CDCl3) δ 188.12, 153.61, 151.63, 148.22, 144.41, 138.91, 134.17, 132.90, 130.45, 124.62, 120.86, 117.98, 108.33, 107.83, 105.60, 101.86, 74.16, 56.16.

(E)-1-(benzo[d][1,3]dioxol-5-yl)-3-(4-chlorophenyl)prop-2-en-1-one (CP07) - pale yellow crystals, yield of 97%, Weight 1.69 g (5,91 mmol), melting point –97.0 – 98.0 °C, HRMS (ESI-TOF+) C16H12ClO3, mm: 286.04 g/mol, HPLC-UV: 5.91 min/ 97%, [M+H]+: calcd m/z = 287.0469; found 287.0475; 1H NMR (400 MHz, CDCl3) δ 7.75 (d, J = 15.6 Hz, 1H), 7.66 (dd, J = 8.1, 1.8 Hz, 1H), 7.57 (d, J = 8.3 Hz, 1H), 7.54 (d, J = 1.7 Hz, 1H), 7.47 (d, J = 15.6 Hz, 1H), 7.40 (d, J = 8.6 Hz, 1H), 6.91 (d, J = 8.1 Hz, 1H), 6.08 (s, 2H). 13C NMR (101 MHz, CDCl3) δ 188.03, 151.96, 148.48, 142.82, 136.38, 133.61, 132.92, 129.65, 129.33, 124.84, 122.22, 108.50, 108.06, 102.04.

(E)-1-(benzo[d][1,3]dioxol-5-yl)-3-(4-(dimethylamino)phenyl)prop-2-en-1-one (CP08) - pale red crystals, yield of 92%, Weight 1.66 g (5,61 mmol), melting point 91.0 – 93.0 °C; HRMS (ESI-TOF+) C18H17NO3, mm: 295.12 g/mol, HPLC-UV: 4.80 min/ 98%, [M+H]+: calcd m/z = 296.1208; found 296.1311; 1H NMR (400 MHz, CDCl3) δ 7.78 (d, J = 15.4 Hz, 1H), 7.63 (dd, J = 8.2, 1.7 Hz, 1H), 7.54 (d, J = 2.4 Hz, 1H), 7.52 (d, J = 1.7 Hz, 2H), 7.52 (s, 1H), 7.29 (d, J = 15.4 Hz, 1H), 6.87 (d, J = 8.1 Hz, 1H), 6.68 (d, J = 8.9 Hz, 2H), 6.03 (s, 2H), 3.02 (s, 6H). 13C NMR (101 MHz, CDCl3) δ 188.49, 152.06, 151.25, 148.19, 145.34, 133.87, 130.40, 124.27, 122.83, 116.54, 111.92, 108.50, 107.91, 101.81, 40.21.

(E)-1-(benzo[d][1,3]dioxol-5-yl)-3-(thiophen-2-yl)prop-2-en-1-one (CP09) – brownish red crystals, yield of 97%, Weight 1.43 g (5,91 mmol), melting point 101.0 – 103.0 °C; HRMS (ESI-TOF+) C14H11O4, mm: 242.06 g/mol, HPLC-UV: 3.98 min/ 99%, [M+H]+: calcd m/z = 243.0663; found 243.0663; 1H NMR (400 MHz, CDCl3) δ 7.65 (dd, J = 8.2, 1.8 Hz, 1H), 7.57 (d, J = 15.3 Hz, 1H), 7.53 (d, J = 1.7 Hz, 2H), 7.51 (d, J = 1.3 Hz, 1H), 7.40 (d, J = 15.3 Hz, 1H), 6.87 (d, J = 8.2 Hz, 1H), 6.69 (d, J = 3.4 Hz, 1H), 6.50 (dd, J = 3.4, 1.8 Hz, 1H), 6.04 (s, 2H). 13C NMR (101 MHz, CDCl3) δ 187.71, 151.80, 148.40, 140.60, 136.77, 133.00, 131.96, 128.68, 128.42, 124.68, 120.57, 108.46, 108.03, 101.98.

(E)-1-(benzo[d][1,3]dioxol-5-yl)-3-(4-fluorophenyl)prop-2-en-1-one (CP10) - pale yellow crystals, yield of 95%, Weight 1.56 g (5,79 mmol), melting point 118.0 – 120.0 °C; HRMS (ESI-TOF+) C16H12FO3, mm: 270.07 g/mol, HPLC-UV: 4.63 min/ 98%, [M+H]+: calcd m/z = 271.0692; found 271.0769; 1H NMR (400 MHz, CDCl3) δ 7.70 (d, J = 2.0 Hz, 1H), 7.66 (d, J = 15.6 Hz, 1H), 7.63 (d, J = 1.7 Hz, 1H), 7.51 (d, J = 1.8 Hz, 1H), 7.45 (d, J = 15.6 Hz, 1H), 6.89 (d, J = 8.2 Hz, 1H), 6.07 (s, 2H). 13C NMR (101 MHz, CDCl3) δ 187.69, 152.15, 148.57, 141.44, 136.00, 135.20, 134.35, 133.41, 132.70, 131.05, 129.79, 127.60, 124.99, 123.34, 108.52, 108.11, 102.11.

2. Evaluation of anti-leishmania activity

*Leishmania infantum* [IOC/L0579(MHOM/BR/1974/PP75)] were cultured in Schneider's medium (Sigma-Aldrich, Missouri, USA), pH 7.0, supplemented with 20% heat-inactivated fetal bovine serum (Thermo Fisher Scientifics, Massachusetts, USA), 2% male human urine, 100 U/ml penicillin and 100 mg/L streptomycin, and the parasites were maintained at 26 °C. Previously described methods (Debrabant et al, 2004) were used to obtain the extracellular axenic amastigote form of *L. infantum*, which were modified using a Schneider medium readapted to pH 5.5 at 37 °C. The culture of promastigotes in stationary phase was centrifuged, and the medium of these cells was replaced and cells differentiated into axenic amastigotes through changes in temperature and pH of the medium. Parasites were maintained in culture for no more than 20 passages.

The compounds were diluted in dimethyl sulfoxide (DMSO) to produce stock solutions with a concentration of 22 mg/mL. Each stock solution was further diluted in culture medium containing a maximum of 0.5% DMSO (as vehicle control) to obtain the desired drug concentrations for the assays. Amphotericin B (UNIANF®; União Química Farmacêutica Nacional S.A, São Paulo, Brazil), an anti-leishmania drug, was used as a positive control. A stock solution of Amphotericin B (10 mg/mL) was prepared in DMSO.

The promastigotes growth inhibition assay was performed following previously described methods (Almeida et al, 2003). Parasites in the promastigote stage in the exponential growth phase were incubated with various concentrations of the tested compounds (ranging from 1012 to 7.9 μM) and Amphotericin B (AmB) as a positive control (10 to 0.078 μM). The plates were then placed in a biological oxygen demand (B.O.D.) incubator and incubated for 72 h at 26 °C in Schneider's medium (consisting of Schneider's Insect Medium 24.5 g/L, L-glutamine 1.8 g/L, 2 g/L glucose, and 0.4 g/L sodium bicarbonate; Sigma-Aldrich—St. Louis—USA) supplemented with appropriate additives. Growth inhibition was evaluated using an 3-4,5-dimethylthiazol-2-yl)-2,5-diphenyltetrazolium bromide (MTT) assay kit (Amresco, Solon, OH, USA) according to the manufacturer's protocol. After 4 h of incubation, 10% sodium dodecyl sulfate was added to dissolve the formazan crystals, and the absorbance at 540 nm was measured using a plate reader (Biosystems model ELx800; Curitiba, PR, Brazil). The same procedure was followed to evaluate the inhibition of the axenic amastigote form using these compounds, with the following modifications: the treatment time was reduced to 24 hours, and the test temperature was raised to 37 °C, at a pH of 5.5. Three independent experiments were performed in triplicate.

## 3. Evaluation of hemolytic activity in human red blood cells

### 3.1. Ethics Statement

The experiments were conducted in compliance with the relevant laws, institutional guidelines, and ethical standards stipulated in the Declaration of Helsinki. Moreover, all the healthy volunteers provided written informed consent,

and the Ethics Committee at the Federal University of Paraiba, Brazil granted its approval for the study (process number: 2.560.067 and CAAE:82944118.5.0000.5188).

3.2. Evaluation of hemolytic activity

The hemolytic activities of chalcones were evaluated using red blood cells obtained from healthy adult humans (n = 3), according to previously described methods (Jain et al, 2015). In summary, 80 µl of a 5% erythrocyte/phosphate buffered saline (PBS) suspension was mixed with the compounds (in concentrations from 1,012 to 7.9 µM) and AmB (in concentrations from 100 to 0, 78 µM), and then incubated for 1 hour at 37 °C. To stop the hemolysis process, 200 µL of PBS (consisting of 1.5 mM KH2PO4, 8.1 mM Na2HPO4, 136.9 mM NaCl and 2.6 mM KCl, pH 7.2) were added and the samples were centrifuged for 10 minutes at 1000 × g. Supernatants were collected and the hemolysis degree was determined by measuring the absorbance at 540 nm using a spectrophotometer. The hemolysis percentage was calculated as [(Abssam − Abscon)/(Abstot − Abscon) × 100], where Abssam is the absorbance of the sample, Abscon is the absorbance of the blank control (no drugs) and Abstot is the absorbance of hemolysis total (obtained by replacing the sample solution with an equal volume of ultrapure water from Direct-Q UV®, Guyancourt, France).

3.3. Cytotoxicity assay

*In vitro* cytotoxicity was evaluated using peripheral blood mononuclear cells (PBMCs) collected from three healthy volunteers (2 males, mean age 23; and 1 female, age 27). PBMCs were separated through density gradient centrifugation (400× g for 40 min) with Ficoll Paque PLUS (GE Healthcare, USA), and resuspended in RPMI 1640 medium, then supplemented with 10% fetal bovine serum, 1% L-glutamine 200 mM (GE Healthcare, USA) and 1% antibiotic solution (penicillin 5000 Units/mL + streptomycin 5000 µg/mL). After 24 h of treatment, cell viability was evaluated by the colorimetric method based on the tetrazolium dye MTT. The MTT assay was used for *in vitro* cytotoxicity as previously described: cells were exposed to serially diluted concentrations of CP03, CP04, CP06 (1,012 to 7.9 µM), and AmB (100 to 0.78 µM). The plates were kept at 37

°C for 24 h. MTT (5 mg/mL) was added and incubated for 4 h at 37 °C, after which the plates were centrifuged, the supernatant was discarded, and DMSO was added, leaving the plates under stirring to solubilize the formazan salts. Absorbance was measured at 540 nm using a plate reader (ELx800; Curitiba, PR, Brazil). The mean percentage of viable cells was calculated relative to the untreated control.

## 4. Statistical analysis

The GraphPadPrism® software program (version 6.0; San Diego, CA, USA) was used to calculate 50% inhibitory concentration (IC50), 50% effective concentration (EC50) and 50% red blood cell concentration (HC50) and 50% cytotoxic concentration (CC50) values. Non-linear regression (curve fitting) was used for statistical analysis. Unless otherwise specified, assays were conducted in triplicate for three independent experiments. Statistical differences between treatments were evaluated using analysis of variance (ANOVA) with Tukey's post hoc test, and a significance level of 0.05 was considered. The mean ± standard error (SEM) was reported for the data.

## 5. *In silico* study

### 5.1. Molecular Docking

Molecular docking was used to investigate the action mechanism of compounds that contribute to antiviral activity through the binding affinity of compounds to CYP-51 enzymes (PDB: 3L4D) (Hargrove, 2009) and Trypanothione reductase (PDB: 5EBK) (Ciccotti, 1986). The 3D structures of the enzymes were obtained from the Protein Data Bank (PDB) (https://www.rcsb.org/pdb/home/home.do) (Saccoliti et al. 2017; Abraham et al., 2015). The compounds under study were initially prepared. The two composites were drawn using Marvin Sketch v. 19.18 (https://chemaxon.com/marvin) (Berendsen et al, 1995) and saved as .sdf files. Then, the compounds were standardized using Standardizer v. 21.2.0 ChemAxon (https://chemaxon.com/standardizer), in which the addition of

hydrogen atoms, standardization of the aromatic ring, salt removal and structure conversion to 3D were performed. After this step, the compounds under study were subjected to molecular docking in the software Molegro Virtual Docker 6.0 (https://molexus.io/molegro-virtual-docker/), using the definitions of the ligand cocrystallized with the protein to identify the active site. Redocking was performed prior to before molecular docking to validate the procedure.

### 5.2. Molecular Dynamics Simulation

Molecular dynamics simulations were performed to estimate the flexibility of interactions between proteins and ligands using the GROMACS 5.0 software program (European Union Horizon 2020 Program, Sweden) (Abraham et al., 2015, Berendsen et al, 1995). Protein and ligand topologies were also prepared using the GROMOS96 54a7 force field. The MD simulation was carried out using the point charge SPC water model, extended in a cubic box (Bondi, 1964). The system was neutralized by the addition of ions (Cl− and Na+) and minimized to remove poor contacts between complex molecules and the solvent. The system was also balanced at 300K using the 100 ps V-rescale algorithm, represented by NVT (constant number of particles, volume and temperature), followed by equilibration at 1 atm pressure using the Parrinello-Rahman algorithm as the NPT (Constant Pressure and Temperature Particle), up to 100 ps. MD simulations were performed in 5,000,000 steps at 10 ns. Next, the RMSD values of all Cα atoms were calculated relative to the initial structures to determine the flexibility of the structure and whether the complex is stable close to the experimental structure. RMSF values were also analyzed to understand the roles played by residues close to the receptor binding site. The RMSD and RMSF graphs were generated in the Grace software program (Grace Development Team, http://plasma-gate.weizmann.ac.il/Grace/) (Pettersen et al., 2021; Nachbagauer et al., 2021).

**Suplementary References**

Abraham MJ, Murtola T, Schulz R, Páll S, Smith JC, Hess B, 2015. GROMACS: High performance molecular simulations through multi-level parallelism from laptops to supercomputers. SoftwareX. 1:19–25.

Berendsen HJC, van der Spoel D, van Drunen R, 1995. GROMACS: a message-passing parallel molecular dynamics implementation. Comp Phys Comm. 91(1–3), 43–56.

Bondi, A. 1964. Van Der Waals Volumes and Radii. J Phys Chem. 68:441–451.

Nachbagauer R, Feser J, Naficy A, Bernstein DI, Guptill J, Walter EB, Berlanda-Scorza F, Stadlbauer D, Wilson PC, Aydillo T, Behzadi MA, Bhavsar D, Bliss C, Capuano C, Carreño JM, Chromikova V, Claeys C, Coughlan L, Freyn AW, Gast C, Javier A, Jiang K, Mariottini C, McMahon M, McNeal M, Solórzano A, Strohmeier S, Sun W, Van der Wielen M, Innis BL, García-Sastre A, Palese P, Krammer F. 2021. A Chimeric Hemagglutinin-Based Universal Influenza Virus Vaccine Approach Induces Broad and Long-Lasting Immunity in a Randomized, Placebo-Controlled Phase I Trial. Nat Med 27:106–114.

Pettersen EF, Goddard TD, Huang CC, Meng EC, Couch GS, Croll TI, Morris JH, Ferrin TE, 2021. UCSF ChimeraX: Structure Visualization for Researchers, Educators, and Developers. Protein Sci. 30:70–82.

Saccoliti F, Angiulli G, Pupo G, Pescatori L. 2017. Inhibition of *Leishmania Infantum* Trypanothione Reductase by Diaryl Sulfide Derivatives. J. Enzyme Inhib. Med. Chem. 32:304–310.

Figure S*26*: Chalcones synthesized via Claisen condensation.

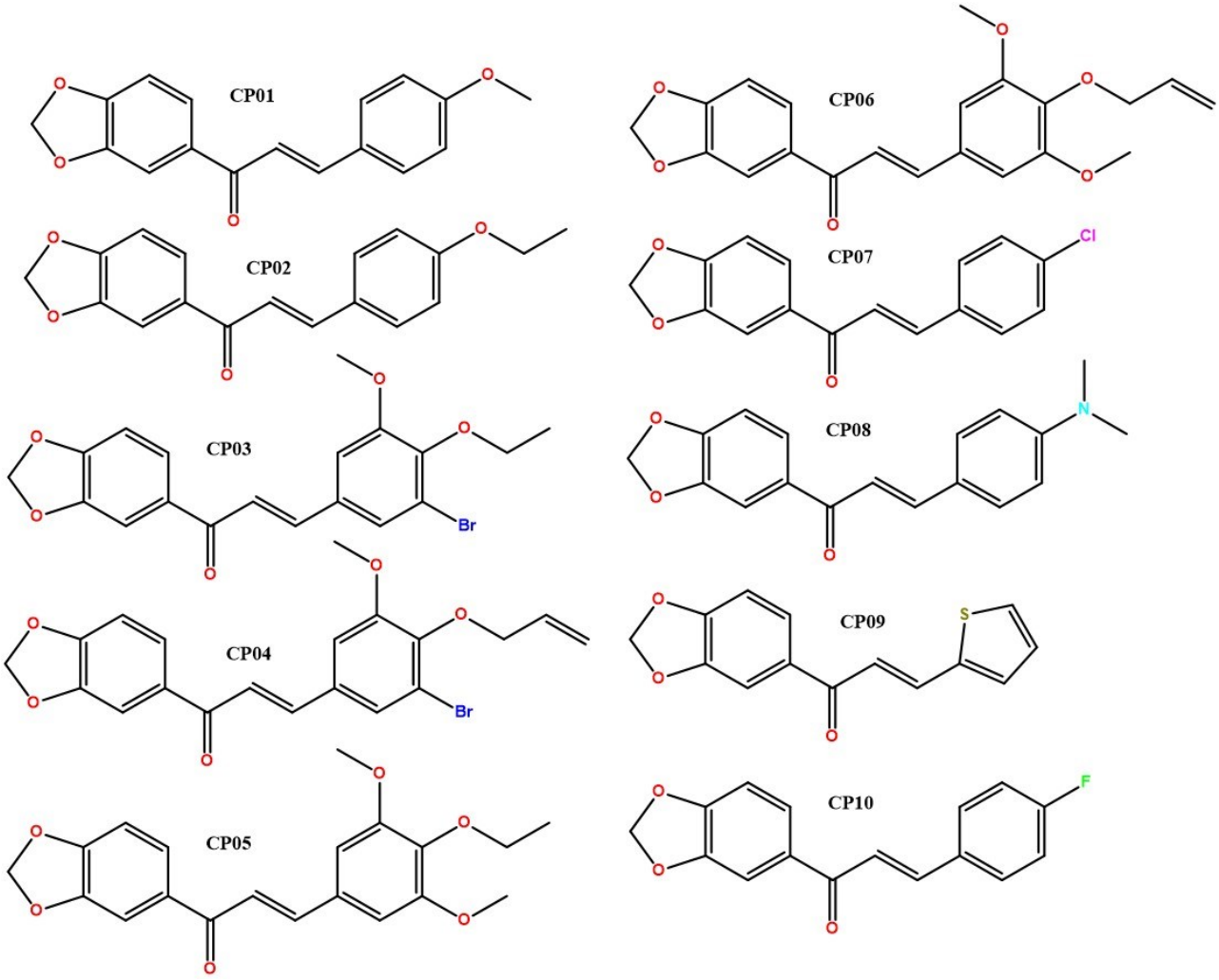

# CAPÍTULO 4

## *In vitro* and *in silico* evaluation of the anti-leishmania activity of synthetic chalcones

A *L. brasiliensis* constituem uma das espécies de *Leishmania* com maior interesse clínico. Estudos *in sílico* e *in vitro* foram realizados com 4 chalconas testadas contra essa espécie, onde o composto FER13 apresentou uma atividade antileishmania promissora. Vale ressaltar que o composto de maior atividade contra a espécie *L. Infantum* foi o mesmo composto, o tornando mais valioso.

Esse estudo foi realizado em colaboração com a doutoranda **Gleice Rayanne da Silva** orientanda do professor doutor **Felipe Queiroga Sarmento Guerra** e foi aceito para publicação na revista “Journal of the Brazilian Chemical Society”, como demonstra o email destacado abaixo.

Qualis Capes: A2

Fatos de Impacto: 2.1

Cite Score: 2.4

Ano vigente 2024

21-May-2024

Dear Prof. QUEIROGA SARMENTO GUERRA:

It is a pleasure to accept your manuscript entitled "Computer-aided drug design studies associated with in vitro antileishmanial tests of new chalcones" in its current form for publication in the Journal of the Brazilian Chemical Society. The comments of the reviewer(s) who reviewed your manuscript are included at the foot of this letter.

You should receive shortly an e-mail from the JBCS Office (publication@jbcs.sbq.org.br) in order to proceed with the payment of the publication fee.
The proofing production will begin only after the JBCS Office verifies the payment was properly credited. The payment process should take no longer than 3 days (the corresponding author will receive a message).

Thank you for your fine contribution. On behalf of the Editors of the Journal of the Brazilian Chemical Society, we look forward to your continued contributions to the Journal.

Sincerely,
Prof. Paula Homem-de-Mello
Associate Editor, Journal of the Brazilian Chemical Society
paula.mello@ufabc.edu.br

*Journal of the Brazilian Chemical Society*

## Graphical Abstract (GA)

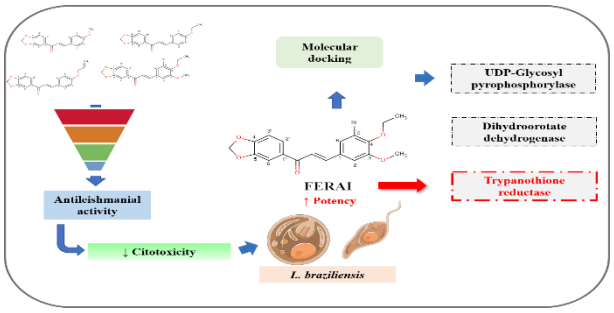


**GA Text:** This study addresses the use of *in silico* tools to predict the pharmacological activity of novel chalcones and possible mechanisms of action in *L. braziliensis* using molecular docking. The molecules proved to be promising.

# Computer-aided drug design studies in association with *in vitro* antileishmanial tests for new chalcones

**Gleice Rayanne da Silva,[a] Francisnaira da Silva Santos,[c,d] Fernando Ferreira Leite,[a] Chonny Alexander Herrera Acevedo,[a] Natália Ferreira de Sousa,[a] Gabriela Bittencourt Grimaldi,[d] Milena Botelho Pereira Soares,[d,e] Elisalva Teixeira Guimarães,[c,d] Marcus Tullius Scotti,[a] Luis Cezar Rodrigues,[f] Francisco Jaime Bezerra Mendonça,[g] Eloísa Helena Campana,[b] José Maria Barbosa Filho,[a] Hemerson Iury Ferreira Guimarães,*[b,h] Felipe Queiroga Sarmento Guerra,[a,b]**

[a]Programa de Pós-Graduação em Produtos Naturais e Sintéticos Bioativos, Centro de Ciências da Saúde, Universidade Federal da Paraíba, CEP:58.051-900, João Pessoa, Paraíba, Brasil

[b]Departamento de Ciências Farmacêuticas, Centro de Ciências da Saúde, Universidade Federal da Paraíba, CEP:58.051-900, João Pessoa, Paraíba, Brasil

[c]Laboratório de Histotécnica e Cultura Celular, Departamento de Ciências da Vida, Universidade do Estado da Bahia, CEP: 41.150-000, Salvador, Bahia, Brasil

[d]Laboratório de Engenharia Tecidual e Imunofarmacologia, Instituto Gonçalo Moniz, Fundação Oswaldo Cruz, CEP:40.296-710, Salvador, Bahia, Brasil

[e]Instituto Senai de Inovação em Sistemas Avançados em Saúde, SENAI/CIMATEC, CEP: 41.650-010, Salvador, Bahia, Brasil

[f]Programa de Pós-Graduação em Desenvolvimento e Inovação Tecnológica em Medicamentos, Universidade Federal da Paraíba, CEP:58.051-900, João Pessoa, Paraíba, Brasil

[g]Laboratório de Síntese e Vetorização de Moléculas, Universidade Estadual da Paraíba, CEP: 58.071-160, João Pessoa, Paraíba, Brasil

[h]Programa de Pós-Graduação em Ciências Farmacêuticas, Departamento de Ciências da Vida, Universidade do Estado da Bahia, CEP: 41.150-000, Salvador, Bahia, Brasil

*fqsg@academico.ufpb.br

ORCID ID: 0000-0003-2057-4821

**Abstract**

*In silico* and *in vitro* tests can reveal promising anti-leishmania activity for natural products and their derivatives. The aim of this study was to investigate *in silico* the pharmacological activities of potential new chalcones and their leishmanicidal potential *in vitro*. The *in silico* study was carried out using the PASS, MolPredictX and *Molegro Virtual Docker* 6.0 programs. Antiparasitic activity was assessed in axenic promastigote and amastigote forms of *L. braziliensis.* The cytotoxicity tests used the J77G8 cell line. The chalcones exhibited $CC_{50}$ values of >50 µM. Chalcone 4 (named FERAI) presented the best activity with $EC_{50s}$ of 9.75 ± 1.7 µM and 10.13 ± 1.7 µM for promastigote and amastigote, respectively. ROS testing presented increased ROS levels in the parasite at the FERAI concentrations of 10 µM (56.33%), 20 µM (61.76%) and 30 µM (67.13%). Molecular docking revealed interactions (binding energy) between FERAI and the enzymes UDP-Glycosyl pyrophosphorylase (-132.276), dihydroorotate-dehydrogenase (-132.276) and trypanothione-reductase (-132.276). Our results demonstrated the anti-leishmanial activity of chalcones, especially FERAI, with a noted raising of ROS levels in the parasite. Molecular docking revealed dihydroorotate dehydrogenase and trypanothione reductase as potential pharmacological targets for FERAI.

**Keywords:** flavonoids, computer-aided drug design, homology modeling, molecular docking, pharmacological activity, MolPredictX

## 1. Introduction

Computer-aided drug design has emerged as a powerful tool with an important role to play in the development of new therapeutic molecules. Structure-based and ligand-based drug design are frequently employed in computer-aided drug design.[1] Computational methods complement *in vitro* and *in vivo* pharmacological testing, potentially reducing costs, experimental time, and even the necessity for animal tests, while enhancing predictive accuracy and safety.[2,3]

Great evolution has taken place in the area of *in silico* drug discovery over the last decade. This space now providing a more targeted and precise approach compared to those of the past, which often required the discovery and identification of active molecules that would subsequently undergo numerous tests in order to be targeted. [4-5] *In silico* analyses provide a powerful tool: the ability to quantitatively predict the activity of compounds and simultaneously study interactions between a test substance and its targets, such as proteins. The combination allows for a more complete understanding of pharmacological activity, as it takes into account binding to specific target proteins.[6-8]

Research with natural products and novel synthetic substances exploits these tools to reach new levels of efficiency and time optimization, providing safer and more reliable results. In this sense, in order to increase knowledge about the therapeutic potential of natural compounds, *in silico* studies are being carried out on various chemical classes, including alkaloids, terpenes, flavonoids and others, all with the aim of obtaining more precise and targeted results.[9-12]

Flavonoids are polyphenolic phytochemical compounds found in many plants, fruits, vegetables and leaves with frequent applications in medicinal chemistry. In the field of scientific research, these compounds stand out for

having a wide range of *in vitro* and *in vivo* pharmacological activity, making them potential candidates for development of new therapies. Anticancer, antioxidant, anti-inflammatory, antiviral and antileishmanial properties have already been reported in the literature for these compounds.[13-14]

In terms of anti-leishmania activity, both natural and synthetic flavonoid compounds have been shown to inhibit parasites. Synthetic derivatives have proven activity against amastigote forms of *L. amazonensis*, eliminating the parasite from mammalian host cells, and demonstrating its pharmacological safety.[15] Dehydrolupinifolinol and sericetin (derived from *Mundulea sericea*) have been shown to be active against drug-sensitive *L. donovani*. Other natural flavonoids as well have presented antileishmanial activity against *L. mexicana*, *L. major,* and *L. braziliensis*.[16-19]

Chalcones are secondary metabolites found in edible and medicinal plants. In the plant kingdom, chalcones play a fundamental role as flavonoid bio-precursors, acting as important intermediaries in the biosynthetic pathway. Chalcones possess a range of pharmacological activities, such as antioxidant, anticancer, antimicrobial, antiviral, anti-plasmodic, and (like flavonoids) antileishmanial.[20]

In Brazil, the first compounds used to treat leishmaniasis were antimonials, followed by pentavalent derivatives ($Sb^{5+}$), which are still used today. Antimoniate-N-methyl glucamine is the drug of choice for treatment of tegumentary and visceral leishmaniasis.[15] In cases of resistance or contraindication, amphotericin B can also be used. The biggest problems involved when using such drugs are their high toxicities, high costs, extended treatment times, serious adverse side effects, and the degree of clinical

resistance.[21-23]

Recognizing the pharmacological potential of chalcones already reported in the literature with regard to their anti-leishmanial activity, and in view of difficulties in adherence and the high toxicity of the drugs currently available for leishmaniasis treatment, the need to study new therapeutic alternatives is evident. The aim of this study was to investigate possible pharmacological activities of four new chalcones *in silico*, their leishmanicidal potential *in vitro*, and evaluate potential mechanisms of action through molecular docking.

## 2. Experimental

### *Test products*

The synthesis of news chalcones was conducted in the Organic Chemistry Laboratory of the Post-graduate Program in Natural Products and Bioactive Synthetics at the Federal University of Paraíba.

Synthesis was carried out through separate methylation, ethylation, and allylation of 4-hydroxybenzaldehyde, with subsequent Claisen-Schmidit condensation, which respectively yielded the first 3 chalcones. The fourth chalcone resulted from bromination on vanillin, followed by ethylation, and aldol condensation (Supplementary material).[24]

### *In silico study - activity spectra prediction (PASS and MolPredictX)*

To predict the biological activity of the structures, the four compounds were submitted to the evaluation of biological activity using two online programs.

The program PASS filter[25] provides quantitative structure reactivity relationships through decomposition of chemical structures into 2D and/or 3D descriptors, with consequent production of models obtained from bioactive ligands. Through analysis, it is possible to predict the estimated activity spectrum

of a compound as probable activity (Pa) and probable inactivity (Pi). The values of Pa and Pi range from 0.000 to 1.000, and a compound can be said to be experimentally active when Pa > Pi. When Pa > 0.7, the probability of experimental pharmacological activity is said to be high, values of 0.5 < Pa < 0.7 indicates an average probability of experimental pharmacological activity, and if Pa < 0.5, the chance of having experimental pharmacological activity is lower, but it can still present a chance of finding a new compound.[26]

MolPredictX is an innovative and freely accessible web interface for predicting the biological activity of query molecules. Utilizing in-house QSAR models, MolPredictX provides 27 qualitative predictions (active or inactive) and quantitative probabilities for bioactivity, including against parasitic organisms such as *Trypanosoma* and *Leishmania.*[27] Specifically, activity against *Leishmania braziliensis* can be evaluated using a Machine Learning model developed by dos Santos Maia *et al.*[28] According to this model, a structure is classified as active when its $pIC_{50}$ value exceeds 4.5. MolPredictX also offers quantitative probability values for activity based on the random forest algorithm utilized in constructing the model.[28]

*Parasite culture*

Promastigote forms of *L. braziliensis* (MHOM/BR88/BA-3456) were cultured in Schneider's medium (Sigma-Aldrich, San Luis, Missouri, USA) containing 10% fetal bovine serum (FBS, GIBCO, Thermo Fisher Scientific, Waltham, MA USA), 50 μg $mL^{-1}$ gentamicin (Life, Carlsbad, CA), pH 7.2, and incubated at 26°C. The parasites were counted daily in a Neubauer chamber for five days. When they reached the stationary growth phase, new *in vitro* passages of the parasites were performed.[29]

*Cytotoxicity test on macrophages in vitro*

Murine macrophages of the J774 strain were used to evaluate the activity of the compounds, being incubated in 96-well plates (1 x $10^4$ cells/well) in Dulbecco's modified Eagle's medium (DMEM; Life Technologies, GIBCO-BRL, Gaithersburg, MD), supplemented with 10% fetal bovine serum (SIGMA) and 50 µg $mL^{-1}$ gentamicin (Life), and maintained for 24 h in an incubator at 37°C, aerated with 5% $CO_2$. Differing concentrations (100, 50, 25, 12.5, 6.25, and 3.125 µM) of the four compounds were tested, in triplicate, being incubated for 72 h. Subsequently, 20 µL of AlamarBlue (Invitrogen, Carlsbad, CA) were added for 6 h. Reading in a spectrophotometer (Microplate reader, Spectramax 190, Molecular Devices, Sunnyvale, California, USA) was performed at 570 and 600 nm. The results were expressed as 50% cytotoxic concentration values ($CC_{50}$). Gentian violet (Synth, São Paulo, SP, Brazil) was used as a positive contro*l.*

*Antileishmanial activity*

Promastigotes of *L. braziliensis* (1 x $10^6$ per well) were grown in a 96-well plate in Schneider's medium (Sigma) supplemented with 10% fetal bovine serum (FBS; GIBCO) and 50 µg $mL^{-1}$ gentamicin (Life) and subjected to treatment with differing concentrations (100, 50, 25, 12.5, 6.25, and 3.125 µM) of the four compounds. The parasites were incubated for 72 h at 26°C. Then, 20 µL well of AlamarBlue (Invitrogen) was added for 24 h, and reading was performed in a spectrophotometer at 570 and 600 nm. The percentage of axenic culture inhibition was determined based on the untreated control.

*Selectivity Index (SI) Evaluation*

The Selectivity Index (SI) was calculated using the ratio between the $CC_{50}$ value obtained for the macrophages and the $IC_{50}$ value obtained in promastigotes

treated with the molecules under study. The SI is used to determine how much more active the tested molecule is against *Leishmania* than toxic for the macrophage, indicating greater selectivity for the parasite without causing damage to the viability of mammalian cells. The SI should be greater than one (>1).[30]

*In vitro infection of macrophages and treatment with FERAI*

Murine J774 macrophages were cultured in 24-well plates at a concentration of 5 x $10^5$ with round coverslips added to the wells beforehand and infected with *L. braziliensis* in stationary phase at a ratio of 10 parasites per macrophage. After washing with DMEM medium, different concentrations of FERAI (20 µM, 10 µM, 5 µM, and 2.5 µM), were added to the wells. AB (5 µM) was used as a positive control. After 24 hours, the cells were fixed in methanol and stained using Giemsa (Dinâmica, Química Contemporânea Ltda, SP, Brazil). The percentage of infected macrophages and the number of amastigotes per macrophage was determined by counting 100 cells/well.

*Evaluation of ROS production*

*L. braziliensis* promastigotes (2 x $10^6$ per well) were grown in a 24-well plate in Schneider's medium, supplemented with 10% fetal bovine serum, 50 µg/mL gentamicin, and then treated with FERAI (5 µM to 30µM). The parasites were incubated for 4h at 26°C. Subsequently, 6µL of $H_2$DCFDA (10mM) (Invitrogen, Eugene, USA) was added to each well, being then kept for 30 min in the absence of light. Data acquisition was performed in a FACSCalibur flow cytometer (Becton Dickinson, Franklin Lakes, NJ, USA) and analyzed in FlowJo_v10.6.1.[31]

*Protein sequence alignment*

Three proteins fundamental to the life maintenance of *Leishmania* species were used in the study: Dihydroorotate Dehydrogenase, Trypanothione-reductase and UDP-glucose pyrophosphorylase. Since these proteins do not have 3D structures in the Protein Data Bank,[32] the corresponding sequences were obtained from the GenBank database.[33] A global alignment was performed using the sequence of a protein with a known three-dimensional structure and the web tool Clustal Omega[34], which aligns protein sequences. The alignment facilitated investigation of the active site, determination of similarity, and shared identity between the proteins.[35]

*Homology modeling*

Target sequences were obtained as amino acid sequences in FASTA format and were imported into the SWISS-MODEL website.[36,37] Quality was predicted for each identified template using alignment resources such as ProMod3, QMEAN and GMQE. The stereo chemical quality of the templates were evaluated using the PSVS (protein structure validation software suite)[38] web server and PROCHECK.[39] PROCHECK generates a Ramachandran plot,[40] for allowed and disallowed regions of the main amino acid chain.

*Molecular docking*

Molecular docking was used to investigate the mechanism of action of the compound presenting more promise in the previous tests ($ChS_4$), and the binding affinity of the compound to the enzymes selected in the study, was used to elucidate a possible route contributing to the leishmanicidal effect. For this, screening with several proteins involved in these effects was performed. The 3D structures of the enzymes that served as templates for the elaborated models

were obtained from the PDB.[34] The proteins selected and detailed information about them are presented in Table 1.

**Table 1.** Information on the proteins selected in the study.

| Protein | PDB ID/Homology | Positive Control |
|---|---|---|
| **Dihydroorotate Dehydrogenase** | Homology | 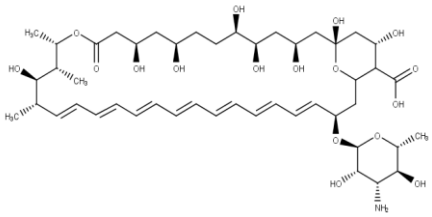 Amphotericin B |
| **Trypanothione Reductase** | | |
| **UDP-glucose pyrophosphorylase** | | |

Molegro Virtual Docker v. 6.0.1 (MVD)[41] software was used with its predefined parameters. The complexed ligand was used to define the active site. The compounds were then imported to analyze the stability of the system through interactions identified with the active site of the enzyme, taking the MolDock Score energy value as reference.[42]

The MolDock SE (Simplex Evolution) algorithm was used with the following parameters: a total of 10 runs with a maximum of 1,500 iterations a population of 50 individuals, 2,000 minimization steps for each flexible residue, and 2,000 global minimization steps per run. The MolDock Score function (GRID) was used to calculate the fitting energy values. The GRID was set to 0.3 A, and the search sphere radius was set to 15 A. Internal electrostatic interactions, internal hydrogen bonds, and sp2-sp2 twists were evaluated for ligand energy

analysis.

*Molecular Dynamics Simulations*

Molecular Dynamics simulations were performed to estimate the flexibility of interactions between proteins and ligands, using the GROMACS 5.0 software (European Union Horizon 2020 Program, Sweden).[43,44] Protein and ligand topologies were also prepared using GROMOS96 54a7 force field, and the MD simulation was performed using the point charge SPC water model, extended in a cubic box.[45] The system was neutralized by addition of $Cl^-$ and $Na^+$ ions and minimized to remove poor contacts between complex molecules and the solvent. The system was also balanced at 300K, using the 100 ps V-rescale algorithm, represented by NVT (constant number of particles, volume, and temperature), followed by equilibration pressure at 1 atm. using the Parrinello-Rahman algorithm as the NPT (particle constant pressure and temperature), up to 100 ps. MD simulations were performed in 5,000,000 steps, at 10 ns. To determine the flexibility of the structure and whether the complex was stable near the experimental structure, the RMSD values of all Cα atoms were calculated relative to the initial structures. RMSF values were also analyzed to verify the roles played by residues close to the receptor binding site. RMSD and RMSF plots were generated in Grace software and protein and ligands were visualized in UCSF Chimera.[46-49]

*Statistical analysis*

The numerical values shown in the pharmacological activity tables correspond to means ± S.E.M, from triplicates of each experiment. Significance in the differences between the groups was evaluated using the one way *ANOVA* test for analysis of variance, and the *Newman Keuls* multiple comparison post-

test for the sample group.[50]

## 3. Results

*PASS filter and MolPredictX predictions*

The *in silico* evaluation aimed at predicting the biological activities of compounds (1-4) based on their structural formulas (in SMILES format). The PASS filter and MolPredictX tools were utilized. The PASS filter indicated that all four chalcones possess antileishmanial activity, being identified among the 15 activities most likely to be exhibited by these substances (see supplementary material). Further, MolPredictX,[28,51] a freely accessible web tool developed at the Laboratory of Cheminformatics of UFPB was employed to predict the potential activity of the chalcones against *Leishmania braziliensis*. The results indicated that all four structures are active, with a probability of activity equal to 0.8 (Table 2).

**Table 2.** Prediction of chalcone biological activity in PASS filter and MolPredictX. *Pa* = Probability to be active*; Pi* = Probability to be inactive.

| | **PASS Filter** | | **MolPredictX** | |
|---|---|---|---|---|
| | Antiprotozoal (*Leishmania*) | | *Leishmania braziliensis* | |
| | *Pa* | *Pi* | *Pa* | *Pi* |
| **Chalcone 1** | 0.704 | 0.009 | 0.80 | 0.20 |
| **Chalcone 2** | 0.649 | 0.011 | 0.80 | 0.20 |
| **Chalcone 3** | 0.78 | 0.005 | 0.80 | 0.20 |
| **Chalcone 4** | 0.753 | 0.007 | 0.80 | 0.20 |

Considering that the studies performed provide only a prediction of the probable, we sought other approaches that might help in the choice of biological activity to be researched. A literature investigation was therefore conducted for the years 2017 to 2021 in the SciELO, PubMed, Medline, LILACS and ScienceDirect databases, using the corresponding chemical class descriptors

"*flavonoids*" OR "*chalcones*", and noting relationships for the selected activities of each compound associated with the pharmacological activity to be researched.

Inclusion criteria included articles that related each chemical class with at least one of the 15 selected pharmacological activities, and which produced promising activity on the targets. The articles were required to be published within the latest five years, and articles that did not demonstrate potentially auspicious activity were excluded.

The results revealed that antileishmanial activity is one of the biological activities most associated with flavonoids (and against the most diverse existing species). A number of studies have reported leishmanicidal activity for compounds of this class, such as: fisetin, a polyphenolic flavonoid, which has potent activity against *Leishmania* spp. in *in vitro* tests;[52] purified dimeric flavonoids from *Arrabidaea brachypoda* with *in vitro* activity against promastigotes and amastigotes forms of *L. amazonensis*;[53] flavonoids isolated from *Polygonum salicifolium* with leishmanicidal *in vitro* activity against *L. Mexicana;*[54] and rusflavone, a biflavonoid isolated from the pollen of *Attalea funifera* presenting activity against promastigote and amastigote forms of *L. amazonensis* through a mechanism that involves the production of reactive oxygen species, mitochondrial dysfunction, and membrane disruption in the parasites.[55]

For chalcones, scientific research can also be found reporting broad leishmanicidal activity against various *Leishmania* species.[56] The studies of Nardella *et al*.[57] indicate that regardless of the assay performed, whether *in vitro* or *in vivo,* the most active compounds against *Leishmania* spp. belong to the chalcone, biflavone, and aurone classes. Phytochemical evaluation of the

chalcones, 2',4'-dimethoxy-6'-hydroxychalcona and 2',5'-dimethoxy-4',6'-dihydroxichalcona has revealed promising antileishmania activity against *L. mexicana*, with no toxicity in human cell line tests.[57] The leishmanicidal activity of 31 synthetic chalcones was analyzed *in vitro,* using promastigotes and amastigotes of *L. donovani, L. tropica, L. major,* and *L. infantum*, and the results indicated that 16 of the compounds were active, while presenting high selectivity, and low toxicity against mammalian cells.[58]

It was decided to initially proceed with *in vitro* antileishmanial activity tests (for screening) followed by more complex studies.

*Cytotoxicity and antileishmanial activity*

Cytotoxicity evaluation ($CC_{50}$) was performed in J774 murine macrophages, and the results for each compound were compared to Gentian violet ($CC_{50}$ = 0.6 ± 0.01 µM), a known cytotoxic drug, or amphotericin B (AB), the antileishmanial reference drug. All chalcones exhibited $CC_{50}$>50, being several times less cytotoxic than amphotericin B ($CC_{50}$ = 3.6 µM) (**Table 3**).

**Table 3.** Cytotoxicity evaluation ($CC_{50}$), half maximal effective concentration for 50% of promastigotes and intracellular parasites forms ($EC_{50}$), and selectivity index of chalcones.

| Compounds | $CC_{50}$ ± S.D. Mφ J774 (µM) | $EC_{50}$ ± S.D. promastigotes *L. braziliensis* (µM) | S.I. promastigotes *L. braziliensis* | $EC_{50}$ amastigotes *L. braziliensis* (µM) | S.I. amastigotes *L. braziliensis* |
|---|---|---|---|---|---|
| 01 | >50 | >50 | - | - | - |
| 02 | >50 | >50 | - | - | - |
| 03 | >50 | >50 | - | - | - |
| 04 (FERAI) | >50 | 9.75 ± 1.7 | 6.8 | 10.13 ±1.7 | 6.6 |
| Amphotericin B (AB) | 3.6 ± 0.50 | 0.32 ± 0.01 | 11.25 | 0.7 ±0.004 | 5.14 |
| Gentian Violet | 0.7 ± 0.09 | - | - | - | - |

GV= Gentian Violet; $CC_{50}$ = 50% cytotoxic concentration; $EC_{50}$ = 50% inhibitory concentration; SI= selectivity index. Values calculated from two independent experiments. S.D. = Standard deviation; S.I. = selectivity index.

Antileishmanial activity in an axenic culture was used to calculate the $EC_{50}$ value and evaluate the activity of the compounds against *L. braziliensis* promastigotes. Molecules 1-3 did not present promising inhibitory potency, obtaining $EC_{50}$ values above 50 μM, as compared to AB used as a positive control ($EC_{50}$ = 0.32 ± 0.01 μM). However, FERAI presented potent activity inhibiting the growth of *L. braziliensis* promastigotes, with an $EC_{50}$ value of 9.75 ± 1.7 μM (Table 3). In view of these results, we decided to continue with the Chalcone 4 tests, now called "FERAI", because it proved to be the most promising compound.

In addition, FERAI demonstrated significant activity against amastigote forms of *L. braziliensis* with an $EC_{50}$ value of 10.13 ± 1.7 μM. Amphotericin B (AB) presented an $EC_{50}$ value of 0.7 ±0.004 μM for this same parasite. The SI, as calculated from the ratio between the $CC_{50}$ and $EC_{50}$ values for FERAI was 6.8 times more selective (SI) for promastigotes, and 6.6 times more potent for *L. braziliensis* amastigotes than for mammalian cells. AB was respectively 11.25 and 5.14 times more selective (SI) (Table 3). Thus, FERAI presented a higher selectivity index for amastigotes than AB, the reference drug.

FERAI also reduced the infection of macrophages by *L. braziliensis*. Murine macrophages of the J774 strain were infected with *L. braziliensis* amastigotes and treated with various concentrations of FERAI, which caused a concentration-dependent reduction in the percentage of macrophages infected, and the number of intracellular parasites per 100 macrophages when compared to the control group. As expected, AB also decreased the number of infected macrophages and the number of amastigotes per 100 cells (Figure 1).

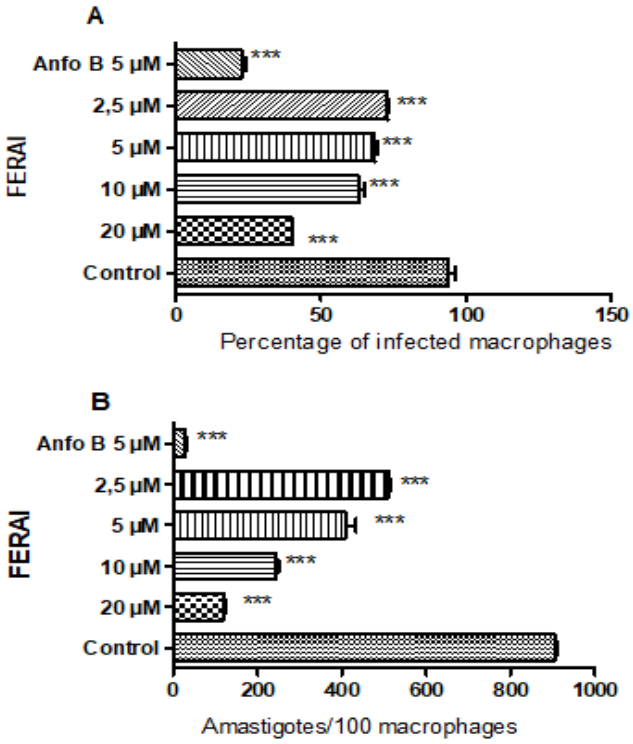


**Figure 1.** Effect of FERAI against intracellular parasites of *L. braziliensis*. Macrophages were infected by *L. braziliensis* (10:1) and treated with four different concentrations of FERAI 1:2 – (2.5 µM to 20 µM) and amphotericin B (5 µM) for 24h. The percentage of infected macrophages (A) and the number of intracellular parasites per 100 macrophages (B) were determined after 24h of treatment.

*FERAI significantly alters the production of ROS in L. braziliensis promastigotes*

ROS levels were measured using the permeable dye $H_2$DCFDA, aiming to investigate whether the leishmanicidal effect of FERAI in *L. braziliensis* promastigotes is due to ROS production. FERAI induced ROS production in promastigotes (with increased ROS levels) noted especially at the highest concentrations used: 10 µM (56.33%), 20 µM (61.76%) and 30 µM (67.13%) compared to the untreated control. Hydrogen peroxide ($H_2O_2$) was used as a positive control (Figure 2).

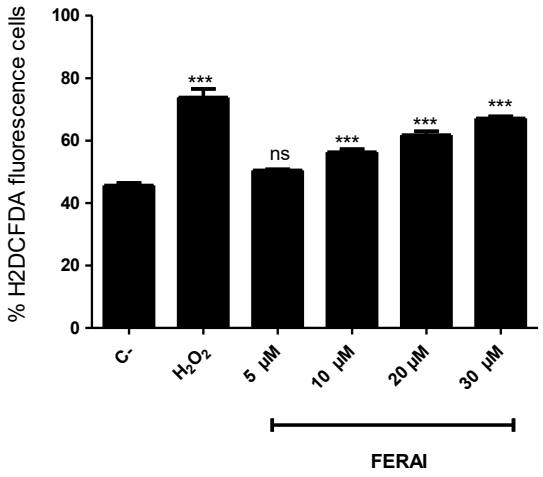


**Figure 2**. Evaluation of intracellular ROS levels in *L. braziliensis* promastigotes. Evaluation of intracellular ROS levels induced using FERAI at different concentrations (5 µM to 30µM) for 24 hours and incubated with $H_2$DCFDA probe for 30 minutes.***p < 0.001 and ns= not significant compared to untreated control.

The average values of the FERAI samples, the positive and negative controls, and the standard deviation were also calculated (Table 4).

**Table 4**. Evaluation of intracellular ROS levels in *L. braziliensis* promastigotes (Mean and standard deviation of positive control and untreated control samples).

| Samples | Mean | Pattern deviation |
|---|---|---|
| **Negative control** | 45.66 | ± 1.14 |
| **$H_2O_2$** | 73.9 | ± 3.74 |
| **FERAI 5 µM** | 50.50 | ± 0.43 |
| **FERAI 10 µM** | 56.33 | ± 1.27 |
| **FERAI 20 µM** | 61.76 | ± 1.58 |
| **FERAI 30 µM** | 67.13 | ± 0.59 |

*Protein sequence alignment*

Shared amino acids between target and template protein sequences were investigated. The results revealed that trypanothione reductase (*L. braziliensis*) possesses 84.01% identity with trypanothione reductase from *L. infantum* (PDB: 3JK6). While dihydroorotate dehydrogenase for *L. braziliensis* possesses 84.66% identity with dihydroorotate dehydrogenase from *L. major* (PDB: 6EBS) (see supplementary material).

UDP-glycosyl pyrophosphorylase from *L. braziliensis*, presented 96.93% identity with UDP-glycosyl pyrophosphorylase from *L. major* (PDB: 2OEF).

*Homology modeling*

The enzyme models for dihydroorotate dehydrogenase, trypanothione reductase and UDP-glycosyl pyrophosphorylase were generated using the homology modeling method. The reliability of the models was assessed using the Ramachandran plot, which represents all possible combinations of dihedral angles Ψ (psi), versus φ (phi) for each amino acid in a protein except glycine, which has no side chains. The models are considered reliable when more than 90% of the amino acids are present in the allowed and/or favored regions (colored regions of the plot). Blank regions represent discrepant values, with poor contacts. The dihydroorotate dehydrogenase model presented 91.8% amino acids in the favored regions and 8.2% in allowed regions. The trypanothione reductase model presented 91.6% of amino acids in the favored regions and 8% in allowed regions. Finally, the UDP-glycosyl pyrophosphorylase model percentages corresponded to 93.5% of amino acids in the favored regions and 6.3% in the allowed regions. Considering the results, the homology models were considered reliable (Figure 3).

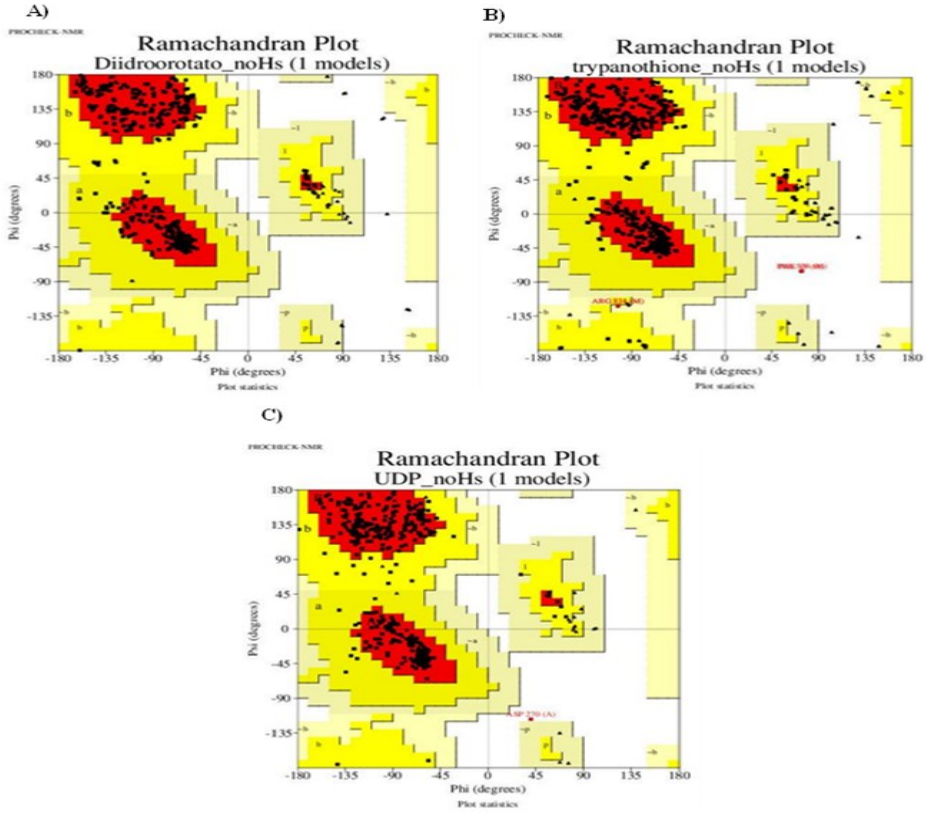


**Figure 3.** Ramachandran plots of the homology modeling generated for the enzymes: Dihydroorotate Dehydrogenase (A), Trypanothione Reductase (B) and UDP-glucose pyrophosphorylase (C).

*Molecular docking*

Chalcone 4 (FERAI) was subjected to screening using molecular docking on 3 proteins. The docking results were generated using two scoring functions, the Moldock Score and the Rerank Score. In most of the scoring functions, the more negative values indicated better predictions. The protein in which the compound obtained binding energy values higher or close to the standard drug in at least one scoring function was considered active (Table 5).

**Table 5.** Binding energy values analyzed in the three selected proteins in the study.

| **Protein** | **Chalcone 4 (FERAI)** | | **Amphotericin B - Positive Control** | |
|---|---|---|---|---|
| | Moldock Score | Rerank Score | Moldock Score | Rerank Score |

| | | | | |
|---|---|---|---|---|
| **Dihydroorotate Dehydrogenase** | -132.276 | -95.1107 | -43.403 | 1141.65 |
| **Trypanothione Reductase** | -151.281 | -317.774 | -102.191 | -282.763 |
| **UDP- Glucose Pyrophosphorylase** | -56.8384 | -39.1568 | -146.389 | -64.8544 |

Of the three proteins analyzed, Chalcone 4 obtained negative energies for all the enzymes under study. Moreover, it obtained better results with dihydroorotate dehydrogenase and trypanothione reductase, and it obtained values close to or higher than the values of MolDockscore and Rerankscore as compared to the controls. Chalcone 4 exhibited greater potency against the proteins dihydroorotate dehydrogenase and trypanothione reductase, with respective binding affinity values of -132.276 and -151.281 Kcal $mol^{-1}$.

We analyzed in detail the interactions and bonds formed with the test compound and the dihydroorotate dehydrogenase and trypanothione reductase proteins.

The test compound (chalcone 4) was capable of forming four hydrophobic interactions with the amino acids Val 22, Ala 19, Cys 249, and Met 70; also forming seven hydrogen bonds with the amino acids Lys 44, Gly 21, Gly 272, Gly 223, Cys 249, Asn 195, and Lys 44 at the active site of the protein dihydroorotate dehydrogenase (Figure 4). Amphotericin B formed seven hydrogen bonds with residues Ser 45, Asn 128, Lys 165, Gly 250, Ile 194, Thr 273, Ala 20, and Met 20; six hydrophobic interactions with residues Pro 73, Glu 29, Met 20, Met 23, Ala 19, and Cys 249; and twelve steric interactions with residues Met 20, Glu 29, Met 23, Val 12, Gln 276, Tyr 59, Ser 198, Gly 122, Asn 199, Ser 98, Lys 44, and Lys 165. Coincidences occurred between the positive control and the test

compound at the hydrophobic interaction of residue Cys 249.

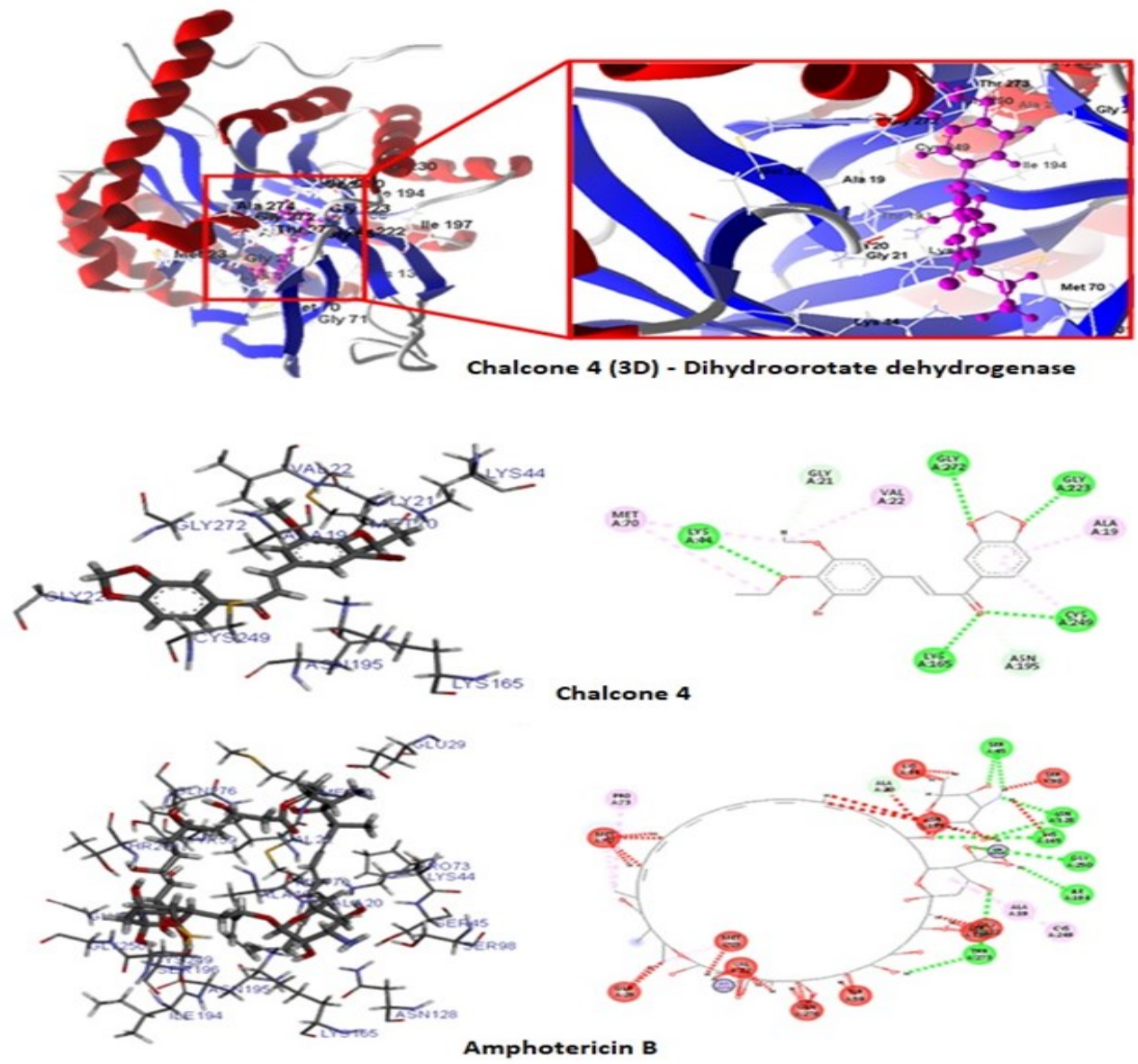


**Figure 4.** 2D and 3D interactions between chalcone 4, Amphotericin B and the protein dihydroorotate dehydrogenase.

For trypanothione reductase, the test compound established six hydrophobic interactions the active site with Thr 160, Ala 398, Ala 159, Val 36, Leu 10, and Val 34; and five hydrogen interactions, which corresponded to Gly 161, Ser 14, Asp 35, and Gly 15 (Figure 5). Amphotericin B, on the other hand, presented five hydrogen bonds with residues Gly 49, Thr 51, Cys 57, Tyr 198,

and Arg; and ten steric interactions with residues Pro 336, Ile 339, Val 53, Cys 52, Ser 14, Asp 327, Met 333, Thr 51, Tyr 198, and Cys 57. A hydrophobic interaction with amino acid Val 53 was also recorded. For this enzyme no similar interactions occurred between the test compound and the positive control.

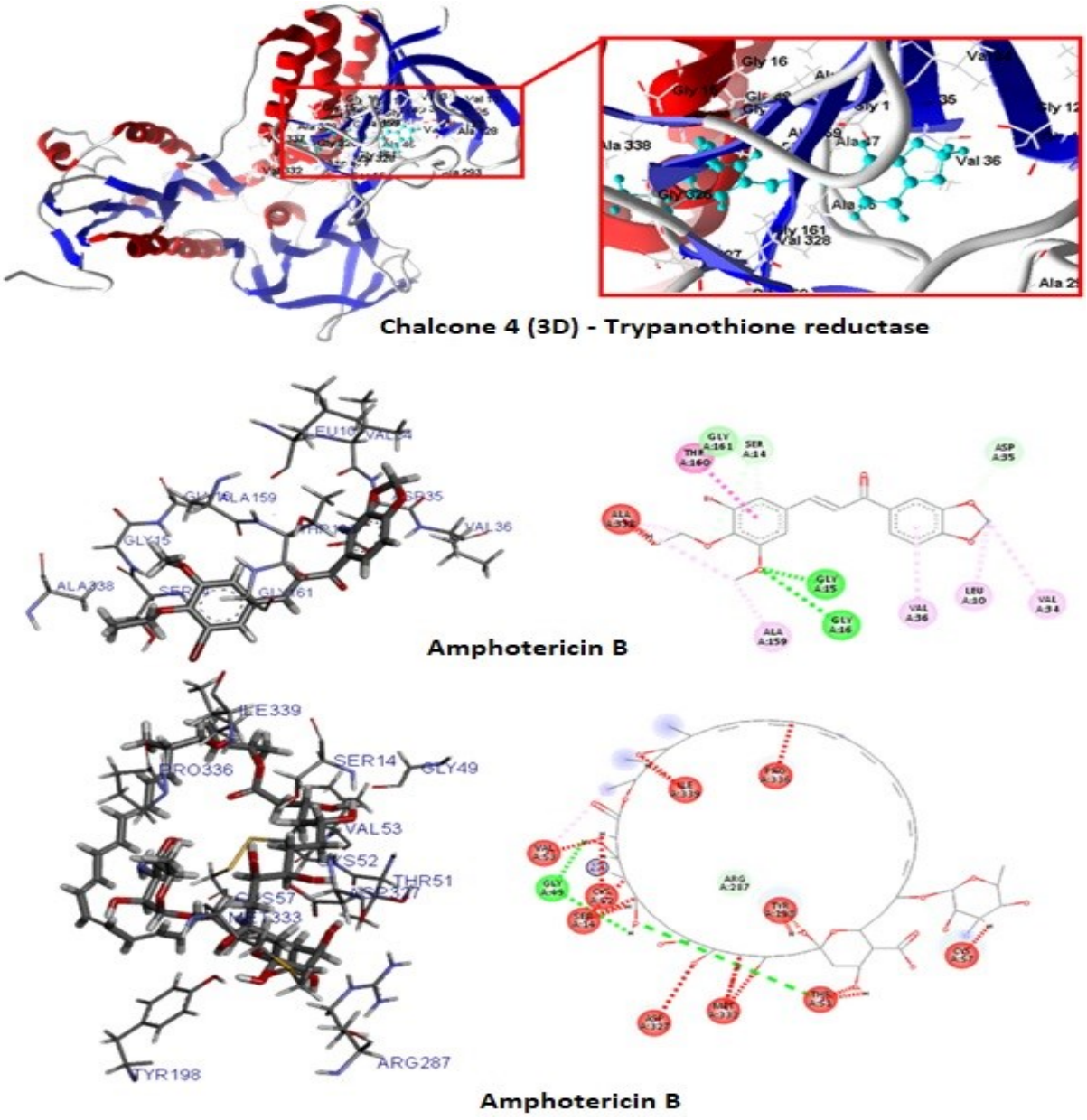


**Figure 5**. 2D and 3D interactions between chalcone 4, Amphotericin B, and trypanothione reductase.

*Trypanothione Reductase*

For trypanothione reductase, analysis of the RMSD metric of the protein

(Figure 6A) revealed that the complexes related to the protein (black line) and compound 4 (FERAI) (red line) presented greater stability than the control drug Amphotericin B (green line); presenting much lower RMSD values. Various fluctuations were also observed in the complex referring to Amphotericin B. For FERAI, it was observed that after a period of 15 ns the RMSD values remained constant at 0.4 nm, remaining without change throughout the total simulation time; denoting high stability. The protein complex presented fluctuations between 30 and 50 ns with RMSD values of up to 0.55 nm, which returned to 0.4 nm after 55 ns. The control drug Amphotericin B was significantly more unstable after 50 ns, as values reached 0.6 nm and remained so until the total time of 100 ns.

When analyzing the stability of the ligands in the presence of solvents (Figure 6B), it was verified that the result corroborated the RMSD results, since FERAI (black line) presented lower RMSD values than the control drug Amphotericin B (red line), which was significantly more unstable.

To better understand the flexibility of residues and amino acids contributing to the conformational change in the trypanothione reductase enzyme, the root mean square fluctuations (RMSF) of each amino acid in the protein were calculated. Residuals with high RMSF values reflect more flexibility and low RMSF values suggest less flexibility. Considering that amino acids with fluctuations above 0.3nm contribute to the flexibility of the channel structure, residues in positions 1-2, 79, 81-87, 89, 305, 355, 458-462, and 480-483 (Figure 7A) contributed to the conformational change and flexibility of the complexed protein.

The Coulomb and Lennard-Jones interaction energies (Table 6) of the protein-ligand complexes were calculated. FERAI demonstrated greater

interaction stability with the active site due to a greater influence of electrostatic and hydrogen interactions. According to Lennard-Jonnes metrics, the control Amphotericin B demonstrated greater stability than FERAI.

**Table 6**. Coulomb and Lennard-Jonnes interaction energy values.

| Energy | Compound 4 (FERAI) | Amphotericin B |
|---|---|---|
| Coulomb (C) | -172.534 | -80.377 |
| Lennard-Jonnes (LJ) | -171.133 | -209.129 |

*Dihydroorotate dehydrogenase*

For dihydroorotate dehydrogenase, according to the protein RMSD metric (Figure 6C), the greater instability observed in the three complexes analyzed reflected the occurrence of a greater number of fluctuations. The control Amphotericin B (green line) presented the greatest stability, with lower RMSD values. FERAI (red line) presented RMSD values of 0.5 nm and fluctuations during the periods at 50 ns and 90 ns.

When analyzing the stability of the ligands in the presence of solvents (Figure 6D), it was found that FERAI (black line) was significantly more unstable than Amphotericin B (red line). FERAI presented RMSD values of 0.4 nm, while Amphotericin B presented values of 0.18 nm.

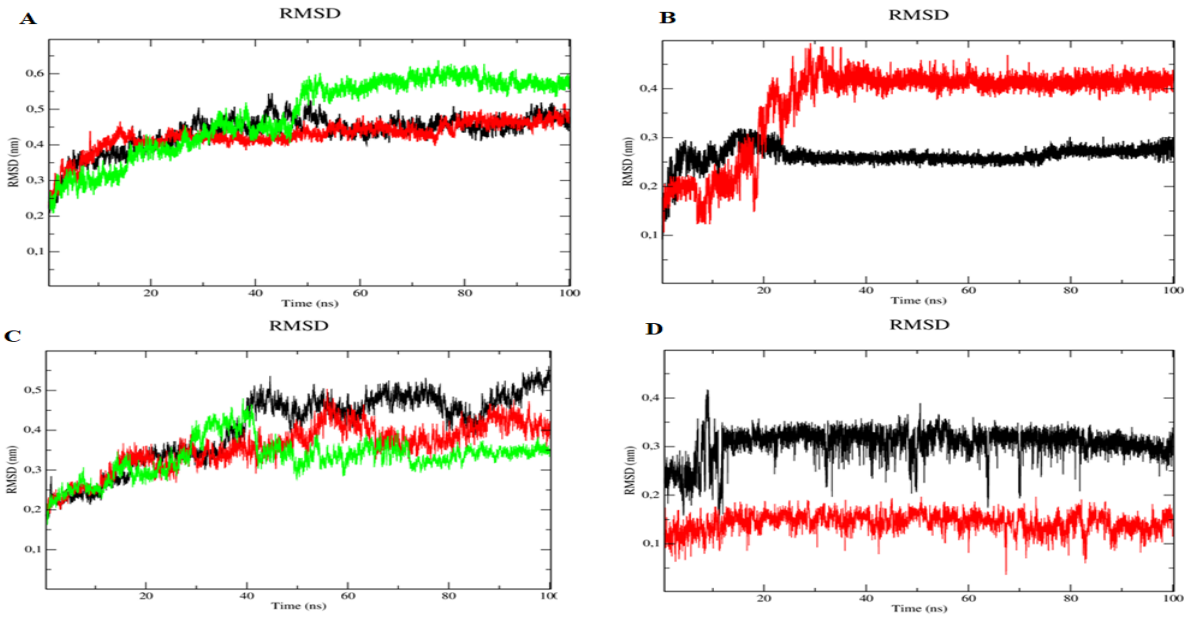


**Figure 6**. RMSD of Cα atoms. A) Trypanothione reductase (black), complexed with FERAI (red) and Amphotericin B (green). B) FERAI (black line), and Amphotericin B (red line). C) Dihydroorotate dehydrogenase (black), complexed with FERAI (red) and Amphotericin B (green). D) FERAI (black line), and Amphotericin B (red line).

To assess the flexibility of the residues and amino acids that contribute to the conformational change in dihydroorotate dehydrogenase, the root mean square fluctuations (RMSF) of each amino acid in the protein were calculated. It was observed that residues at positions 201, 204- 209, 216, and 310-312 contribute to the conformational change of the protein complexed with FERAI (Figure 7B).

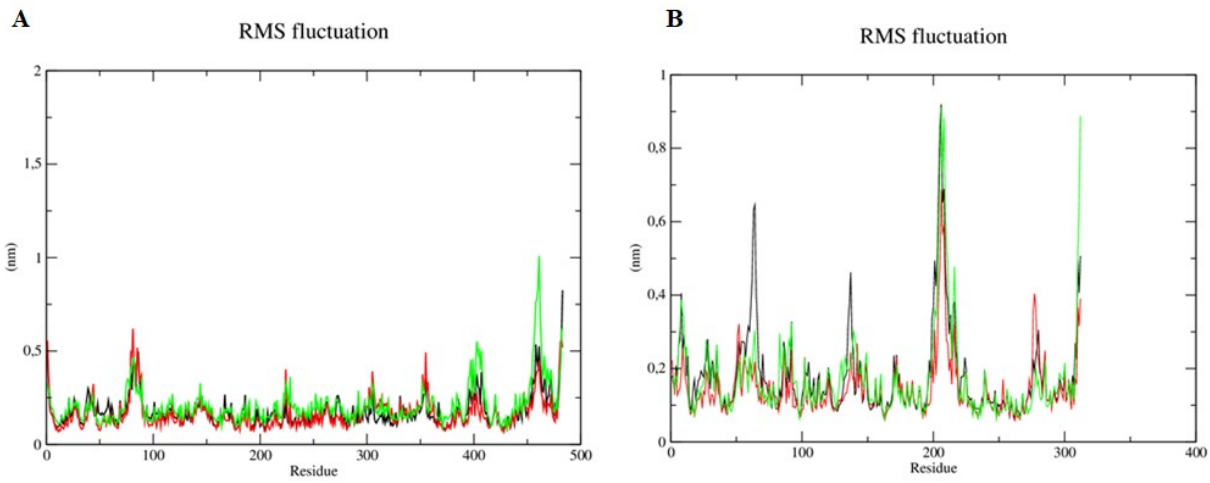


**Figure 7**. RMSF of atoms. A) Enzyme (black line) complexed to FERAI (red line) and Amphotericin B (green line). B) Enzyme Dihydroorotate dehydrogenase (black line) complexed to FERAI (red line) and Amphotericin B (green line).

The Coulomb and Lennard-Jones interaction energies (Table 7) of the protein-ligand complexes were calculated. FERAI demonstrated greater interaction stability with the active site through Lennard-Jonnes energy calculations, which denotes a greater influence of Van der Waals interactions. According to the Coulomb metrics, the Amphotericin B control demonstrated greater stability than FERAI.

**Table 7**. Coulomb and Lennard-Jonnes interaction energy values.

| Energy | Compound 4 (FERAI) | Amphotericin B |
|---|---|---|
| Coulomb (C) | -58.6761 | -83.475 |
| Lennard-Jonnes (LJ) | -158.865 | -126.96 |

## Discussion

Through the use of computer simulations, computational chemistry and bioinformatics have taken an innovative role in directing studies and drug planning.[59] In this context, the use of *in silico* models has evolved with remarkable progress in many areas such as: correlation, prediction, simplification,

automation, among other expressive aspects.[60]

Development of new drugs is a complex process that requires both time and financial resources. Computer-aided studies aim to create new approaches that boost research and provide avenues for further testing. Virtual screening for identification and optimization of other testing methodologies is an advantage of these studies, as it is possible to predict pharmacological activity for a specific molecule, quantifying activity and inactivity with a probability score.[61-62]

As an initial screening regarding pharmacological activity, it was possible to observe in both the PASS and MolPredictX studies that the four chalcones presented similar results for the 15 activities with higher probabilities of occurrence in both. The fact that the four substances belong to the same class could explain the occurrence of similar results among them, taking into account that the tests work using decomposition of the molecular structure into 2D and 3D descriptors which they are expected to have in common.

Based on the literature, and seeking to elect the pharmacological activity most associated with chalcones, it was observed that antileishmania activity has been well researched and that these substances present promising activity with regard to potency and efficacy against various species.[63-65]

A number of studies have reported leishmanicidal activity for this class of compounds, such as: fisetin, a polyphenolic flavonoid, which has potent *in vitro* action against *Leishmania* spp.,[52] purified dimeric flavonoids from *Arrabidaea brachypoda* with *in vitro* action against promastigotes and amastigotes forms of *L. amazonensis*,[53] flavonoids isolated from *Polygonum salicifolium* with *in vitro* leishmanicidal activity against *L. mexicana*,[54] and rusflavone, a biflavonoid isolated from the pollen of *Attalea funifera*, which has been shown to act against

the promastigote and amastigote forms of *L. amazonensis*, through a mechanism that involves the production of ROS, mitochondrial dysfunction, and membrane disruption in the parasites.[55]

As for chalcones, scientific research can also be found indicating broad leishmanicidal activity against various species of the genus *Leishmania.*[56] The studies of Nardella *et al*.[57] indicated that regardless of the assay performed, whether *in vitro* or *in vivo,* the most active compounds against *Leishmania* spp. belong to the chalcone, biflavone, and aurone classes. The phytochemical evaluations of the chalcones, 2',4'-dimethoxy-6'-hydroxychalcone and 2',5'-dimethoxy-4',6'-dihydroxichalcone presented promising antileishmania activity against *L. mexicana*, with no toxicity in tests with a human cell line.[48] The leishmanicidal activity of 31 synthetic chalcones was analyzed *in vitro* using promastigotes and amastigotes of *L. donovani, L. tropica, L. major,* and *L. infantum.* The results indicated that 16 of the compounds were active against the strains, showing high selectivity and low toxicity against mammalian cells.[52] In view of this, it was decided to continue our research in this area.

Cytotoxicity assays at the beginning of studies with natural products are among the principal *in vitro* tests used. They predict toxicity, and provide a means for evaluation, safety screening, and classification of compounds. The monitoring of cell response within these assays provides reliable results and can serve as a basis for measuring other parameters such as cell viability and SI.[66-67]

When compared using gentian violet, the cytotoxicity test results for murine macrophages demonstrated the low cytotoxicity of the four chalcones ($CC_{50}$ = 0.6 ± 0.01 μM), with $CC_{50}$ values above 50 μM. These were encouraging results, as it is essential that new antileishmanial drug candidates present

reduced cytotoxicity to overcome the disadvantages of drugs currently used in therapy.

Another study investigating the effects of twenty brominated chalcones against four cancer cell lines reported similar results, the tested substances exhibited lower cytotoxicity for non-malignant gastric epithelial cells than for diseased ones, demonstrating selectivity.[68] Researchers investigated the *in vitro* cytotoxicity of ten chalcones against the HeLa cell line through the MTT viability assay and SI calculation, and the results revealed the low cytotoxicity of these substances in this cell type.[69]

It was observed during the axenic culture analysis for antileishmanial activity that Chalcones 1, 2, and 3 did not present promising inhibitory potency ($IC_{50}$). However Chalcone 4, which was the most potent in inhibiting the growth of *L. braziliensis*, presented low cytotoxicity when compared to AB, being therefore a promising candidate for future tests.

A number of studies have reported chalcones with potent antileishmanial activity against *L. braziliensis*.[61,65,70] Two synthetic chalcones were evaluated *in vitro* against *L. braziliensis* promastigotes for inhibitory activity and cytotoxicity against macrophages. The $IC_{50}$ and $CC_{50}$ results were respectively, 1.38 ± 1.09; 6.36 ± 2.04 μM, and 13.49 ± 3.13; 199.43 ± 4.11 μM, and both presented effects against *L. braziliensis* promastigotes, with low toxicity to mammalian cells.[63]

Similar results were found in a study involving three methoxy chalcones, which presented significant *in vitro* antileishmanial activity against *L. braziliensis* promastigotes ($IC_{50}$ = 2.7 μM, 3.9 μM, and 4.6 μM), with more potent activity than the control drug pentamidine ($IC_{50}$ = 6.0 μM).[71]

The potential for FERAI activity to involve increased ROS levels in *L.*

*braziliensis* promastigotes was also investigated. The results indicated an increase in ROS levels, at concentrations of 10 μM (56.33%), 20 μM (61.76%), and 30 μM (67.13%) compared to the untreated control. Similar results were found by Santiago-Silva et al.[72], who evaluated the production of ROS by chalcone ((E)-1-(4,8-dimethoxynaphthalen-1-yl)-3-(4-nitrophenyl) prop-2-en-1-one), which induced several morphological and ultrastructural changes in free promastigotes, including loss of plasma membrane integrity, and an increase in ROS.

Given our results, it was hypothesized that the addition of bromine to molecule 4 optimized its antileishmanial effects. Reports in the literature already report that brominated synthetic substances possess superior bioactive potential, and although the mechanisms that explain these results are not yet fully elucidated, one can cite possibilities. High lipophilicity and permeability through biological membranes, increased half-life, and the ability to form intermolecular bonds (attractive interactions) between the electrophilic region of the molecule containing bromine atoms and nucleophilic active sites of the biomolecule. Bromination can lead to increased therapeutic potency and research in the area of chemoinformatics can provide important contributions to elucidate its molecular interactions.[73] Thus, we decided to continue our studies with Chalcone 4, with tests investigating its action on *L. braziliensis* amastigotes, and evaluating its SI.

*L. braziliensis* is associated with both metastasis and the mucosal form of leishmaniasis, and underlies the importance of developing more effective and less toxic drugs for treatment.[74-75] When the pharmacological activity of FERAI was evaluated against amastigotes of *L. braziliensis*, an $IC_{50}$ value of 10.13 ± 1.7

μM was observed. AB, a drug commercially available for the treatment of leishmaniasis, presented an $IC_{50}$ value of 0.7 ± 0.004 μM. Although FERAI presented a higher inhibitory concentration, the result still presents promise when its low toxicity compared to AB is considered. FERAI may yet be a future drug candidate for leishmaniasis treatment since macrophages infected with *L. braziliensis* amastigotes and treated with FERAI resulted in a reductions both in the number of infected macrophages and in the number of amastigotes per macrophage, confirming its significant activity on intracellular forms of *L. braziliensis.*

Protein sequence alignment helps to verify the similarity and identity the same protein in different species or different proteins from the same species. With this technique, it is possible to analyze conserved regions and identify common residues in the active site. In addition, it is possible to point out differences and structural similarities that can contribute to drug development. Amino acids shared between the sequences of the target and template proteins have been investigated.[76-77]

Alignment of the *L. braziliensis* trypanothione-reductase protein sequences with trypanothione reductase from *L. infantum*; the *L. braziliensis* dihydroorotate dehydrogenase with dihydroorotate dehydrogenase from *L. major;* and *L. braziliensis* UDP-glycosyl pyrophosphorylase with UDP-glycosyl pyrophosphorylase from *L. major*, revealed a high degree of identity and similarity, which enabled the construction of reliable homology models for these proteins.

Molecular docking, when applied to analyze natural products as candidates for new drugs, makes it possible to obtain data on mechanisms of

action, molecular interactions, and substance - target binding.[78-79] Molecular docking is a fast, low-cost and efficient technique, and is very useful for working with both natural and synthetic products, allowing reduction of material losses, and better use of the substances.[9, 80]

In the molecular docking results, chalcone 4 (FERAI) obtained negative energies for all of the enzymes under study, demonstrating interaction with all the targets. Further, FERAI interacted more specifically with dihydroorotate dehydrogenase and trypanothione reductase, and this may reflect a certain specificity of the compound, since it presented higher energy in two specific targets.

After analyzing the potential activity of FERAI in relation to important mechanisms for evaluating antileishmanial activity, molecular dynamics simulations were carried out to evaluate the flexibility of the enzymes and the stability of interactions in the presence of factors such as solvent, ions, pressure, and temperature. Such information is important because it complements docking results and allows us to evaluate whether the compound remains strongly bound to the studied enzymes in the presence of factors that are found in the host organism. For this analysis, the enzymes trypanothione reductase and dihydroorotate dehydrogenase were chosen since FERAI presented greater affinity for these proteins. RMSD was calculated separately for the Cα atoms of the complexed enzyme and the structures of each ligand.

Ligand stability is essential in pharmacological activity studies, as this factor, for keeping compounds bound to the active site, can be a determining factor in both potency and efficacy.[81-82] The trypanothione reductase protein complex proved to be more stable than the dihydroorotate dehydrogenase

complex, which in turn was the most unstable complex, as it presented the highest RMSD values, corresponding to 0.5 nm.

Similar to Amphotericin B, FERAI was capable of establishing strong bonds with the active site, tending to remain even in the presence of solvents, ions, and other factors. Enzyme conformational flexibility is necessary for the production of certain effects, and the evidence suggests that enzyme folding and unfolding may indicate a loss of enzyme activity that precedes any marked changes in protein conformation.[83] Flexibility results for the amino acid residues of trypanothione reductase revealed that of the amino acids present in the protein, the residues in positions 1-2, 79, 81-87, 89, 305, 355, 458-462, and 480-483 favored conformational changes and protein flexibility when complexed with the compound. This may be related to the fact that the protein under study was constructed using homology modeling.

The Coulomb and Lennard-Jones interaction energy calculations for the protein-ligand complexes and compound 4 (FERAI) demonstrated stable RMSD and interaction energies which in addition to enabling interaction, flexibility and stability, suggests that compound 04 interacts at the active site of the trypanothione reductase enzyme. It was also observed that the RMSD of FERAI did not present high stability for dihydroorotate dehydrogenase, suggesting that the compound does not interact significantly with this enzyme.

## 4. Conclusions

Based on our results, the four compounds tested did not present significant cytotoxicity compared to Amphotericin B. However, of the compounds tested, FERAI presented the highest potency against *L. braziliensis*

promastigotes and amastigotes, and was also able to reduce the both percentage of *Leishmania* infected macrophages, and the number of intracellular parasites *in vitro*. The ROS test results indicated that the compound possibly acts by increasing ROS in the parasite and may be one of the mechanisms of action involved in FERAI's antileishmanial activity. Molecular docking revealed that FERAI interacts with UDP-Glycosyl pyrophosphorylase, with stronger, more potent inhibition of dihydroorotate dehydrogenase, and trypanothione reductase. Trypanothione reductase, a possible target for FERAI in *L. braziliensis* presented more stable RMSD and Coulomb and Lennard-Jones interaction energies as well.

## Supplementary Information

Supplementary information concerning the synthesis of the molecules, characterization and extra information on the protein-binding sequence of the enzymes involved in this study are available free of charge at http://jbcs.sbq.org.br.

## Acknowledgments

We thank the Federal University of Paraíba and its Postgraduate Program in Natural Products and Bioactive Synthetics for their institutional support, and also the Oswaldo Cruz Foundation (Fiocruz), Bahia-BR for instrumental and technological support.

## Author Contributions

Silva, G. R., Sousa, N. F., Leite, F. F., (Investigation, writing original draft,

validation); Santos, F. S., Acevedo, C. A. H., Grimaldi, G. B. (Conceptualization, formal analysis); Soares, M. B. P., Guimarães, E. T., Rodrigues, L. C., Campana, E. H. (Funding acquisition, project administration); Scotti, M. T., Mendonça, F. J. B. (Resources, Validation, Visualization); Barbosa Filho, J. M., Guimarães, H. I. F., Guerra, F. Q. S. (Writing-review & editing).

**References**


1. Mohammad, B.; Khurshid, A.; Sudeep, R.; Jalaluddin, M. A.; Mohd, A.; Mohammad, H. S.; Saif, K.; Mohammad, A. K.; Ivo, P.; Inho, C.; *Current Pharmaceutical Design* **2016**, *22*, 5, 572-581. [https://doi.org/10.2174/1381612822666151125000550]
2. Raies, A. B.; Bajic, V. B.; *Computational Molecular Science* **2016**, *6*, 2, 147-172. [https://doi.org/10.1002/wcms.1240]
3. Yang, X.; Wang, Y.; Byrne, R.; Schneider, G.; Yang, S.; *Chemical Reviews* **2019**, *119*, 18, 10520-10594. [https://doi.org/10.1021/acs.chemrev.8b00728]
4. Aliper, A.; Plis, S.; Artemov, A.; Ulloa, A.; Mamoshina, P.; Zhavoronkov, A.; *Molecular Pharmaceuticals* **2016**, *13*, 7, 2524-2530. [https://doi.org/10.1021/acs.molpharmaceut.6b00248]
5. Gloriozova, T. A.; Dembitsky, V. M.; *International Journal of Chemical Studies* **2018**, *6*, 1, 832-839. [https://doi.org/10.1007/s13659-016-0117-3]
6. Jiao, X.; Jin, X.; Ma, Y.; Yang, Y.; Li, J.; Liang, L.; Liu, R.; Li, Z.; *Computational Biology and Chemistry* **2021**, *90*. [https://doi.org/10.1016/j.compbiolchem.2020.107402]
7. Sakai, M.; Nagayasu, K.; Shibui, N.; Andoh, C.; Takayama, K.; Shirakawa, H.; Kaneko, S.; *Scientific Reports* **2021**, *11*, 525. [https://doi.org/10.1038/s41598-020-80113-7]
8. Gupta, M.; Sharma, R.; Kumar, A.; *Biology and Chemistry* **2018**, *76*, 210-217. [https://doi.org/10.1016/j.compbiolchem.2018.06.005]
9. Zaid, N. A. M.; Sekar, M.; Bonam, S. R.; Gan, S. H.; Lum, P. T.; Begum, M. Y.; Rani, N. N. I. M.; Vaijanathappa, J.; Wu, Y. S.; Subramaniyan, V.; Fuloria, N. K.; Fuloria, S.; *Drug Desing, Development and Therapy* **2022**, *16.* [https://doi.org/10.2147/DDDT.S326332]
10. Al-Shuaeeb, R. A. A.; El-Mageed, H.; R.; A.; Ahmed, S.; Mohamed, H. S.; Hamza, Z. S.; Rafi, M. O.; Ahmad, I.; Patel, H.; *Journal of*

*Biomolecular Structure and Dynamics* **2023**, *41*, 23. [https://doi.org/10.1080/07391102.2023.2212778]

11. Thayumanavan, G.; Jeyabalan, S.; Fuloria, S.; Sekar, M.; Ravi, M.; Selvaraj, L. K.; Bala, L.; Chidambaram, K.; Gan, S. H.; Rani, N. N. I. M.; Begum, M. Y.; Subramanaiyan, V.; Sathasivam, K. V.; Meenakshi, D. U.; Fuloria, N. K.; *Molecules* **2022**, *27*, 8, 2572. [https://doi.org/10.3390/molecules27082572]
12. Njogu, P. M.; Guantai, E. M.; Pavadai, E.; Chibale, K.; ACS Infectious Diseases **2015**, *2*, 1, 8–31. [https://doi.org/10.1021/acsinfecdis.5b00093]
13. Ullah, A.; Munir, S.; Badshah, S. L.; Khan, N.; Gani, L.; Poulson, B. G.; Emwas, H.; Jaremko, M.; *Molecules* **2020**, *25*, 22. [https://doi.org/10.3390/molecules25225243]
14. Moradian, N.; Hatam, G.; Hamedi, A.; Pasdaran, A.; *Chemical Biology & Drug Design* **2023**, *101,* 6. [https://doi.org/10.1111/cbdd.14226]
15. Lourenço, E. M. G.; Silva, F.; Neves, A. R.; Bonfá, I. S.; Ferreira, A. M. T.; Menezes, A. C. G.; Silva, M. C. E.; Santos, J. T.; Martines, M. A. U.; Perdomo, R. T.; Toffoli-Kadri, M. C.; Barbosa, E. G.; Sabá, S.; Beatriz, A.; Rafique, J.; Arruda, C. C. P.; Lima, D. P.; *ACS Infect. Dis.* **2023,** 9, 10, 2048-2061. [https://doi.org/10.1021/acsinfecdis.3c00336]
16. Chepkirui, C.; Ochieng, P. J.; Sarkar, B.; Hussain, A.; Pal, C.; Yangc, J.; Coghi, P.; Akala, H. M.; Derese, S.; Ndakala, A.; Heydenreich, M.; Wong, V. K. W.; Erdélyi, M.; Yenesew, A.; *Fitoterapia* **2021,** 149. [https://doi.org/10.1016/j.fitote.2020.104796]
17. Al-Huqail, A. A.; Bekhit, A. A.; Ullah, H.; Ayaz, M.; Mostafa, N. M.; *Agronomy* **2023**, 13, 11, 2765. [https://doi.org/10.3390/agronomy13112765]
18. Hernandéz-Rivera, J. L.; Espinoza-Hicks, J. C.; Chacón-Vargas, K. F.; Carrillo-Campos, J.; Sánchez-Torres, L. E.; Camacho-Dávila, A. A.; *Molecular Diversity* **2023,** *27*, 2073-2092. [https://doi.org/10.1007/s11030-022-10542-1]
19. Santos, R. F.; Silva, T.; Brito, A. C. S.; Inácio, J. D.; Ventura, B. D.; Mendes, M. A. P.; Azevedo, B. F.; Siqueira, L. M.; Almeida-Amaral, E. E.; Dutra, P. M. L.; Da-Silva, S. A. G.; *Frontiers in Cellular and Infection Microbiology* **2023,** *12*. [https://doi.org/10.3389/fcimb.2022.1059168]
20. Rudrapal, M.; Khan, J.; Dukhyil, A. A. B.; Alarousy, R. M. I. I.; Attah, E. I.; Sharma, T.; Khairnar, S. J.; Bendale, A. R.; *Molecules* **2021,** 26, 23, 7177. [https://doi.org/10.3390/molecules26237177]
21. Ministério da Saúde; *Manual de vigilância e controle da leishmaniose visceral*; Brasília, 2014. [https://bvsms.saude.gov.br/bvs/publicacoes/manual_vigilancia_controle_leishmaniose_visceral_1edicao.pdf] acessed in March 2023

22. Ministério da Saúde; *Manual de Leishmaniose Visceral*; Brasília, 2021. [https://www.gov.br/saude/pt-br/assuntos/saude-de-a-a-z/l/leishmaniose-visceral] acessed in March 2023
23. Tiwari, N.; Gedda, M. R.; Tiwari, V. K.; Singh, S. P.; Singh, R. K.; *Mini-Reviews in Medicinal Chemistry* **2017**, *18*, 1. [https://doi.org/10.2174/1389557517666170425105129]
24. Winter, C.; Caetano, J. N.; Araújo, A. B. C.; Chaves, A. R.; Ostroski, I. C.; Vaz, B. G.; Pérez, C. N.; Alonso, C. G.; *Chemical Engineering Journal* **2016**, *303*, 604–610. [https://doi.org/10.1016/j.cej.2016.06.058]
25. PASS filter online, *version 2.0*; Way2Drug; Moscow, Russia.
26. Goel, R. K.; Singh, D.; Lagunin, A; Poroikov, V.; *Medicinal Chemistry Research* **2010***, 20*, 9, 1509–1514. [https://doi.org/10.1007/s00044-010-9398-y]
27. Scotti, M. T.; Herrera-Acevedo, C.; Menezes, R.; Martin, H. J.; Muratov, E.; Silva, Á. Í. D. S.; Albuquerque, E. F.; Calado, L. F.; Coy-Barrera, E.; Scotti, L.; *Molecular Informatics* **2022,** *41*, 12. [https://doi.org/10.1002/minf.202200133]
28. Maia, M. S.; Silva, J. P. R.; Nunes, T. A. L.; Sousa, J. M. S.; Rodrigues, G. C. S.; Monteiro, A. F. M.; Tavares, J. F.; Rodrigues, A. F.; Mendonça-Junior, F. J. B.; Scotti, L.; Scotti, M. T.; *Molecules* **2020**, *25,* 10, 2281. [https://doi.org/10.3390/molecules25102281]
29. Magalhães, T. B. S.; Silva, D. K. C.; Teixeira, J. S.; de Lima, J. D. T.; Barbosa-Filho, J. M.; Moreira, D. R. M.; Guimarães, E. T.; Soares, M. B. P.; *Frontiers in Pharmacology* **2022**, *13,* 1-13. [https://doi.org/10.3389/fphar.2022.846123]
30. Passos, C. L. A.; Ferreira, C.; Soares, D. C.; Saraiva, E. M.; *PLOS ONE* **2015,** *10,* 10, e0141778. [https://doi.org/10.1371/journal.pone.0141778]
31. FlowJo, *version* 10.6.1; Becton, Dickinson and Company, Ashland, OR, USA.
32. Research Collaboratory for Structural Bioinformatics, https://www.rcsb.org/pdb/home/home.do, accessed in February 2023.
33. National Library of Medicine, https://www.ncbi.nlm.nih.gov/, accessed in February 2023.
34. European Molecular Biology Laboratory, https://www.ebi.ac.uk/Tools/msa/clustalo/, accessed in February 2023.
35. Bernstein, F. C.; Koetzle, T. F.; Williams, G. J. B.; Meyer, E. F.; Brice, M. D.; Rodgers, J. R.; Kennard, O.; Shimanouchi, T.; Tasumi, M.; *Journal of Molecular Biology* **1977**, *112,* 3, 535–542. [https://doi.org/10.1016/s0022-2836(77)80200-3]
36. Waterhouse, A.; Bertoni, M.; Bienert, S.; Studer, G.; Tauriello, G.; Gumienny, R.; Heer, F. T.; de Beer, T. A. P.; Rempfer, C.; Bordoli, L.;

Lepore, R; Schwede, T.; *Nucleic Acids Research* **2018**, *46,* 296-303. [https://doi.org/10.1093/nar/gky427]
37. Swiss-Model, https://swissmodel.expasy.org/, accessed in February 2023.
38. Protein Structure Validation Software Suite, http://psvs-1_5-dev.nesg.org/, accessed in February 2023.
39. Laskowski, R. A.; MacArthur, M. W.; Moss, D. S.; Thornton, J. M.; *Journal of Applied Crystallography* **1993***, 26,* 2, 283–291. [https://doi.org/10.1107/s0021889892009944]
40. Lovell, S. C.; Davis, I. W.; Arendall, W. B.; de Bakker, P. I. W.; Word, J. M.; Prisant, M. G.; Richardson, J. S.; Richardson, D. C.; *Proteins: Structure, Function, and Bioinformatics* **2003**, *50,* 3, 437–450. [https://doi.org/10.1002/prot.10286]
41. Molegro Virtual Docker*, version 6.0.1*; Molexus IVS, Denmark.
42. Thomsen, R.; Christensen, M. H.; *Docking. Journal of Medicinal Chemistry* **2006**, *49*, 11, 3315–3321. [https://doi.org/10.1021/jm051197e]
43. Abraham, M. J.; Murtola, T.; Schulz, R.; Páll, S.; Smith, J. C.; Hess, B.; Lindahl, E.; *SoftwareX* **2015**, *1,* 19–25. [https://doi.org/10.1016/j.softx.2015.06.001]
44. GROMACS, *version* 2.1; Sphinx&Alabaster, Netherlands.
45. Bondi, A. Van Der Waals Volumes and Radii. *J. Phys. Chem*. **1964**, *68*, 441–451. [https://doi.org/10.1021/J100785A001]
46. RBVI UCSF Chimera; Chimera Commercial Licensing, California, USA.
47. Pettersen, E. F.; Goddard, T. D.; Huang, C. C.; Meng, E. C.; Couch, G. S.; Croll, T. I.; Morris, J. H.; Ferrin, T. E.; *Protein Science* **2021**, *30*, 70–82. [https://doi.org/10.1002/pro.3943]
48. Nachbagauer, R.; Feser, J.; Naficy, A.; Bernstein, D. I.; Guptill, J.; Walter, E. B.; Berlanda-Scorza, F.; Stadlbauer, D.; Wilson, P. C.; Aydillo, T.; *Nat. Med*. **2021**, *27*, 106–114. [https://doi.org/10.1038/s41591-020-1118-7]
49. Grace Development Team, http://plasma-gate.weizmann.ac.il/Grace/, accessed in March 2023.
50. GraphPad Prism, *version* 9.5.1; GraphPad Software, Boston, MA, USA.
51. MolPredictX, https://www.molpredictx.ufpb.br/, accessed in March 2023.
52. Adinehbeigi, K.; Razi Jalali, M. H.; Shahriari, A.; Bahrami, S.; *Pathogens and Global Health* **2017**, *111*, 4, 176–185. [https://doi.org/10.1080/20477724.2017.1312777]
53. Rocha, V.; Quintino da Rocha, C.; Ferreira Queiroz, E.; Marcourt, L.; Vilegas, W.; Grimaldi, G.; Furrer, P.; Allémann, É.; Wolfender, J. L.;

Soares, M.; *Molecules* **2018**, *24*, 1, 1. [https://doi.org/10.3390/molecules24010001]
54. Zheoat, A. M.; Alenezi, S.; Elmahallawy, E. K.; Ungogo, M. A.; Alghamdi, A. H.; Watson, D. G.; Igoli, J. O.; Gray, A. I.; de Koning, H. P.; Ferro, V. A.; *Pathogens* **2021,** *10*, 2, 175. [https://doi.org/10.3390/pathogens10020175]
55. Gomes, A. N. P.; Camara, C. A.; Sousa, A. S.; Santos, F. A. R.; Santana Filho, P. C.; Dorneles, G. P.; Romão, P. R. T.; Silva, T. M. S.; *Revista Brasileira de Farmacognosia* **2021**, *31*, 2, 176–183. [https://doi.org/10.1007/s43450-021-00130-z]
56. Alonso, L.; Menegatti, R.; Gomes, R. S.; Dorta, M. L.; Luzin, R. M.; Lião, L. M.; Alonso, A.; *European Journal of Pharmaceutical Sciences* **2020**, *151*, 105407. [https://doi.org/10.1016/j.ejps.2020.105407]
57. Nardella, F.; Gallé, J. B.; Bourjot, M.; Weniger, B.; Vonthron-Sénécheau, C.; *Cham: Springer International Publishing* **2018,** 163–194. [https://doi.org/10.1007/978-3-319-67045-4_7]
58. Ortalli, M.; Ilari, A.; Colotti, G.; De Ionna, I.; Battista, T.; Bisi, A.; Gobbi, S.; Rampa, A.; Di Martino, R. M. C.; Gentilomi, G. A.; Varani, S.; Belluti, F.; *European Journal of Medicinal Chemistry* **2018,** *152*, 527–541. [https://doi.org/10.1016/j.ejmech.2018.04.057]
59. Oprea, T. I.; *Chemoinformatics in Drug Discovery* **2005**. [https://doi.org/10.1002/3527603743]
60. Cruz, J. H. D. A.; Moreira, I. C. D. S.; Alves, M. D. F. V.; Oliveira, H. M. B. F. D.; Oliveira Filho, A. A. D.; Alves, M. A. S. G.; *Archives of Health Investigation* **2020**, *8,* 11. [https://doi.org/10.21270/archi.v8i11.4314]
61. Surabhi, S.; Singh, B.; *Journal of Drug Delivery and Therapeutics* **2018**, *8,* 5, 504–509. [https://doi.org/10.22270/jddt.v8i5.1894]
62. Yu, W.; MacKerell, A. D.; *Methods in Molecular Biology* **2016,** 85–106. [https://doi.org/10.1007/978-1-4939-6634-9_5]
63. Mello, M. V. P.; Abrahim-Vieira, B. D. A.; Domingos, T. F. S.; de Jesus, J. B.; de Sousa, A. C. C.; Rodrigues, C. R.; Souza, A. M. T. D.; *European Journal of Medicinal Chemistry* **2018**, *150*, 920–929. [https://doi.org/10.1016/j.ejmech.2018.03.047]
64. N'guessan, D. U. J. P.; Alzain, A. A.; Adouko, E. M.; *Journal of Applied Pharmaceutical Sciences and Research* **2021,** *4*, 3. [https://doi.org/10.31069/japsr.v4i3.4]
65. Osman, M. S.; Awad, T. A.; Shantier, S. W.; Garenalbi, E. A.; Osman, W.; Mothana, R. A.; Nasr, F. S.; Elhag, E. R.; *Arabian Journal of Chemistry* **2022**, *15*, 4. [https://doi.org/10.1016/j.arabjc.2022.103717]
66. Tolosa, L.; Donato, M. T.; Gómez-Lechón, M. J.; *Methods in Molecular Biology*. New York, NY: Springer New York, **2014**, 333–348.

67. Costa, C. A.; Lopes, R. M.; Ferraz, L. S.; Esteves, G. N. N.; Di Iorio, J. F.; Souza, A. A.; de Oliveira, I. M.; Manarin, F.; Judice, W. A. S.; Stefani, H. A.; Rodrigues, T.; *Bioorganic & Medicinal Chemistry* **2020**, *28*, 11, 115511. [https://doi.org/10.1016/j.bmc.2020.115511]
68. Zhang, S.; Li, T.; Zhang, Y.; Xu, H.; Li, Y.; Zi, X.; Yu, H.; Li, J.; Jin, C. Y.; Liu, H. M.; *Toxicology and Applied Pharmacology* **2016**, *309*, 77–86. [https://doi.org/10.1016/j.taap.2016.08.023]
69. Sinha, S.; Batovska, D. I.; Medhi, B.; Radotra, B. D.;, Bhalla, A.; Markova, N.; Sehgal, R.; *Malaria Journal* **2019**, *18*, 1. [https://doi.org/10.1186/s12936-019-3060-z]
70. Escrivani, D. O.; Charlton, R. L.; Caruso, M. B.; Burle-Caldas, G. A.; Borsodi, M. P. G.; Zingali, R. B.; Arruda-Costa, N.; Pameira-Mello, M. V.; Jesus, J. B.; Souza, A. M. T.; Abrahim-Vieira, B.; Freitag-Pohl, S.; Pohl, E.; Steel, P. G.; *PLOS Neglected Tropical Diseases* **2021**, *15*, 11. [https://doi.org/10.1371/journal.pntd.0009951]
71. Bello, M. L.; Chiaradia, L. D.; Dias, L. R. S.; Pacheco, L. K.; Stumpf, T. R.; Mascarello, A.; Steindel, M.; Yunes, R. A.; Castro, H. C.; Nunes, R. J.; Rodrigues, C. R.; *Bioorganic & Medicinal Chemistry* **2011**, *19*, 16, 5046–5052. [https://doi.org/10.1016/j.bmc.2011.06.023]
72. Santiago-Silva, K. M.; Bortoleti, B. T. S.; Oliveira, L. N.; Maia, L. F. A.; Castro, J. C.; Costa, I. C.; Lazarin, D. B.; Wardell, J. L.; Wardell, S. M. S. V.; Albuquerque, M. G.; Lima, C. H. S.; Pavanelli, W. R.; Bispo, M. L. F.; Gonçalves, R. S. B.; *Antibiotics* **2022**, *11*, 1402. [https://doi.org/10.3390/antibiotics11101402]
73. Jitareanu, A.; Tataringa, G.; Zbancioc, A. M.; Trifan, A.; *The Medical-Surgical Journal* **2018**, *122*, 3.
74. Ministério da Saúde; *Manual de Leishmaniose Tegumentar*; Brasília, 2017. [https://bvsms.saude.gov.br/bvs/publicacoes/manual_vigilancia_leishmaniose_tegumentar.pdf] acessed in March 2023
75. Vasconcelos, J. M.; Gomes, C. G.; Sousa, A.; Teixeira, A. B.; Lima, J. M.; *Revista Brasileira de Análises Clínicas* **2018,** *50*, 3, 221-227. [https://doi.org/10.21877/2448-3877.201800722]
76. Kong, L.; Ju, F.; Zheng, W.; Zhu, J.; Sun, S.; Xu, J.; Bu, D.; *Journal of Computational Biology* **2022**. [https://doi.org/10.1089/cmb.2021.0430]
77. Gao, M.; Skolnick, J.; *Bioinformatics* **2020**. [https://doi.org/10.1093/bioinformatics/btaa810]
78. Fu, Y.; Zhao, J.; Chen, Z.; *Computational and Mathematical Methods in Medicine* **2018**, 1–12. [https://doi.org/10.1155/2018/3502514]
79. Pinzi, L.; Rastelli, G.; *International Journal of Molecular Sciences* **2019**, *20*, 18, 4331. [https://doi.org/10.3390/ijms20184331-]
80. Fan, J.; Fu, A.; Zhang, L.; *Quantitative Biology* **2019**, *7*, 2, 83–89. [https://doi.org/10.1007/s40484-019-0172-y]

81. Zhang, X.; Stevens, R. C.; Xu, F.; *Trends in Biochemical Sciences* **2015,** *40*, 2. [https://doi.org/10.1016/j.tibs.2014.12.005]
82. Tripathi, M. K.; Ahmad, S.; Tyagi, R.; Dahiya, V.; Yadav, M. K.; *Computer Aided Drug Design (CADD): From Ligand-Based Methods to Structure-Based Approaches* **2022.** [https://doi.org/10.1016/8978-0-323-90608-1.00001-0]
83. Yan, B. X.; Sun, Y. Q.; *Journal of Biological Chemistry* **1997,** *272*, 6. [https://doi.org/10.1074/jbc.272.6.3190]

# Conclusões e Perspectivas

## CONCLUSÕES E PERSPECTIVAS

Em conclusão, um total de 18 compostos foram sintetizados, sendo 2 dímeros de chalcona FER26 e FER23(A), 1 monômero FER23(B) e 15 chalconas. Desses, 9 estão sendo relatadas pela primeira vez na literatura. Os compostos foram sintetizados partindo de reagentes simples, baratos e de fácil acesso. Foram usadas técnicas conhecidas na literatura, como alquilações, alilações, acilações e condensações de Claisem.

Dos compostos sintetizados, 10 foram avaliados frente a formas promastigotas e amastigotas de *Leishmania infantum*, em que 6 apresentaram atividade inibitória, sendo 3 considerados os mais promissores, dentre eles o composto CP03 ganhou destaque, apresentando uma $IC_{50}$ de 10 µm, além de apresentar ausência de hemólise em eritrócitos. Com isso destacamos a importância da classe chalcona com relação a suas propriedades farmacológicas, sendo candidatos terapêuticos com grande potencial.

Ainda dos compostos sintetizados, 4 foram testados *in vitro* e in sílico contra *Leishmania brasiliensis,* dentre eles o composto FER13 se mostrou mais promissor frente ao parasita. O composto demonstrou maior poder de inibição entre as 2 espécies de Leishmania testadas, se tornando um candidato promissor a criação de novos derivados.

Novas sínteses com a formação desses derivados podem ser consideradas, utilizando os compostos ativos como protótipos para a formação de novos derivados, possibilitando potencializar ainda mais essas propriedades.

# Material Suplementar

**MATERIAL SUPLEMENTAR**

ACILAÇÃO DA RESORCINA

Em balão de fundo redondo foi pesado e adicionado 5 g (1 eq, 45,409 mmol) de resorcina e solubilizados em 5,2 mL (1,1 eq, 49,95 mmol) de anidrido acético. Após total solubilização, foi adicionado 21,5 mL (3,5 eq, 158,931 mmol) de trifluoreto de boroeterato ($BF_3.Et_2O$). O sistema foi deixado sob agitação magnética em temperatura ambiente por 24 h sendo monitorada por Cromatografia em Camada Delgada Analítica (CCDA) (Schimidt NG & KROUTIL W. 2017). Após o tempo de reação foi feito uma partição com água, gelo e acetato de etila. A fase orgânica foi lavada por 3 vezes, sendo seca em sulfato de sódio anidro e purificada por recristalização em hexano, obtendo um sólido esbranquiçado (Esquema 8).

Esquema 3: Acilação da resorcina.

Acilação da resorcina.

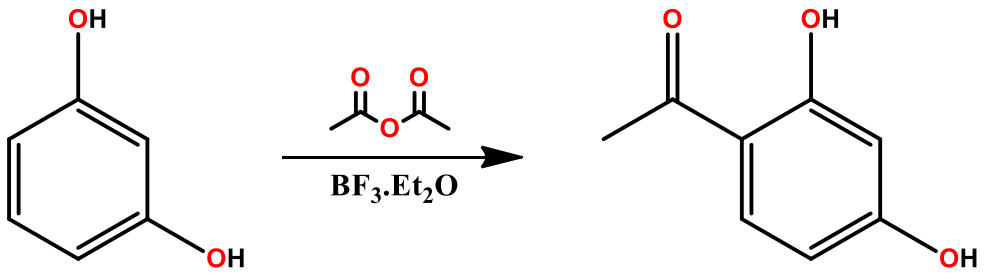


resorcinol 1-(2,4-dihidroxifenil)etanona

Fonte: autor, 2024

DIMERIZAÇÃO DA VANILINA

Em um erlemeyer de 50 mL foram solubilizados 2g de vanilina (1 eq, 13,14 mmol) sob agitação magnética a 50 °C. Um segundo erlemeyer de 50 mL foi solubilizado 2,4 g (1 eq, 13,14 mmol) de cloreto férrico hexahidratado ($FeCl_3.6H_2O$) (Esquema 9). A solução de cloreto férrico foi adicionada a solução contendo a vanilina, sendo observado uma mudança de coloração imediata, partindo de um transparente límpido para um tom roxo. A reação foi deixada sob agitação magnética, em temperatura ambiente por 24 h, sendo monitorada por CCDA. Foi observado a formação de um sólido de coloração cinza. Após as 24 h o sólido foi filtrado em placa porosa e kitassato sob sistema de vácuo. O sólido foi lavado por 3 vezes com água destilada e 3 vezes com metanol, sendo seco

em dessecador a vácuo, apresentando um rendimento aproximado de 25% (~500 mg).

Esquema 4: Dimerização da vanilina.

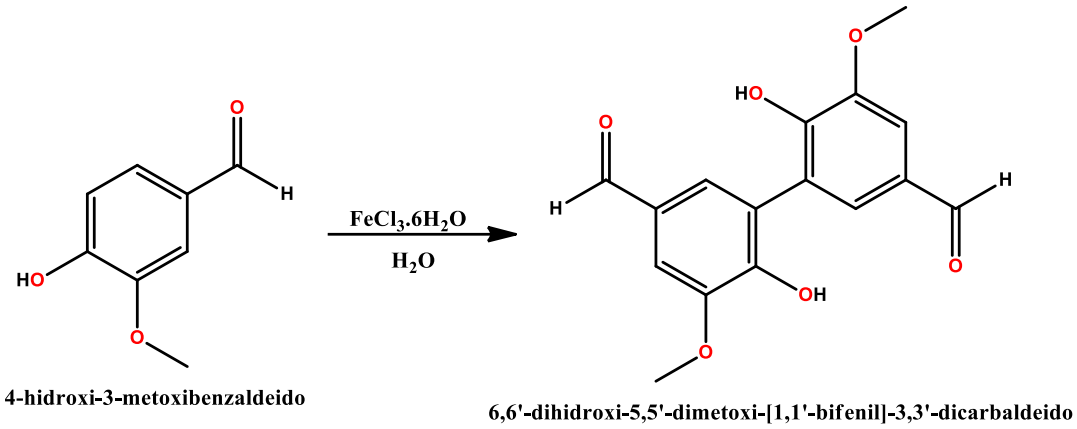


4-hidroxi-3-metoxibenzaldeido

6,6'-dihidroxi-5,5'-dimetoxi-[1,1'-bifenil]-3,3'-dicarbaldeido

Fonte: autor, 2023.

BROMAÇÃO DA VANILINA

Em erlemeyer de 500 mL foi pesado 2 g de vanilina (1 eq, 13,14 mmol) e solubilizado em 100 mL de solução (0,32 molar) contendo ácido acético e bromo ($Br_2$), a reação (Esquema 10) foi deixada sob agitação magnética por 24 h, sendo monitorada por CCDA. Foi observado uma mudança de coloração partindo de um laranja forte para um laranja mais claro com um pó suspenso turvando o meio reacional. Após o tempo de reação a agitação foi suspensa, promovendo uma decantação do sólido. Foi feita uma filtração do sólido sob vácuo, em funil de placa porosa e kitassato, sendo lavado por 3 vezes com água destilada. O produto resultante foi seco em dessecador, obtendo um rendimento aproximado de 45%.

Esquema 5: Bromação da vanilina.

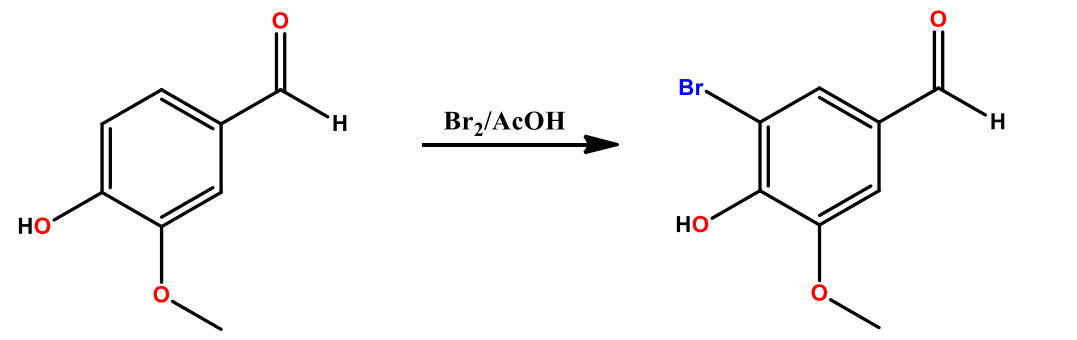


4-hidroxi-3-metoxibenzaldeido

3-bromo-4-hidroxi-5-metoxibenzaldeido

Fonte: autor, 2024.

ADIÇÃO DE GRUPOS ALQUILA E ALILA

Um procedimento geral para as adições de grupamentos alquila e alila foi utilizado, sendo comum em todas as reações.

Foram pesados e adicionados em erlemeyer de 250 mL, 2 g do acetil resorcinol (1 eq, 13,15 mmol) e solubilizado em dimetil-formamida (DMF) (Esquema 11). Foi adicionado 5,6 g (3 eq, 39,45 mmol) de iodo metano ($ICH_3$) e 5,4 g (3 eq, 39,45 mmol) de carbonato de potássio ($K_2CO_3$). A reação foi deixada sob agitação magnética por 24 h, sendo monitorada por CCDA. Após o tempo de reação foi feito uma partição com acetato de etila e água destilada, a fase orgânica foi seca em sulfato de sódio anidro. Foi obtido um rendimento aproximado de 95%.

Esquema 6: Metilação da acetofenona da resorcina.

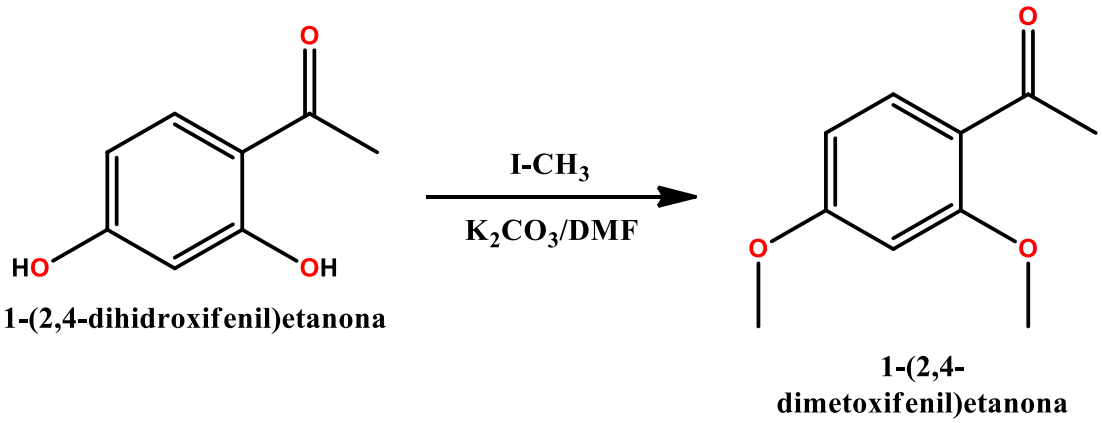


1-(2,4-dihidroxifenil)etanona

1-(2,4-dimetoxifenil)etanona

Fonte: Autor, 2024.

ETERIFICAÇÕES NA BROMO-VANILINA

Foram pesados e adicionados em erlemeyer de 250 mL 1 g de bromo vanilina (1 eq, 6,58 mmol), 1,2 g de carbonato de potássio (2 eq, 13,16 mmol) e os respectivos reagentes iodeto de metila 0,93 g (1 eq, 6,58 mmol), bromo etano 0, 72 g (1 eq, 6,58 mmol) e brometo de alila 0,79 g (1 eq, 6,58 mmol). As reações foram submetidas ao mesmo método, sendo solubilizadas em DMF e deixadas sob agitação magnética por 24 h (Esquema 12), a temperatura ambiente e sendo monitoradas por CCDA. Após consumo dos reagentes foram purificadas por partição com acetato de etila e água destilada, sendo lavadas por 3x e secada com sulfato de sódio anidro. Foram obtidos rendimentos entre 87-95%.

Esquema 7: Reações de eterificação na bromo-vanilina.

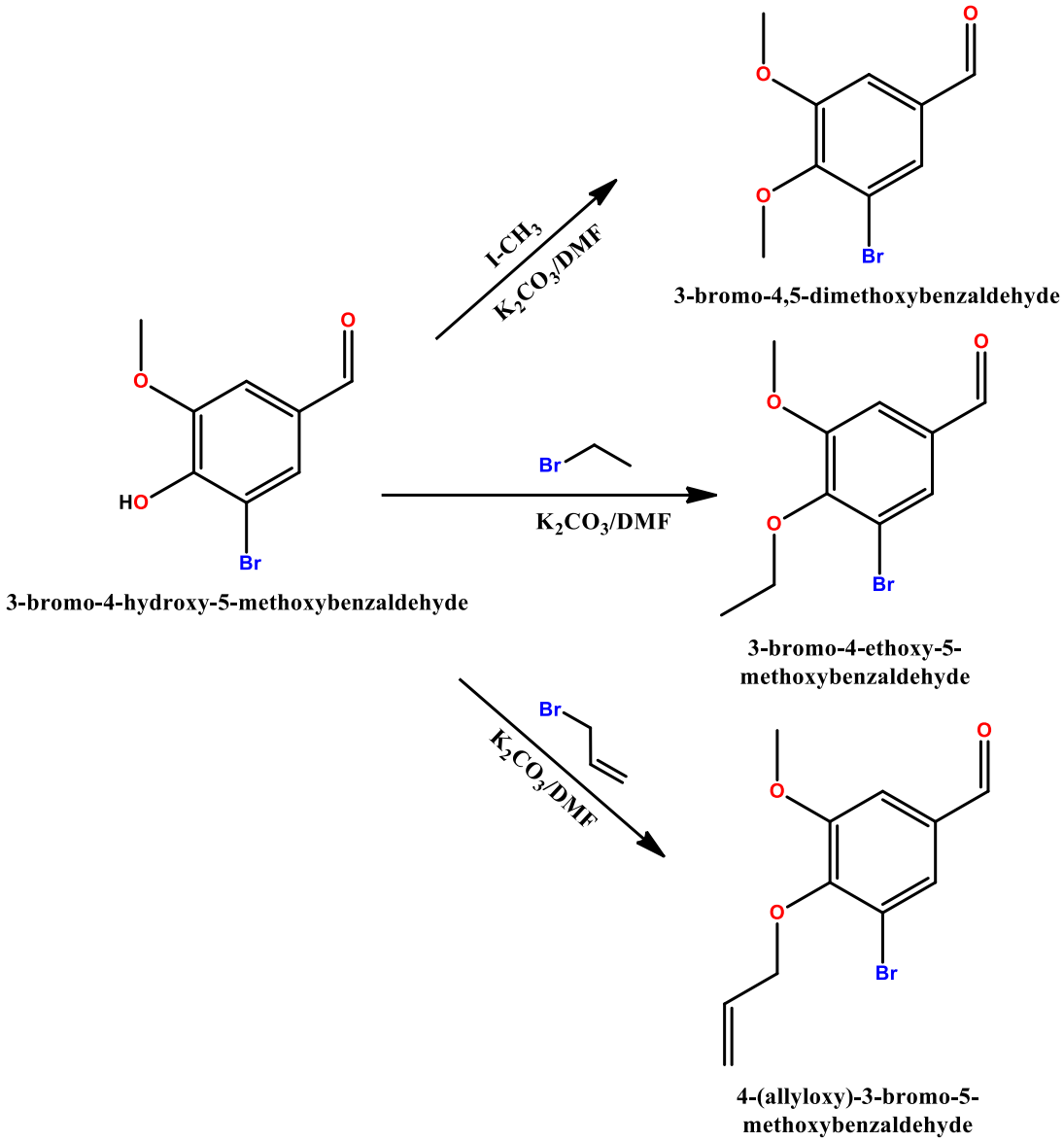


Fonte: Autor, 2024.

SÍNTESE DA BICHALCONA 1-(2,3-DIMETOXIFENIL)-3-(5'-(3-(2,4-DIMETOXIFENIL)-3-OXOPROP-1-EN-1-IL)-2',3',5,6-TETRAMETOXI-[1,1'-BIFENIL]-3-IL)PROP-2-EN-1-ONA (FER26)

Em um erlemeyer de 500 mL foi adicionado 0,1 g (1 eq: 0,30 mmol) de dimetil divanilina e 0,108 g (2 eq: 0,60) de 2,4-dimetoxi acetofenona, ambos foram solubilizados em 50 ml de etanol, e deixado em agitação magnética (Esquema 13). Em seguida foi adicionado 50 mL de uma solução de hidróxido de sódio (NaOH a 10%), havendo uma precipitação de um sólido amarelado. O sólido foi

filtrado e purificado em CCDP com sistema de eluição hexano: acetato de etila na proporção 8:3 com 3 eluições, com um rendimento aproximado de 40%.

Esquema 8: Síntese da bichalcona via condensação de Claisem.

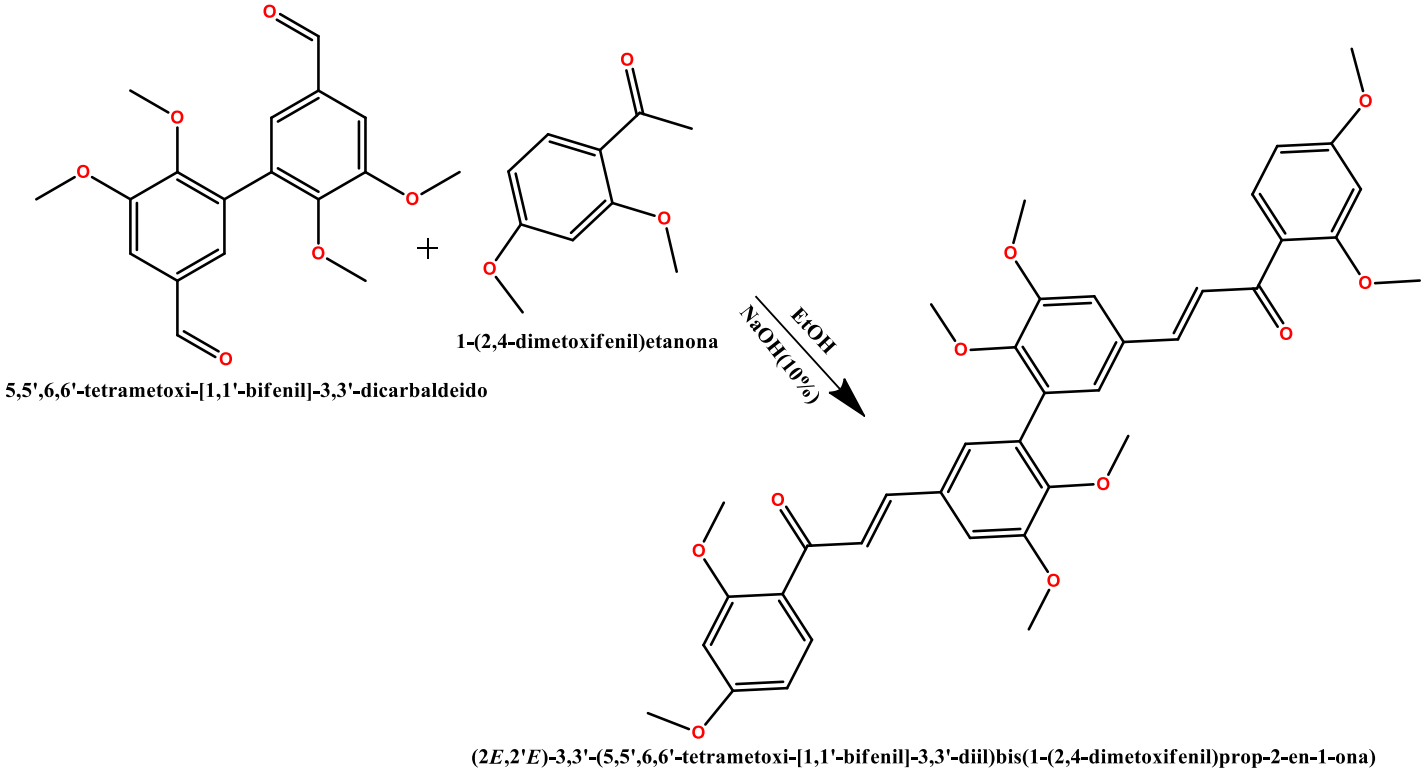


Fonte: autor, 2024.

SÍNTESE DA BICHALCONA (2E,2'E)-3,3'-(5,5',6,6'-tetrametoxi-[1,1'-bifenil]-3,3'-diil)bis(1-(benzo[d][1,3]dioxol-5-il)prop-2-en-1-ona) (FER23(A))

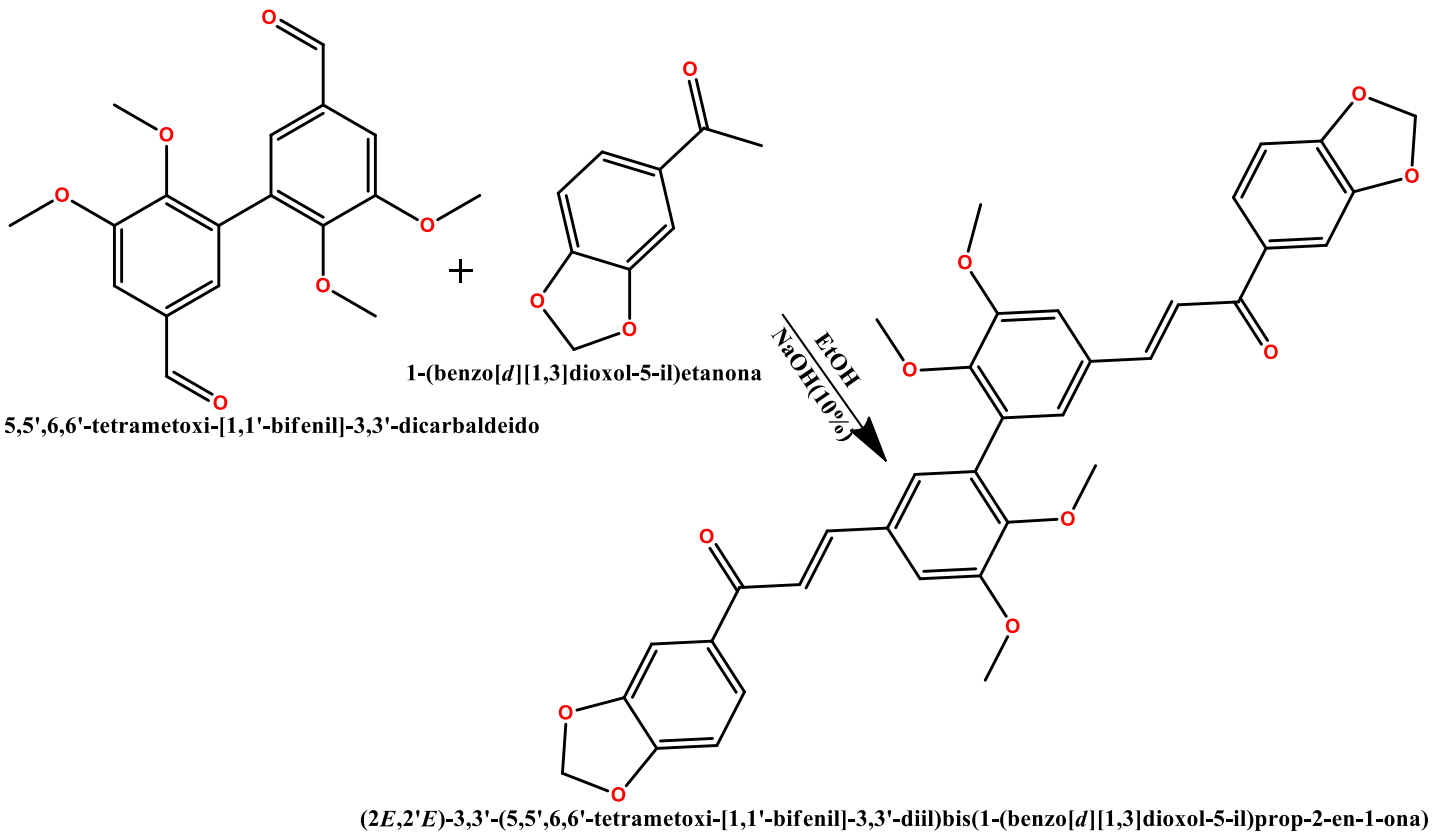


A metodologia utilizada na síntese da (2E,2'E)-3,3'-(5,5',6,6'-tetrametoxi-[1,1'-bifenil]-3,3'-diil)bis(1-(benzo[d][1,3]dioxol-5-il)prop-2-en-1-ona) foi semelhante à descrita no subitem 4.13. Em um erlemeyer de 500 mL foi adicionado 0,5 g (1 eq: 1,51 mmol) de divanilina (subitem 4.9) e 0,250 g (2 eq: 1,51) de 3,4-metilenodioxi acetofenona, ambos foram solubilizados em 50 ml de etanol, e deixado em agitação magnética (Esquema 14). Em seguida foi adicionado 50 mL de uma solução de hidróxido de sódio (NaOH a 10%), havendo uma precipitação de um sólido amarelado. O sólido foi filtrado e purificado em CCDP com sistema de eluição hexano: acetato de etila na proporção 8:2 com 3 eluições, com um rendimento aproximado de 40%.

SÍNTESE DA MONOCHALCONA 5'-(3-(BENZO[1,3]DIOXOL-5-IL)-3-OXOPROP-1-EN-1-IL)-2',3',5,6-TETRAMETOXI-[1,1'-BIFENIL]-3-CARBALDEÍDO (FER23(B))

*O* composto 5'-(3-(benzo[1,3]dioxol-5-il)-3-oxoprop-1-en-1-il)-2',3',5,6-tetrametoxi-[1,1'-bifenil]-3-carbaldeído (Esquema 14) foi obtido como produto secundário da bichalcona descrita em 7.14. A partir da CCDP foi purificado e analisado em espectroscopia de RMN $^{1}H$ e $^{13}C$. Para o composto FER23(B) foi obtido um rendimento de 25%.

Esquema 9: Síntese do FER23(B) via condensação de Claisem.

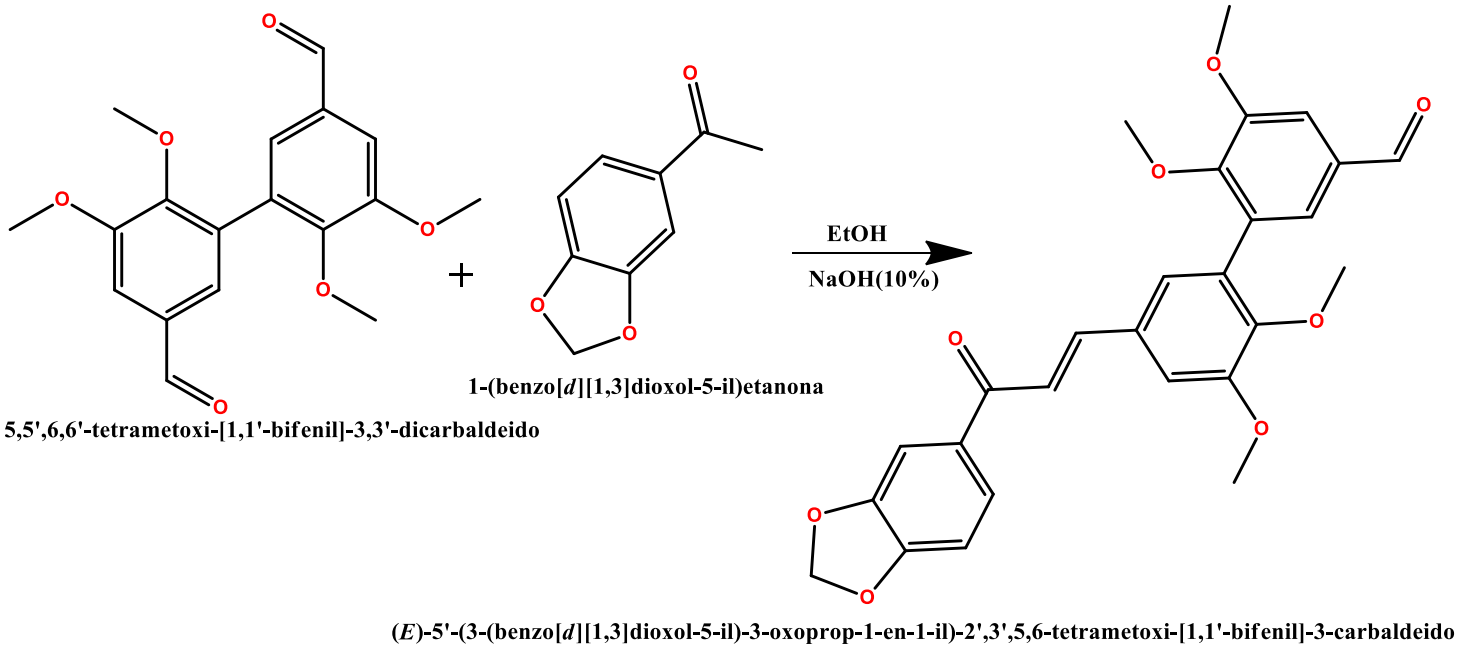


5,5',6,6'-tetrametoxi-[1,1'-bifenil]-3,3'-dicarbaldeido

1-(benzo[*d*][1,3]dioxol-5-il)etanona

(*E*)-5'-(3-(benzo[*d*][1,3]dioxol-5-il)-3-oxoprop-1-en-1-il)-2',3',5,6-tetrametoxi-[1,1'-bifenil]-3-carbaldeido

Fonte: autor, 2024.

PROCEDIMENTO GERAL PARA A SÍNTESE DAS CHALCONAS

Na síntese das chalconas foi utilizado um procedimento comum a todos os compostos, sendo derivadas da acetofenona 1-(benzo[d][1,3]dioxol-5-il)etanona com diferentes benzaldeídos.

Foram pesados e adicionados a um erlemeyer de 250 mL (1 eq, 3,05 mmol) de 1-(benzo[d][1,3]dioxol-5-il)etanona, (3 eq, 9,15 mmol) de hidróxido de potássio e (1 eq, 3,05 mmol) do respectivo aldeído (Esquema 15). Todas as reações foram feitas com metanol como solvente, sendo aplicado agitação magnética por 24 h a temperatura ambiente, sendo monitoradas por CCDA. Após o período de reação em todos os casos o produto precipitou, sendo extraído com

filtração a vácuo e lavado por 3x com metanol. Foram obtidos rendimentos que variam entre 70-90%.

Esquema 10: Procedimento geral na síntese das chalconas.

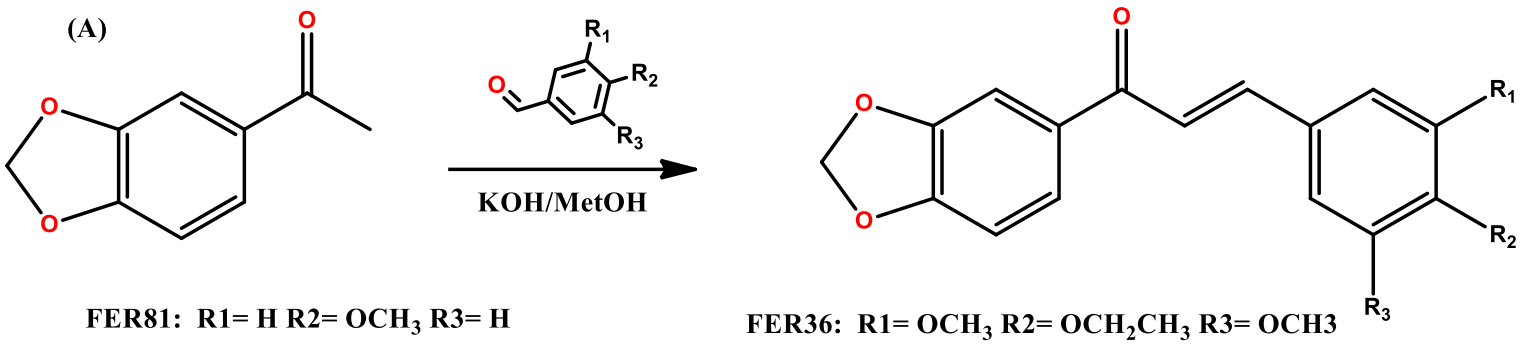


**FER81:** R1= H R2= $OCH_3$ R3= H

**FER18:** R1= H R2= $OCH_2CH_3$ R3= H

**FER89:** R1= H R2= $OCH_2CHCH_2$ R3=H

**FER08:** R1= $OCH_3$ R2= $OCH_3$ R3= Br

**FER13:** R1= $OCH_3$ R2= $OCH_2CH_3$ R3=Br

**FER12:** R1= $OCH_3$ R2= $OCH_2CHCH_2$ R3= Br

**FER36:** R1= $OCH_3$ R2= $OCH_2CH_3$ R3= OCH3

**FER37:** R1= $OCH_3$ R2= $OCH_2CHCH_2$ $R_3$= $OCH_3$

**FER41:** R1= H R2= Cl R3= H

**FER44:** R1= H R2= Cl R3= Cl

**FER42:** R1= H R2= $NH_2$ R3= H

**FER45:** R1= H R2= F R3= H

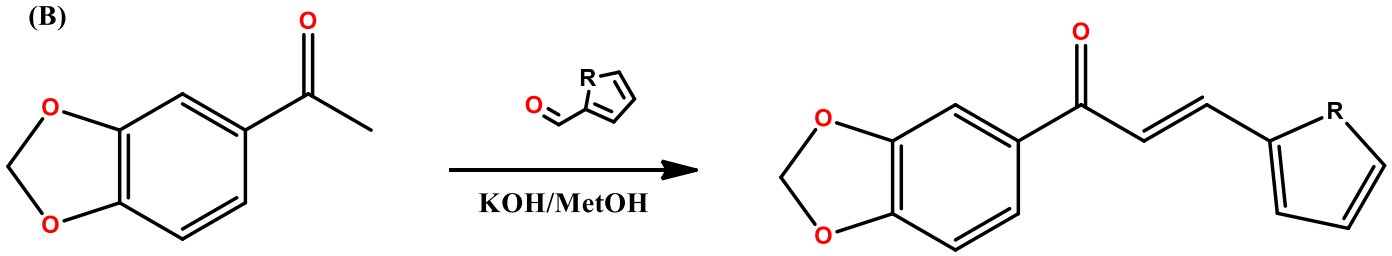


**FER38: R= O**
**FER39: R= S**

Fonte: autor, 2024.

**ANEXOS**

(2E,2'E)-3,3'-(5,5',6,6'-tetrametoxi-[1,1'-bifenil]-3,3'-diil)bis(1-(2,4-dimetoxifenil)prop-2-en-1-ona) (**FER26**)

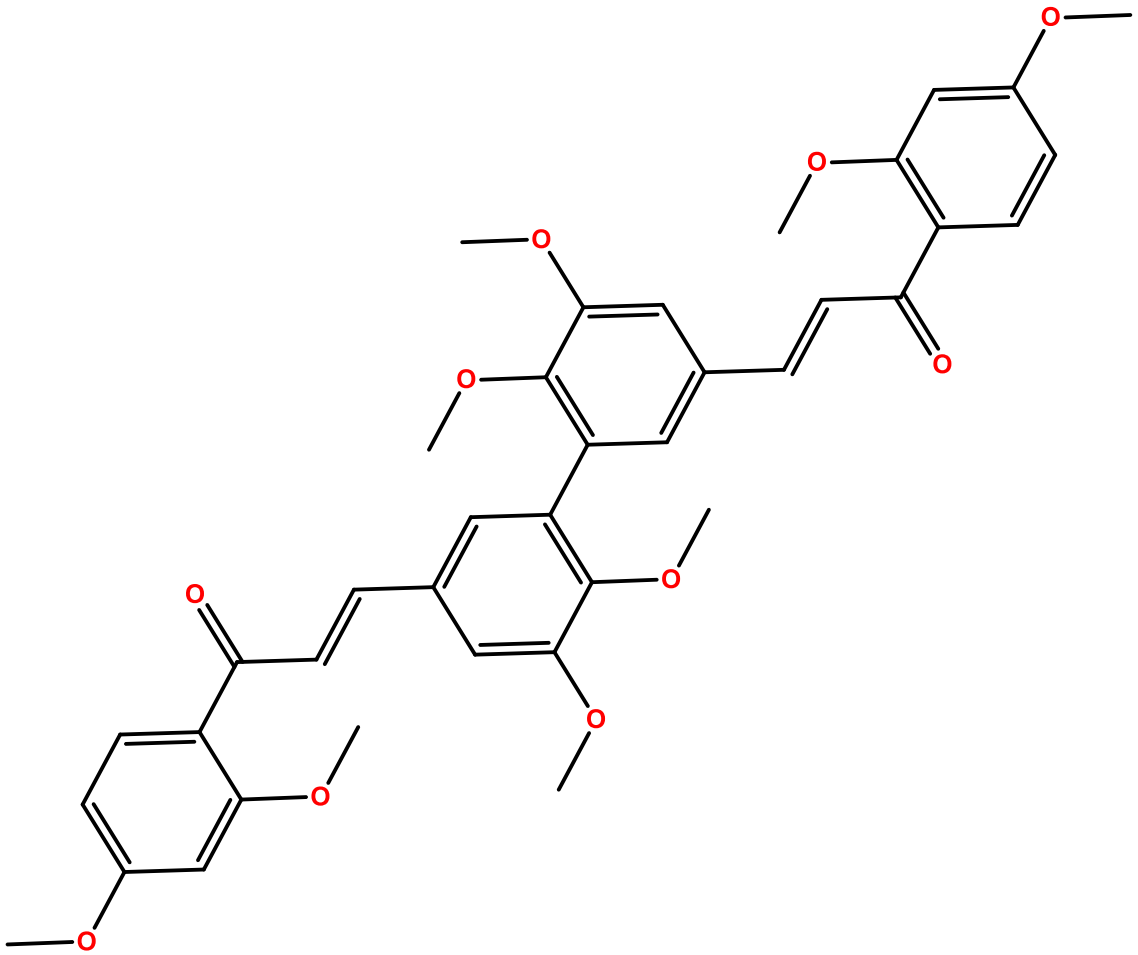

**Chemical Formula:** $C_{38}H_{38}O_{10}$
**Exact Mass: 654,25**

Sólido pastoso, de coloração verde – FM: $C_{38}H_{38}O_{10}$ [M+]: 665.2537 g/mol; PF: 148 – 149 °C; Tempo de reação 24 hrs; Rendimento: 40%; RMN $^{1}H$ (400 MHz, $CDCl_3$) $\delta_H$ 7.72 (d, *J* = 8.6 Hz, 2H); 7.62 (d, *J* = 15.7 Hz, 2H); 7.39 (d, *J* = 15.7 Hz, 2H); 7.15 (dd, *J* = 12.2, 2.0 Hz, 4H); 6.55 (dd, *J* = 8.6, 2.3 Hz, 2H); 6.49 (d, *J* = 2.2 Hz, 2H); 3.95 (s, 6H); 3.87 (s, 6H); 3.86 (s, 6H); 3.71 (s, 6H). $^{13}C$ NMR (125 MHz, $CDCl_3$) $\delta_C$ 190.78, 164.21, 160.42, 153.01, 148.82, 142.10, 132.85, 132.61, 131.03, 126.71, 123.81, 122.43, 114.19, 111.60, 105.28, 98.85, 60.99, 56.05, 55.94, 55.68.

(2E,2'E)-3,3'-(5,5',6,6'-tetrametoxi-[1,1'-bifenil]-3,3'-diil)bis(1-(benzo[d][1,3]dioxol-5-il)prop-2-en-1-ona) (**FER(A)**)

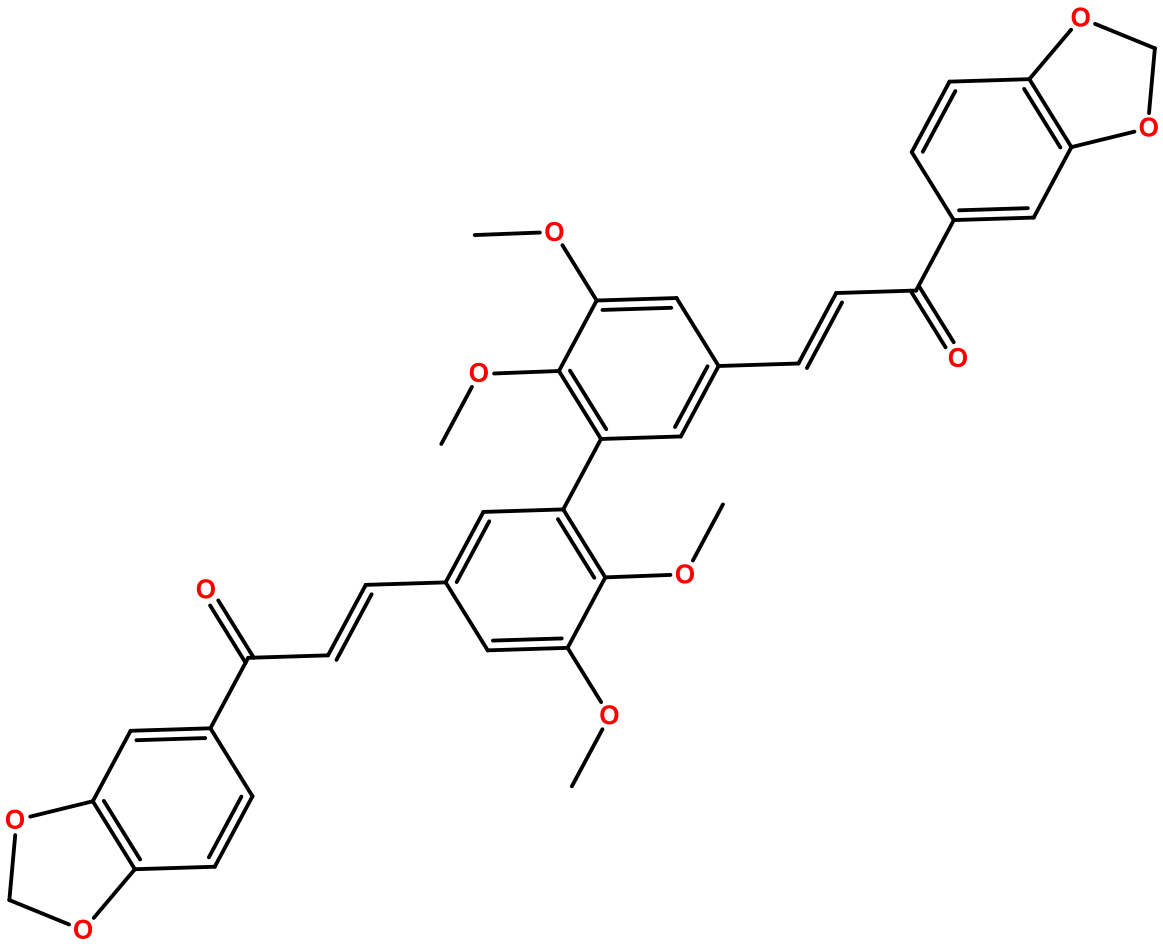

**Chemical Formula:** $C_{36}H_{30}O_{10}$
**Exact Mass: 622,18**

Sólido pastoso de coloração verde – FM: $C_{36}H_{30}O_{10}$; MM: 622,18 g/mol; PF: 157 - 158 °C; Tempode reação: 24 hrs; Rendimento: 40%. $^{1}$H NMR (500 MHz, $CDCl_3$) δ 7.76 (d, *J* = 15.6 Hz, 2H); 7.64 (dd, *J* = 8.2, 1.8 Hz, 2H); 7.52 (d, *J* = 1.7 Hz, 2H); 7.41 (d, *J* = 15.6 Hz, 2H); 7.20 (dd, *J* = 14.5, 2.0 Hz, 4H); 6.88 (d, *J* = 8.1 Hz, 2H); 6.05 (s, 4H); 3.98 (s, 6H); 3.73 (s, 6H). $^{13}$C NMR (125 MHz, $CDCl_3$) δ 188.30, 153.11, 151.81, 149.13, 148.43, 144.07, 133.15, 132.61, 130.61, 124.80, 123.66, 121.19, 111.97, 108.56, 108.04, 102.00, 61.04, 56.15.

(E)-5'-(3-(benzo[d][1,3]dioxol-5-yl)-3-oxoprop-1-en-1-il)-2',3',5,6-tetrametoxi-[1,1'-bifenil]-3-carbaldeido (**FER23(B)**)

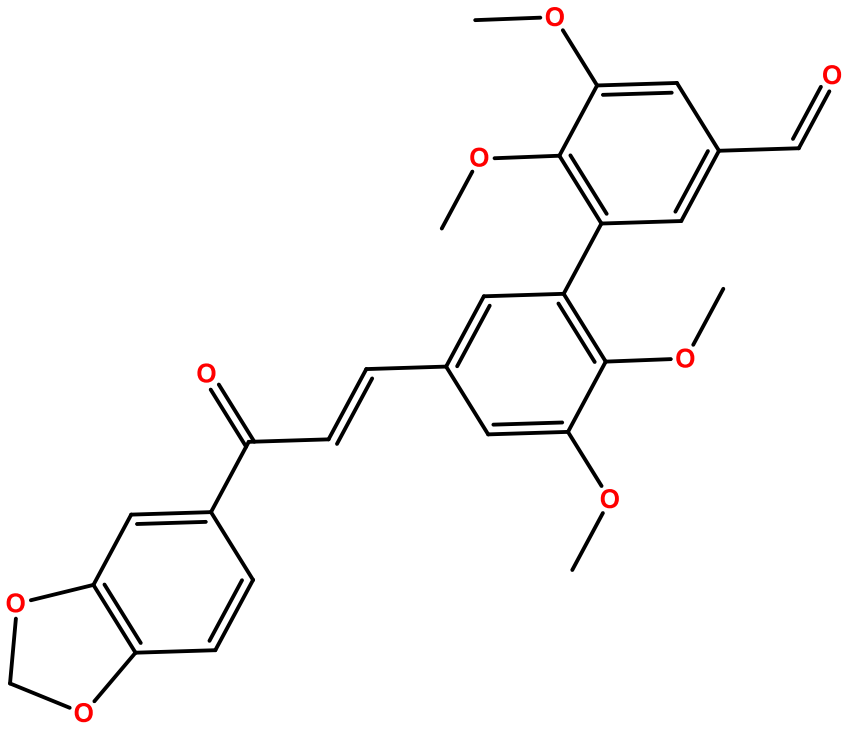

**Chemical Formula:** $C_{27}H_{24}O_8$
**Exact Mass: 476,15**

Sólido pastoso de coloração verde – FM: $C_{27}H_{24}O_8$ [M+]: 447.1532 g/mol; PF: 136 - 137 °C; Tempode reação: 24 hrs; Rendimento: 25%. RMN $^{1}H$ (400 MHz, $CDCl_3$) $\delta_H$ 9.91 (s, 1H); 7.75 (d, *J* = 15.6 Hz, 1H); 7.64 (dd, *J* = 8.2, 1.7 Hz, 1H); 7.51 (dd, *J* = 8.4, 1.8 Hz, 2H); 7.40 (d, *J* = 15.6 Hz, 1H); 7.41 (d, *J* = 2.0 Hz, 1H); 7.19 (s, 2H); 6.88 (d, *J* = 8.2 Hz, 1H); 6.88 (d, *J* = 8.2 Hz, 2H); 3.98 (s, 3H); 3.98 (s, 3H); 3.78 (s, 3H); 3.71 (s, 3H). $^{13}C$ NMR (125 MHz, $CDCl_3$) $\delta_C$ 191.25, 188.28, 153.53, 153.13, 152.57, 151.85, 149.07, 148.45, 143.95, 133.13, 132.35, 132.14, 132.10, 130.75, 128.02, 124.82, 123.51, 121.30, 114.21, 112.15, 110.18, 108.58, 108.06, 102.02, 61.12, 61.04, 56.18, 56.17.

(E)-1-(benzo[d][1,3]dioxol-5-yl)-3-(3,4-dimetoxifenil)prop-2-en-1-ona (**FER23**)

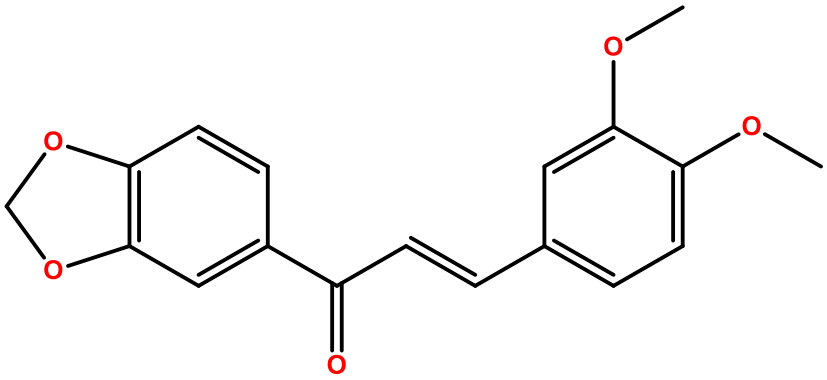

Sólido amorfo, de coloração branco esverdeado – FM: $C_{18}H_{16}O_5$; MM: 312,10 g/mol; PF: 98 – 100 °C; Tempo de reação: 24 horas; Rendimento: 86%. RMN $^1H$ (400 MHz, $CDCl_3$) $\delta_H$ 7.74 (d, *J* = 15.5 Hz, 1H); 7.64 (dd, *J* = 8.2, 1.7 Hz, 1H); 7.52 (d, *J* = 1.6 Hz, 1H); 7.34 (d, *J* = 15.5 Hz, 1H); 7.22 (dd, *J* = 8.4, 1.9 Hz, 1H); 7.15 (d, *J* = 2.1 Hz, 1H); 6.89 (d, *J* = 8.2 Hz, 2H); 6.06 (s, 2H); 3.95 (s, 3H); 3.93 (s, 3H). $^{13}C$ NMR (125 MHz, $CDCl_3$) $\delta_C$ 188.33, 151.36, 149.27, 148.25, 144.45, 133.22, 127.99, 124.52, 123.07, 119.66, 114.07, 111.15, 110.09, 108.46, 107.90, 101.85, 56.01, 55.99.

(E)-1-(benzo[d][1,3]dioxol-5-yl)-3-(4-metoxifenil)prop-2-en-1-ona (**FER81**)

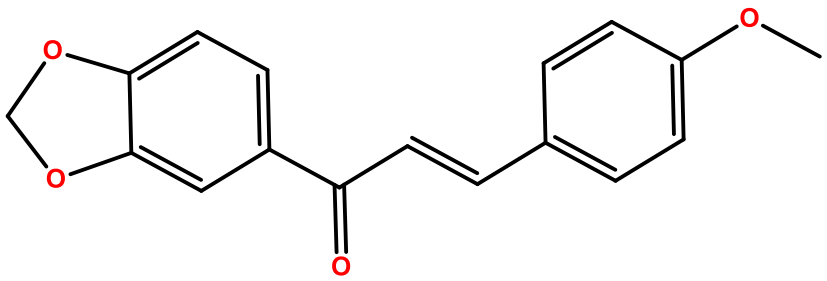

Sólido amorfo, de coloração branco esverdeado - FM: $C_{17}H_{14}O_4$; MM: 282,09 g/mol; PF: 118 – 119 °C; Tempo de reação: 24 horas; Rendimento: 87%. RMN $^1H$ (500 MHz, $CDCl_3$) $\delta_H$ 7.75 (d, J = 15.5 Hz, 1H); 7.62 (dd, *J* = 8.1, 1.7 Hz, 1H); 7.57 (d, *J* = 8.7 Hz, 2H); 7.51 (d, *J* = 1.7 Hz, 1H); 7.35 (d, *J* = 15.5 Hz, 1H); 6.91 (d, *J* = 8.8 Hz, 2H); 6.87 (d, *J* = 8.1 Hz, 1H); 6.03 (s, 2H); 3.83 (s, 3H). $^{13}C$ NMR (125 MHz, $CDCl_3$) $\delta_C$ 188.33, 161.66, 151.59, 148.31, 144.14, 133.32, 130.20, 127.81, 124.54, 119.47, 114.48, 108.49, 107.95, 101.90, 55.47.

Figura 27: Espectro de RMN $^{1}H$ (500 MHz, $CDCl_3$) de FER81.

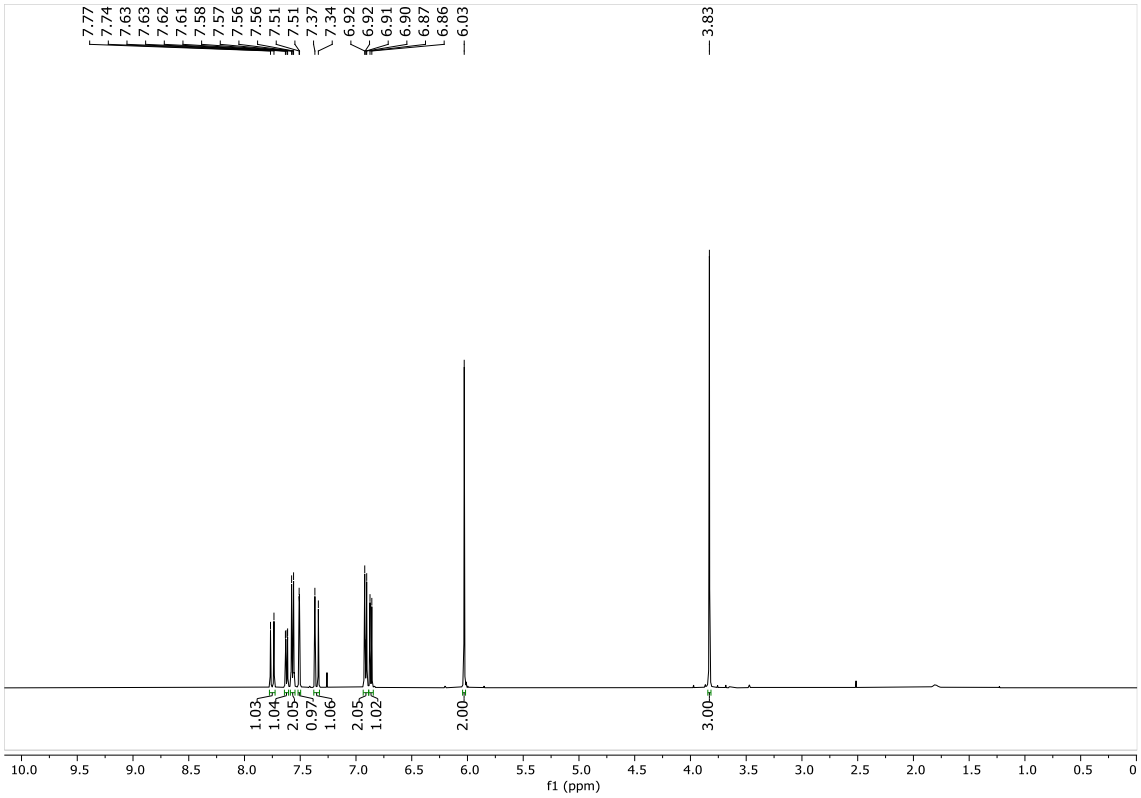


Figura 28: Expansão do espectro de RMN $^{1}H$ (500 MHz, $CDCl_3$) de FER81 na região 6.80 - 7.80 ppm.

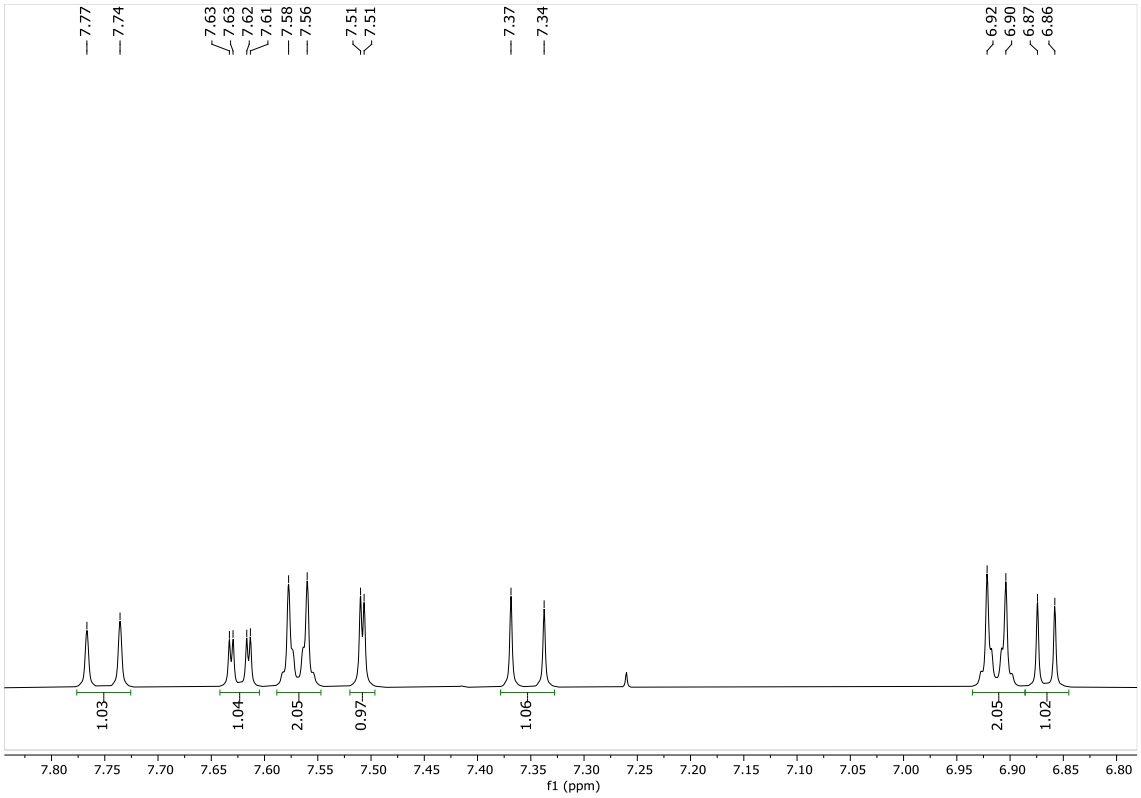

Figura 29: Espectro de RMN $^{13}C$ (125 MHz, $CDCl_3$) de FER81.

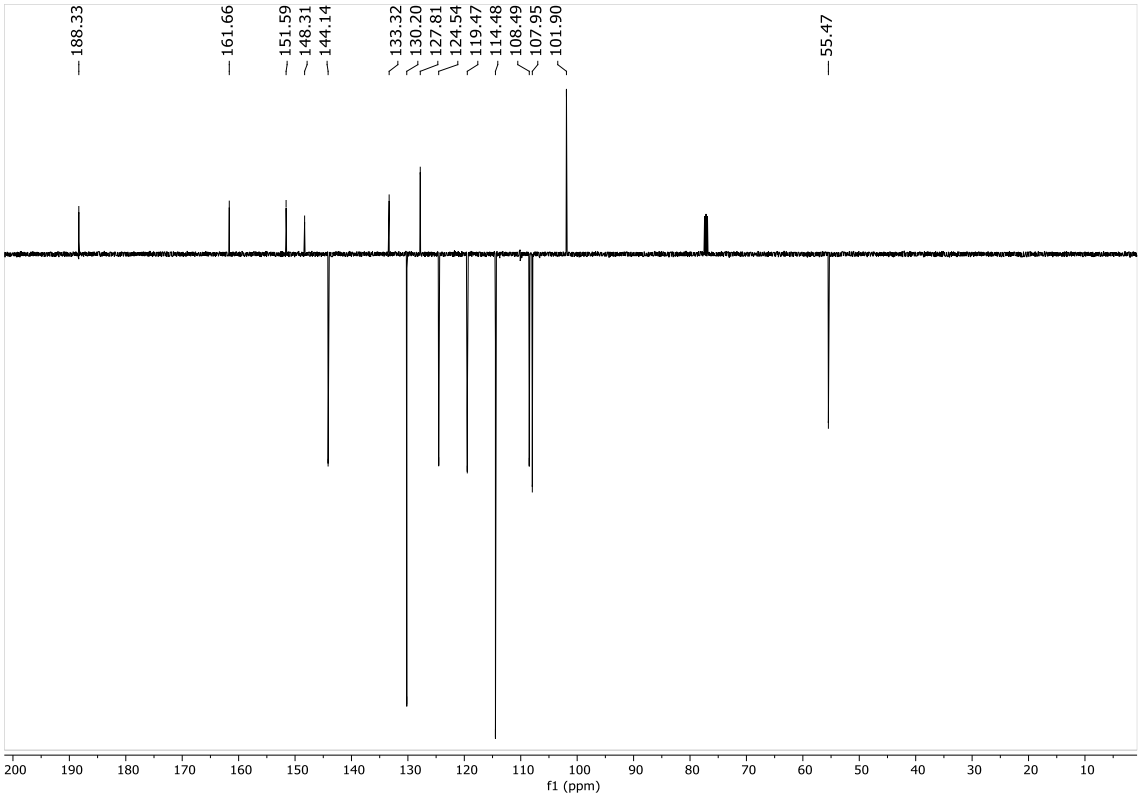


Figura 30: Expansão do espectro de RMN $^{13}C$ (125 MHz, $CDCl_3$) de FER81 na região 102 - 162 ppm.

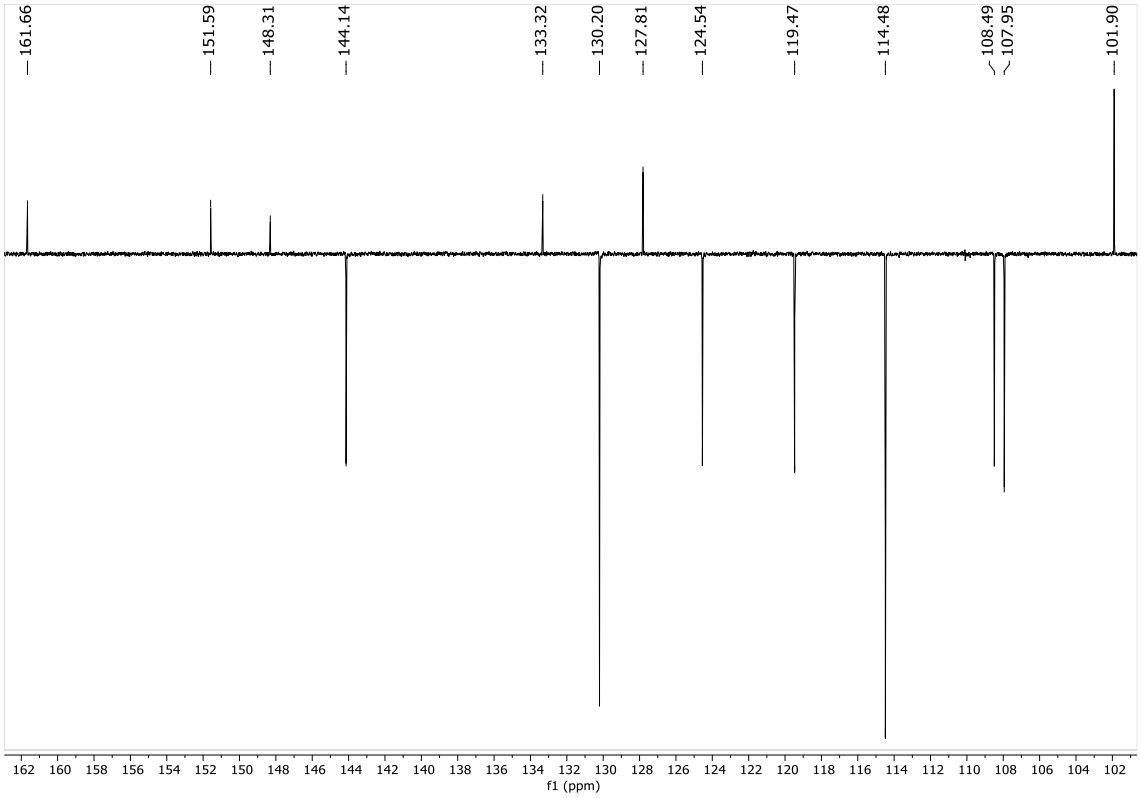

(E)-1-(benzo[d][1,3]dioxol-5-yl)-3-(4-etoxifenil)prop-2-en-1-ona (**FER18**)

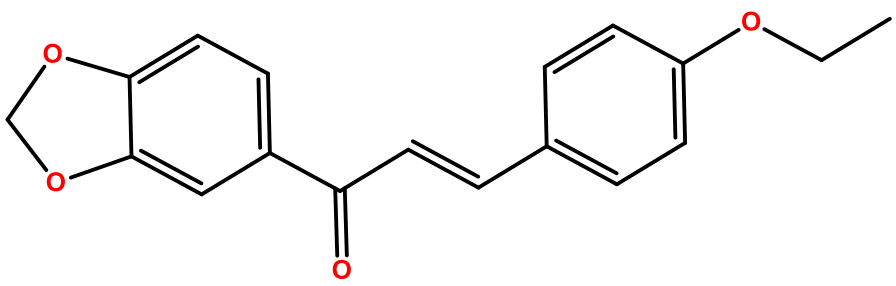

Sólido amorfo, de coloração branco esverdeado - FM: $C_{18}H_{16}O_4$ [M+]: 297.1132 g/mol; PF: 125.0 - 126.0 °C; Tempo de reação: 24 horas; Rendimento: 95%. $^1$H NMR (400 MHz, $CDCl_3$) δ 7.73 (d, *J* = 15.5 Hz, 1H), 7.60 (dd, *J* = 8.2, 1.7 Hz, 1H), 7.54 (d, *J* = 8.7 Hz, 2H), 7.49 (d, *J* = 1.7 Hz, 1H), 7.33 (d, *J* = 15.5 Hz, 1H), 6.88 (d, *J* = 8.8 Hz, 2H), 6.85 (d, *J* = 8.1 Hz, 1H), 6.01 (s, 2H), 4.04 (q, *J* = 7.0 Hz, 2H), 1.40 (t, *J* = 7.0 Hz, 3H). $^{13}$C NMR (101 MHz, $CDCl_3$) δ 188.19, 160.94, 151.42, 148.15, 144.08, 133.20, 130.07, 127.47, 124.38, 119.17, 114.80, 108.34, 107.79, 101.74, 63.57, 14.65.

Figura 31: Espectro de RMN $^1$H (500 MHz, $CDCl_3$) de FER18.

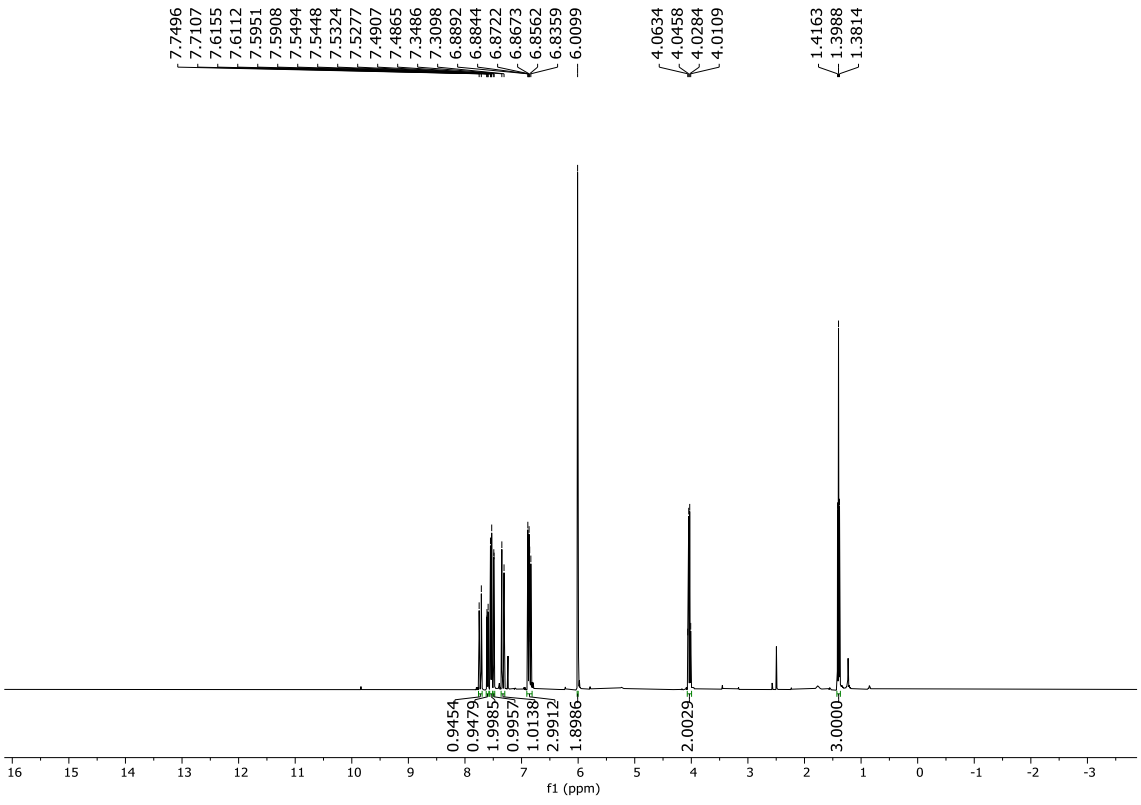

Figura 32: Expansão do espectro de RMN $^{1}H$ (500 MHz, $CDCl_3$) de FER18 na região 6.70 - 7.85 ppm.

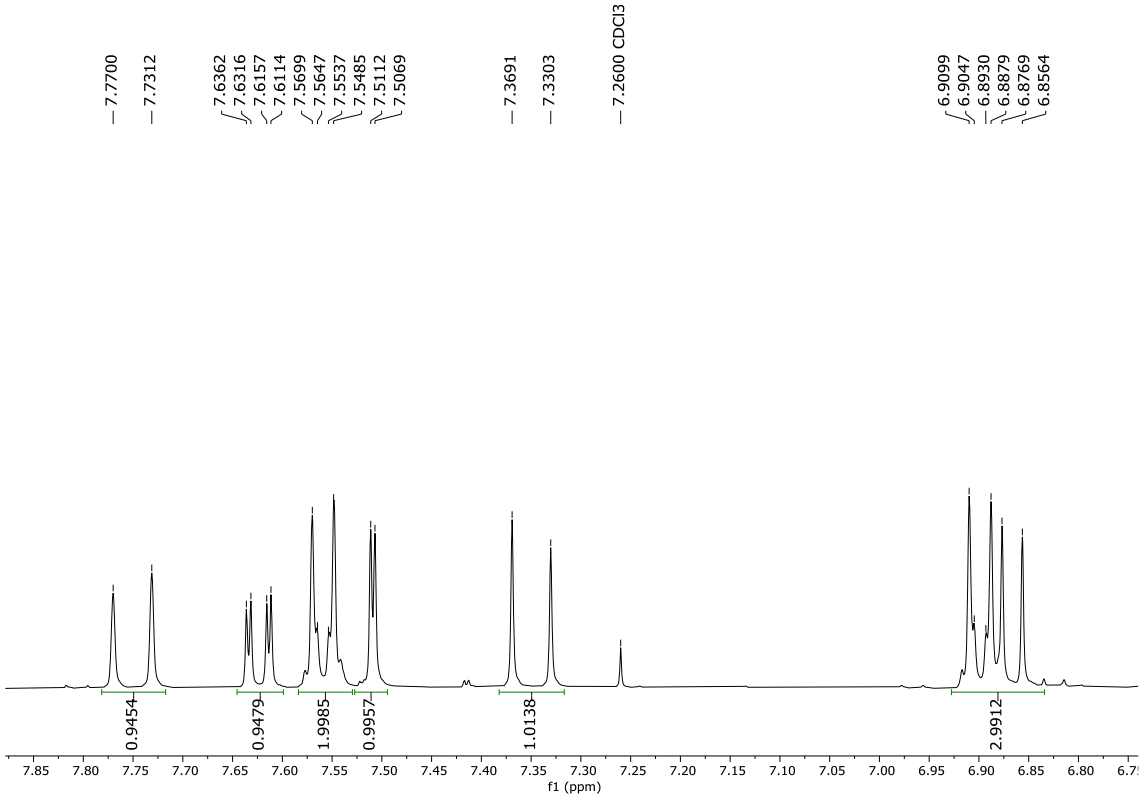


Figura 33: Espectro de RMN $^{13}C$ (125 MHz, $CDCl_3$) de FER18.

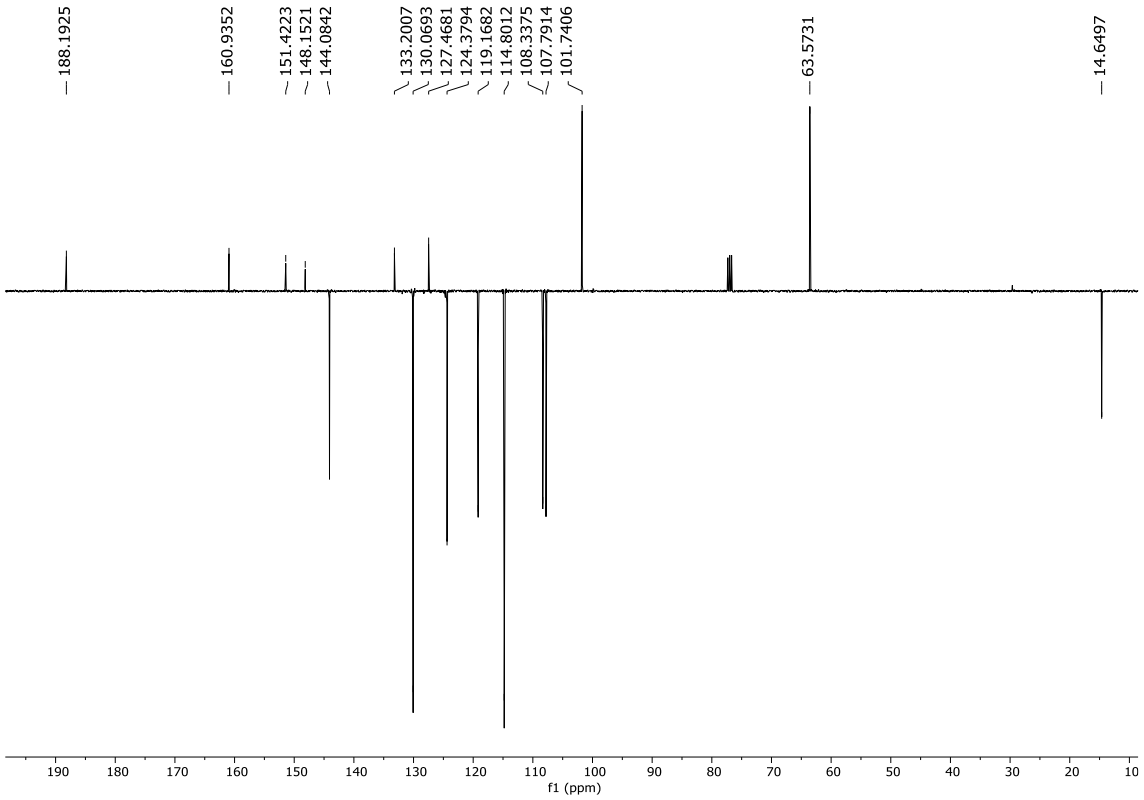

Figura 34: Expansão do espectro de RMN $^{13}C$ (125 MHz, $CDCl_3$) de FER18 na região 102 - 162 ppm.

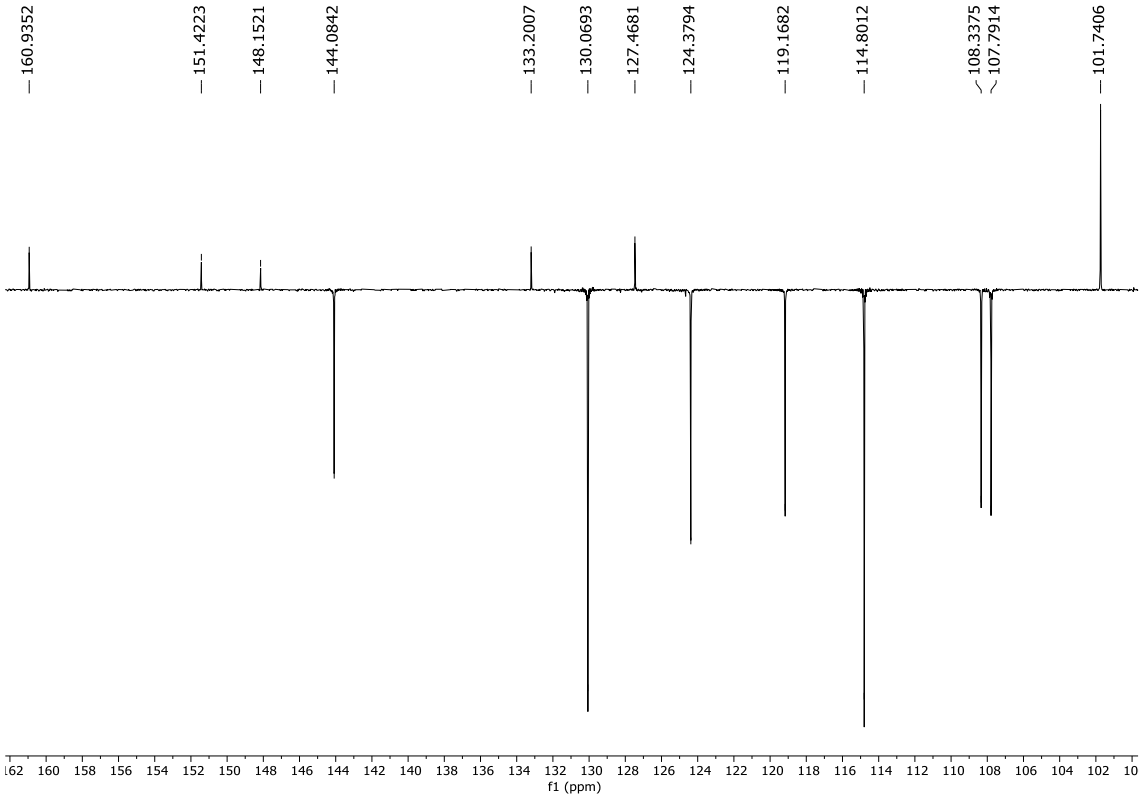


Figura 35: Espectro de massas [M+] de FER13.

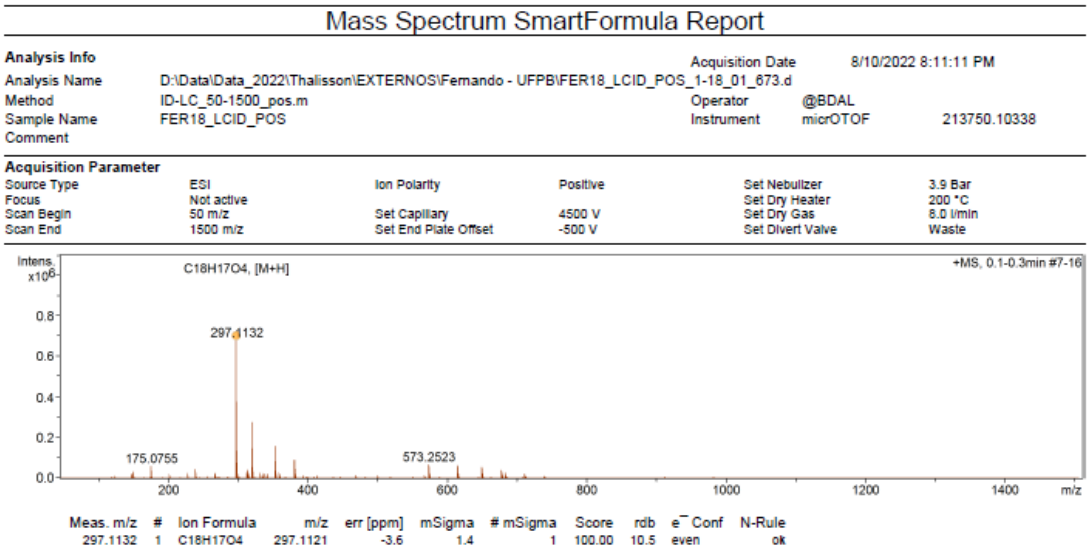

Mass Spectrum SmartFormula Report

**Analysis Info**

| | | | |
|---|---|---|---|
| Analysis Name | D:\Data\Data_2022\Thalisson\EXTERNOS\Fernando - UFPB\FER18_LCID_POS_1-18_01_673.d | Acquisition Date | 8/10/2022 8:11:11 PM |
| Method | ID-LC_50-1500_pos.m | Operator | @BDAL |
| Sample Name | FER18_LCID_POS | Instrument | micrOTOF 213750.10338 |
| Comment | | | |

**Acquisition Parameter**

| | | | | | |
|---|---|---|---|---|---|
| Source Type | ESI | Ion Polarity | Positive | Set Nebulizer | 3.9 Bar |
| Focus | Not active | | | Set Dry Heater | 200 °C |
| Scan Begin | 50 m/z | Set Capillary | 4500 V | Set Dry Gas | 8.0 l/min |
| Scan End | 1500 m/z | Set End Plate Offset | -500 V | Set Divert Valve | Waste |



| Meas. m/z | # | Ion Formula | m/z | err [ppm] | mSigma | # mSigma | Score | rdb | e⁻ Conf | N-Rule |
|---|---|---|---|---|---|---|---|---|---|---|
| 297.1132 | 1 | C18H17O4 | 297.1121 | -3.6 | 1.4 | 1 | 100.00 | 10.5 | even | ok |

(E)-3-(4-(alliloxi)fenil)-1-(benzo[d][1,3]dioxol-5-il)prop-2-en-1-ona (**FER89**)

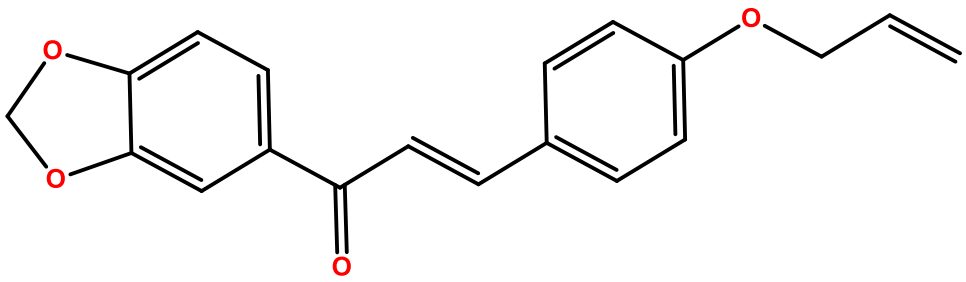

Sólido amorfo, de coloração branco esverdeado - FM: $C_{19}H_{16}O_4$; MM: 308,10 g/mol; PF: °C; Tempo de reação: 24 horas; Rendimento: 93%. $^1$H NMR (400 MHz, $CDCl_3$) δ 7.75 (d, *J* = 15.6 Hz, 1H); 7.63 (dd, *J* = 8.2, 1.6 Hz, 1H); 7.57 (d, *J* = 8.7 Hz, 2H); 7.51 (d, *J* = 1.5 Hz, 1H); 7.36 (d, *J* = 15.5 Hz, 1H); 6.93 (d, *J* = 8.7 Hz, 2H); 6.88 (d, *J* = 8.1 Hz, 1H); 6.15 – 5.91 (m, 3H); 5.42 (dd, *J* = 17.3, 1.4 Hz, 2H); 5.36 – 5.27 (m, 2H); 4.57 (d, *J* = 5.3 Hz, 3H). $^{13}$C NMR (100 MHz, $CDCl_3$) δ 188.39, 160.69, 151.63, 148.35, 144.16, 133.36, 132.87, 130.22, 127.97, 124.58, 119.58, 118.14, 115.26, 108.53, 107.99, 101.93, 68.99.

Figura 36: Espectro de RMN $^1$H (500 MHz, $CDCl_3$) de FER89.

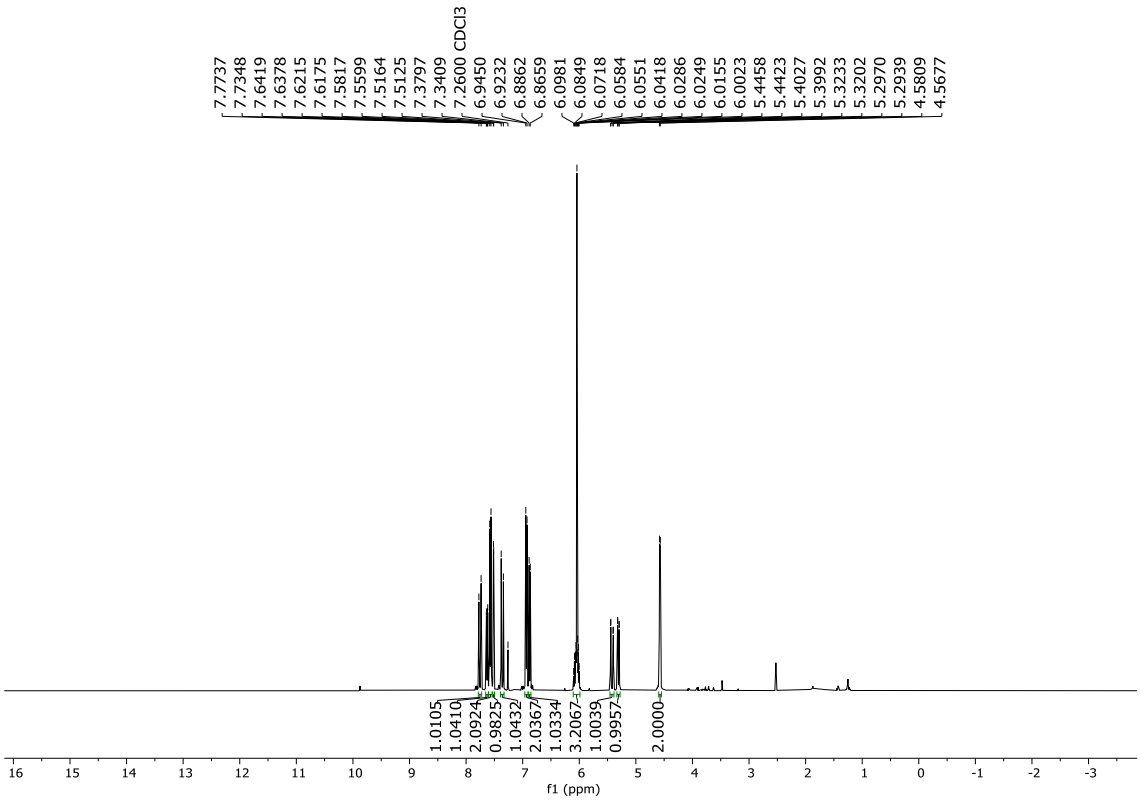

Figura 37: Expansão do espectro de RMN $^{1}H$ (500 MHz, $CDCl_3$) de FER89 na região 6.85 - 7.80 ppm.

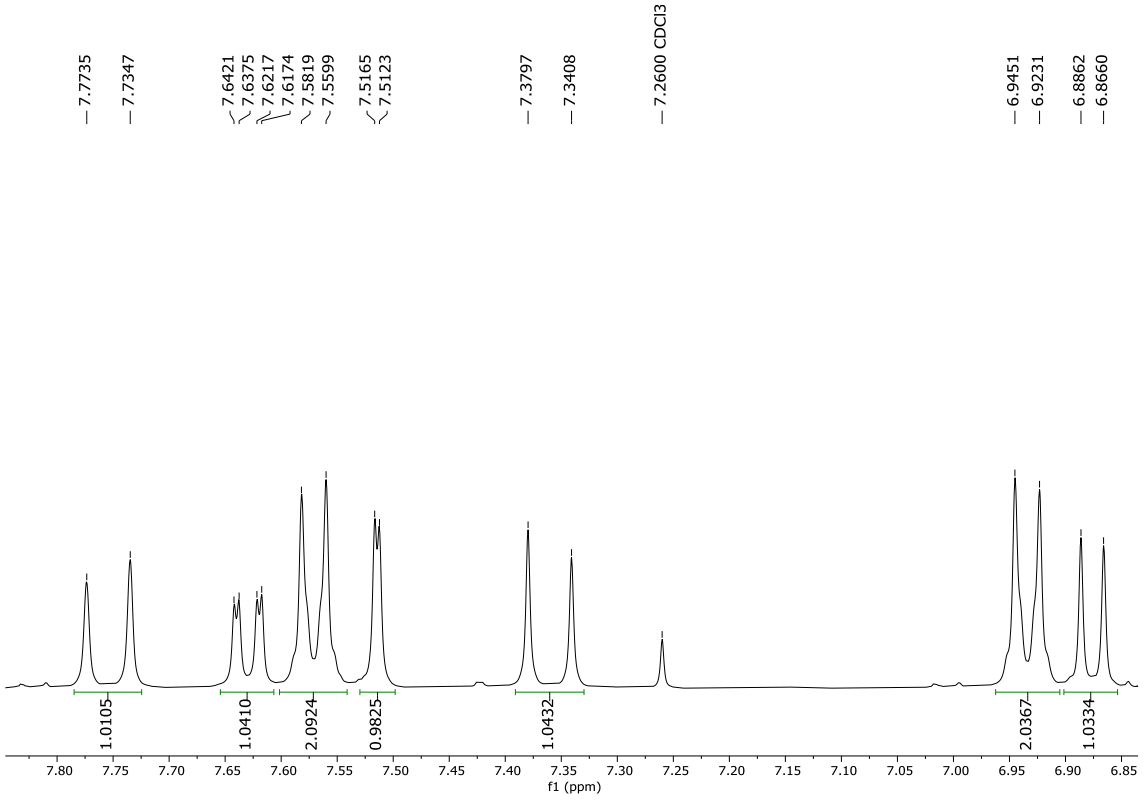


Figura 38: Espectro de RMN $^{13}C$ (125 MHz, $CDCl_3$) de FER89.

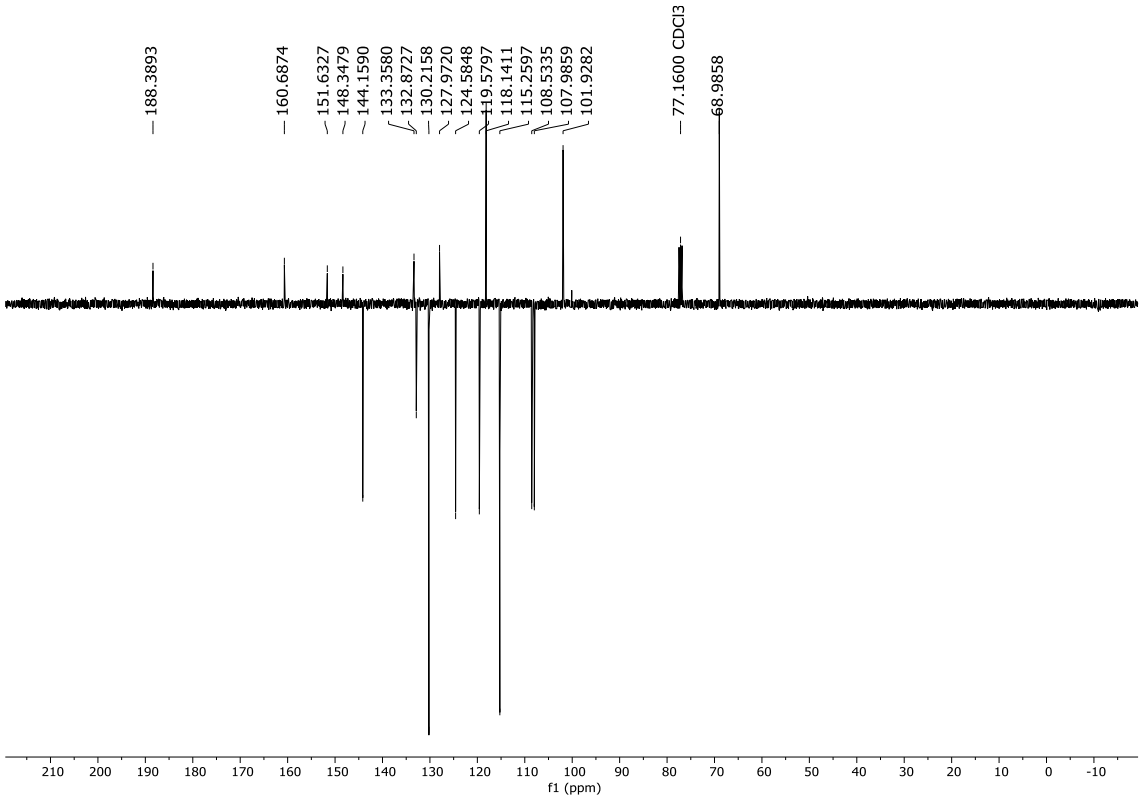

Figura 39: Expansão do espectro de RMN $^{13}C$ (125 MHz, $CDCl_3$) de FER89 na região 102 - 162 ppm.

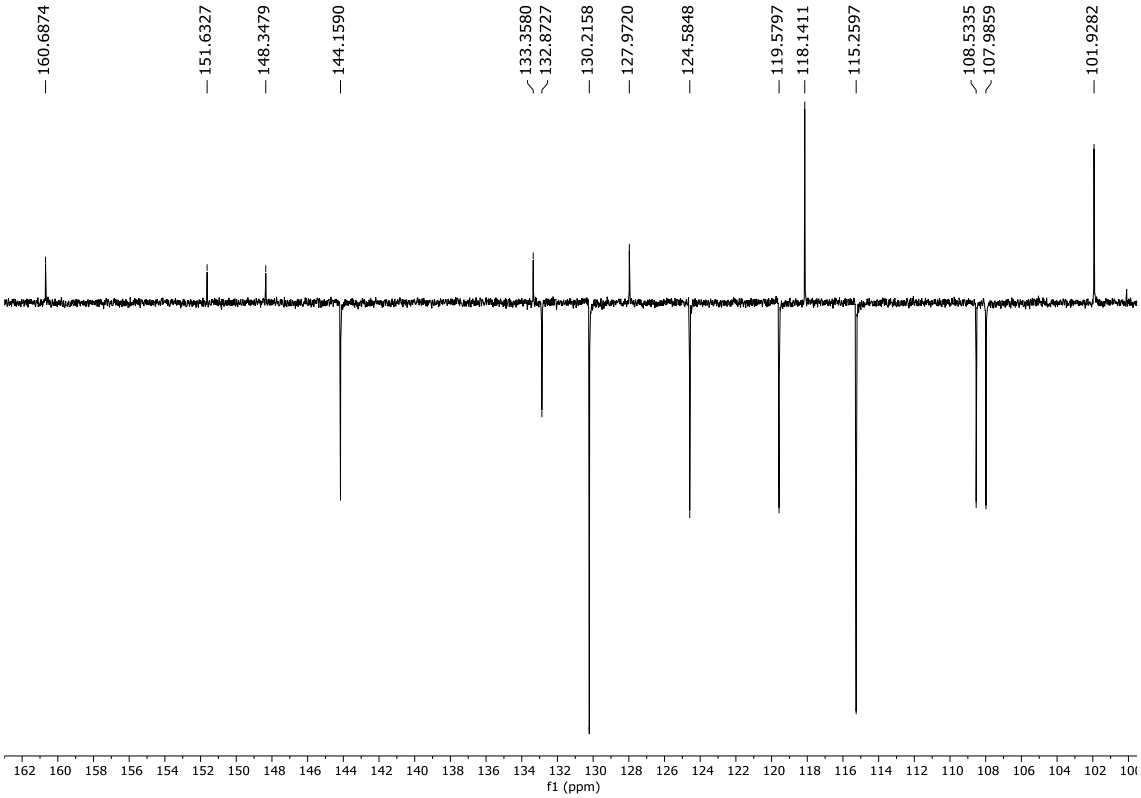


(E)-1-(benzo[d][1,3]dioxol-5-yl)-3-(3-bromo-4,5-dimetoxifenil)prop-2-en-1-ona (**FER08**)

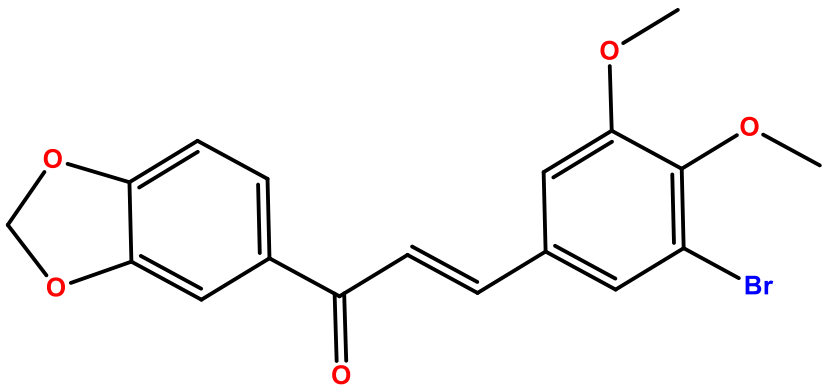


Sólido amorfo, de coloração branco esverdeado - FM: $C_{18}H_{15}BrO_5$ [M+]: 391.0185 g/mol; PF: 108,8 – 110,3 °C; Tempo de reação: 24 horas; Rendimento: 92%. $^1H$ NMR (400 MHz, $CDCl_3$) 7.62 (d, *J* = 15.5 Hz, 1H), 7.63 (dd, *J* = 8.2, 1.7 Hz, 1H), 7.50 (d, *J* = 1.6 Hz, 1H), 7.50 (d, *J* = 1.6 Hz, 1H), 7.36 (d, *J* = 15.5 Hz, 1H), 7.05 (d, *J* = 1.9 Hz, 1H), 7.05 (d, *J* = 1.9 Hz, 1H), 6.05 (s, 2H), 3.91 (s, 3H), 3.89 (s, 3H). $^{13}C$ NMR (101 MHz, $CDCl_3$) δ 187.82, 153.79, 151.85, 148.35,

148.25, 142.50, 132.77, 132.09, 124.77, 122.01, 118.16, 111.56, 108.40, 107.95, 101.95, 60.78, 56.23.

Figura 40: Espectro de RMN $^{1}H$ (500 MHz, $CDCl_3$) de FER08.

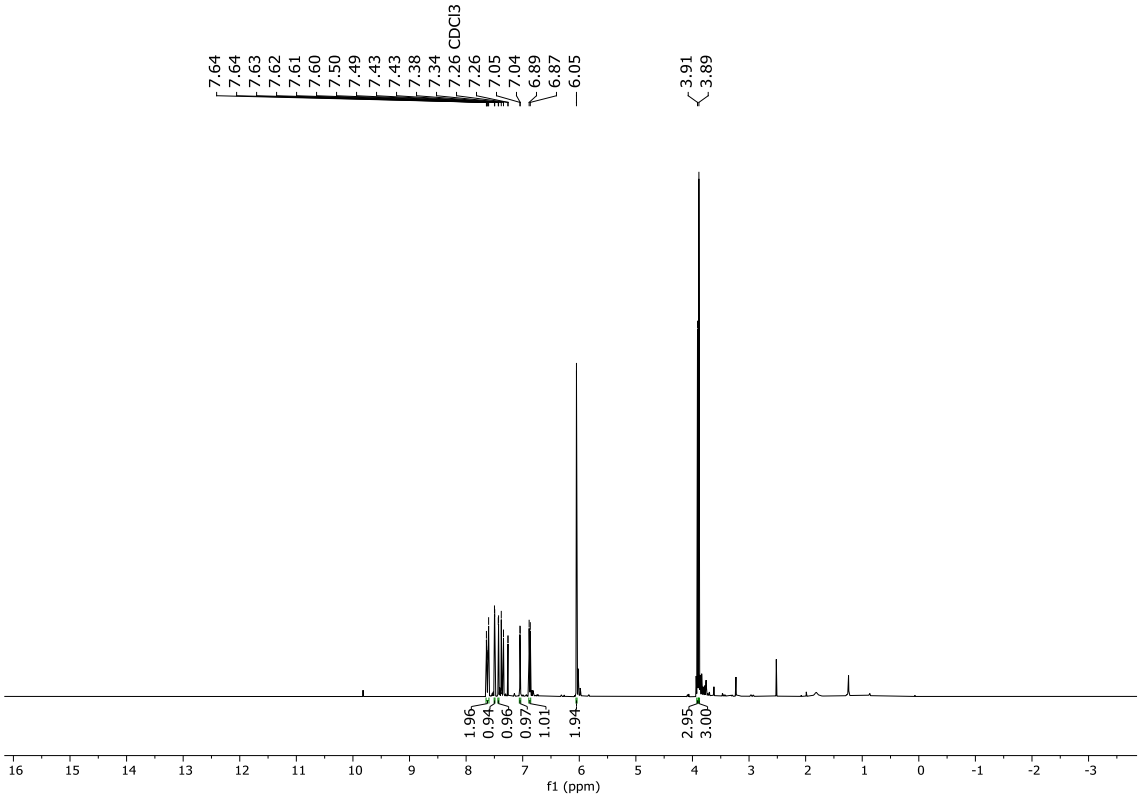

Figura 41: Expansão do espectro de RMN $^{1}H$ (500 MHz, $CDCl_3$) de FER08 na região 6.85 - 7.65 ppm.

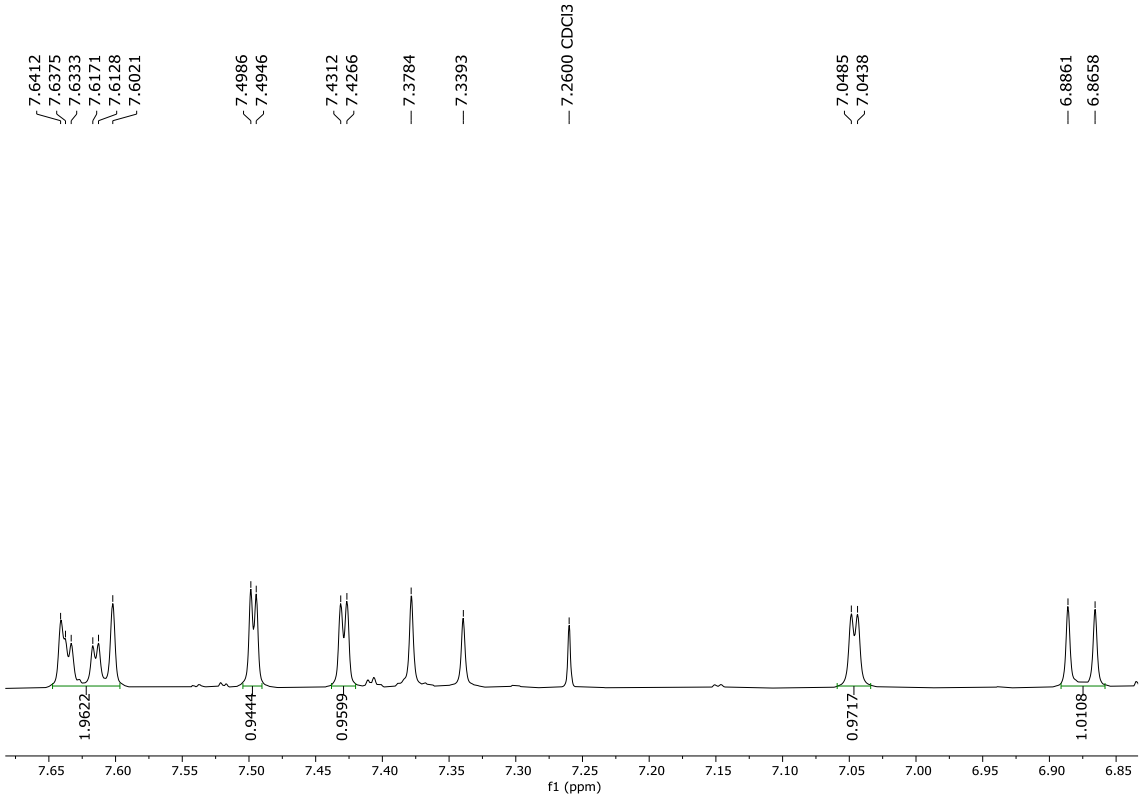


Figura 42: Espectro de RMN $^{13}C$ (125 MHz, $CDCl_3$) de FER08.

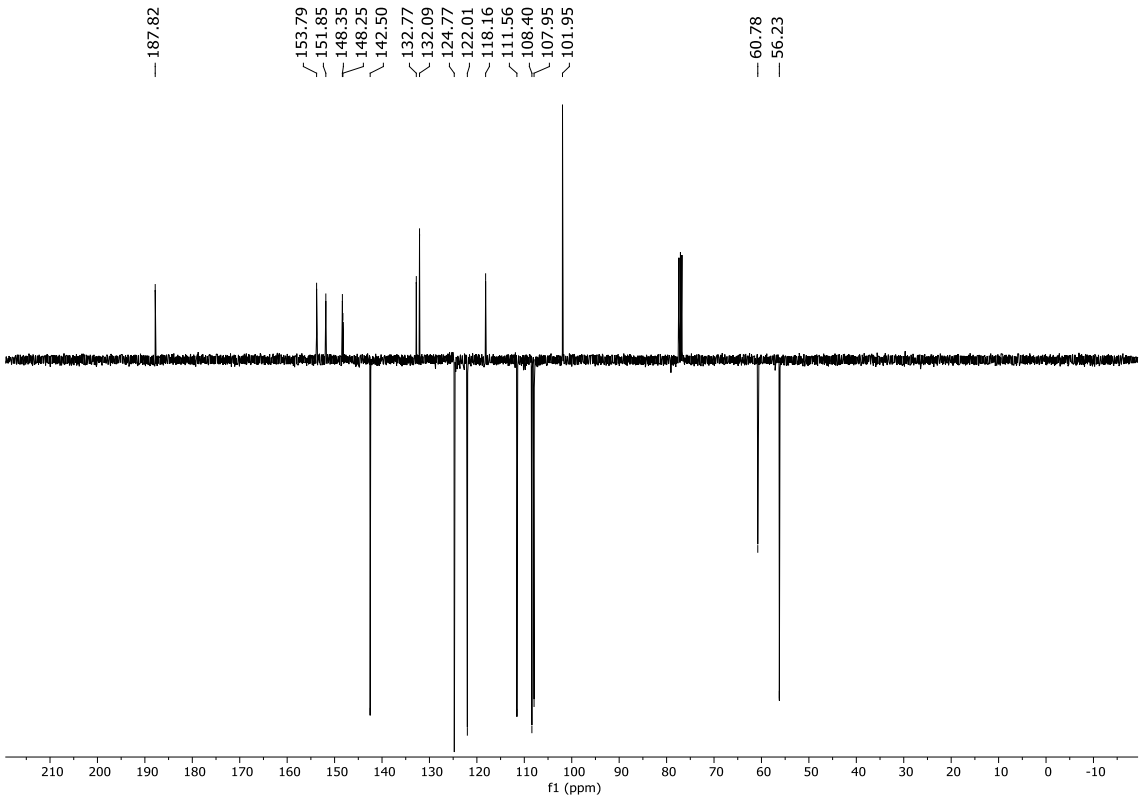

Figura 43: Expansão do espectro de RMN $^{13}C$ (125 MHz, $CDCl_3$) de FER08 na região 102 - 154 ppm.

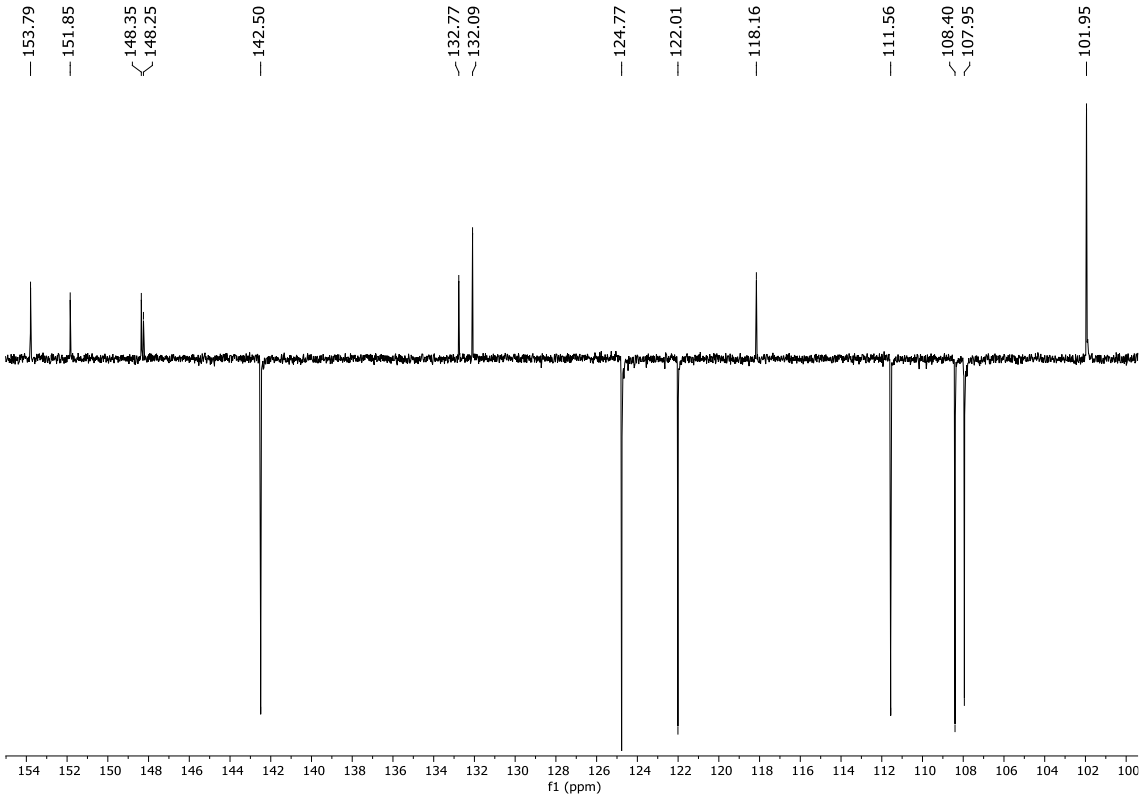


Figura 44: Espectro de massas [M+] de FER08.

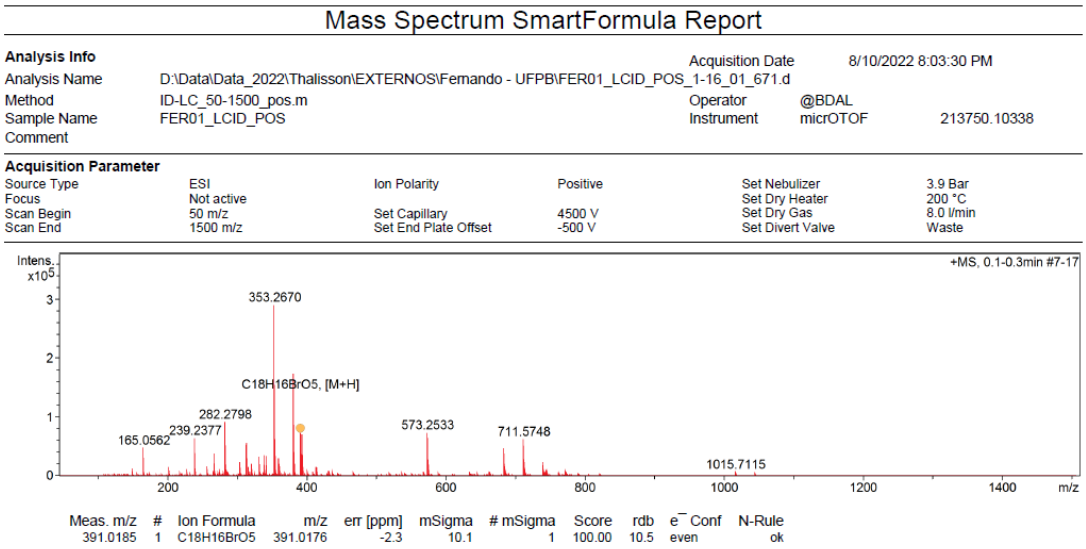

(E)-1-(benzo[d][1,3]dioxol-5-il)-3-(3-bromo-4-etoxi-5-metoxifenil)prop-2-en-1-ona (**FER13**)

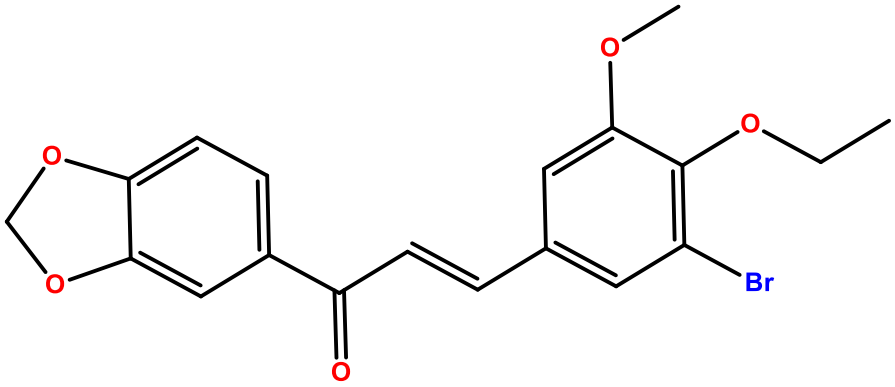


Sólido amorfo, de coloração branco esverdeado - FM: $C_{19}H_{17}BrO_5$; MM: 404.03 g/mol; PF: 112.6 - 115.2 °C; Tempo de reação: 24 horas; Rendimento: 87%. $^1$H NMR (400 MHz, $CDCl_3$) δ 7.37 (d, *J* = 15.5 Hz, 1H), 7.64 (dd, *J* = 8.2, 1.7 Hz, 1H), 7.52 (d, *J* = 1.4 Hz, 1H), 7.46 (d, *J* = 1.9 Hz, 1H), 7.37 (d, *J* = 15.5 Hz, 1H), 7.05 (d, *J* = 1.9 Hz, 1H), 6.90 (d, *J* = 8.1 Hz, 1H), 6.07 (s, 2H), 4.13 (q, *J* = 7.1 Hz, 2H), 3.91 (s, 3H), 1.43 (t, *J* = 7.1 Hz, 3H). $^{13}$C NMR (101 MHz, $CDCl_3$) δ 187.89, 153.91, 151.81, 148.34, 147.53, 142.61, 132.80, 131.83, 124.80, 124.73, 121.88, 118.63, 111.50, 108.40, 107.93, 101.90, 69.43, 56.19, 15.58.

Figura 45: Espectro de RMN $^1$H (500 MHz, $CDCl_3$) de FER13.

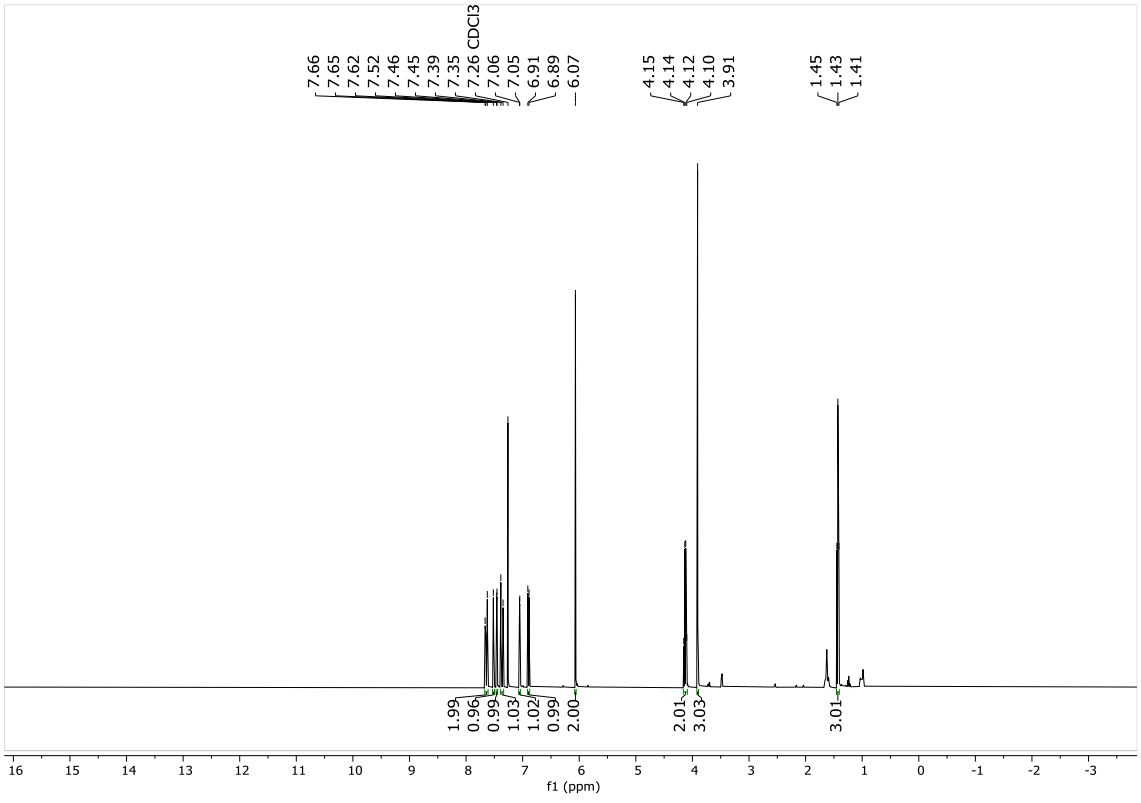

Figura 46: Expansão do espectro de RMN $^{1}H$ (500 MHz, $CDCl_3$) de FER13 na região 6.80 - 7.75 ppm.

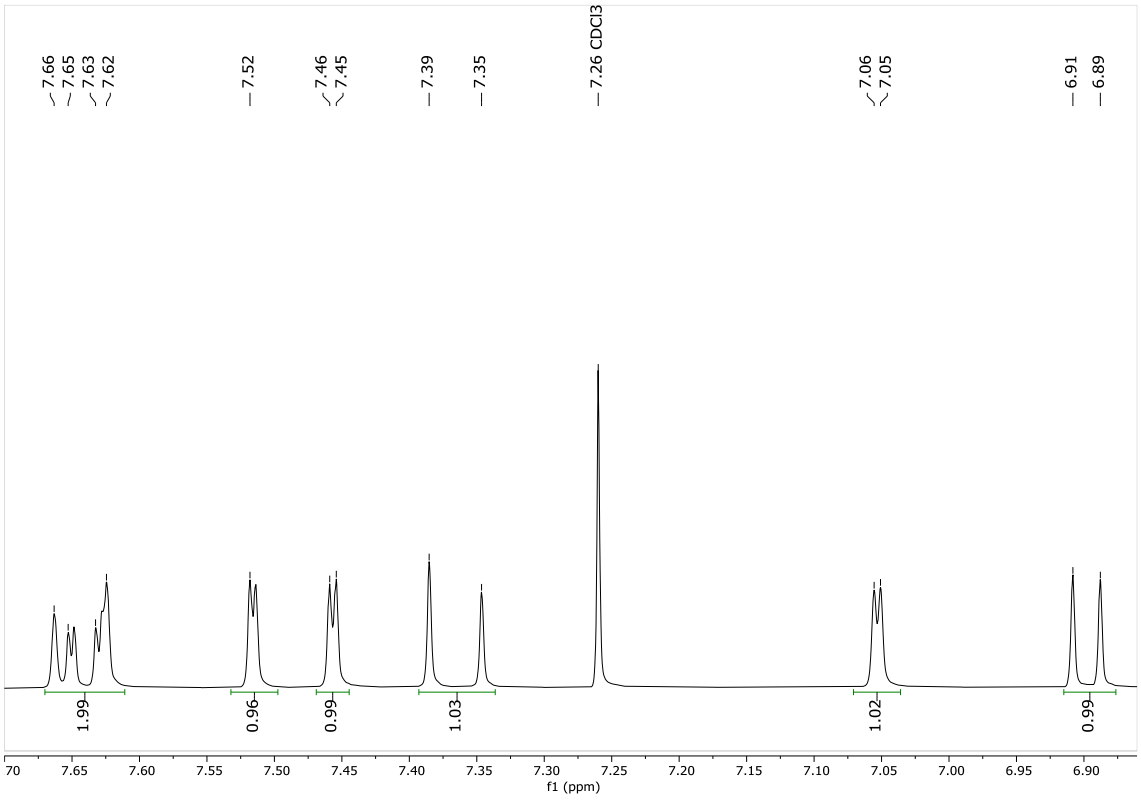


Figura 47: Espectro de RMN $^{13}C$ (125 MHz, $CDCl_3$) de FER13.

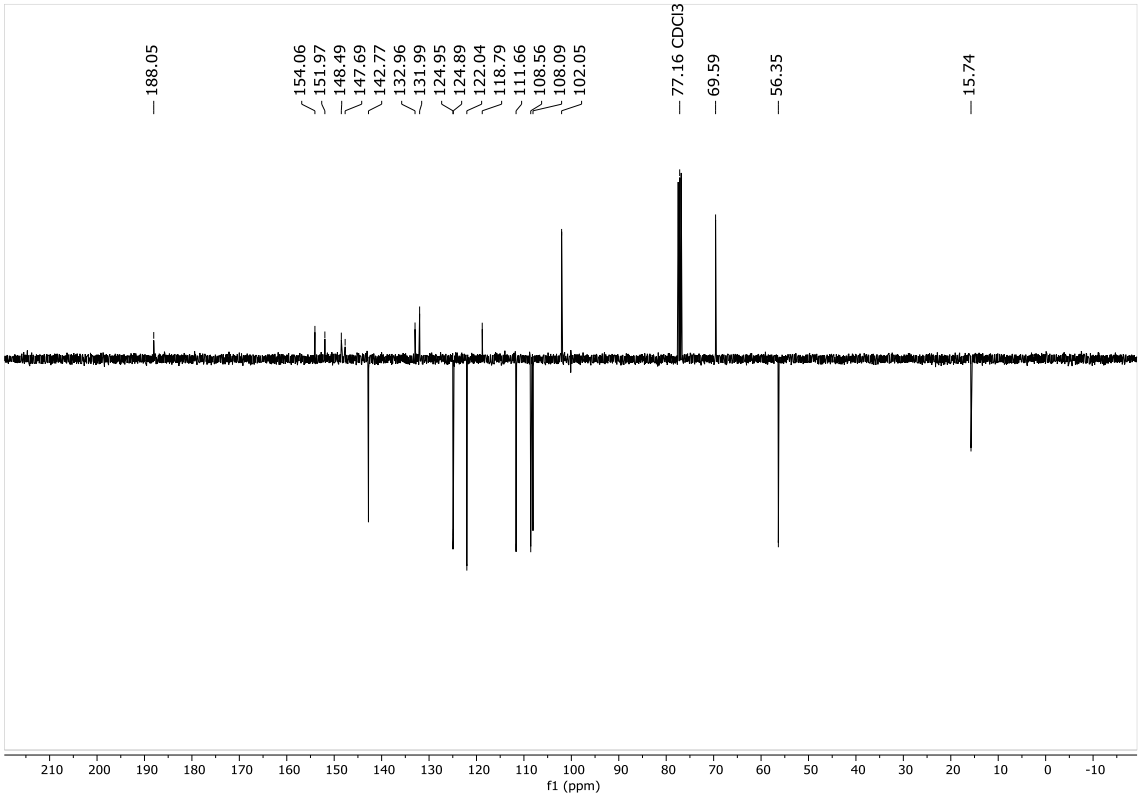

Figura 48: Expansão do espectro de RMN $^{13}C$ (125 MHz, $CDCl_3$) de FER13 na região 102 - 154 ppm.

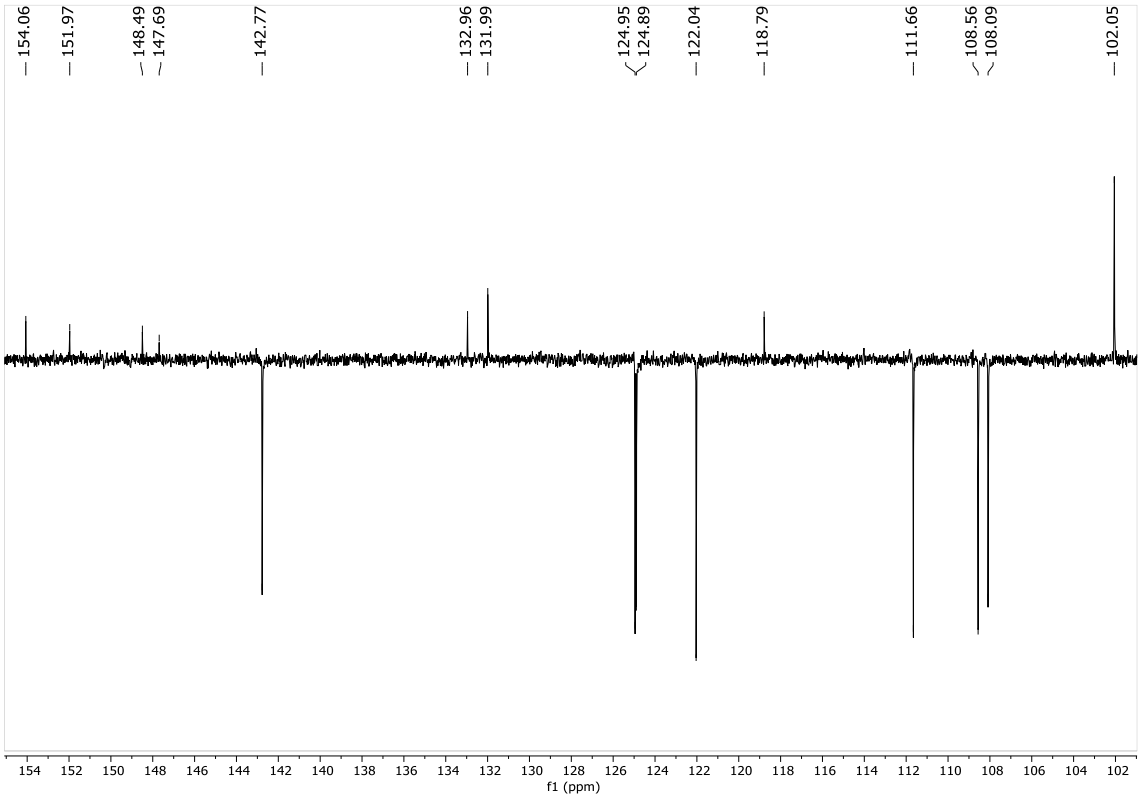


8.2.1. (E)-3-(4-(alliloxi)-3-bromo-5-metoxifenil)-1-(benzo[d][1,3]dioxol-5-il)prop-2-en-1-ona (**FER12**)

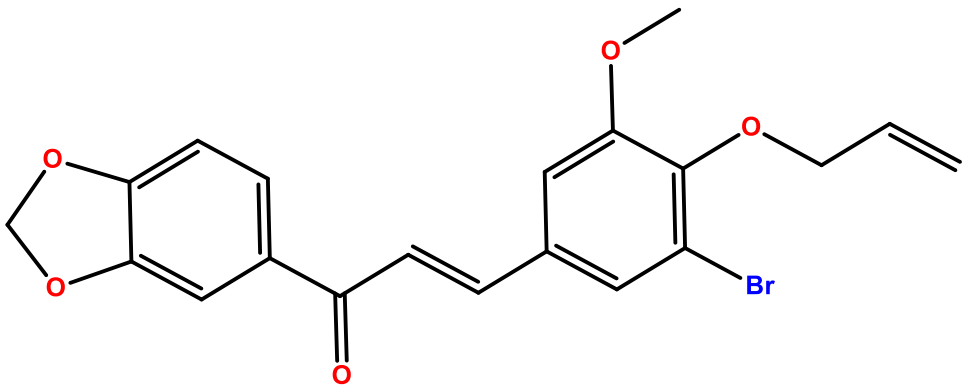


Sólido amorfo, de coloração branco esverdeado - FM: $C_{20}H_{17}BrO_5$ [M+]417.0335 g/mol; PF: 123.7 - 125.8 °C; Tempo de reação: 24 horas; Rendimento: 95%. $^1H$ NMR (400 MHz, $CDCl_3$) δ 7.62 (d, *J* = 15.6 Hz, 1H), 7.62 (dd, *J* = 8.2, 1.7 Hz, 2H), .49 (d, *J* = 1.6 Hz, 1H), 7.43 (d, *J* = 1.8 Hz, 1H), 7.34 (d, *J* = 15.6 Hz, 1H), 7.03 (d, *J* = 1.9 Hz, 1H), 6.87 (d, *J* = 8.2 Hz, 1H), 6.11 (ddt, *J* = 17.2, 10.3, 6.0 Hz, 1H), 6.04 (s, 2H), 5.37 (dq, *J* = 17.2, 1.5 Hz, 1H), 5.23 (dq, *J*

= 10.4, 1.1 Hz, 1H), 4.57 (dt, *J* = 6.0, 1.3 Hz, 2H), 3.89 (s, 3H). $^{13}C$ NMR (101 MHz, $CDCl_3$) δ 187.86, 153.85, 151.84, 148.37, 147.08, 142.54, 133.56, 132.82, 132.04, 124.82, 124.76, 122.00, 118.59, 118.47, 111.54, 108.43, 107.95, 101.93, 74.25, 56.22.

Figura 49: Espectro de RMN $^1H$ (500 MHz, $CDCl_3$) de FER12.

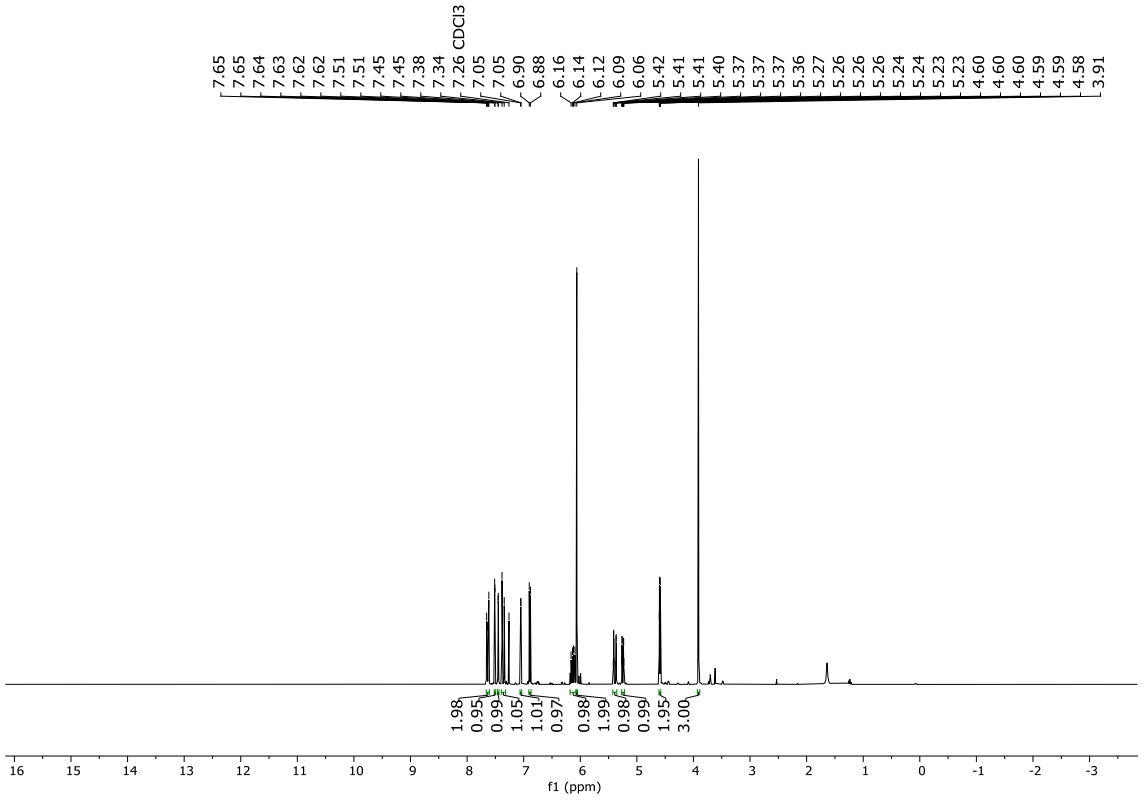

Figura 50: Expansão do espectro de RMN $^{1}H$ (500 MHz, $CDCl_3$) de FER12 na região 5.20 - 6.20 ppm.

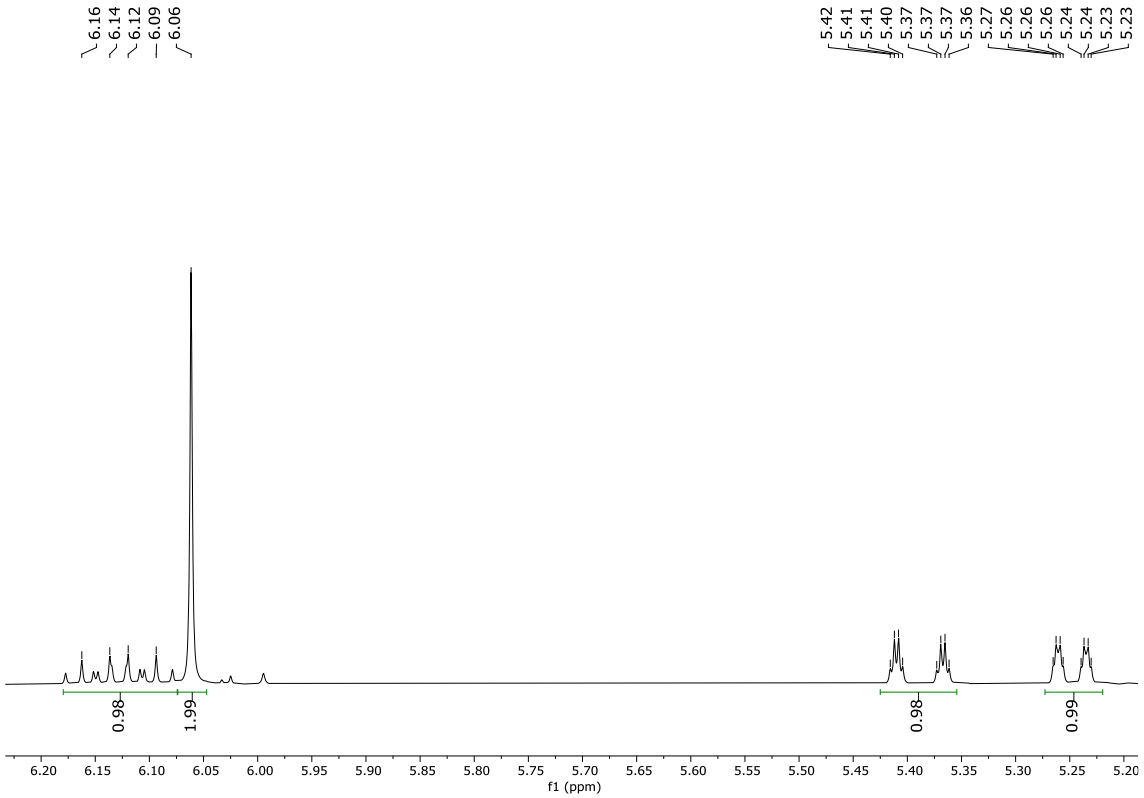


Figura 51: Expansão do espectro de RMN $^{1}H$ (500 MHz, $CDCl_3$) de FER12 na região 6.80 - 7.90 ppm.

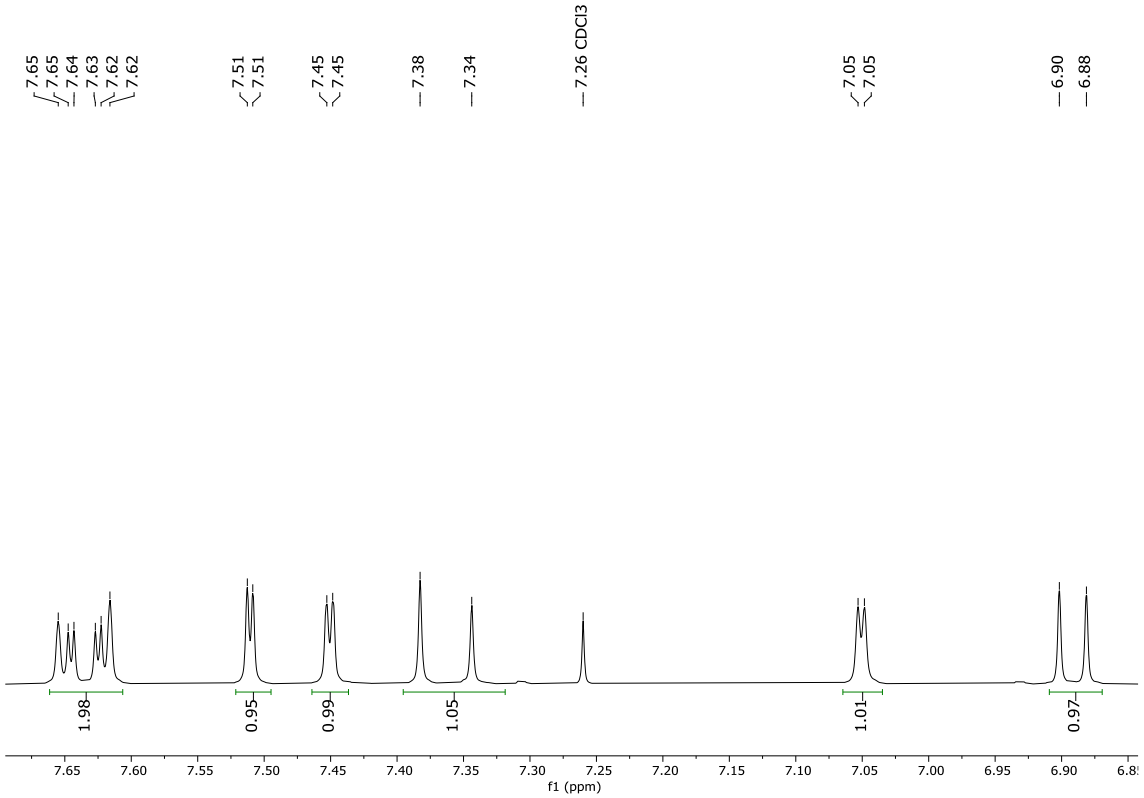

Figura 52: Espectro de RMN $^{13}C$ (125 MHz, $CDCl_3$) de FER12.

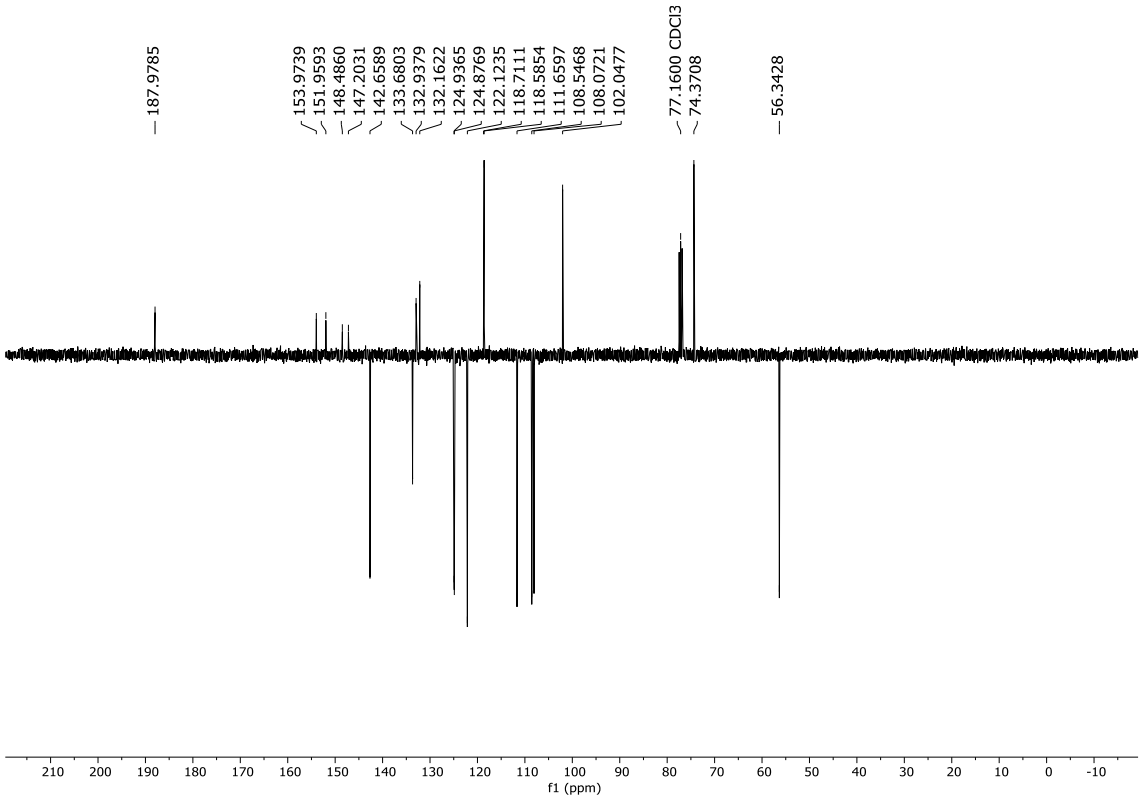


Figura 53: Expansão do espectro de RMN $^{13}C$ (125 MHz, $CDCl_3$) de FER12 na região 102 - 154 ppm.

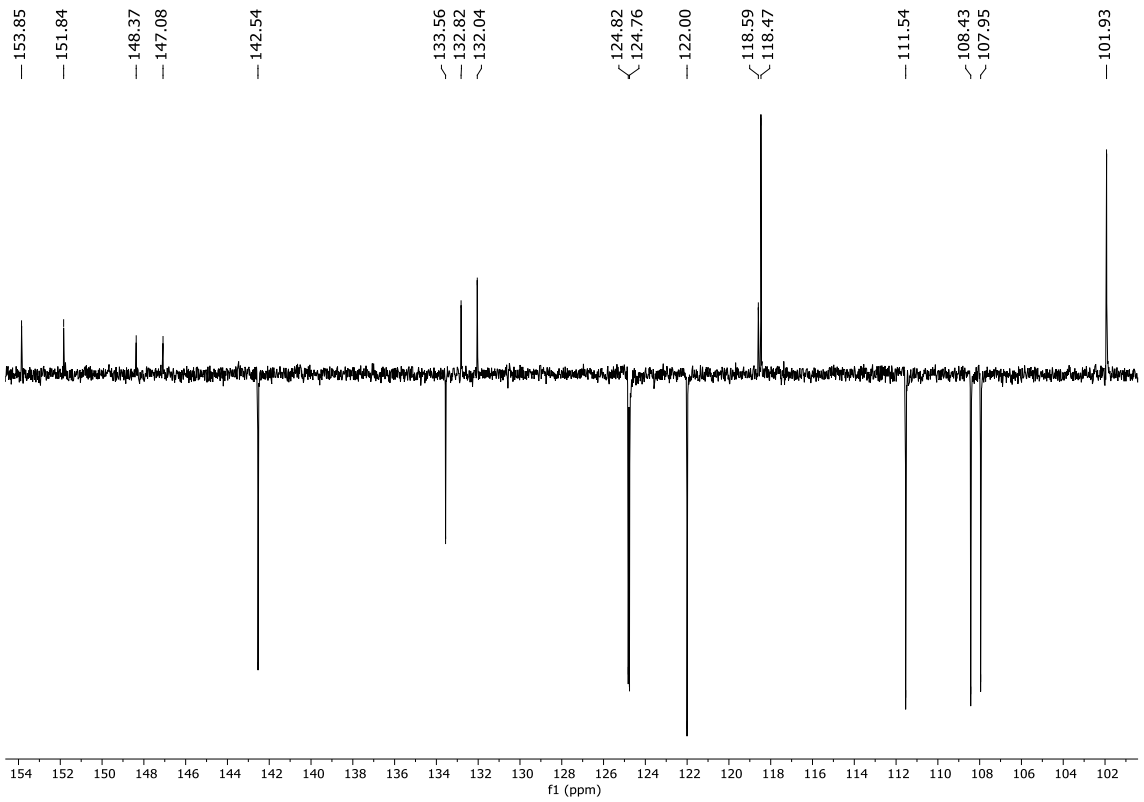

Figura 54: Espectro de massas [M+] de FER12.

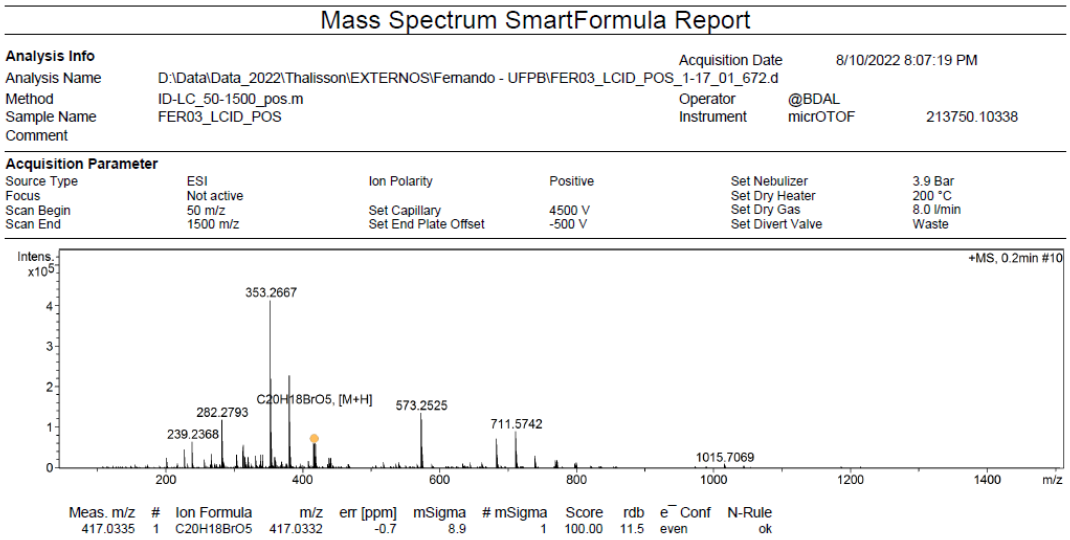


(E)-1-(benzo[d][1,3]dioxol-5-il)-3-(4-etoxi-3,5-dimetoxifenil)prop-2-en-1-ona (**FER36**)

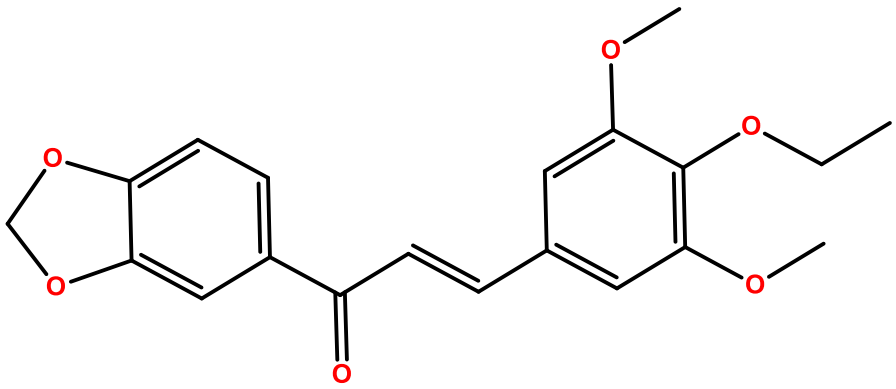

Sólido amorfo, de coloração branco esverdeado - FM: $C_{20}H_{20}O_6$ [M+]: 357.1346 g/mol; PF: 131.0 – 133.0 °C; Tempo de reação: 24 horas; Rendimento: 87%. $^1$H NMR (400 MHz, $CDCl_3$) δ 7.69 (d, *J* = 15.6 Hz, 1H), 7.63 (dd, *J* = 8.2, 1.8 Hz, 1H), 7.51 (d, *J* = 1.8 Hz, 1H), 7.35 (d, *J* = 15.6 Hz, 1H), 6.88 (d, *J* = 8.1 Hz, 1H), 6.84 (s, 2H), 6.05 (s, 2H), 4.10 (q, *J* = 7.1 Hz, 2H), 3.89 (s, 6H), 1.36 (t, *J* = 7.0 Hz, 3H). $^{13}$C NMR (101 MHz, $CDCl_3$) δ 188.36, 153.89, 151.76, 148.38, 144.64, 139.48, 133.13, 130.43, 124.74, 121.02, 108.55, 108.02, 105.76, 101.98, 69.24, 56.34, 15.64.

Figura 55Espectro de RMN $^{1}H$ (500 MHz, $CDCl_3$) de FER36.

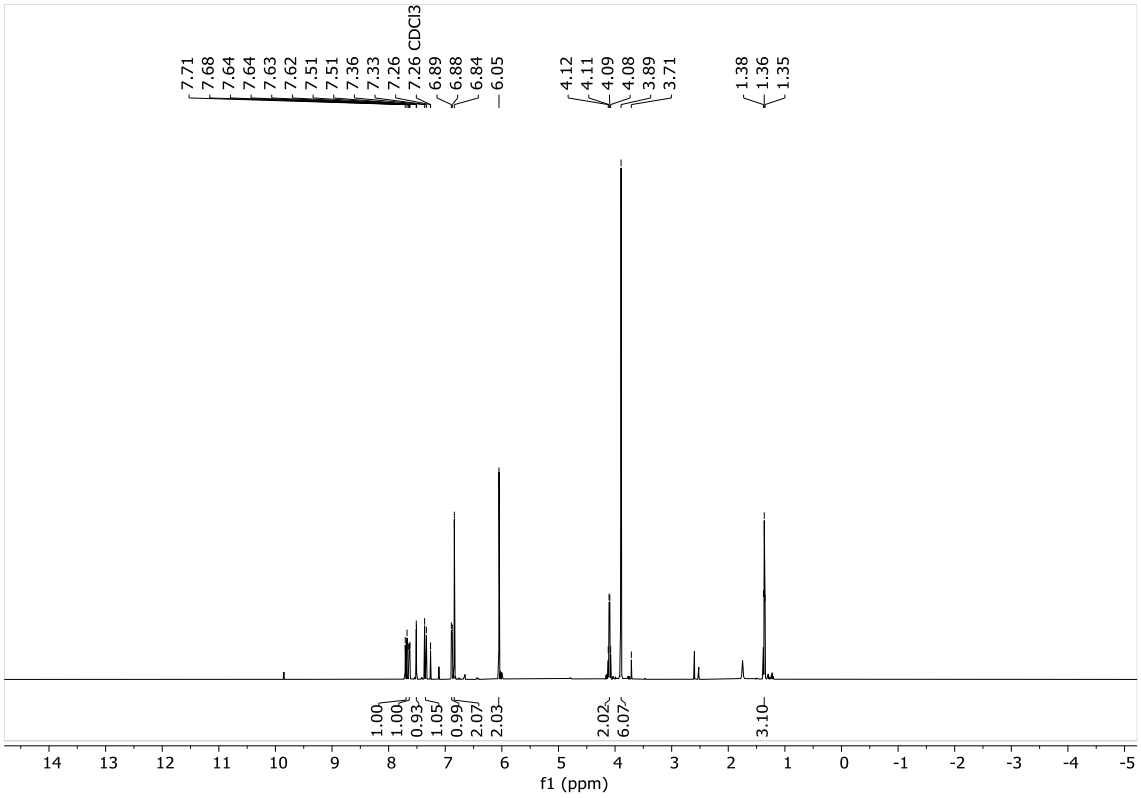


Figura 56Expansão do espectro de RMN $^{1}H$ (500 MHz, $CDCl_3$) de FER36 na região 1.50 - 4.20 ppm.

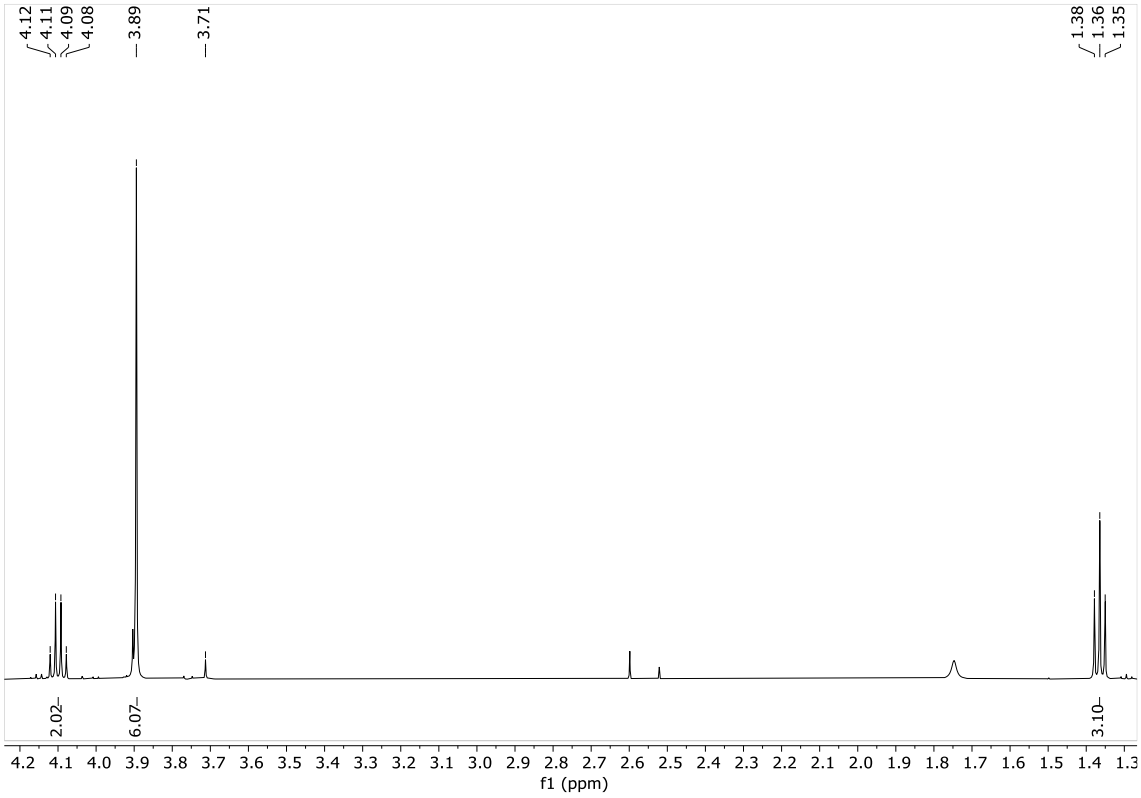

Figura 57Expansão do espectro de RMN $^{1}H$ (500 MHz, $CDCl_3$) de FER36 na região 6.80 - 7.70 ppm.

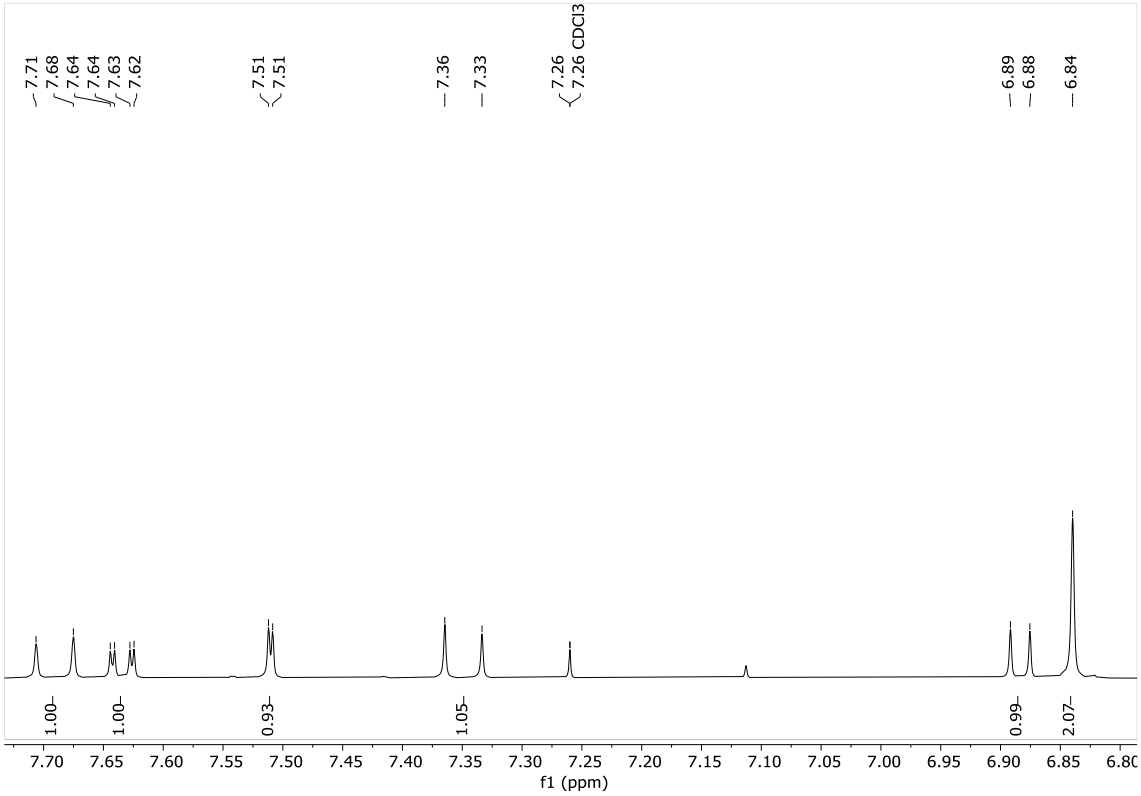


Figura 58Espectro de RMN $^{13}C$ (125 MHz, $CDCl_3$) de FER36.

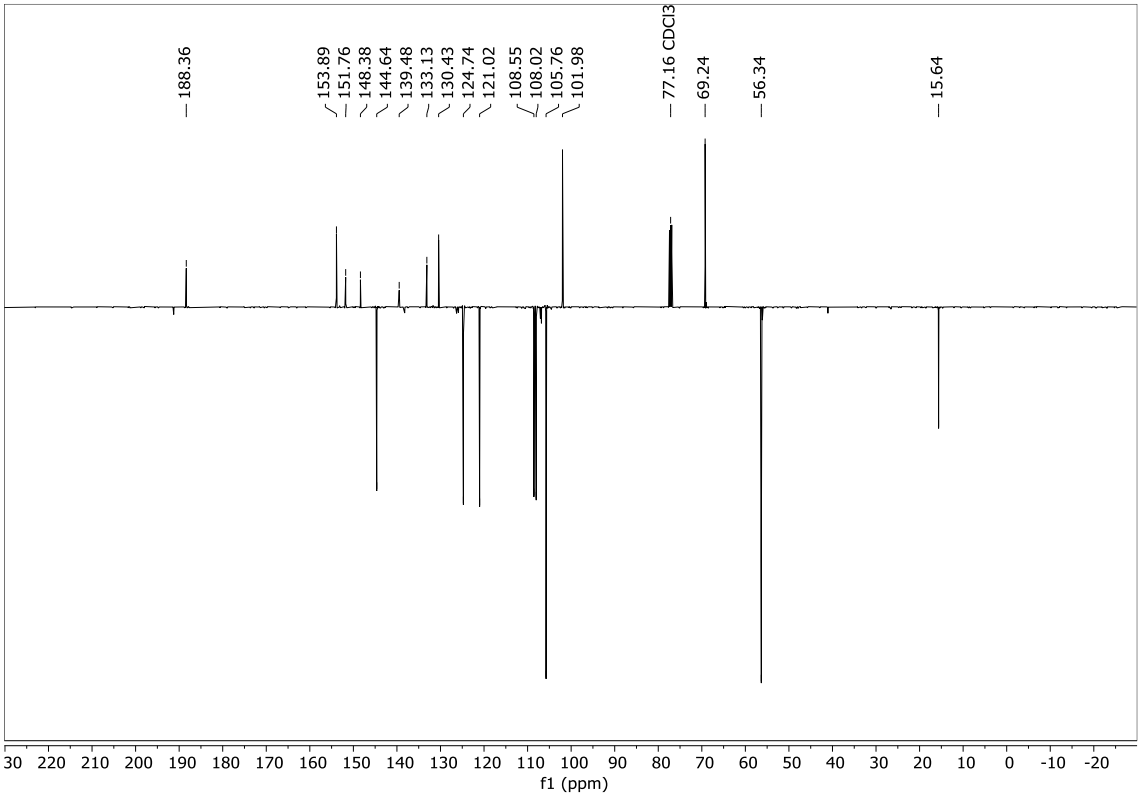

Figura 59Expansão do espectro de RMN $^{13}C$ (125 MHz, $CDCl_3$) de FER36 na região 102 - 155 ppm.

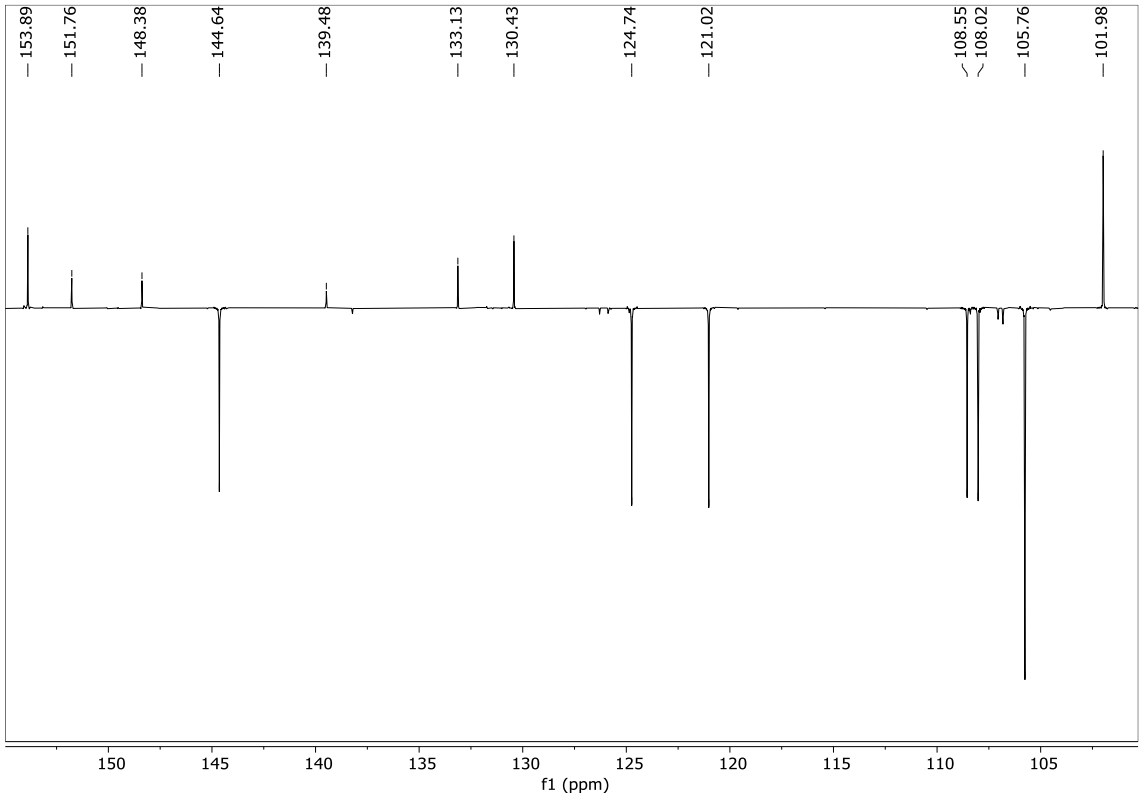


Figura 60: Espectro de massas [M+] de FER36.

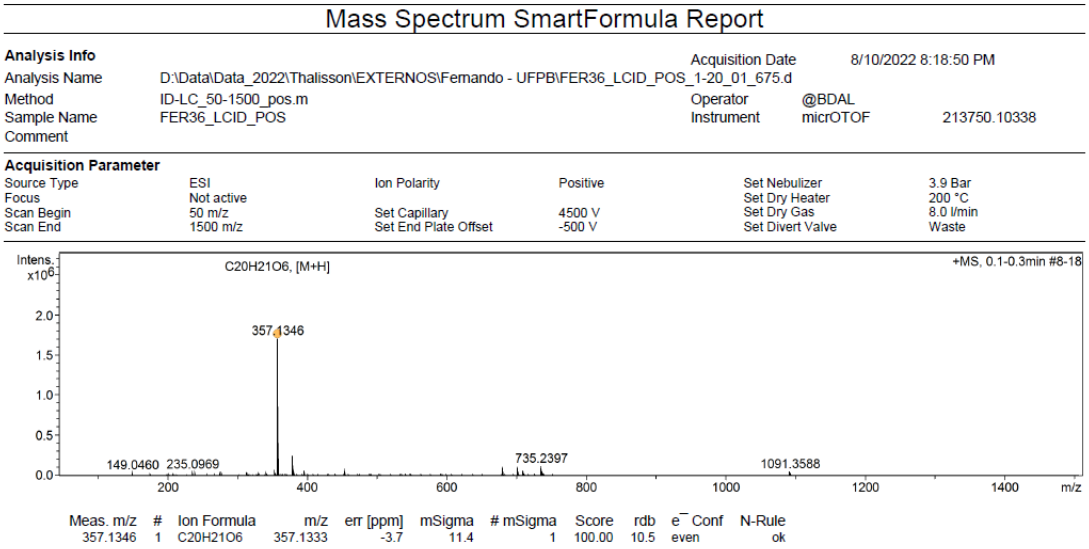

(E)-3-(4-(alliloxi)-3,5-dimetoxifenil)-1-(benzo[d][1,3]dioxol-5-il)prop-2-en-1-ona (**FER37**)

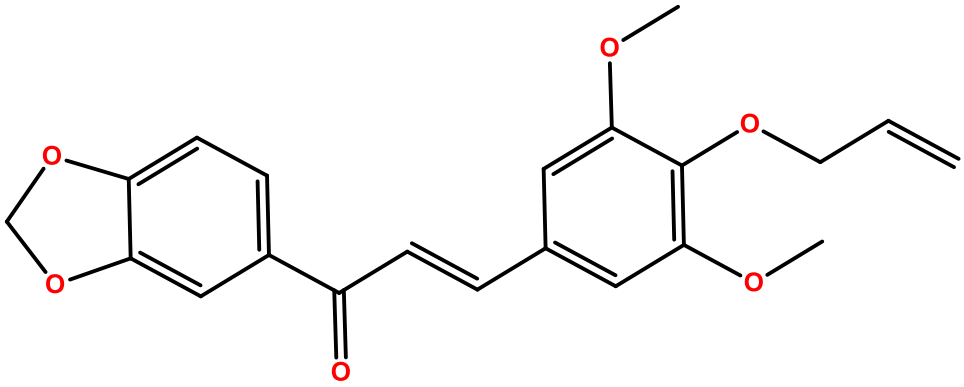

Sólido amorfo, de coloração branco esverdeado - FM: $C_{21}H_{20}O_6$ [M+]: 369.1339 g/mol; PF: 136.0 – 137.0 °C; Tempo de reação: 24 horas; Rendimento: 92%. $^1$H NMR (400 MHz, $CDCl_3$) δ 7.60 (d, *J* = 15.5 Hz, 1H), 7.68 – 7.55 (m, 2H), 7.49 – 7.42 (m, 1H), 7.32 (d, *J* = 15.5 Hz, 1H), 6.85 – 6.75 (m, 3H), 5.99 (s, 2H), 6.11 – 6.01 (m, 1H), 5.28 (dt, *J* = 17.2, 1.7 Hz, 1H), 5.15 (dt, *J* = 10.4, 1.5 Hz, 1H), 5.15 (dt, *J* = 10.4, 1.5 Hz, 1H), 3.85 (d, *J* = 2.4 Hz, 8H). $^{13}$C NMR (101 MHz, $CDCl_3$) δ 188.12, 153.61, 151.63, 148.22, 144.41, 138.91, 134.17, 132.90, 130.45, 124.62, 120.86, 117.98, 108.33, 107.83, 105.60, 101.86, 74.16, 56.16.

Figura 61: Espectro de RMN $^1$H (500 MHz, $CDCl_3$) de FER37.

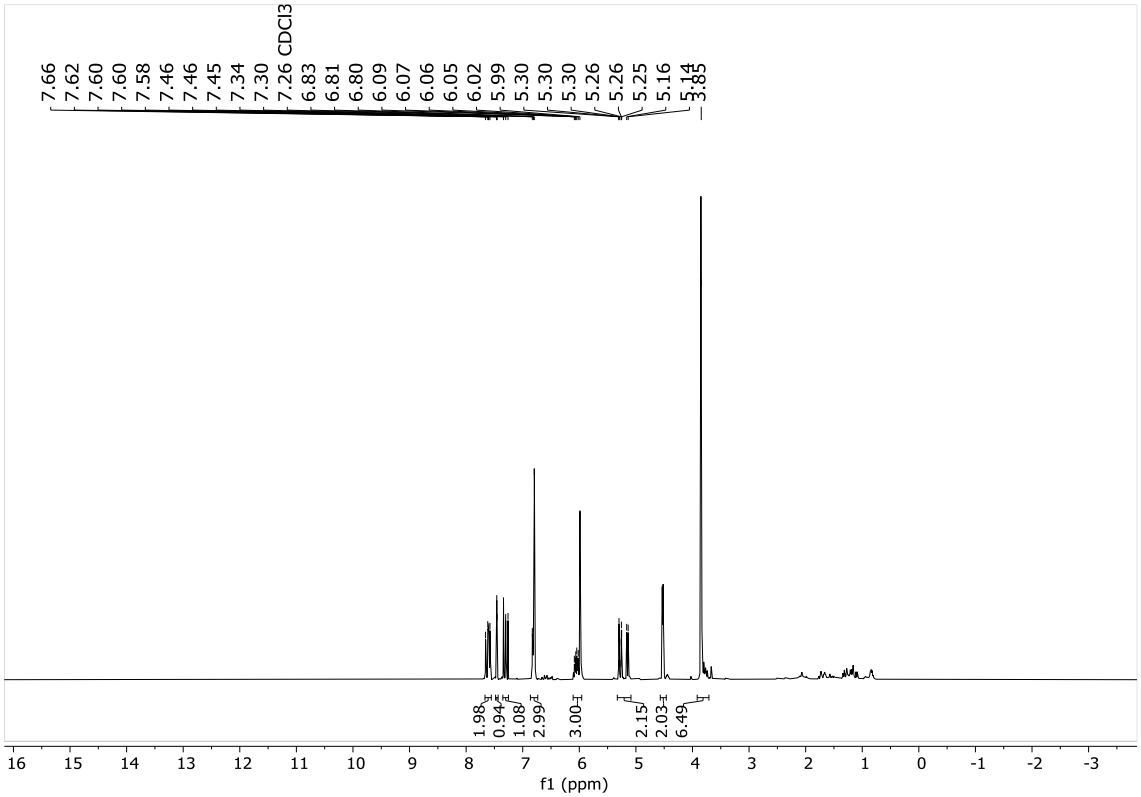

Figura 62: Expansão do espectro de RMN $^{1}H$ (500 MHz, $CDCl_3$) de FER37 na região 3.75 - 7.65 ppm.

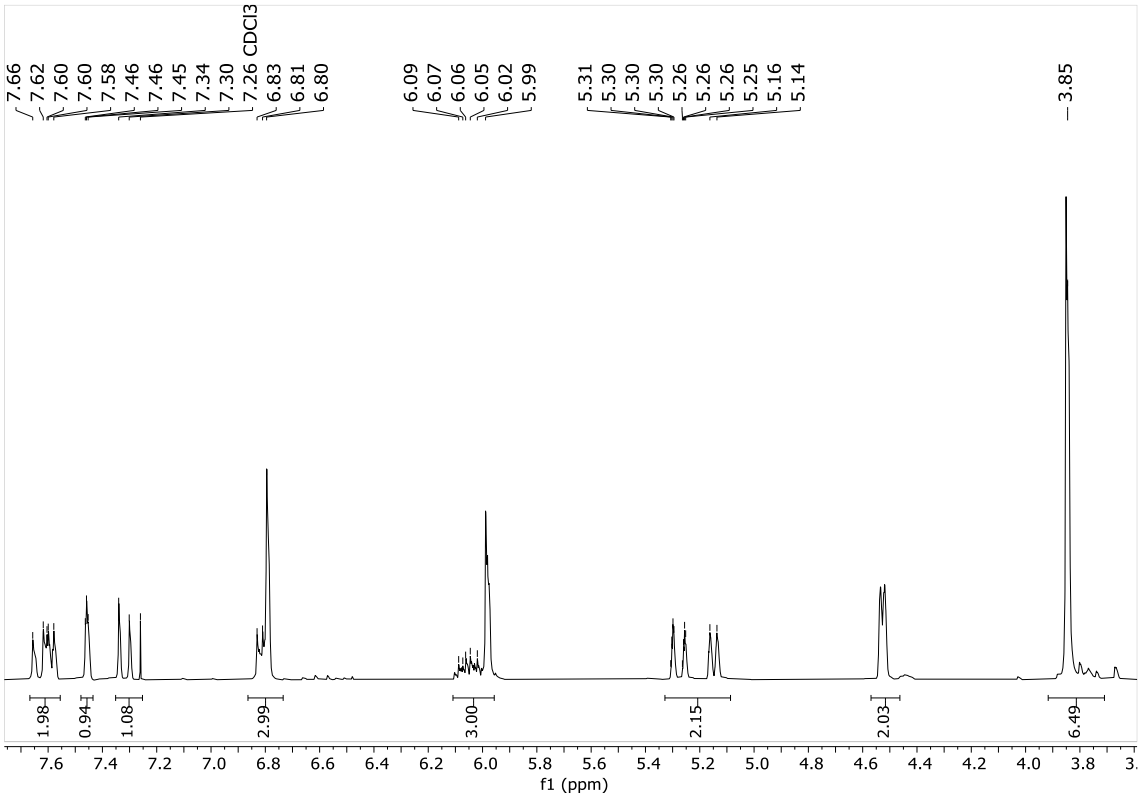


Figura 63: Espectro de RMN $^{13}C$ (125 MHz, $CDCl_3$) de FER37.

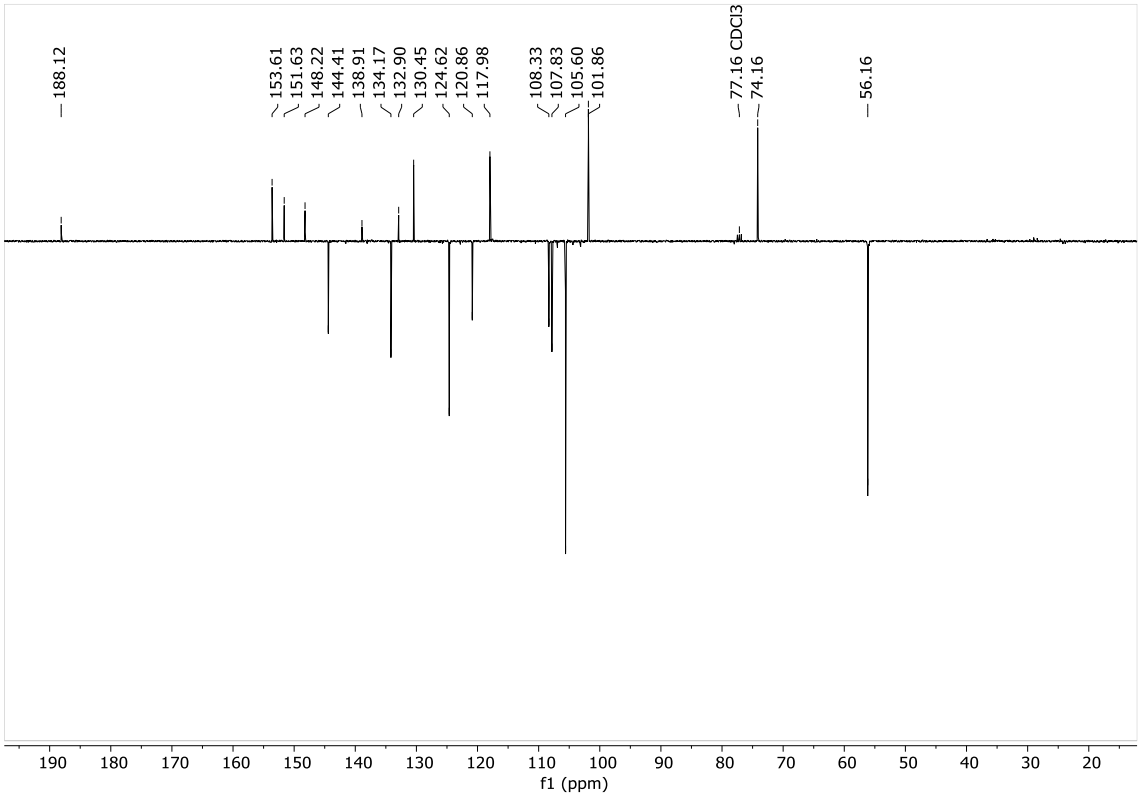

Figura 64: Expansão do espectro de RMN $^{13}C$ (125 MHz, $CDCl_3$) de FER37 na região 102 - 156 ppm.

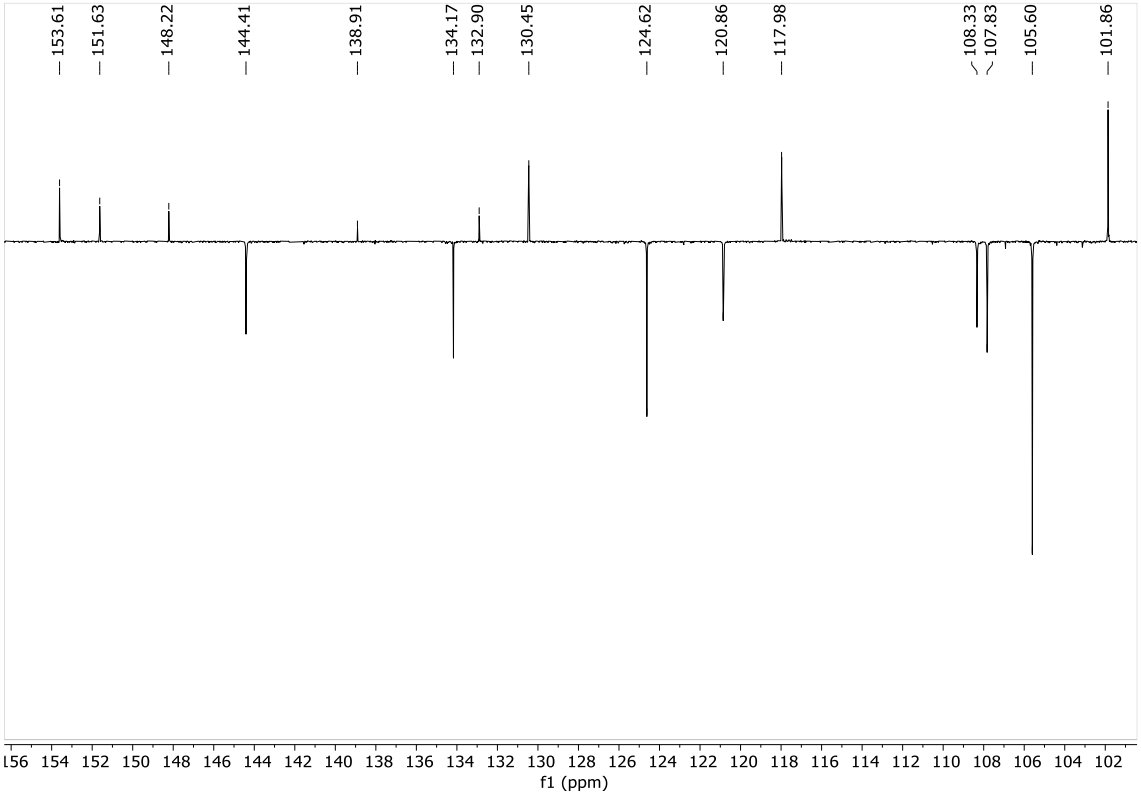


Figura 65: Espectro de massas [M+] de FER37.

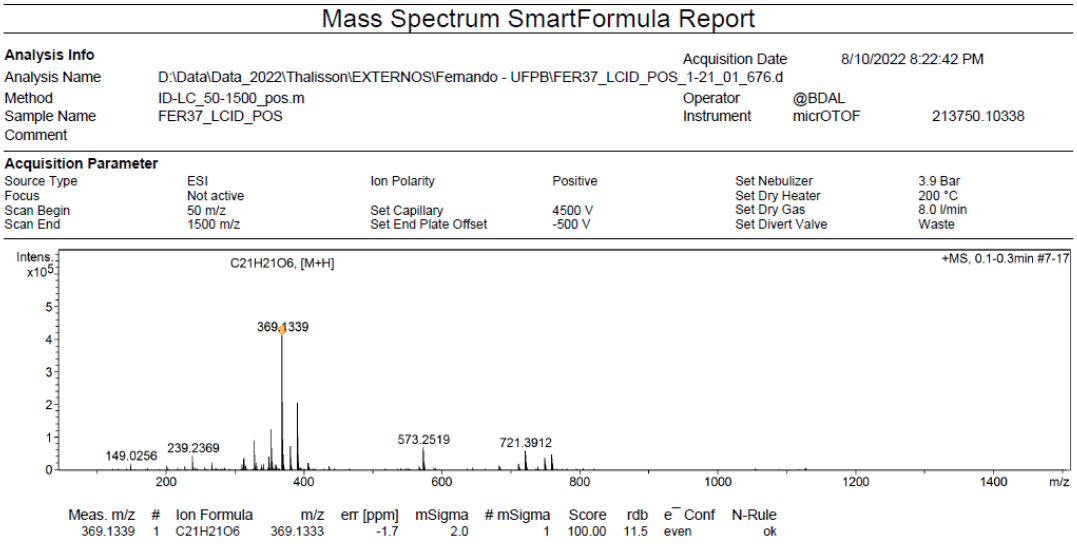

(E)-1-(benzo[d][1,3]dioxol-5-il)-3-(4-clorofenil)prop-2-en-1-ona (**FER41**)

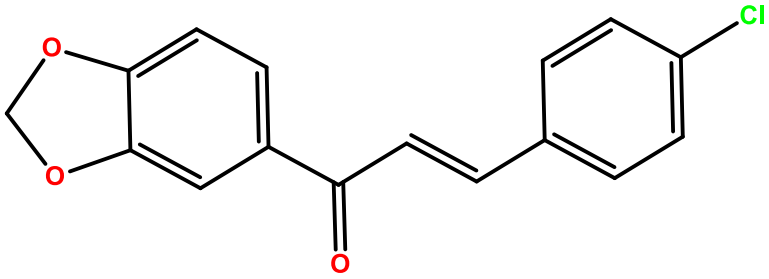


Sólido amorfo, de coloração branco esverdeado - FM: $C_{16}H_{11}ClO_3$ [M+]: 287.0475 g/mol; PF: 97.0 – 98.0 °C; Tempo de reação: 24 horas; Rendimento: 97%. $^1$H NMR (400 MHz, $CDCl_3$) δ 7.75 (d, *J* = 15.6 Hz, 1H), 7.66 (dd, *J* = 8.1, 1.8 Hz, 1H), 7.57 (d, *J* = 8.3 Hz, 1H), 7.54 (d, *J* = 1.7 Hz, 1H), 7.47 (d, *J* = 15.6 Hz, 1H), 7.40 (d, *J* = 8.6 Hz, 1H), 6.91 (d, *J* = 8.1 Hz, 1H), 6.08 (s, 2H). $^{13}$C NMR (101 MHz, $CDCl_3$) δ 188.03, 151.96, 148.48, 142.82, 136.38, 133.61, 132.92, 129.65, 129.33, 124.84, 122.22, 108.50, 108.06, 102.04.

Figura 66: Espectro de RMN $^1$H (500 MHz, $CDCl_3$) de FER41.

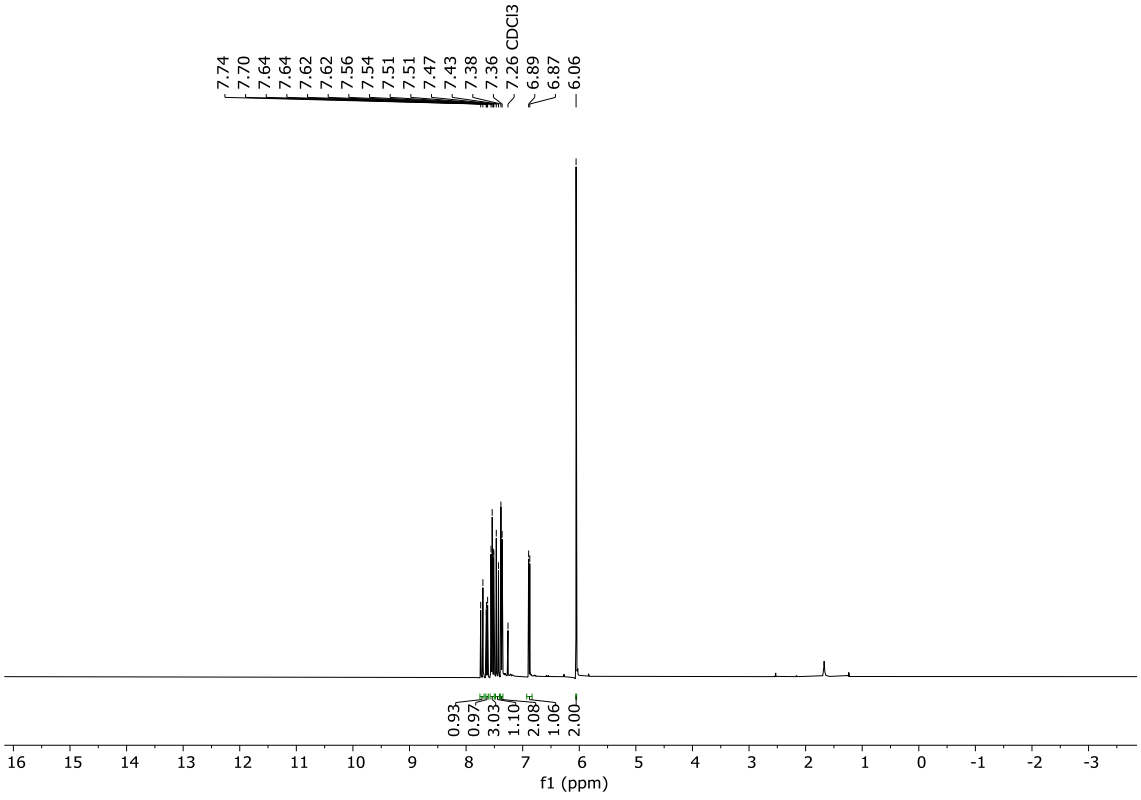

Figura 67: Expansão do espectro de RMN $^{1}H$ (500 MHz, $CDCl_3$) de FER41 na região 6.00 - 7.80 ppm.

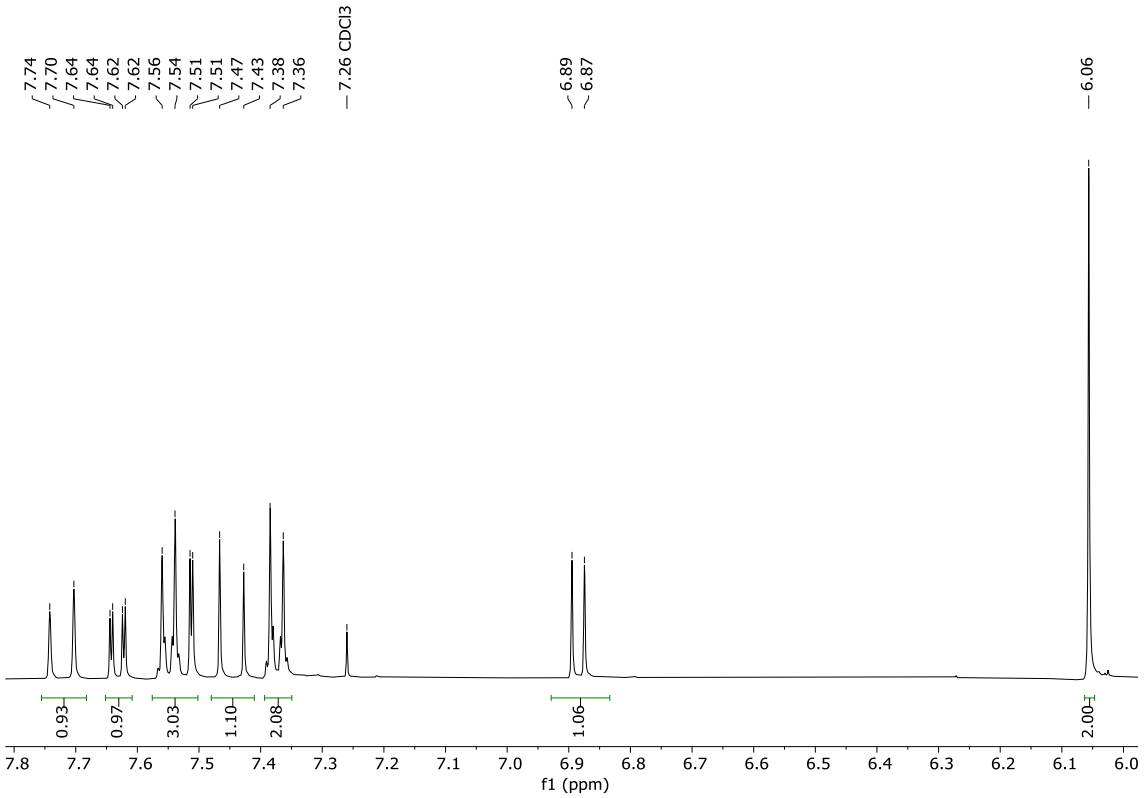


Figura 68: Espectro de RMN $^{13}C$ (125 MHz, $CDCl_3$) de FER41.

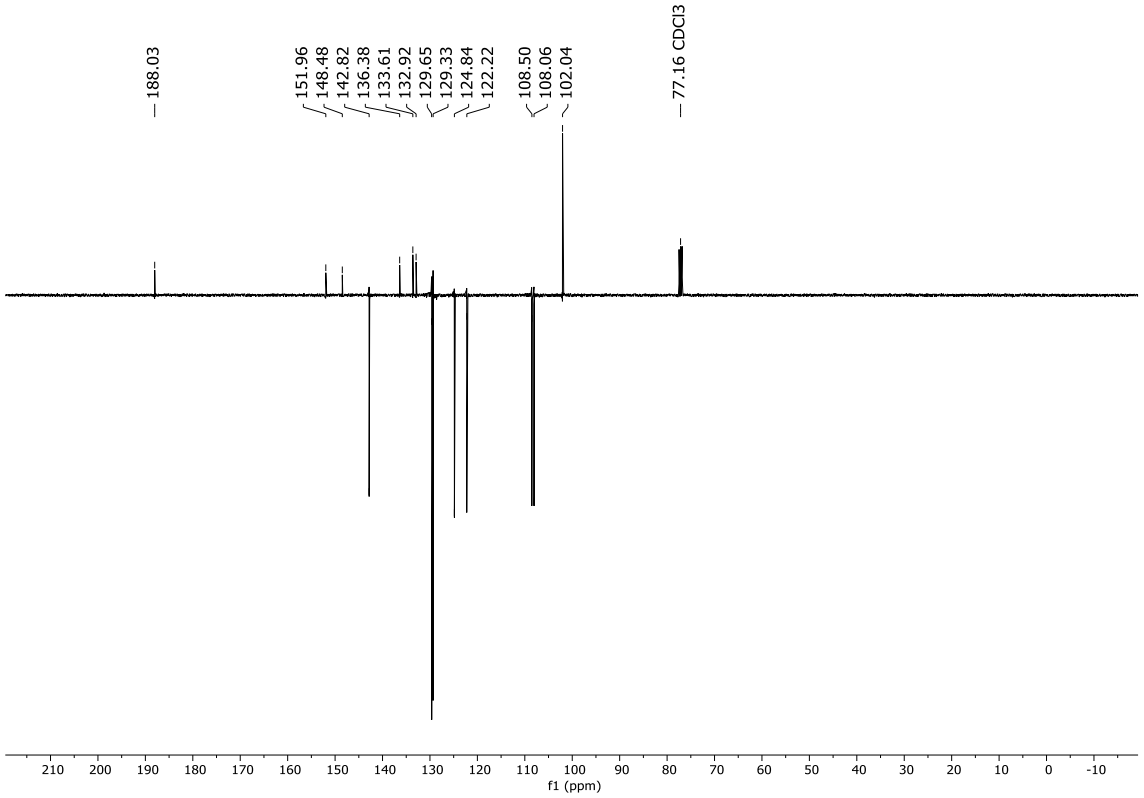

Figura 69: Expansão do espectro de RMN $^{13}C$ (125 MHz, $CDCl_3$) de FER41 na região 102 - 152 ppm.

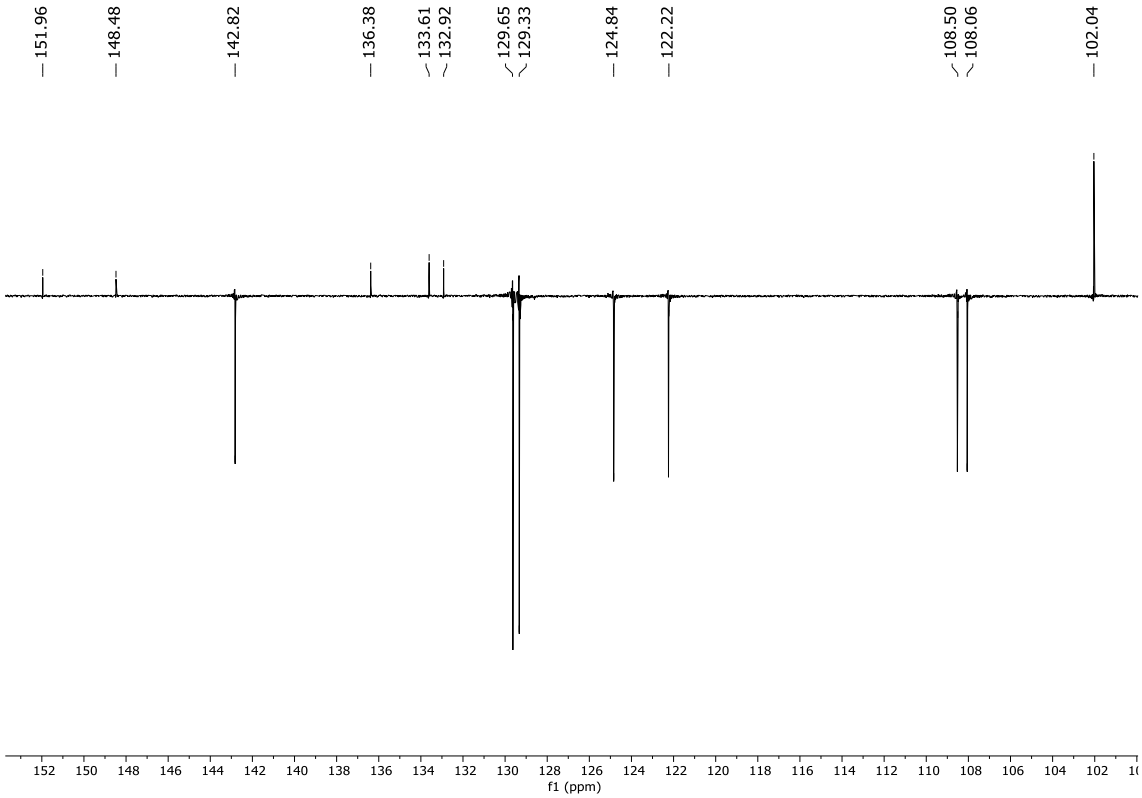


Figura 70: Espectro de massas [M+] de FER41.

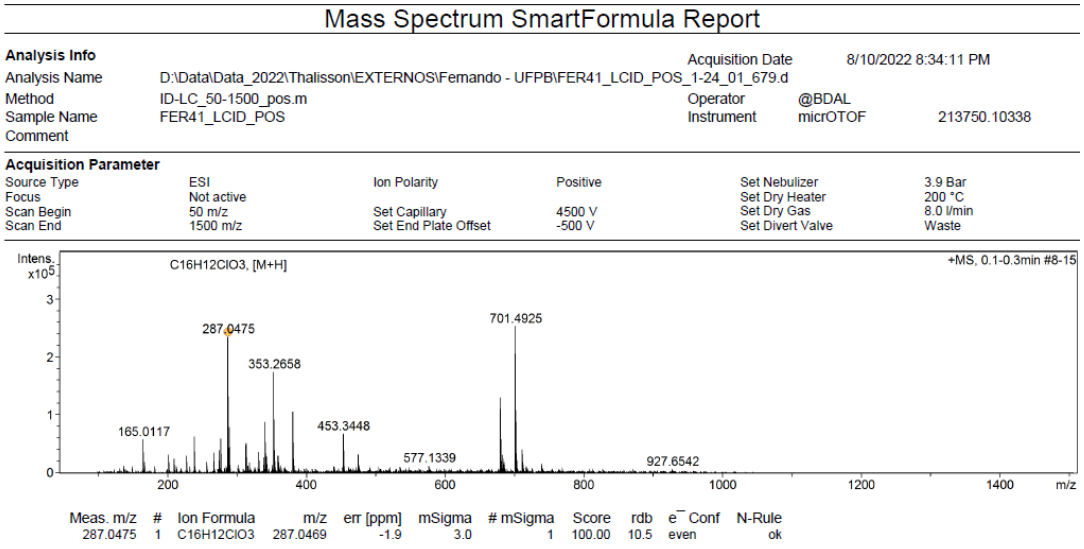


(E)-1-(benzo[d][1,3]dioxol-5-il)-3-(3,4-diclorofenil)prop-2-en-1-ona (**FER44**)

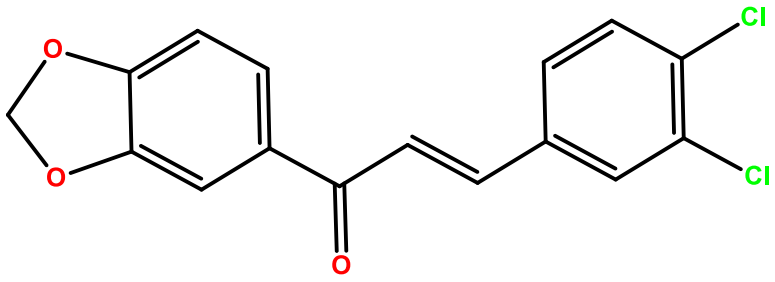


Sólido amorfo, de coloração branco esverdeado - FM: $C_{16}H_{10}Cl_2O_3$ [M+]: 321,0085 g/mol; PF: 99.0 – 101.0 °C; Tempo de reação: 24 horas; Rendimento: 96%. $^{1}H$ NMR (500 MHz, $CDCl_3$) 7.73 (d, J = 15.6 Hz, 1H), 7.66 – 7.56 (m, 3H), 7.51 (d, *J* = 1.7 Hz, 1H), 7.40 (d, J = 15.9 Hz, 1H), 7.09 (t, J = 8.6 Hz, 2H), 6.87 (d, J = 8.2 Hz, 1H), 6.04 (s, 2H). $^{13}C$ NMR (126 MHz, $CDCl_3$) δ 188.09, 165.06, 163.06, 151.86, 148.42, 142.98, 132.96, 131.32, 130.31, 124.76, 121.50, 116.26, 116.08, 108.49, 108.01, 102.00.

Figura 71: Espectro de RMN $^{1}H$ (500 MHz, $CDCl_3$) de FER44.

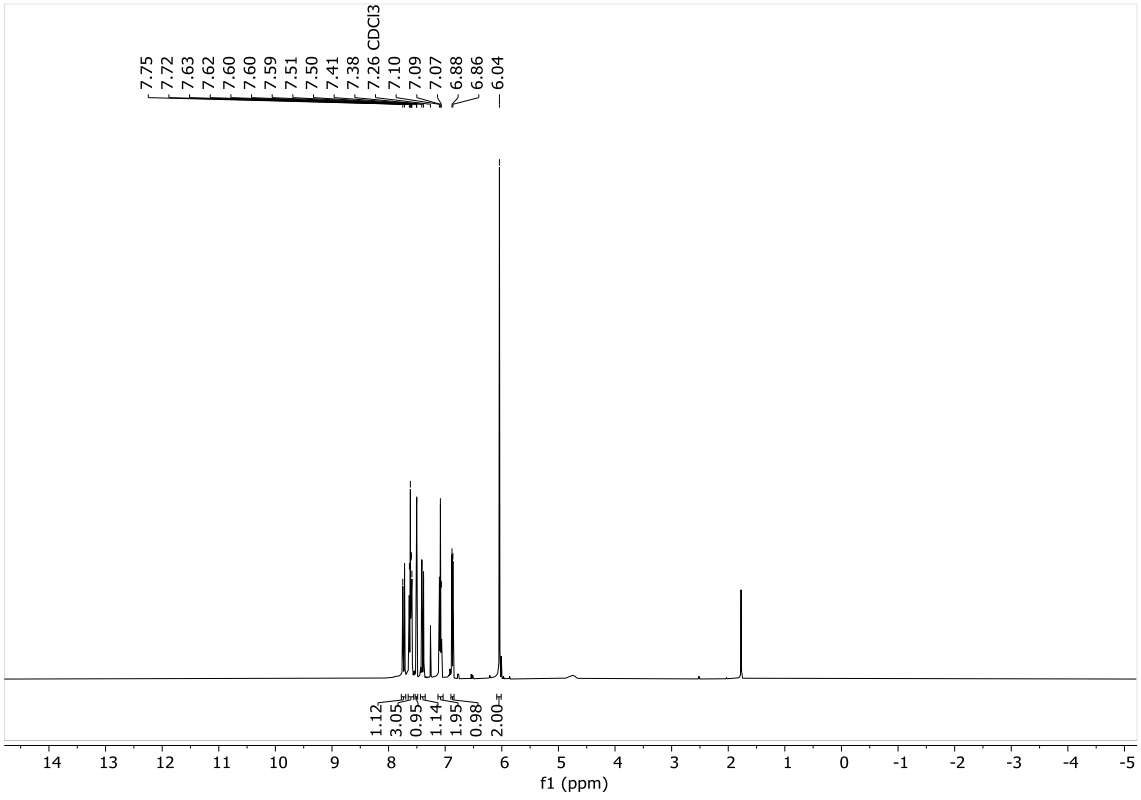

Figura 72: Expansão do espectro de RMN $^{1}H$ (500 MHz, $CDCl_3$) de FER44 na região 5.90 - 7.90 ppm.

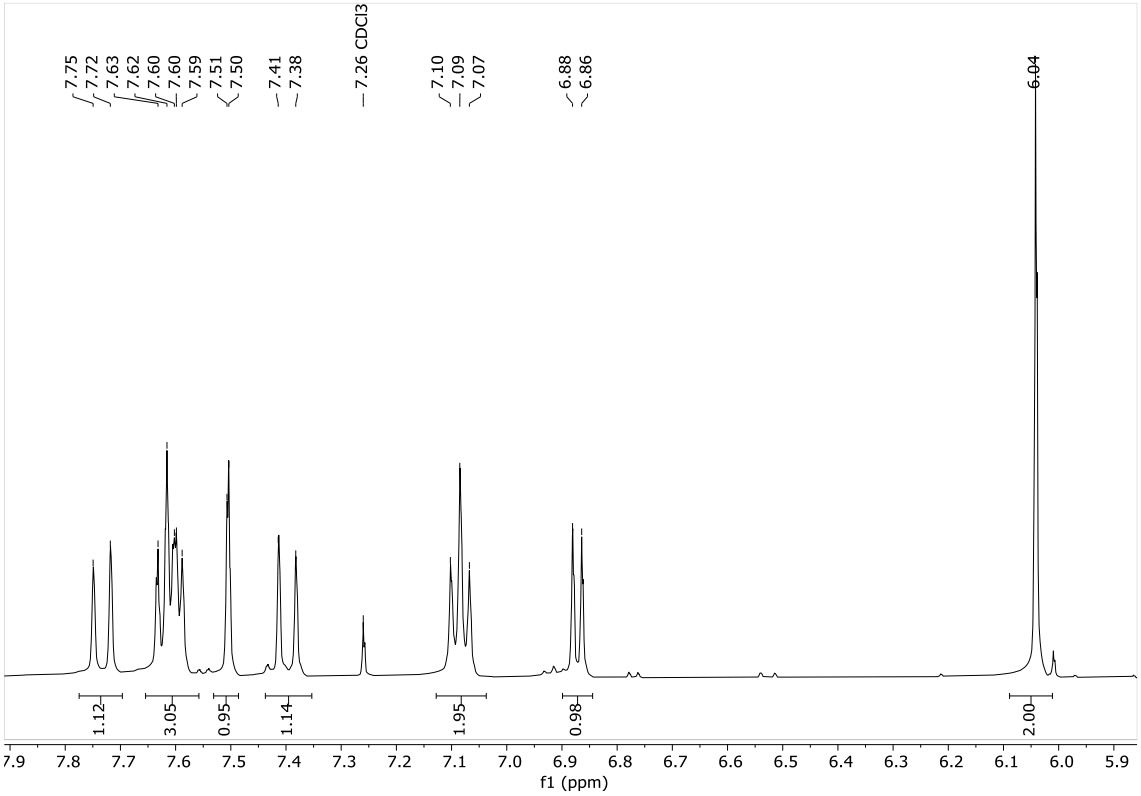


Figura 73: Espectro de RMN $^{13}C$ (125 MHz, $CDCl_3$) de FER44.

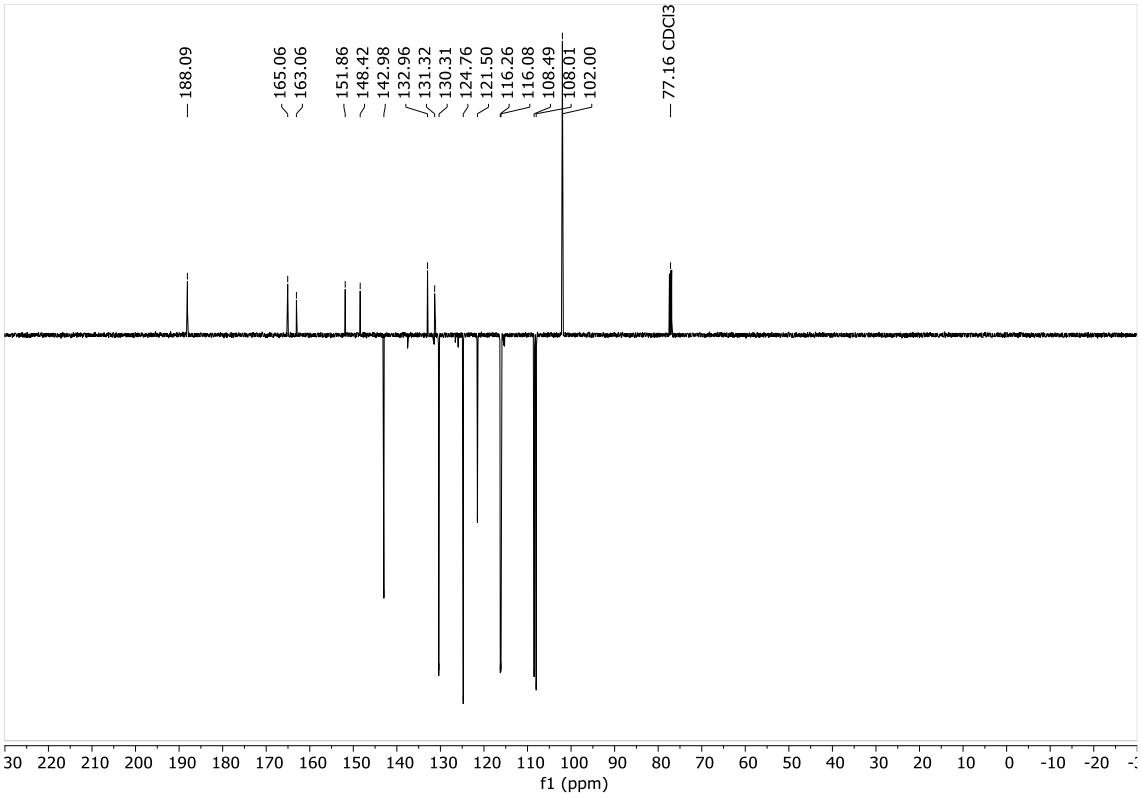

Figura 74: Expansão do espectro de RMN $^{13}C$ (125 MHz, $CDCl_3$) de FER44 na região 102 - 168 ppm.

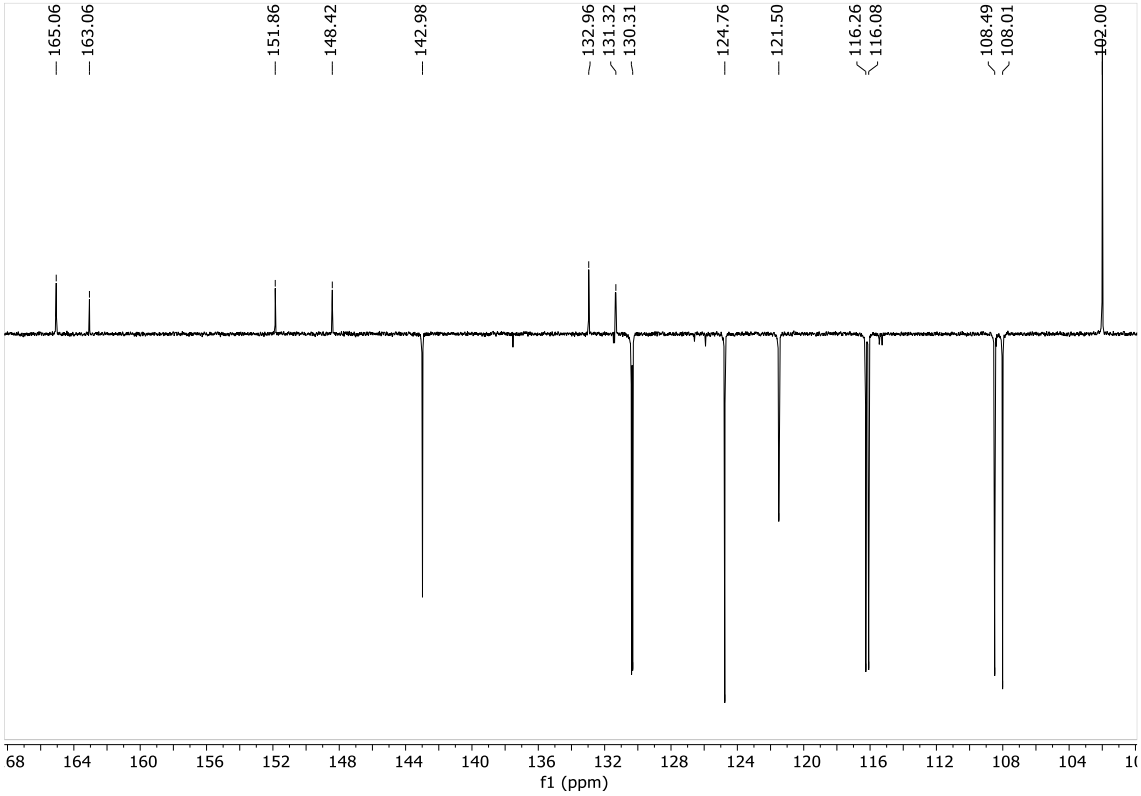


Figura 75: Espectro de massas [M+] de FER44.

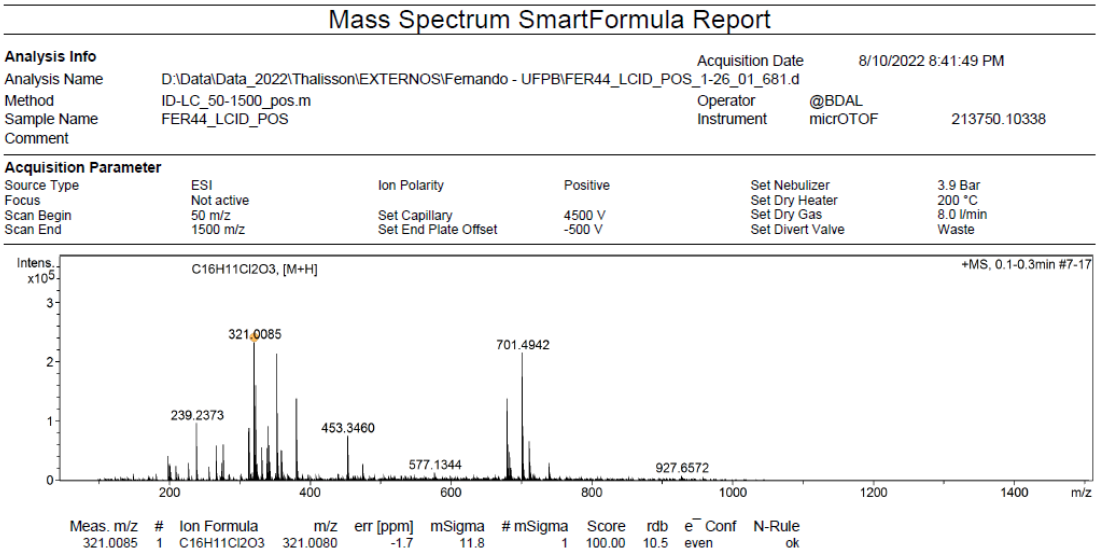

(E)-1-(benzo[d][1,3]dioxol-5-il)-3-(4-(dimetilamino)fenil)prop-2-en-1-ona (**FER42**)

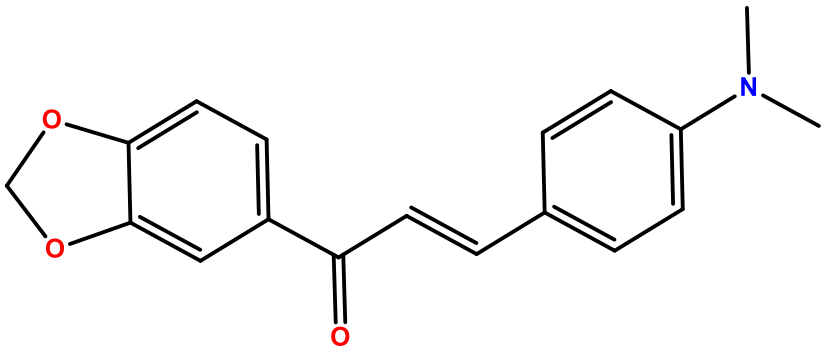


Sólido amorfo, de coloração vermelho alaranjado - FM: $C_{18}H_{17}NO_3$ [M+]: 296.1311 g/mol; PF: 91.0 – 93.0 °C; Tempo de reação: 24 horas; Rendimento: 98%. $^{1}$H NMR (400 MHz, $CDCl_3$) δ 7.78 (d, *J* = 15.4 Hz, 1H), 7.63 (dd, *J* = 8.2, 1.7 Hz, 1H), 7.54 (d, *J* = 2.4 Hz, 1H), 7.52 (d, *J* = 1.7 Hz, 2H), 7.52 (s, 1H), 7.29 (d, *J* = 15.4 Hz, 1H), 6.87 (d, *J* = 8.1 Hz, 1H), 6.68 (d, *J* = 8.9 Hz, 2H), 6.03 (s, 2H), 3.02 (s, 6H). $^{13}$C NMR (101 MHz, $CDCl_3$) δ 188.49, 152.06, 151.25, 148.19, 145.34, 133.87, 130.40, 124.27, 122.83, 116.54, 111.92, 108.50, 107.91, 101.81, 40.21.

Figura 76: Espectro de RMN $^{1}$H (500 MHz, $CDCl_3$) de FER42.

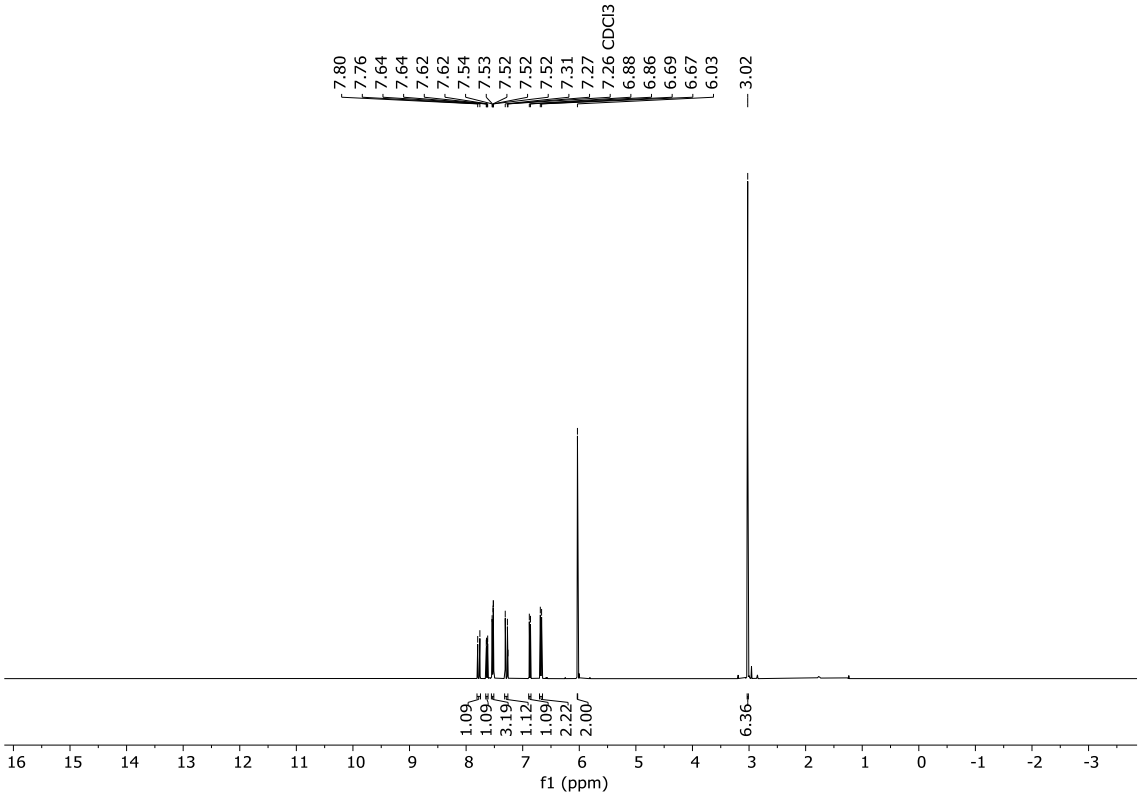

Figura 77: Expansão do espectro de RMN $^{1}H$ (500 MHz, $CDCl_3$) de FER42 na região 5.90 - 8.00 ppm.

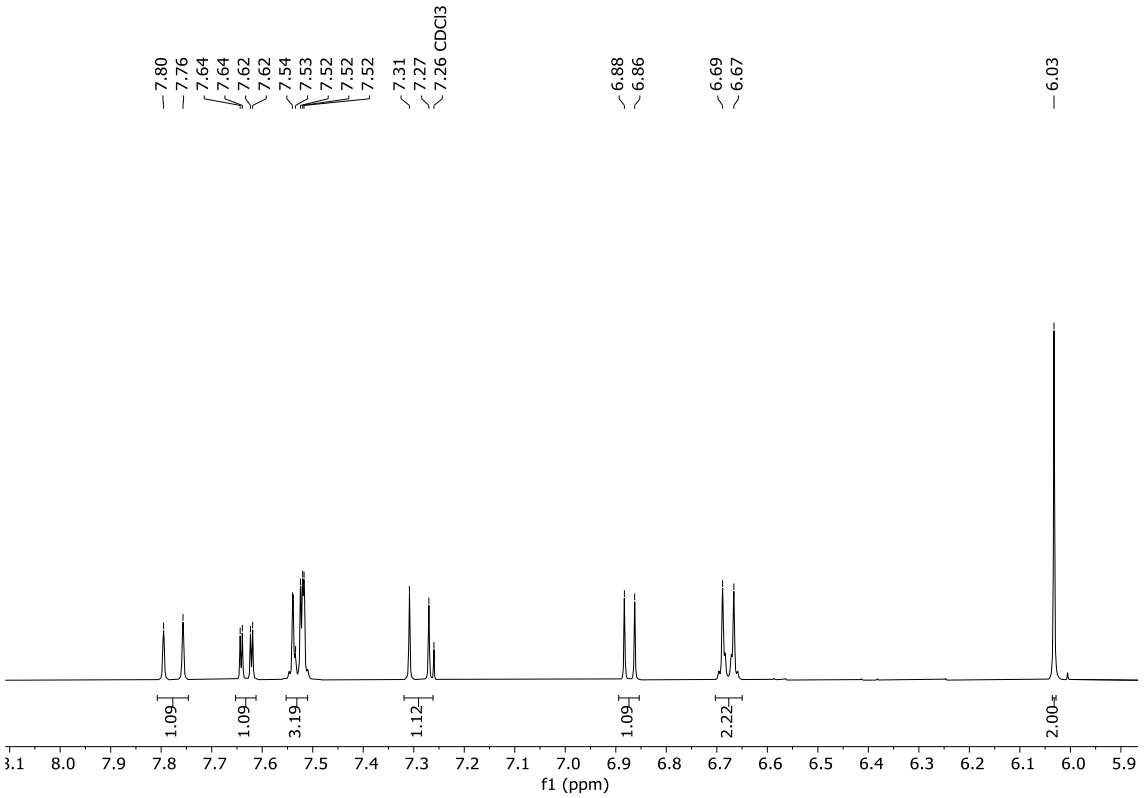


Figura 78: Espectro de RMN $^{13}C$ (125 MHz, $CDCl_3$) de FER42.

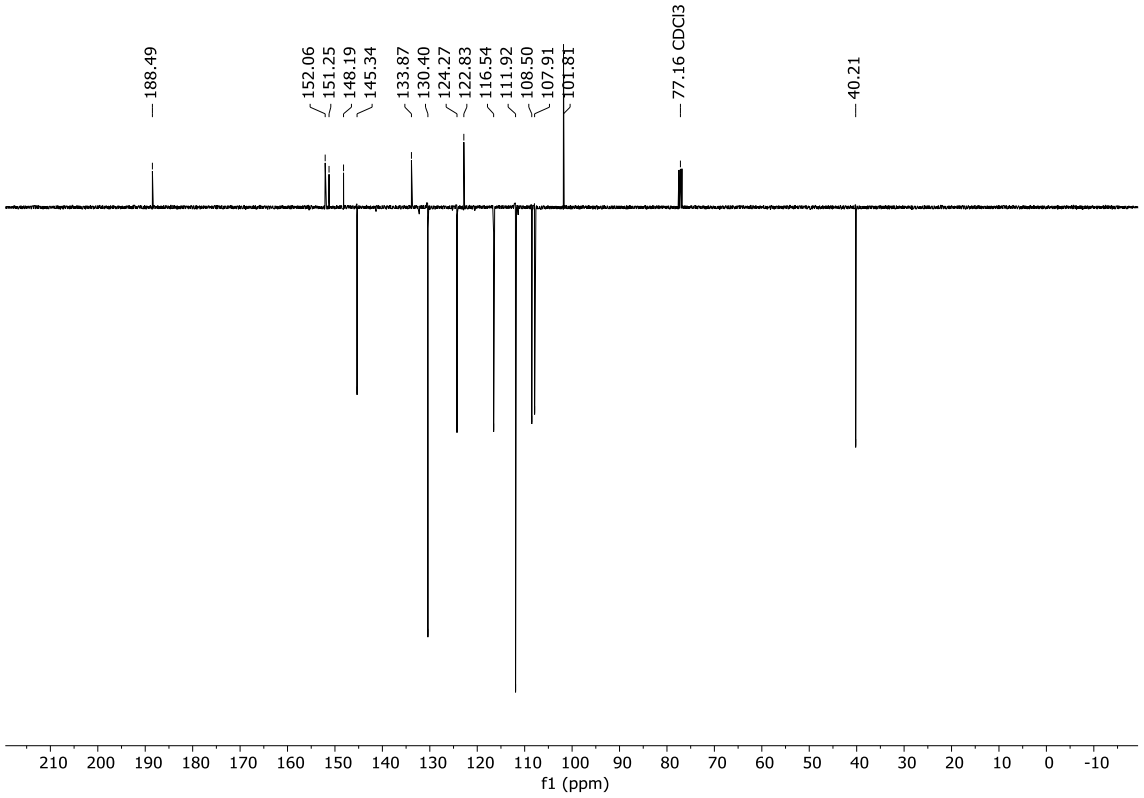

Figura 79: Expansão do espectro de RMN $^{13}C$ (125 MHz, $CDCl_3$) de FER42 na região 100 - 154 ppm.

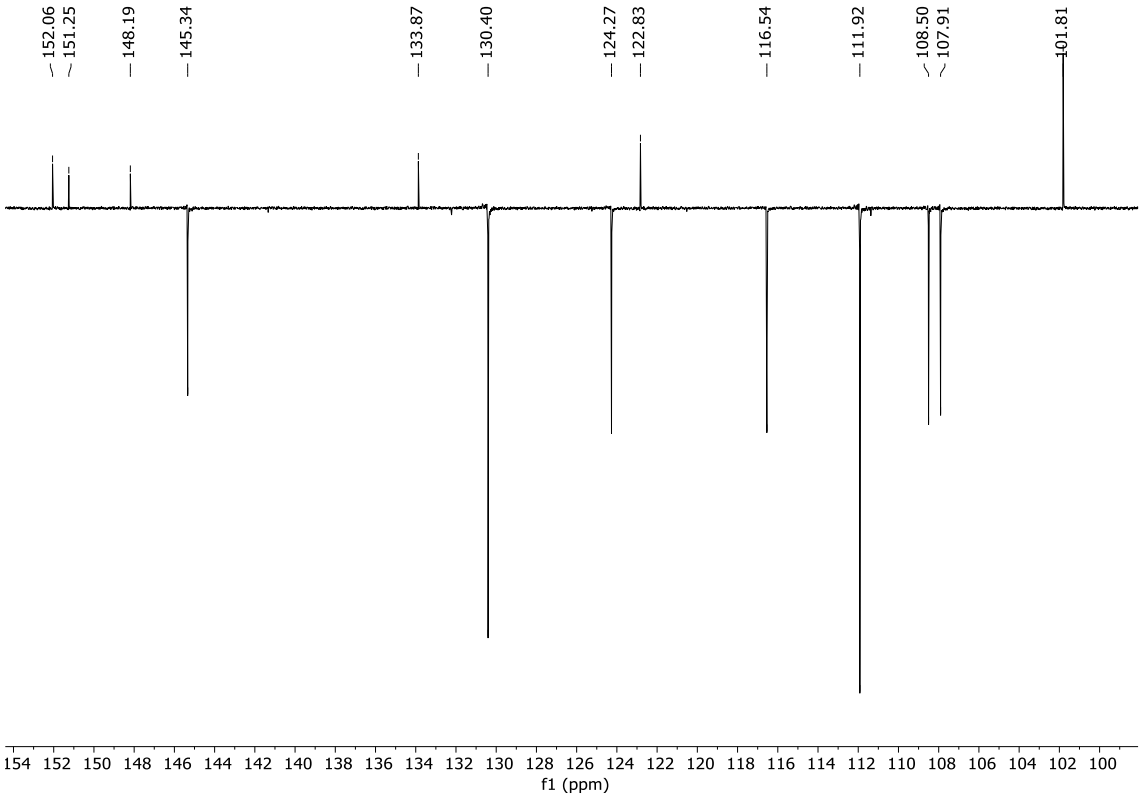


Figura 80: Espectro de massas [M+] de FER42.

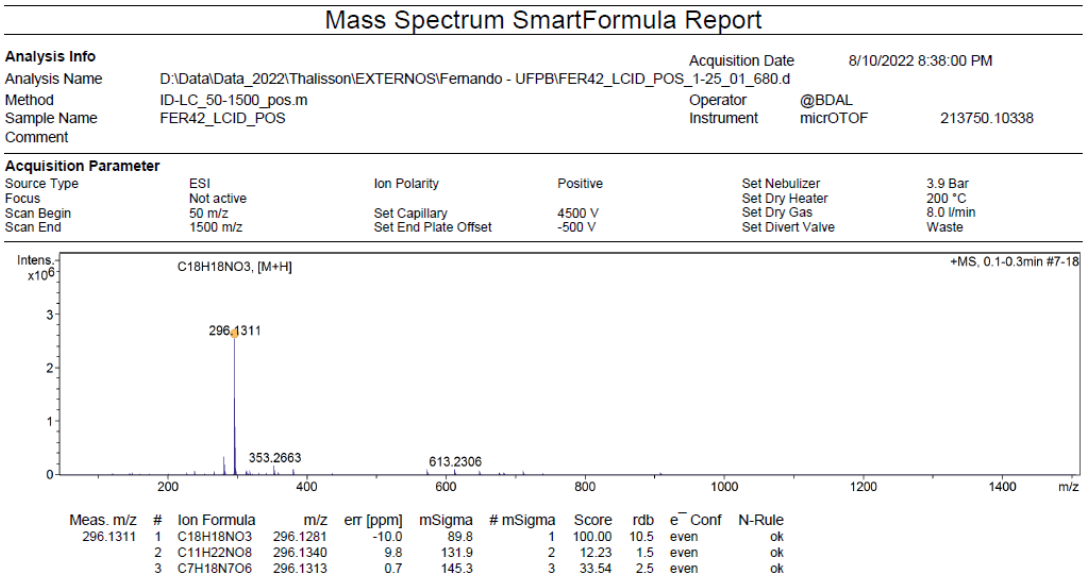

Mass Spectrum SmartFormula Report

**Analysis Info**

| | | | |
|---|---|---|---|
| Analysis Name | D:\Data\Data_2022\Thalisson\EXTERNOS\Fernando - UFPB\FER42_LCID_POS_1-25_01_680.d | Acquisition Date | 8/10/2022 8:38:00 PM |
| Method | ID-LC_50-1500_pos.m | Operator | @BDAL |
| Sample Name | FER42_LCID_POS | Instrument | micrOTOF 213750.10338 |
| Comment | | | |

**Acquisition Parameter**

| | | | | | |
|---|---|---|---|---|---|
| Source Type | ESI | Ion Polarity | Positive | Set Nebulizer | 3.9 Bar |
| Focus | Not active | | | Set Dry Heater | 200 °C |
| Scan Begin | 50 m/z | Set Capillary | 4500 V | Set Dry Gas | 8.0 l/min |
| Scan End | 1500 m/z | Set End Plate Offset | -500 V | Set Divert Valve | Waste |



| Meas. m/z | # | Ion Formula | m/z | err [ppm] | mSigma | # mSigma | Score | rdb | e⁻ Conf | N-Rule |
|---|---|---|---|---|---|---|---|---|---|---|
| 296.1311 | 1 | C18H18NO3 | 296.1281 | -10.0 | 89.8 | 1 | 100.00 | 10.5 | even | ok |
| | 2 | C11H22NO8 | 296.1340 | 9.8 | 131.9 | 2 | 12.23 | 1.5 | even | ok |
| | 3 | C7H18N7O6 | 296.1313 | 0.7 | 145.3 | 3 | 33.54 | 2.5 | even | ok |

(E)-1-(benzo[d][1,3]dioxol-5-il)-3-(4-fluorofenil)prop-2-en-1-ona (**FER45**)

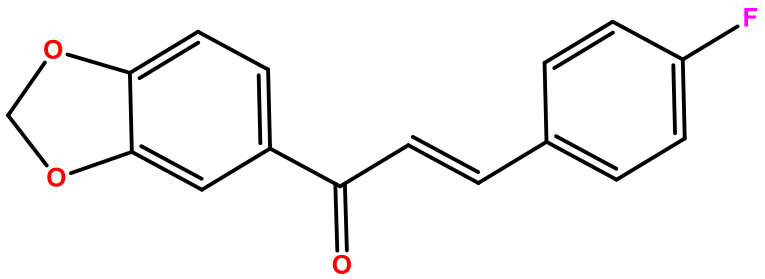


Sólido amorfo, de coloração branco esverdeado - FM: $C_{16}H_{11}FO_3$ [M+]: 271.0769 g/mol; PF: 118.0 – 120.0 °C; Tempo de reação: 24 horas; Rendimento: 98%. $^1$H NMR (400 MHz, $CDCl_3$) δ 7.70 (d, *J* = 2.0 Hz, 1H), 7.66 (d, *J* = 15.6 Hz, 1H), 7.63 (d, *J* = 1.7 Hz, 1H), 7.51 (d, *J* = 1.8 Hz, 1H), 7.45 (d, *J* = 15.6 Hz, 1H), 6.89 (d, *J* = 8.2 Hz, 1H), 6.07 (s, 2H). $^{13}$C NMR (101 MHz, $CDCl_3$) δ 187.69, 152.15, 148.57, 141.44, 136.00, 135.20, 134.35, 133.41, 132.70, 131.05, 129.79, 127.60, 124.99, 123.34, 108.52, 108.11, 102.11.

Figura 81: Espectro de RMN $^1$H (500 MHz, $CDCl_3$) de FER45.

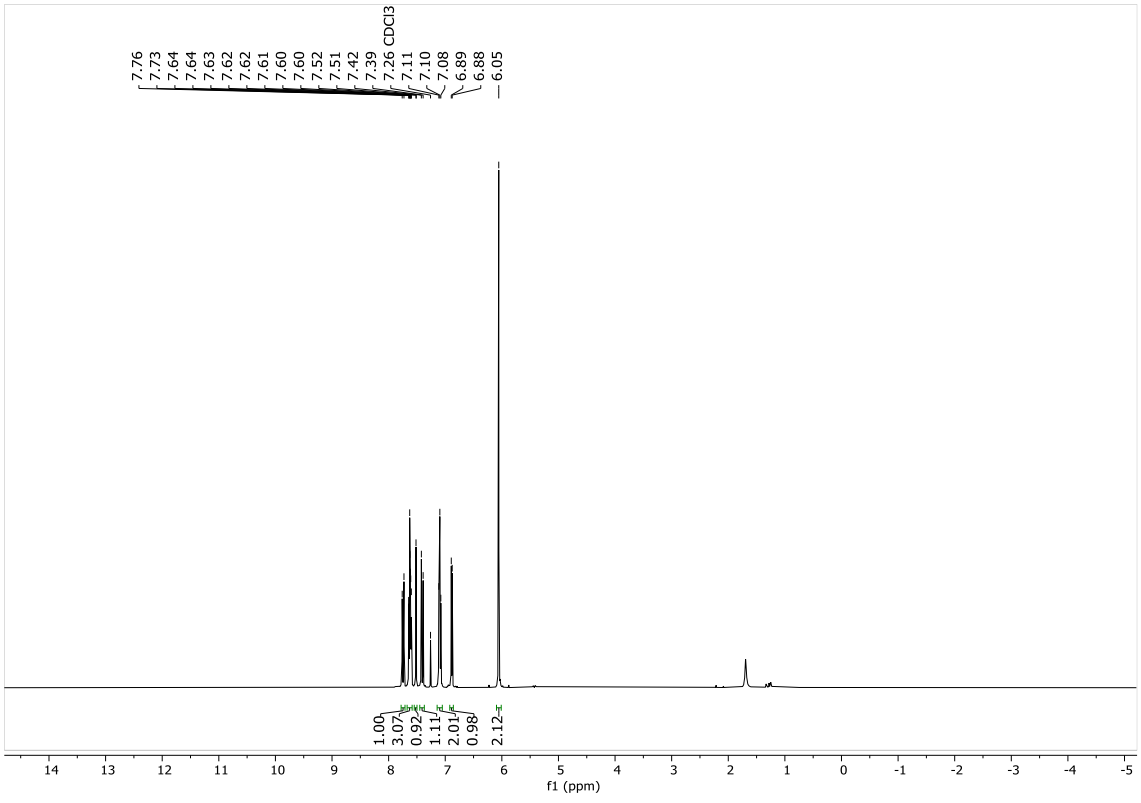

Figura 82: Expansão do espectro de RMN $^{1}H$ (500 MHz, $CDCl_3$) de FER45 na região 6.00 - 7.80 ppm.

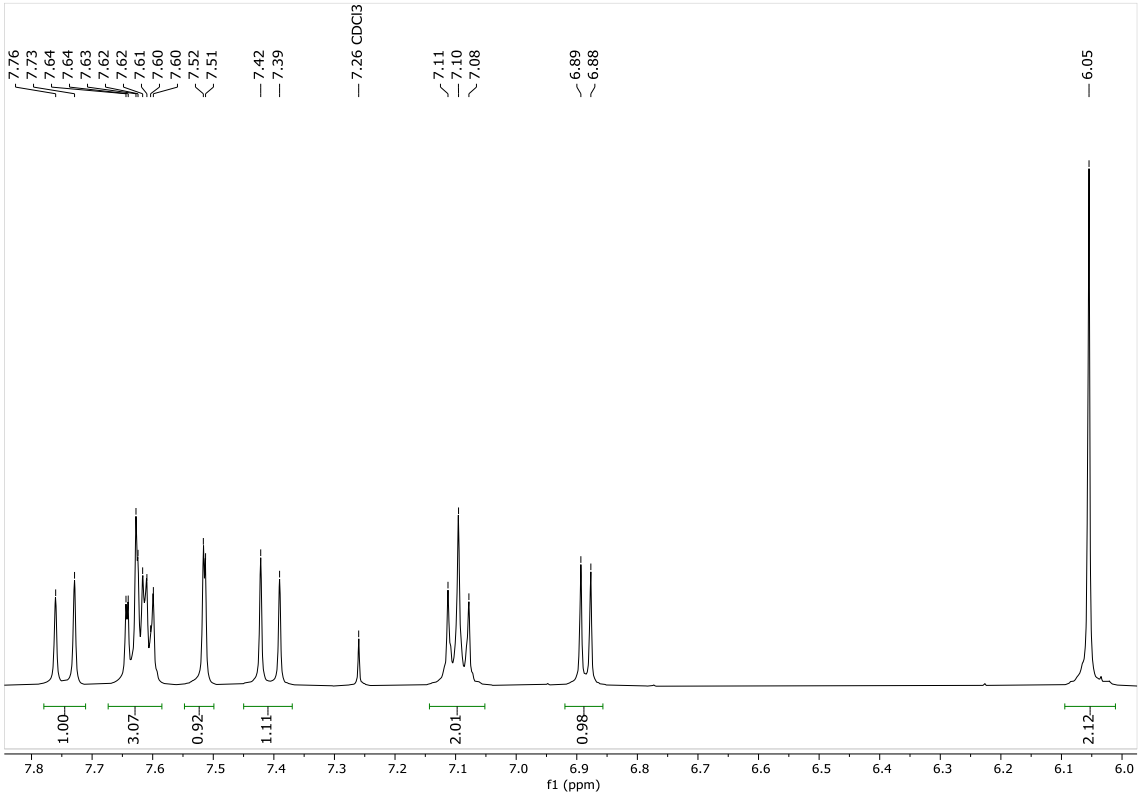


Figura 83: Espectro de RMN $^{13}C$ (125 MHz, $CDCl_3$) de FER45.

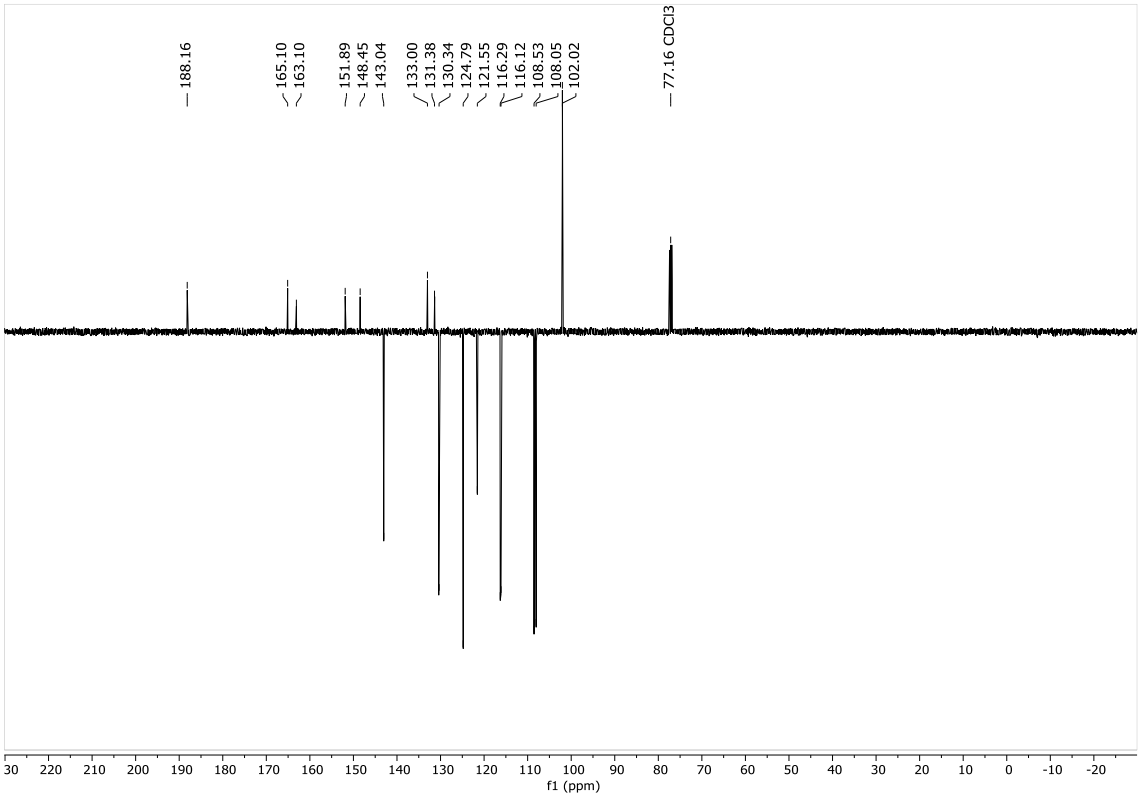

Figura 84: Expansão do espectro de RMN $^{13}C$ (125 MHz, $CDCl_3$) de FER45 na região 102 - 165 ppm.

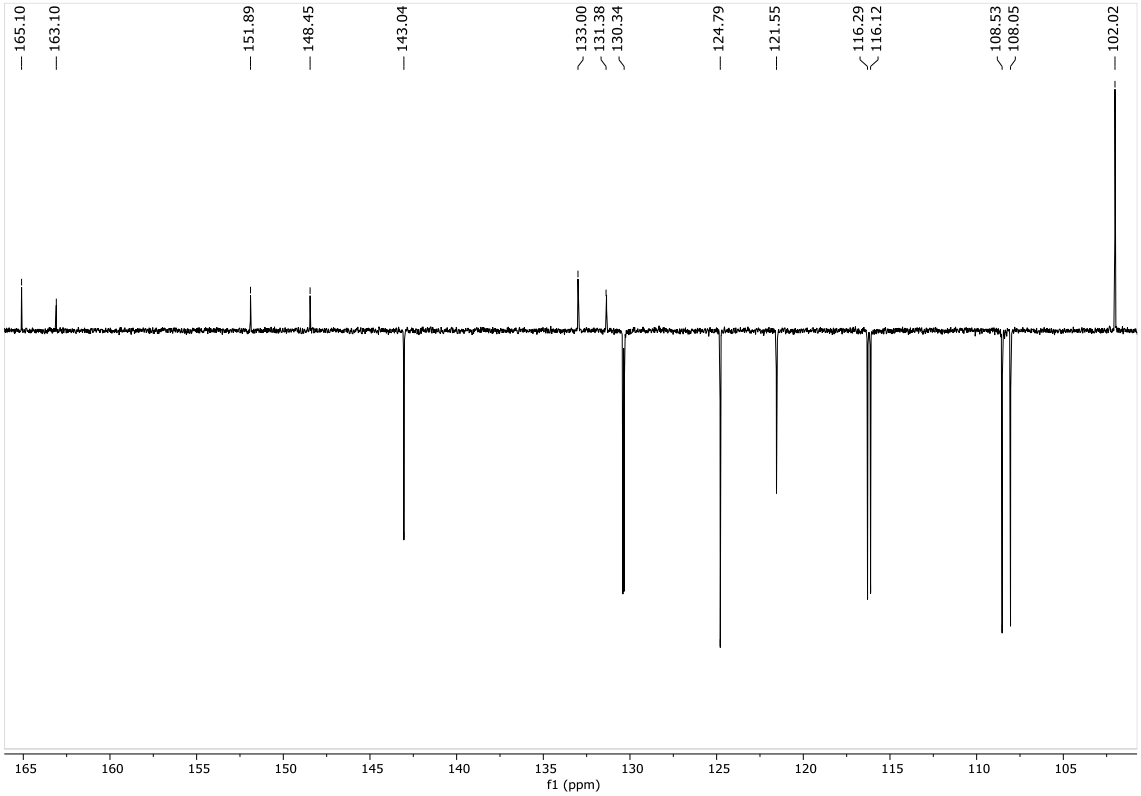


Figura 85: Espectro de massas [M+] de FER45.

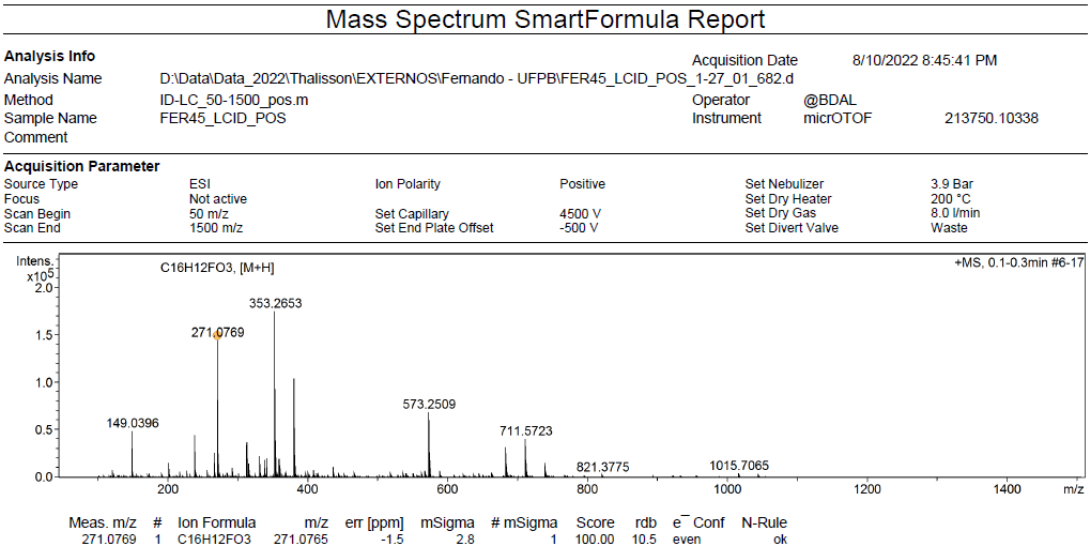

Mass Spectrum SmartFormula Report

**Analysis Info**

| | | | |
|---|---|---|---|
| Analysis Name | D:\Data\Data_2022\Thalisson\EXTERNOS\Fernando - UFPB\FER45_LCID_POS_1-27_01_682.d | Acquisition Date | 8/10/2022 8:45:41 PM |
| Method | ID-LC_50-1500_pos.m | Operator | @BDAL |
| Sample Name | FER45_LCID_POS | Instrument | micrOTOF 213750.10338 |
| Comment | | | |

**Acquisition Parameter**

| | | | | | |
|---|---|---|---|---|---|
| Source Type | ESI | Ion Polarity | Positive | Set Nebulizer | 3.9 Bar |
| Focus | Not active | | | Set Dry Heater | 200 °C |
| Scan Begin | 50 m/z | Set Capillary | 4500 V | Set Dry Gas | 8.0 l/min |
| Scan End | 1500 m/z | Set End Plate Offset | -500 V | Set Divert Valve | Waste |



| Meas. m/z | # | Ion Formula | m/z | err [ppm] | mSigma | # mSigma | Score | rdb | e⁻ Conf | N-Rule |
|---|---|---|---|---|---|---|---|---|---|---|
| 271.0769 | 1 | C16H12FO3 | 271.0765 | -1.5 | 2.8 | 1 | 100.00 | 10.5 | even | ok |

(E)-1-(benzo[d][1,3]dioxol-5-il)-3-(tiofen-2-il)prop-2-en-1-ona (**FER38**)

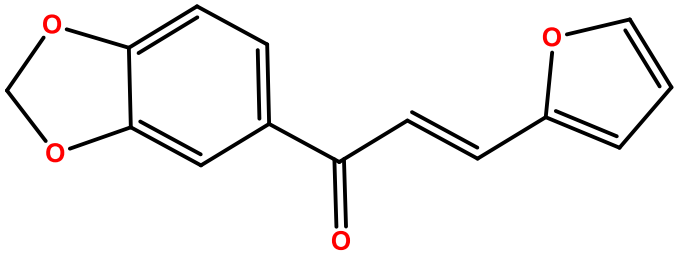


Sólido amorfo, de coloração marrom tijolo - FM: $C_{14}H_{10}O_4$ [M+]: 243.0636 g/mol; PF: 101.0 – 103.0 °C; Tempo de reação: 24 horas; Rendimento: 99%. $^1$H NMR (400 MHz, $CDCl_3$) δ 7.65 (dd, *J* = 8.2, 1.8 Hz, 1H), 7.57 (d, *J* = 15.3 Hz, 1H), 7.53 (d, *J* = 1.7 Hz, 2H), 7.51 (d, *J* = 1.3 Hz, 1H), 7.40 (d, *J* = 15.3 Hz, 1H), 6.87 (d, *J* = 8.2 Hz, 1H), 6.69 (d, *J* = 3.4 Hz, 1H), 6.50 (dd, *J* = 3.4, 1.8 Hz, 1H), 6.04 (s, 2H). $^{13}$C NMR (101 MHz, $CDCl_3$) δ 187.63, 151.80, 151.73, 148.33, 144.84, 133.00, 130.22, 124.66, 119.09, 115.98, 112.68, 108.37, 107.95, 101.91.

Figura 86: Espectro de RMN $^1$H (500 MHz, $CDCl_3$) de FER38.

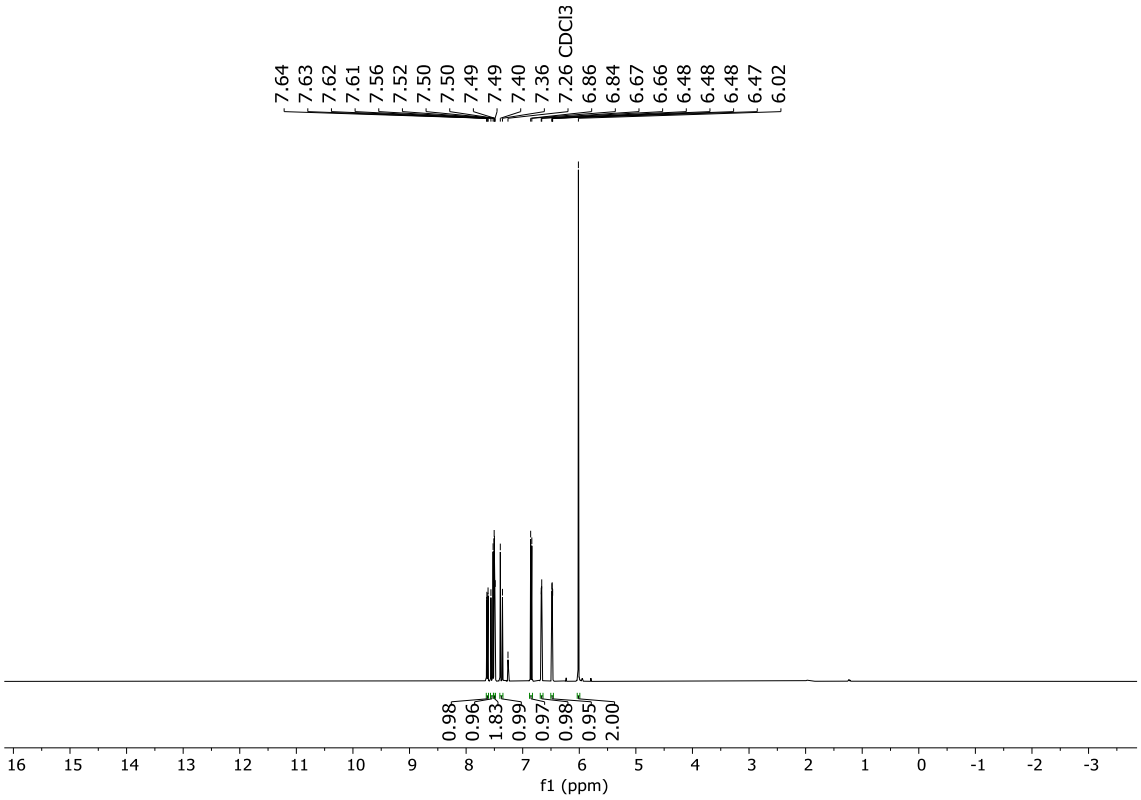

Figura 87: Expansão do espectro de RMN $^{1}H$ (500 MHz, $CDCl_3$) de FER38 na região 6.00 - 7.70 ppm.

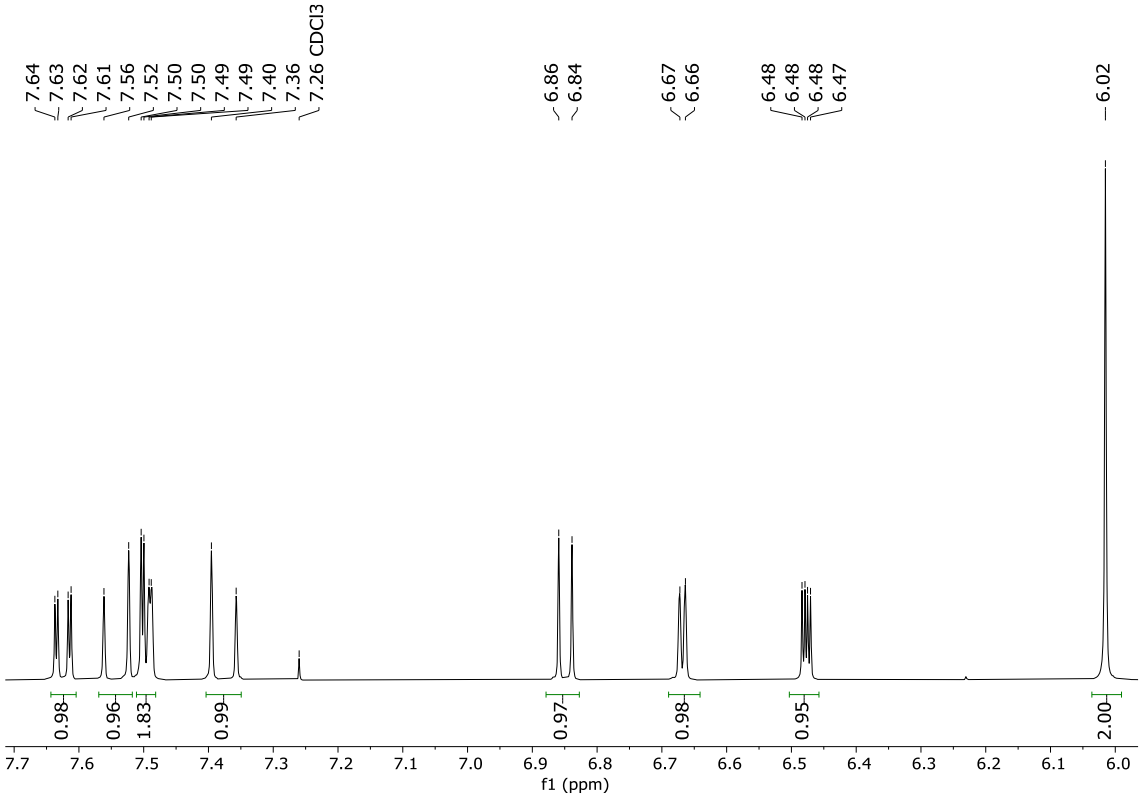


Figura 88: Espectro de RMN $^{13}C$ (125 MHz, $CDCl_3$) de FER38.

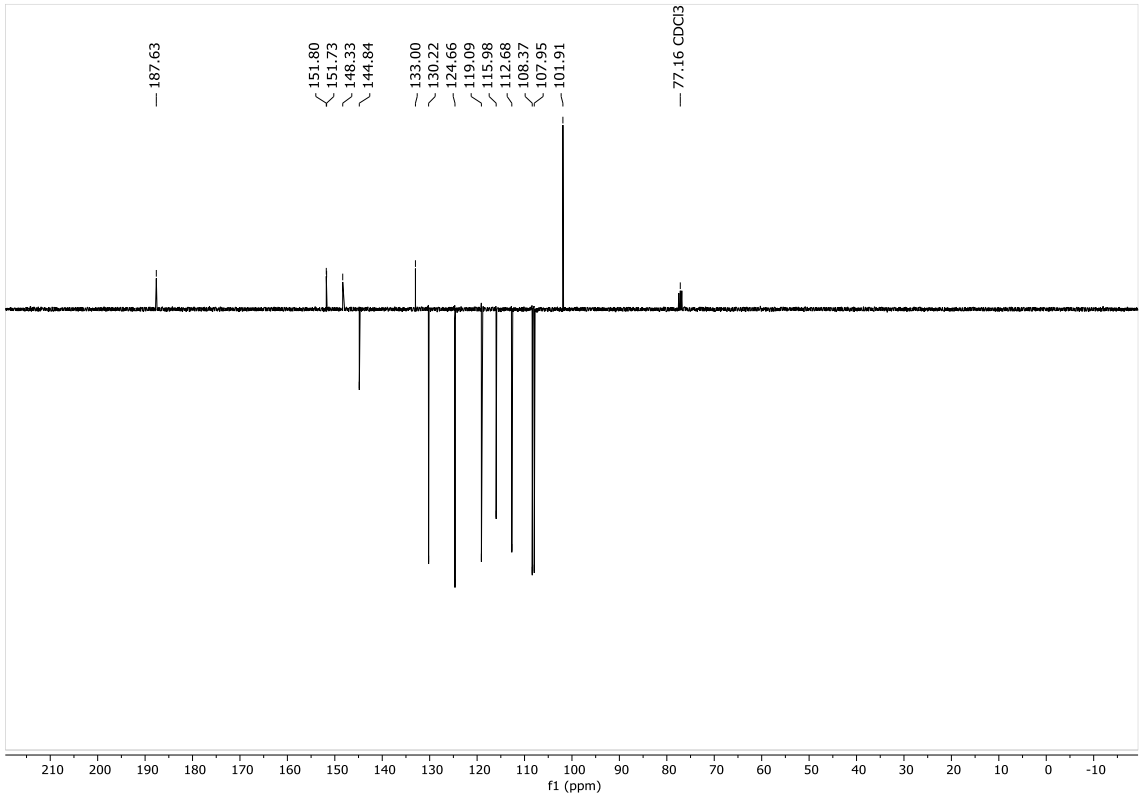

Figura 89: Expansão do espectro de RMN $^{13}C$ (125 MHz, $CDCl_3$) de FER38 na região 102 - 152 ppm.

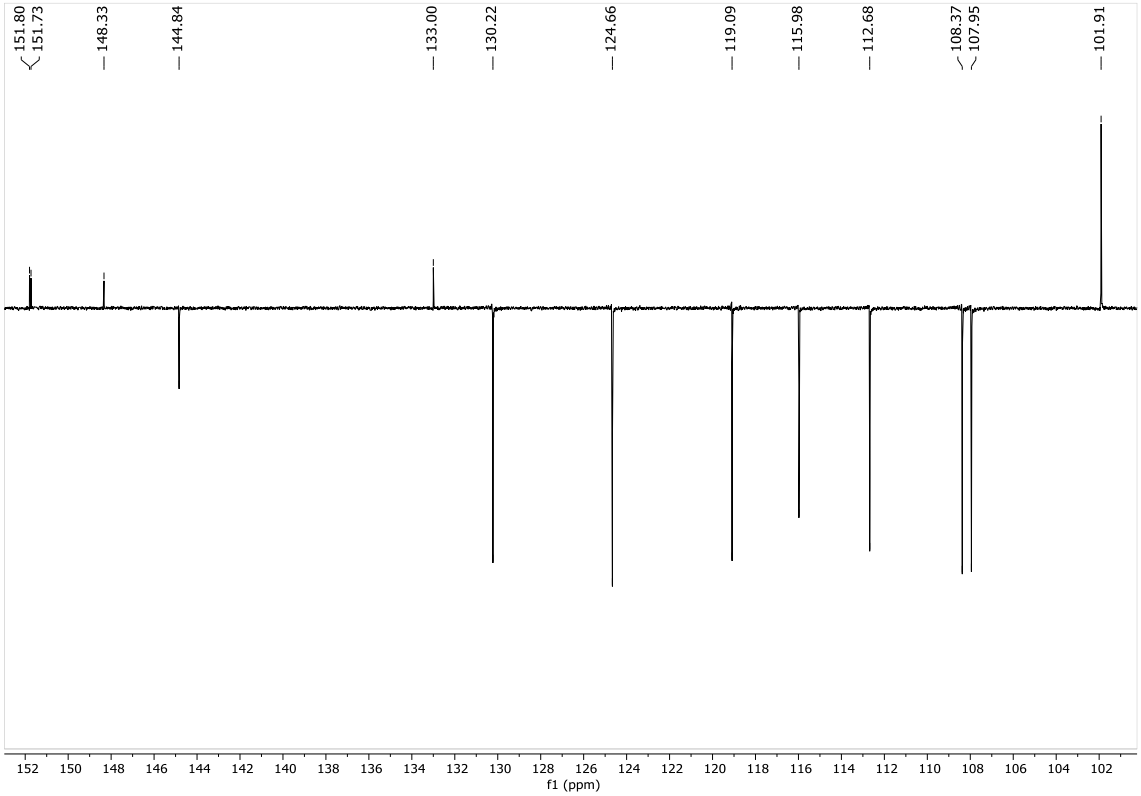


Figura 90: Espectro de massas [M+] de FER38.

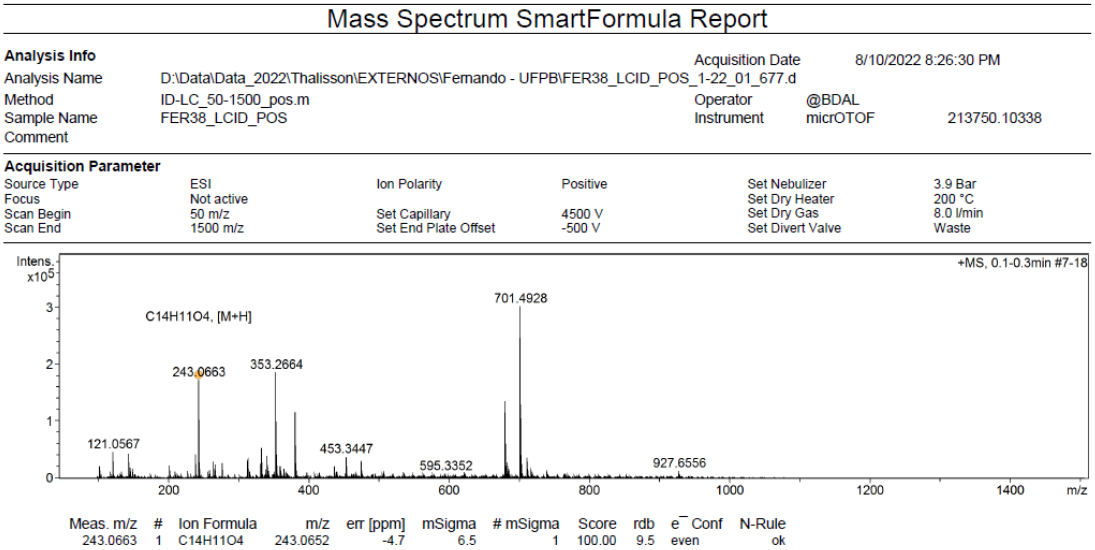

Mass Spectrum SmartFormula Report

**Analysis Info**

| | | | |
|---|---|---|---|
| Analysis Name | D:\Data\Data_2022\Thalisson\EXTERNOS\Fernando - UFPB\FER38_LCID_POS_1-22_01_677.d | Acquisition Date | 8/10/2022 8:26:30 PM |
| Method | ID-LC_50-1500_pos.m | Operator | @BDAL |
| Sample Name | FER38_LCID_POS | Instrument | micrOTOF 213750.10338 |
| Comment | | | |

**Acquisition Parameter**

| | | | | | |
|---|---|---|---|---|---|
| Source Type | ESI | Ion Polarity | Positive | Set Nebulizer | 3.9 Bar |
| Focus | Not active | | | Set Dry Heater | 200 °C |
| Scan Begin | 50 m/z | Set Capillary | 4500 V | Set Dry Gas | 8.0 l/min |
| Scan End | 1500 m/z | Set End Plate Offset | -500 V | Set Divert Valve | Waste |



| Meas. m/z | # | Ion Formula | m/z | err [ppm] | mSigma | # mSigma | Score | rdb | e⁻ Conf | N-Rule |
|---|---|---|---|---|---|---|---|---|---|---|
| 243.0663 | 1 | C14H11O4 | 243.0652 | -4.7 | 6.5 | 1 | 100.00 | 9.5 | even | ok |

(E)-1-(benzo[d][1,3]dioxol-5-il)-3-(furan-2-il)prop-2-en-1-ona (**FER39**)

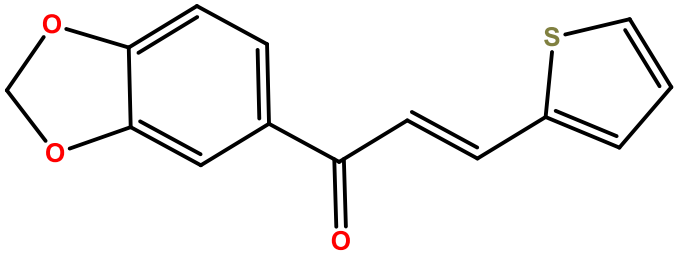


Sólido amorfo, de coloração branco esverdeado - FM: $C_{14}H_{10}O_3S$ [M+]: 259,0430 g/mol; PF: 103.0 – 105.0°C; Tempo de reação: 24 horas; Rendimento: 99%. $^1$H NMR (400 MHz, $CDCl_3$) δ 7.91 (d, *J* = 15.3 Hz, 1H), 7.62 (dd, *J* = 8.2, 1.8 Hz, 1H), 7.62 (dd, *J* = 8.2, 1.8 Hz, 2H), 7.40 (d, *J* = 5.1 Hz, 1H), 7.34 (d, *J* = 3.7 Hz, 1H), 7.28 (d, *J* = 15.3 Hz, 2H), 7.08 (dd, *J* = 5.1, 3.7 Hz, 2H), 6.88 (d, *J* = 8.1 Hz, 2H), 6.05 (s, 4H). $^{13}$C NMR (101 MHz, $CDCl_3$) δ 187.71, 151.80, 148.40, 140.60, 136.77, 133.00, 131.96, 128.68, 128.42, 124.68, 120.57, 108.46, 108.03, 101.98.

Figura 91: Espectro de RMN $^1$H (500 MHz, $CDCl_3$) de FER39.

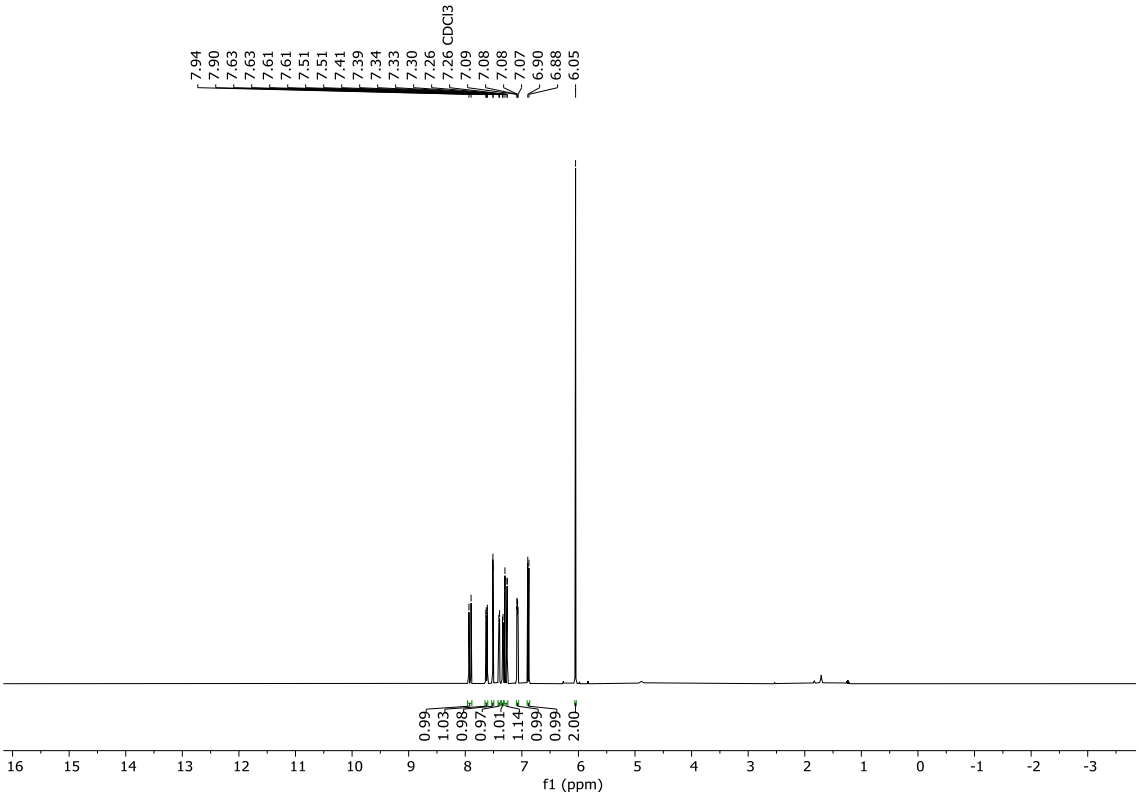

Figura 92: Expansão do espectro de RMN $^{1}H$ (500 MHz, $CDCl_3$) de FER39 na região 6.00 - 8.00 ppm.

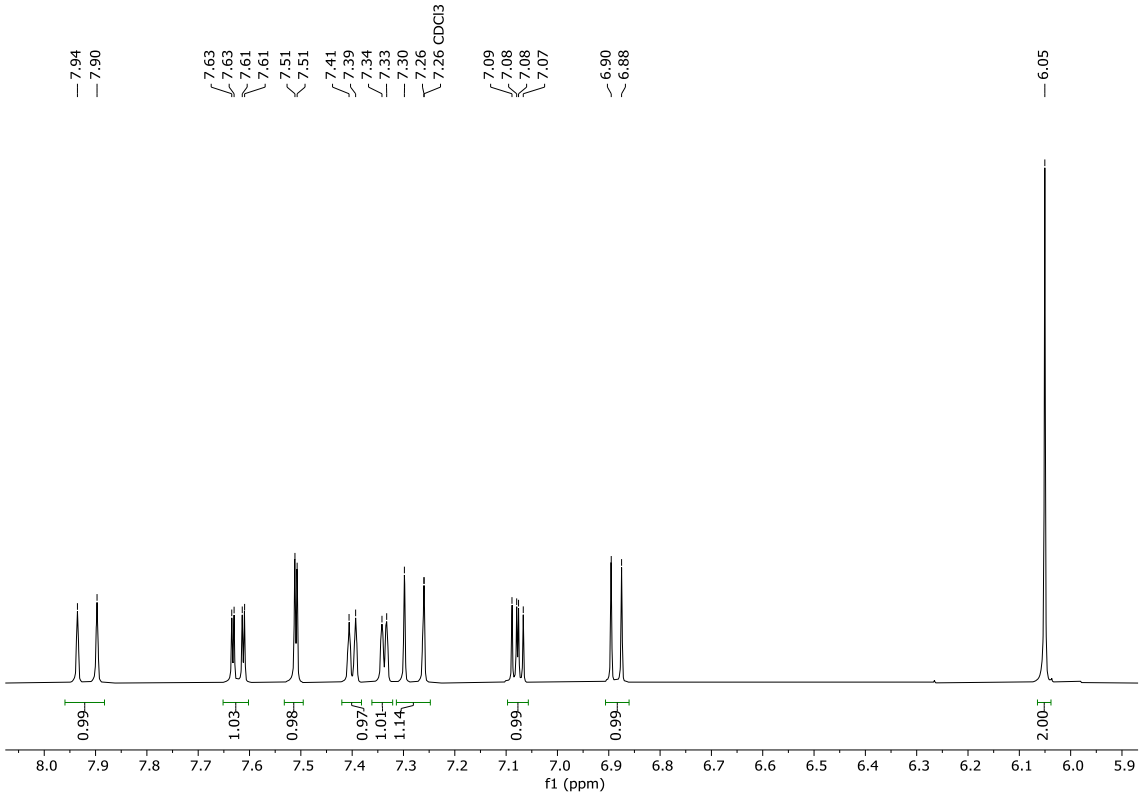


Figura 93: Espectro de RMN $^{13}C$ (125 MHz, $CDCl_3$) de FER39.

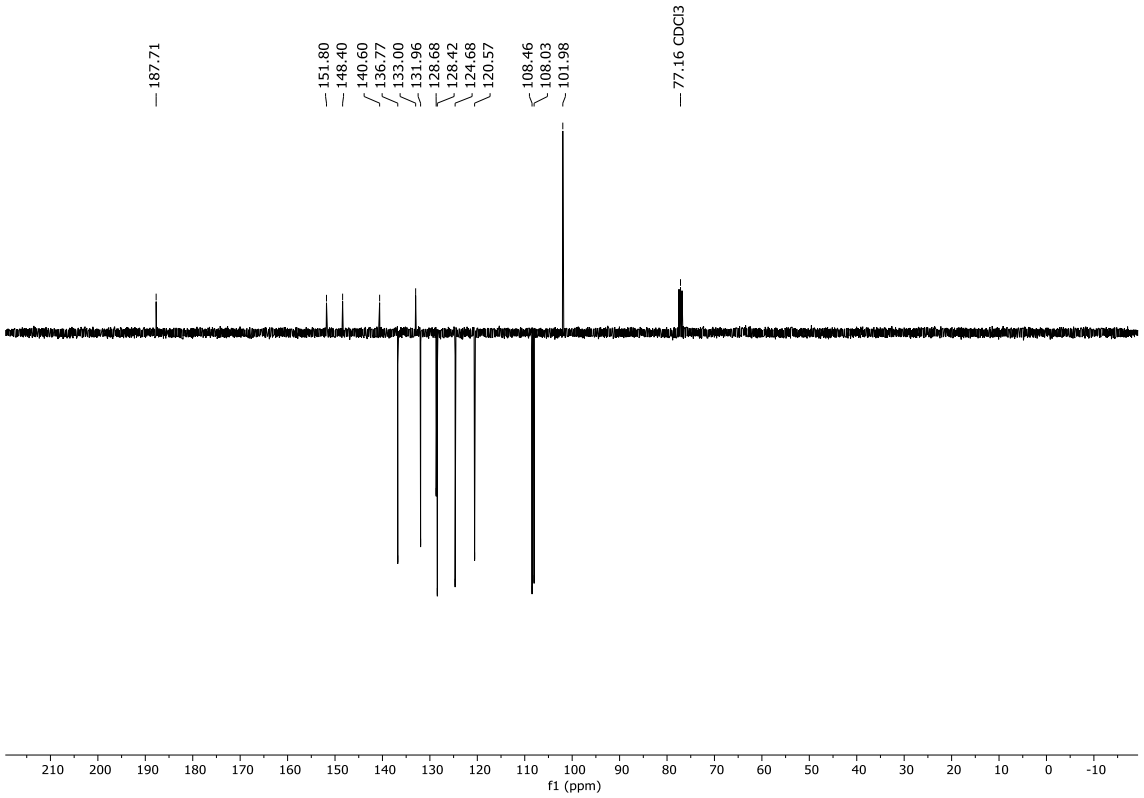

Figura 94: Expansão do espectro de RMN $^{13}C$ (125 MHz, $CDCl_3$) de FER39 na região 102 - 152 ppm.

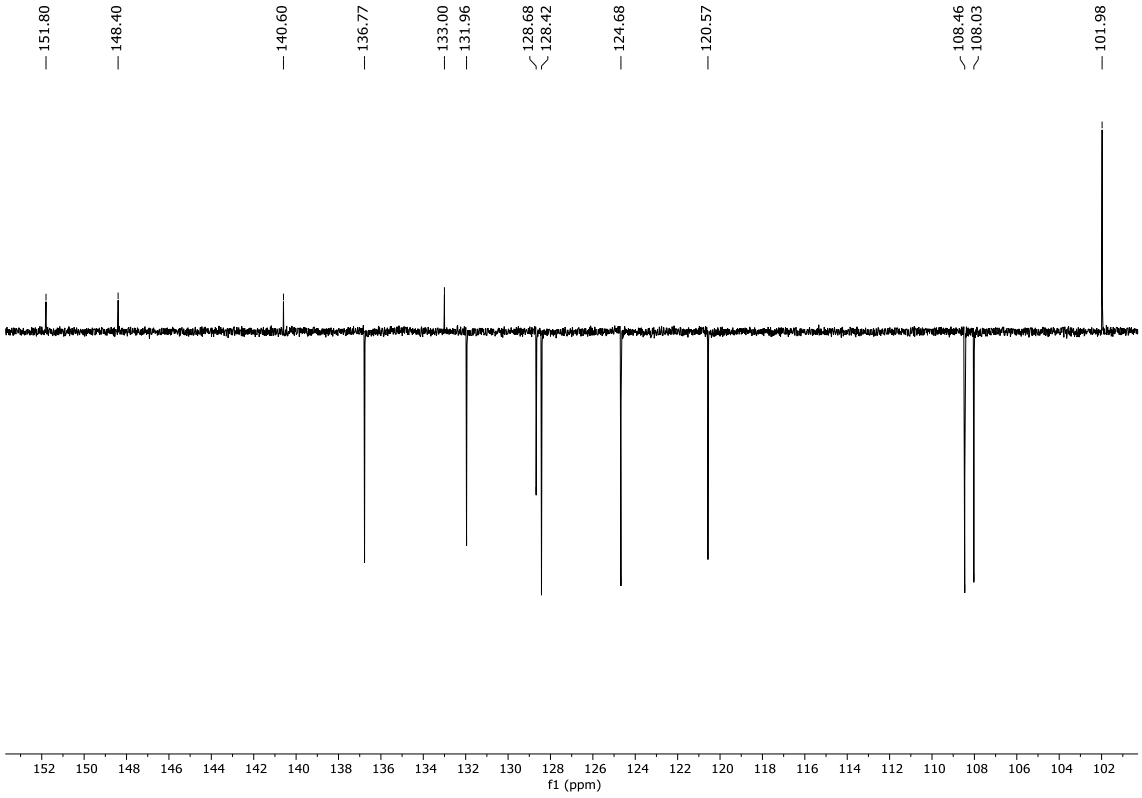


Figura 95: Espectro de massas [M+] de FER39.

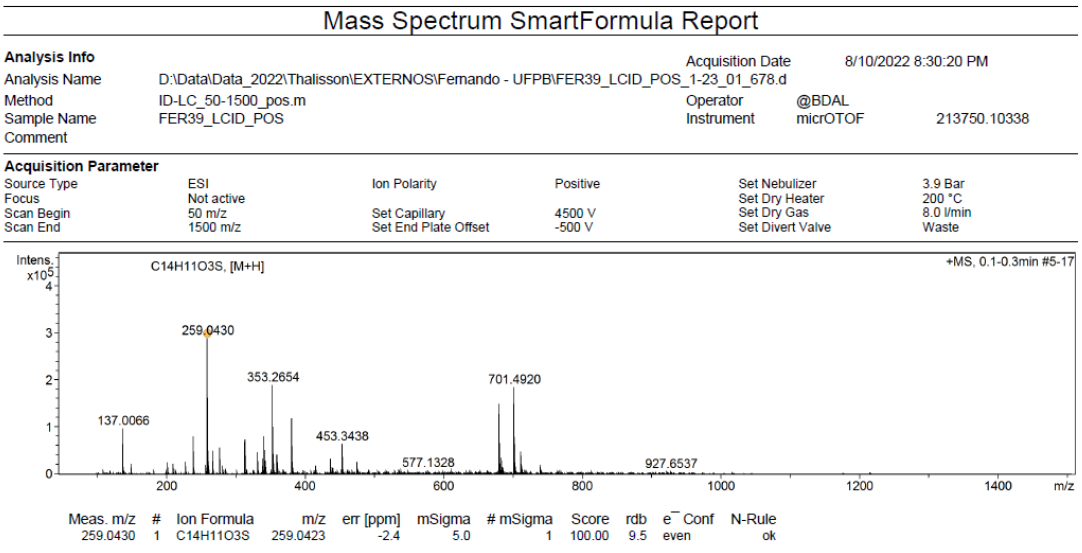

Mass Spectrum SmartFormula Report

**Analysis Info**

| | | | |
|---|---|---|---|
| Analysis Name | D:\Data\Data_2022\Thalisson\EXTERNOS\Fernando - UFPB\FER39_LCID_POS_1-23_01_678.d | Acquisition Date | 8/10/2022 8:30:20 PM |
| Method | ID-LC_50-1500_pos.m | Operator | @BDAL |
| Sample Name | FER39_LCID_POS | Instrument | micrOTOF 213750.10338 |
| Comment | | | |

**Acquisition Parameter**

| | | | | | |
|---|---|---|---|---|---|
| Source Type | ESI | Ion Polarity | Positive | Set Nebulizer | 3.9 Bar |
| Focus | Not active | | | Set Dry Heater | 200 °C |
| Scan Begin | 50 m/z | Set Capillary | 4500 V | Set Dry Gas | 8.0 l/min |
| Scan End | 1500 m/z | Set End Plate Offset | -500 V | Set Divert Valve | Waste |



| Meas. m/z | # | Ion Formula | m/z | err [ppm] | mSigma | # mSigma | Score | rdb | e⁻ Conf | N-Rule |
|---|---|---|---|---|---|---|---|---|---|---|
| 259.0430 | 1 | C14H11O3S | 259.0423 | -2.4 | 5.0 | 1 | 100.00 | 9.5 | even | ok |